On the stability of mycobacterial ribosomes during stasis

Andrej Trauner

Thesis submitted for the degree of Doctor of Philosophy of Imperial College London

October, 2010

Division of Biology, Department of Life Sciences, Imperial College London

Exhibition road, SW7 2AZ London, United Kingdom

Declaration of originality

I hereby declare that I have performed all the work and analysed all the data presented in this report. The exception was the operation of the mass spectrometer – performed by Mr Mark Bennett and the determination of viability presented in Fig. 4.47, which was performed by Dr Huw D. Williams.

Ko dobrave se mrače,
k meni spo glasovi tihi
kakor tožbe tajni vzdihi
src, ki v žalosti žive.

Mir, ah, lega na zemljo,
meni ni ga moč dobiti,
ni mogoče potopiti
duše v spanje mi sladko.

Tihi, polunočni čas,
trepetanje zvezd v višavi,
glas vpijočega v puščavi,
trs samotni to sem jaz!

Pridite, nevihte ve,
pridi, burno ti življenje,
pridi, šumno koprnenje,
in prevpijte mi srce!

Jasnih, jasnih, sončnih dni,
polnih borb, polnih ječanja!
Tiho, tiho dalje sanja
noč z bleščečimi očmi.

JOSIP MURN, KO DOBRAVE SE MRAČE

Mojim.

Andrej

Abstract

Latent tuberculosis is estimated to account for over 99% of *Mycobacterium tuberculosis* infections globally. Bacteria are believed to enter a non-replicating persistent (NRP) state to counter the effect of oxygen and nutrient limitation during latent infection. While NRP bacteria are believed to retain some metabolic activity, it is not known how the stability and functionality of the biosynthetic apparatus is maintained. Using the Wayne hypoxia model, we focused on mycobacterial ribosomes and found that, in contrast to enteric bacteria, no higher order structures (e.g. ribosomal dimers) are formed upon entry into stasis. We devised a strategy incorporating microfluidic, proteomic and ribosomal profiling techniques to elucidate the fate of mycobacterial ribosomes during NRP. We compared the stability of wild-type ribosomes to those of mutants in the transcriptional regulator DosR, which cannot survive prolonged oxygen starvation. While stability was comparable under conditions of active growth and normoxic stasis, Δ*dosR* mutants showed a marked decrease in levels of 70S ribosomes and 30S ribosomal subunits under hypoxia. Microfluidic analyses were consistent with these observations and pointed to a progressive degradation of rRNA during prolonged hypoxia, with evidence of discrete rRNA cleavage. Proteomic analysis also supported a gradual degradation of ribosomes and led to the identification of S30AE proteins as possible ribosome stabilisation factors. There is an S30AE domain protein is the DosR regulon and it may contribute to the observed destabilisation of the ribosome during hypoxia in Δ*dosR* mutants.

Macromolecular stability is further compromised during infection by the presence of reactive oxygen and nitrogen species. We used mass spectrometry to assess the impact of oxidative stress on mycobacterial nucleic acids. We found that RNA was more susceptible to damage. Since only limited RNA synthesis occurs in NRP, the ability of cells to preserve intact ribosomes could be crucial for long-term survival.

Acknowledgements

I would like to thank Dr Huw Williams for his guidance and help with all the aspects of the project – our discussions have kept me going and pulled me back on track on several occasions. I would also like to express my profound gratitude to Mr Mark Bennett for teaching me the ropes of mass spectrometry and without whom there would be no nucleoside analysis or proteomic analysis of ribosomes.

I would like to thank Prof Martin Buck and Dr Brian Robertson who have followed my progress and offered much appreciated comments on the direction of my work. I would also like to extend my gratitude to Dr Samantha Sampson for allowing me to use the Bioanalyzer, members of the Robertson Lab, in particular Mr Graham Joyce, for his help with mycobacterial recombineering, all things related to cloning and measuring luminescence for the transcription-translation assay. In addition I would like to thank Dr Eric Rubin for hosting me in his lab, while I attempted to carry out the TraSH experiment, Prof Neil Fairweather for allowing me to use his anaerobic cabinet, Dr Robert Coutts for lending me the refractometer, the Leak Lab for the French press and BIA Separations for their kind gift of the chromatographic columns as well as the technical support. I am also grateful to Mr Ian Morris and Ms Fiona May for their assistance with many a "crisis" during my time at Imperial.

Last but not least, I would like to thank everybody who has had to put up with me during the writing of this thesis for their patience. In particular Anna, who has been there for me in the thickest of it all, armed with coffee and cookies.

Finally, I am very grateful to the Wellcome Trust for their generous patronage.

Table of contents

DECLARATION OF ORIGINALITY 2
ABSTRACT 4
ACKNOWLEDGEMENTS 5
TABLE OF CONTENTS 6
LIST OF FIGURES 10
LIST OF TABLES 14
1. GENERAL INTRODUCTION 15
1.1 Scope of introduction 16
1.2 Tuberculosis 16
1.2.1 A brief overview of current numbers 16
1.2.2 Natural course of tuberculosis 18
1.2.3 Treating tuberculosis 20
1.2.3.1 Relapse 21
1.2.3.2 Relapsing *Mtb* during infection 22
1.3 Latent tuberculosis 23
1.3.1 Latency/dormancy/persistence 23
1.3.1.1 Definition 23
1.3.1.2 Bacterial persisters and persistence 24
1.3.2 The granuloma 24
1.3.2.1 Granuloma formation and dynamics 26
1.3.2.2 Granuloma as an environmental niche 27
1.3.3 Modelling latent tuberculosis 27
1.3.3.1 *In vivo* models 28
1.3.3.2 *In vitro* models 29
1.3.3.3 Model organisms 31
1.4 The persistent mycobacterium 32
1.4.1 Physiological adaptations during persistence 32
1.4.1.1 Energy generation 33
1.4.1.2 Anabolic metabolism 34
1.4.1.3 Stability 35
1.4.1.4 Sporulation 36
1.4.2 Regulation of persistence 37
1.4.2.1 DosR regulon 37
1.4.2.2 DosR regulon or Enduring Hypoxic Response 39
1.4.2.3 Stringent response and persistence 41
1.4.2.4 Stringent response regulation of the ribosome 41
1.4.3 Ribosomal stability as a survival strategy 43
1.4.3.1 Ribosomal stability in *E. coli* 44
1.5 The stressed persistent mycobacterium 45
1.5.1 Oxidative and nitrosative damage 45
1.5.1.1 Sources of damage 47
1.5.1.2 Targets for damage 48
1.5.1.3 General mitigation of damage 49
1.5.2 Implications of damage 50
1.5.2.1 Selective targeting 50
1.5.2.2 Downstream effects of DNA and RNA damage 51
1.5.2.3 Repair of oxidative damage to DNA 52
1.5.2.4 Repair of oxidative damage to RNA 54
1.6 Summary of aims 55
2. MATERIALS AND METHODS 57
2.1.1 Bacterial strains and growth media 58
2.1.2 Viability determination 59
2.1.3 Toxicity assay 59
2.1.4 Methylene blue toxicity 60
2.1.4.1 Photo-oxidation with methylene blue 60
2.1.5 Biosynthesis determination 60
2.1.5.1 Protein synthesis 60

2.1.5.2 RNA synthesis 61
2.2 Molecular biology techniques *61*
2.2.1 Protein precipitation 61
2.2.1.1 Colorimetric Protein Quantitation 62
2.2.2 SDS-PAGE 62
2.2.3 Western blot analysis 62
2.2.3.1 Densitometric analysis 63
2.2.4 Nucleic acid isolation 63
2.2.4.1 Isolation of DNA 63
2.2.4.2 Isolation of RNA 64
2.2.4.3 Spectrophotometric analysis 65
2.2.4.4 Bioanalyzer analysis 65
2.2.5 Polymerase chain reaction 65
2.2.5.1 Agarose gel electrophoresis 66
2.2.5.2 Restriction enzyme digestion and ligation 66
2.2.6 Recombineering mutagenesis 66
2.2.6.1 Complementation of ΔMSMEG_3935 67
2.2.7 Transformation 71
2.2.7.1 Transformation of *E. coli* 71
2.2.7.2 Transformation of *Msm* 72
2.3 Ribosomal profiling *72*
2.3.1 Cell lysis 72
2.3.2 Ribosomal profiling 73
2.3.3 Sucrose gradient preparation 73
2.4 Fast protein liquid chromatography (FPLC) of ribosomes *74*
2.4.1 Fast protein liquid chromatography 74
2.4.2 Coupled transcription-translation assay 75
2.4.3 [^{3}H]-erythromycin binding assay 76
2.5 Mass spectrometric analysis of peptides *76*
2.5.1 Trypsin digestion 76
2.5.2 iTRAQ labelling 77
2.5.2.1 Sample cleanup 77
2.5.3 HPLC of peptides 78
2.5.4 Mass spectrometric analysis 78
2.5.4.1 Mass windows 78
2.5.4.2 Data analysis 79
2.5.5 Multiple reaction monitoring approach to specific protein detection 79
2.6 Nucleoside analysis *80*
2.6.1 induction of oxidative stress 80
2.6.2 Nucleic acid extraction 81
2.6.3 nucleic acid digestion 81
2.6.4 HPLC 82
2.6.4.1 HPLC prior to mass spectrometry 82
2.6.4.2 HPLC prior to electrochemical detection 82
2.6.5 Tandem mass spectrometry 83
2.6.6 Electrochemical detection 84
2.6.6.1 Hydrodynamic voltammograms 84
2.6.6.2 Nucleoside detection 84
2.6.7 Sample quantification 84
2.7 Trash experiment *85*
2.7.1 Phage stock preparation 85
2.7.2 Transposon mutant library construction 86
3. PERSISTENT PHYSIOLOGY 87
3.1 Introduction *88*
3.2 Stationary phase survival *89*
3.2.1 Long-term viability of Msm 89
3.2.1.1 Persistence model parameters 89
3.2.1.2 Stationary phase survival of ΔdosR *Msm* 90
3.2.2 Mbo BCG ΔdosR mutant 92
3.3 Toxicity studies *93*
3.3.1 Effect of H_2O_2 on Msm growth 93
3.3.2 Susceptibility of static Msm to nucleic acid damaging agents 94
3.4 Biosynthesis *96*

3.4.1 Measuring biosynthesis by [^{3}H]-label incorporation ... 96
3.4.1.1 Amino acid incorporation ... 96
3.4.1.2 Uracil incorporation ... 98
3.4.2 RNA biosynthesis during stasis ... 99
3.4.2.1 Hypoxia ... 99
3.4.2.2 C-starvation ... 101
3.5 Discussion ... 103
3.5.1 Biosynthesis in the Wayne model of persistence ... 103
4. RIBOSOMAL STABILITY IN STASIS ... 108
4.1 Introduction and aims ... 109
4.2 Ribosomal profiling (method development) ... 109
4.2.1 Ribosomal profiling – sample preparation ... 110
4.2.2 Ribosomal profiling – buffer composition ... 111
4.2.3 Ribosomal profiling – Ultracentrifugation parameters ... 114
4.3 Ribosomal profiling (results) ... 118
4.3.1 The mycobacterial ribosome during growth and stasis ... 118
4.3.2 Ribosomal stability during hypoxia – a role for DosR? ... 120
4.3.3 Ribosomal stability during carbon starvation ... 124
4.3.4 DosR regulon in ribosomal stability ... 125
4.3.4.1 HspX ... 126
4.3.4.2 USPs ... 128
4.4 rRNA stability ... 130
4.4.1 Explanation of the approach ... 131
4.4.2 rRNA stability during hypoxia ... 134
4.4.3 rRNA stability during carbon starvation ... 136
4.4.4 rRNA stability during CCCP-induced energy starvation ... 137
4.5 Compositional analysis of ribosomes ... 139
4.5.1 Proteomic analysis of "Pre-spin" ribosomal pellets ... 139
4.5.2 Chromatographic purification of ribosomes ... 142
4.5.2.1 Cell fractionation using monolith chromatography ... 144
4.5.2.2 Ribosomal profiling using chromatography ... 148
4.5.2.3 Optimal isolation of ribosomes from crude extracts ... 152
4.5.2.4 Function of chromatography purified ribosomes ... 153
4.6 Evaluation of FPLC as a tool for compositional analysis ... 155
4.6.1 Quantitative proteomics using iTRAQ – method implementation ... 156
4.6.1.1 Troubleshooting of iTRAQ implementation ... 157
4.6.1.2 Optimisation of iTRAQ - labelled peptide purification ... 160
4.6.1.3 Optimisation of iTRAQ – data acquisition ... 161
4.6.2 iTRAQ compositional analysis – FPLC purification scrutiny ... 170
4.7 Compositional analysis of ribosomes during stasis ... 171
4.7.1 Choice of samples ... 172
4.7.2 iTRAQ of ribosomal samples ... 175
4.7.2.1 Ribosomal proteins ... 175
4.7.2.2 Non-ribosomal proteins ... 178
4.7.2.3 Ribosome-associated proteins ... 179
4.8 S30AE domain proteins of Msm ... 182
4.8.1 MSMEG_3935 and MSMEG_1878 interact with the ribosome ... 184
4.8.2 MSMEG_3935 mutagenesis and complementation ... 187
4.8.3 ΔMSMEG_3935 viability and rRNA stability during hypoxia ... 189
4.9 Discussion ... 192
4.9.1 Mycobacterial ribosomes – stabilised by association? ... 192
4.9.1.1 Slow-growing vs fast-growing mycobacteria ... 195
4.9.1.2 rRNA stability in stasis ... 195
4.9.2 On the role of DosR in ribosomal stability ... 198
4.9.3 MSMEG_3935 & MSMEG_1878 – keepers of the ribosome? ... 199
4.9.4 The ribosome during stasis – conclusions ... 202
5. OXIDATIVE STRESS TO NUCLEIC ACIDS ... 204
5.1 Introduction and aims ... 205
5.2 HPLC analysis method implementation ... 205
5.2.1 HPLC-MS method development ... 205
5.2.1.1 Choice of chromatography ... 206
5.2.1.2 Setting up the MRM parameters ... 208
5.2.1.3 Sample preparation evaluation ... 209

5.2.2 HPLC-ECD method development 211
5.2.2.1 Hydrodynamic voltammograms of nucleosides 211
5.2.2.2 Sensitivity of ECD compared to mass spectrometry 212
5.3 Nucleic acid damage 216
5.3.1 Hydrogen peroxide oxidative damage to nucleic acids 216
5.3.1.1 Dose dependent damage to nucleic acids 216
5.3.1.2 Time-course of oxidative damage 219
5.3.1.3 ΔdosR and oxidative damage 220
5.3.1.4 Hydrogen peroxide – a suitable stress agent? 221
5.3.2 Methylene blue photo-oxidation 222
5.3.2.1 Toxicity 223
5.3.2.2 Damage to nucleic acids 224
5.4 Exploring oxidative damage in mycobacteria using TraSH 225
5.4.1 Choice of mutants 226
5.4.2 Mutagenesis 228
5.4.3 TraSH experiment – transposon mutant library construction 229
5.5 Discussion 230
5.5.1 Measuring oxidative damage in mycobacteria – what have we learned? 230
5.5.2 Implications of greater susceptibility of RNA to oxidative damage 233
6. GENERAL DISCUSSION 235
Can RafH be a regulator of mycobacterial growth? 236
Is ribosomal stability important for survival in mycobacterial persistence? 239
7. REFERENCES 242

List of Figures

Chapter 1 – General Introduction

FIG. 1.1 The global burden of tuberculosis. *17*

FIG. 1.2 The "life-cycle" of *Mtb* – progression of tuberculosis. *20*

FIG. 1.3 The classic granuloma. *25*

FIG. 1.4 The Wayne model of persistence. *30*

FIG. 1.5 The respiratory system of mycobacteria. *34*

FIG. 1.6 Impact of biologically relevant ROS and RNS interactions. *48*

FIG. 1.7 The Fenton reaction. *49*

FIG. 1.8 Modified nucleobases exhibit non Watson-Crick base pairing and are actively removed from DNA. *53*

Chapter 3 – Persistent Physiology

FIG. 3.1 The viability of ΔdosR *Msm* is compromised during prolonged hypoxic stasis, but not prolonged carbon starvation. *91*

FIG. 3.2 *Mbo* BCG putative *dosR* mutants harbour active DosR. *93*

FIG. 3.3 H_2O_2 has a concentration-dependent effect on active growth of *Msm*. *93*

FIG. 3.4 DosR does not play a role in the resistance to nucleic acid damaging agents during stasis. *95*

FIG. 3.5 [^{3}H]-label from [4,5-^{3}H]-leucine and [methyl-^{3}H]-methionine is poorly incorporated into proteins by *Msm*. *97*

FIG. 3.6 [^{3}H]-label from [5,6-^{3}H]-uracil is incorporated readily into cellular RNA in *Msm*. *98*

FIG. 3.7 RNA biosynthesis is reduced to a lesser extent in ΔdosR than wild type during prolonged hypoxia. *100*

FIG. 3.8 [^{3}H]-uracil incorporation into RNA during prolonged carbon starvation. *101*

Chapter 4 – Ribosomal Stability in Stasis

FIG. 4.1 Mycobacterial cells are lysed more efficiently by passage through the French press. *111*

FIG. 4.2 Polysomes, intact ribosomes and ribosomal subunits form part of the ribosomal population of *Msm* during active growth. *113*

FIG. 4.3 Sucrose concentration gradients were linear. *114*

FIG. 4.4 Pre-spin improves the resolution of ribosomal profiles and removes cytosolic proteins. *115*

FIG. 4.5 Resolution is comparable when different combination of gradient range and spin times are used. *116*

FIG. 4.6 Summary flow chart of the ribosomal profiling protocol. *117*

FIG. 4.7 Ribosomal profiles of actively growing and stationary phase bacteria during normoxia. *118*

FIG. 4.8 Ribosomal profiles of actively growing and stationary phase *Msm* ΔdosR during normoxia. *120*

FIG. 4.9 *Msm* ΔdosR ribosomes are destabilised during hypoxic stasis. *122*

FIG. 4.10 *Msm* ΔdosR ribosomes during hypoxia are the same as wild type ribosomes. *123*

FIG. 4.11 Ribosomal profiles of 4-day-old hypoxic cultures of *Msm*. *124*

FIG. 4.12 Ribosomal profiles during carbon starvation. *125*

FIG. 4.13 α-crystallin does not associate exclusively to the ribosome in *Mbo* BCG. *127*

FIG. 4.14 Western blots used for the quantitation of HspX association shown in Fig. 4.13. *128*

FIG. 4.15 Anti-His_6-Rv1636 antibodies cross-react with *Msm* cellular extracts. *130*

FIG. 4.16 Ribosomal RNA profiles of actively growing *Msm* cells. *132*

FIG. 4.17 Ribosomal RNA profiles – data processing. *133*

FIG. 4.18 rRNA stability during prolonged hypoxic stasis. *135*

FIG. 4.19 rRNA stability during prolonged carbon-starved stasis. *136*

FIG. 4.20 Wild type *Msm* is more susceptible to CCCP when grown to normoxic stationary phase in rich medium. *137*

FIG. 4.21 rRNA stability of cultures exposed to CCCP. *138*

FIG. 4.22 "Pre-spin" ribosomal preparations contain proteins from all cellular compartments. *140*

FIG. 4.23 Fractionation of *Msm* cell extracts on DEAE monolithic columns. *144*

FIG. 4.24 Monolith-FPLC fraction F2 alone contains ribosomal subunits. *146*

FIG. 4.25 The composition of chromatographic fraction F2 (see Fig. 4.24) and sucrose-purified ribosomes is comparable. *147*

FIG. 4.26 Eluting ribosomes with NH_4Cl preserves associated ribosomes. *149*

FIG. 4.27 Chromatographic profiling of *Msm* cell extracts. *150*

FIG. 4.28 Outline of chromatographic gradients used for the elution of ribosomal fractions during FPLC analysis. *151*

FIG. 4.29 Purification of *Msm* ribosomes using monolithic QA columns. *153*

FIG. 4.30 Monolith-FPLC purified ribosomes show modest biological activity. *154*

FIG. 4.31 Schematic representation of the iTRAQ tag. *156*

FIG. 4.32 The pH of iTRAQ labelled peptides need to be adjusted prior to SCEX cleanup of the samples. *158*

FIG. 4.33 Monolith-FPLC purified ribosomal preparations cannot be labelled with iTRAQ if eluted with 1 M NH_4Cl. *160*

FIG. 4.34 Summary flow chart for iTRAQ labelling of tryptic peptides. *161*

FIG. 4.35 Increasing the depth of analysis by setting up m/z windows for mass spectrometric analysis. *165*

FIG. 4.36 A combination of acquisition methods yields a higher depth of analysis. *166*

FIG. 4.37 The total number of proteins identified and the sequence coverage of each protein is improved by combining acquisition methods. *168*

FIG. 4.38 Equivalent samples are comparable when labelled with different iTRAQ tags. *169*

FIG. 4.39 rRNA profiles reflect the status of the ribosomal population. *172*

FIG. 4.40 rRNA profiles of samples used for iTRAQ. *173*

FIG. 4.41 Hypoxic stasis results in the progressive degradation of the ribosome, manifested by an imbalance in the 30S/50S ratio. *177*

FIG. 4.42 MSMEG_3935 has a putative DosR responsive element upstream of its start codon. *181*

FIG. 4.43 S30AE proteins of *E. coli*, *Msm* and *Mtb*. *182*

FIG. 4.44 Phylogenetic tree of selected mycobacterial S30AE proteins. *183*

FIG. 4.45 MSMEG_3935 is absent from hypoxic *Msm* ΔdosR cultures. *186*

FIG. 4.46 Knocking out MSMEG_3935. *189*

FIG. 4.47 The viability of ΔMSMEG_3935 *Msm* is compromised during prolonged hypoxic stasis, but but to a lesser extent than that of ΔdosR. *190*

FIG. 4.48 rRNA stability of ΔMSMEG_3935 is compromised during prolonged hypoxic stasis. *191*

FIG. 4.49 Model of ribosomal stability during stasis. *203*

Chapter 5 – Oxidative Stress to Nucleic Acids

FIG. 5.1 Definition of chromatographic resolution (R). *207*

FIG. 5.2 Nuclease P1 efficiently digests DNA at 57.5˚C. *209*

FIG. 5.3 H_2O_2 treatment causes an increase in 8-OG levels in tRNA after *in vitro* exposure. *210*

FIG. 5.4 Hydrodynamic voltammograms for guanine nucleosides and their 8-hydroxyl derivatives. *212*

FIG. 5.5 Pump noise drastically reduces the sensitivity of our HPLC-ECD system. *213*

FIG. 5.6 Summary flow-chart of the nucleoside detection method. *215*

FIG. 5.7 H_2O_2 causes more detectable oxidative damage in hypoxic cultures of wild type *Msm*. *217*

FIG. 5.8 Time-course of nucleic acid oxidation in wild type *Msm* during active growth. *219*

FIG. 5.9 Sub-lethal concentrations of H_2O_2 lead to a greater oxidation of cellular nucleic acids during hypoxia. *220*

FIG. 5.10 Methylene blue photo-oxidation inhibits *Msm* wild type growth. *223*

FIG. 5.11 Methylene blue photo-oxidation gives rise to 8-O(d)G in wild type *Msm in vivo*. *224*

FIG. 5.12 Interplay between oxidative damage and antioxidant defences in mycobacteria during infection. *227*

List of Tables

Chapter 2 – Materials and Methods

TABLE 2.1 Bacterial strains used during this study. *58*

TABLE 2.2 Growth media formulation. *59*

TABLE 2.3 Primers used for PCR and *Msm* mutagenesis *68*

TABLE 2.4 Plasmids used during this study *71*

TABLE 2.5 Peptides used for MRM analysis *80*

TABLE 2.6 m/z transitions and collision energies for nucleoside analysis *83*

Chapter 4 – Ribosomal Stability in Stasis

TABLE 4.1 rProteins and ribosome-associated proteins in "Pre-spin" ribosomal preparations as identified by ProteinPilot. *141*

TABLE 4.2 Comparative iTRAQ analysis of *M. smegmatis* ribosomal fractions by mass spectrometry *170*

TABLE 4.3 Proteins detected during iTRAQ analysis of *M. smegmatis* ribosomal fractions *178*

TABLE 4.4 Comparative levels of detected ribosome-associated proteins during *Msm* stasis. *179*

TABLE 4.5 MSMEG_1878 and MSMEG_3935 peptides used for MRM analysis *185*

Chapter 5 – Oxidative Stress to Nucleic Acids

TABLE 5.1 R values for key nucleosides using different column chemistries. *207*

TABLE 5.2 Detection and quantitation thresholds for 8-OG and 8-OdG using HPLC-ECD. *213*

TABLE 5.3 Summary of *Msm* mutagenesis for oxidative stress TraSH. *228*

1. General Introduction

1.1 Scope of introduction

This introduction is not intended to provide an extensive review of the literature, but rather offer a guide to the existing knowledge and ideas that have formed the conceptual framework of my work. There are a multitude of recent reviews that deal with many of the themes that I will address, so I felt that the best contribution I could give was to pick the relevant topics and summarise them.

I consider latent human infection to be the natural state of *Mycobacterium tuberculosis*. As a result, I perceive the physiology of the persistent bacterium to be defined by its limited capacity to generate chemical energy imposed on it by a scarce availability of oxygen and nutrients. The bacterium is very well adapted to the limiting environment in which it exists, and it is able to survive within it by conserving energy and exploiting several aspects of macrophage biology. In this introduction I will try to summarise what is known about the persistent bacterium, while drawing attention to an important aspect of its physiology that has not yet been fully explored – that of RNA damage and stability.

1.2 Tuberculosis

1.2.1 A brief overview of current numbers

Few diseases have played such a prominent role in human history, as did tuberculosis – evidence of which was found in some of the earliest human civilisations. Its first descriptions effectively coincide with the emergence of medicine (Dormandy, 1999, Gandy, 2003). Historically referred to as phthisis, consumption or the white plague, it is caused by the slow-growing Gram positive bacillus *Mycobacterium tuberculosis* (*Mtb*) and to a lesser extent *Mycobacterium bovis* (*Mbo*). With the advent of the antibiotic era and the improvement of public health measures, tuberculosis was considered an all but managed disease in the developed world (Gandy, 2003). However a high prevalence of

disease remained in less developed countries, as well as lower social strata of developed societies. The latter is illustrated by two recent epidemics of tuberculosis in New York and London (Story and Citron, 2003, Wallace and Wallace, 2003).

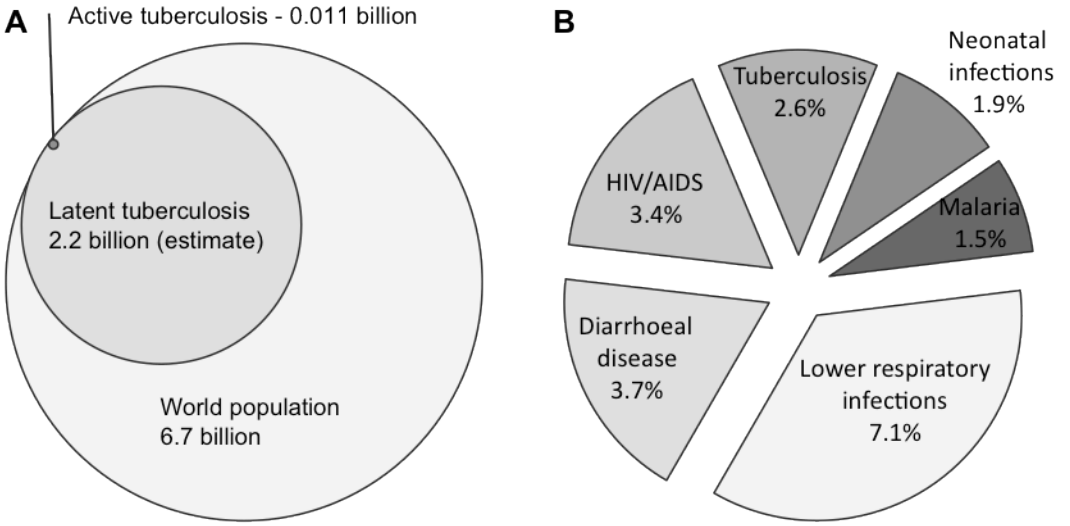


FIG. 1.1 The global burden of tuberculosis. (**A**) Representation of the prevalence of active and estimated latent tuberculosis as a proportion of the global population. (**B**) The contribution of infectious diseases to the global burden of disease. These infections are included in the list of the twenty leading causes of death (WHO, 2004).

According to the last report on the global burden of diseases published by the World Health Organisation (WHO) 58.8 million people died in 2004. Approximately 2.6% of these deaths were caused by tuberculosis (see Fig. 1.1), making it 7th among the leading causes of death globally (WHO, 2004). The latest statistics indicate that 2008 saw 9.4 million new cases of tuberculosis that, together with pre-existing infections, led to a total of 1.3 million deaths globally. This number does not include 0.5 million people who died due to coinfection with human immunodeficiency virus (HIV) and *Mtb* (WHO, 2009). There is a large disparity in the burden of tuberculosis between developed and developing nations (Blanc and Uplekar, 2003), with 22 "high burden countries"[1]

[1] High burden countries are defined as "countries that rank first to 22nd in terms of absolute numbers of cases and which have received particular attention at the global level since 2000". They include Afganistan, Bangladesh, Brazil, Cambodia,

accounting for as much as 80% of the global incidence and mortality (WHO, 2009). The main contributing factors to this disparity are the concurrent global HIV epidemic (Corbett et al., 2003) and socio-economic factors such as poverty, conflicts and an inadequate health care provision (Walls and Shingadia, 2004, Gandy and Zumla, 2002), exacerbated further by the emergence and spread of antibiotic resistance (WHO, 2009).

It is important to note that prevalence of active tuberculosis is dwarfed by the calculated number of latent infections (see Fig. 1.1). The WHO estimates that less than 1% of people infected with *Mtb* present with active tuberculosis. The vast majority are asymptomatic, but show a delayed-hypersensitivity (positive) reaction when injected subcutaneously with the purified protein derivative (PPD) of *Mtb*. By definition, these individuals harbour latent tuberculosis (WHO, 2009). Latent infection can reactivate with a probability of 10% during the lifetime of a person (Vynnycky and Fine 1997). The probability rises to 8-10% *per annum* if HIV positive (Girardi *et al.*, 2000), creating a reservoir of infection and posing a considerable public health problem (Lin and Flynn, 2010). Understanding latent disease is therefore paramount if we are to fulfil the goal of eliminating TB as a public health problem by 2050 in line with WHO's global STOP TB strategy (WHO, 2009).

1.2.2 Natural course of tuberculosis

The progression of *Mtb* infection in humans can be summarised as follows. *Mtb* enters the lung via the aerosol route – liquid droplets containing even a single bacterium are believed to be able to cause infection (Russell, 2007). Once in the lung, bacteria are taken up by alveolar macrophages, which then infiltrate the lung epithelium. In the initial stages, infected macrophages produce a host of pro-inflammatory cytokines, key amongst which is tumour necrosis factor alpha (TNFα). TNFα secretion mediates the

China, DR Congo, Ethiopia, India, Indonesia, Kenya, Mozambique, Myanmar, Nigeria, Pakistan, Philippines, Russian federation, South Africa, Thailand, Uganda, UR Tanzania, Viet Nam, Zimbabwe.

migration and aggregation of phagocytic cells that will serve as the basis for a developing granuloma (Russell, 2007). The bacteria are cleared by the immune system at this point in approximately 65-70% of immunocompetent individuals (Lin and Flynn, 2010). In the remaining 30% *Mtb* undergoes a period of exponential growth despite, or perhaps because of (Davis and Ramakrishnan, 2009), this initial inflammatory response. The expansion is halted by the establishment of adaptive immunity, mediated primarily by interferon-gamma (IFNγ) secreting T-lymphocytes, which are clonally selected in the mediastinal lymph nodes (Lin and Flynn, 2010). The pivotal role of IFNγ in controlling exponential growth of *Mtb* is illustrated by the fact that IFNγ$^{-/-}$ mice are unable to control *Mtb* infection and succumb to infection more rapidly than wild type mice (Cooper *et al.*, 1993, Flynn *et al.*, 1993). Broadly speaking, the progression of infection at this point can result in one of two possible outcomes: active or latent disease. 5-10% of successfully colonised individuals will develop active disease – in approximately 87% of the cases as pulmonary tuberculosis, otherwise as extrapulmonary infection (Hopewell, 2008). The vast majority of infected people – up to 95%, will establish long-lasting latent infection (Mathema *et al.*, 2006) that is characterised by an absence of clinical symptoms, and is determined by virtue of measuring the immune response to PPD (Barry *et al.*, 2009).

The ratio of active to latent disease appears to be somewhat surprising for a pathogen. However, if we consider the possibility that *Mtb* infection of humans predates the establishment of dense settlements (Gutierrez *et al.*, 2005), then epidemiological principles dictate that for *Mtb* to persist in a human population composed of small and disseminated tribes it would have to evolve appropriate survival mechanisms. One such mechanism could be the establishment of latent disease (Dye and Borgdorff, 2008). The consequences of this trait have important implications for the management of disease.

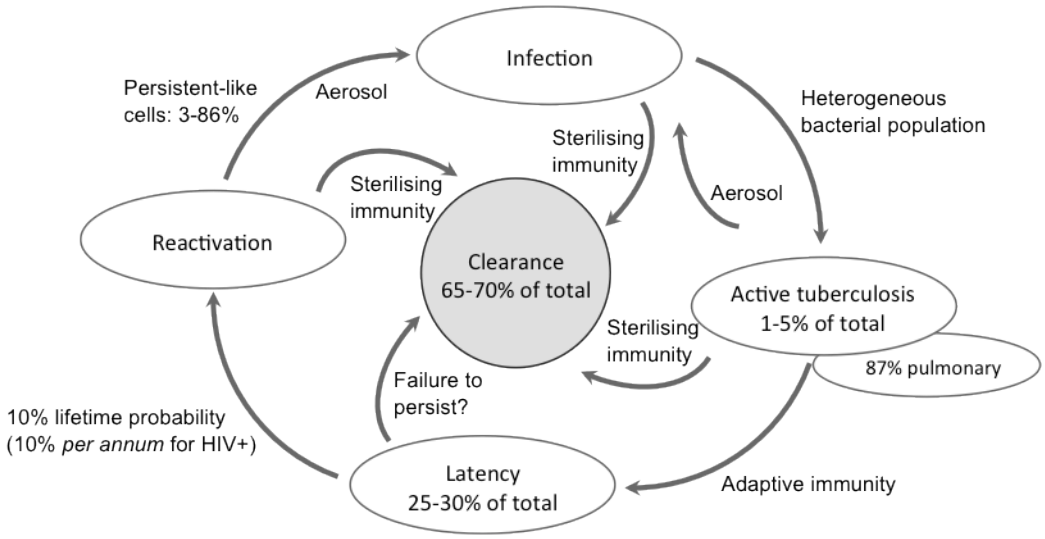


FIG. 1.2 The "life-cycle" of *Mtb* – progression of tuberculosis. The proportion of clearance, active disease and latency was derived from Lin and Flynn (2010) and Mathema *et al.* (2006). The rate of reactivation was adapted from Vynnycky and Fine (1997) and Girardi *et al.* (2000). The proportion of persistent-like cells were derived from Garton *et al.* (2008).

1.2.3 Treating tuberculosis

The challenges of tuberculosis chemotherapy became clear ever since the Medical Research Council carried out the first randomised trial, testing the efficacy of streptomycin against pulmonary tuberculosis (MRC, 1948). While the trial was successful in proving that streptomycin did lead to significant improvements in patient health, it also showed that antibiotic resistance occurred rapidly, followed closely by relapse. Ultimately there was no improvement in the death rate when compared to the untreated group after 5 years. The MRC went on to carry out a number of additional trials (Fox *et al.*, 1999) leading to the conclusion that the only effective treatment for tuberculosis is prolonged chemotherapy with multiple antibiotics (Schluger, 2008). This approach was designed to have the highest therapeutic effect, while minimising relapse and antibiotic resistance.

Antimicrobial chemotherapy of tuberculosis in immunocompetent patients involves a prolonged course (six months) of a combination of first-line antibiotics usually consisting of isoniazid, pyrazinamide, rifampicin and either streptomycin or

ethambutol for the first two months, followed by a treatment with isoniazid and rifampicin for a further four months (Schluger, 2008).

1.2.3.1 Relapse

Results obtained during the development of the current chemotherapeutic approach showed that understanding the observations from the clinic can inform us on the physiological properties of *Mtb* during infection (Mitchison, 1965).

It has become apparent that bacterial killing occurs in two stages during treatment. The majority of bacteria are killed within the first two weeks of treatment (Jindani *et al.*, 1980). The killing of the remainder of the bacteria takes considerably longer than two weeks and is required to minimise the rate of relapse (Mitchison, 1992). For example, clinical trials have revealed that a six-month treatment with streptomycin and isoniazid resulted in a relapse rate of 29% after two years; adding another drug to the mix decreased the relapse rate to 8% if the third drug was pyrazinamide and 3% if it was rifampicin (Mitchison, 1992).

It was the data from different clinical trials that led Mitchison to propose the "Special populations" hypothesis in 1979. He postulated that the majority of *Mtb* cells are actively growing during infection, and they are therefore highly susceptible to antibiotics such as isoniazid and streptomycin. Since evidence from clinical trials indicated that using isoniazid and streptomycin alone led to a high rate of relapse, he hypothesised that other *Mtb* populations must be present. The metabolic activity of these cells, he hypothesised, was lower than that of the rest of the population and as such would be protective against antibiotic treatment (Mitchison, 1979, Mitchison, 1992).

How does the hypothesis of special populations relate to the establishment of latent infection? It is possible to claim that the end result of antibiotic treatment is similar to that of an effective immune response – i.e. a decline of the population of *Mtb*.

Moreover, just as the antibiotic tolerant population can subside and re-emerge leading to relapse in a clinical context, the same population may also lead to reactivation after the establishment of latent infection – this premise has been used as the basis for the Cornell model of latent tuberculosis (McCune *et al.*, 1966, see 1.3.3.1).

1.2.3.2 Relapsing *Mtb* during infection

The sub-population of *Mtb* that is refractive to isoniazid and streptomycin treatment can be described as non-replicating, with a slow metabolic rate and a limited capability of ATP synthesis (see section 1.4.1). Together, these three features define the non-replicating persistent (NRP) state. Cells enter the NRP state to endure adverse conditions, and are very therefore stable.

The stability of non-replicating bacilli is exemplified by their ability to resume growth after survival in this state for several decades, both *in vitro* (Corper and Cohn, 1951) and *in vivo* (Lillebaek *et al.*, 2003). Although the precise mechanism of reactivation is unclear, it has been shown to include the establishment of a growing population, since prolonged prophylactic treatment with isoniazid reduces the rate of relapse (Comstock *et al.*, 1979). Reactivation is also dependent on the levels of TNFα in the host – anti-TNFα therapy being correlated with a higher rate of tuberculosis, most probably due to reactivation of existing disease (Keane *et al.*, 2001). It is important to note that reactivation does not appear to occur simultaneously in all bacteria within a granuloma. In fact a proportion ranging from 3 to 86% of *Mtb* in the sputum of individuals with active disease show characteristics of persistent bacteria (Garton *et al.*, 2008, see section 1.3.1).

Understanding the physiology of the NRP state could allow the development of approaches that are better suited to target this troublesome sub-population. For instance, preventing the establishment of non-replicating state, disrupting the

mechanisms by which this state is maintained or even "locking" *Mtb* in this state to avoid reactivation (Wayne and Sohaskey, 2001).

1.3 Latent tuberculosis

1.3.1 Latency/dormancy/persistence

When investigating latent tuberculosis researchers often refer to mycobacterial latency, dormancy and/or persistence, and they sometimes use these terms interchangeably. In order to avoid confusion, I would like to define these terms as I intend to use them in my thesis.

1.3.1.1 Definition

I use *latency* and *latent tuberculosis* to refer to the clinical asymptomatic manifestation of the disease. An individual is considered latently infected if she/he shows to have cellular immunity to purified protein derivative of *Mtb* manifested as a delayed hypersensitive reaction to the antigen, while not showing any overt clinical symptoms.

By *persistence* I mean a non-replicating state, with slow but appreciable metabolic activity and reduced susceptibility to antibiotic treatment. I perceive this state to be commonly established during the treatment in the clinic and during *in vivo* and *in vitro* modelling of latent tuberculosis. Persistent cells can resume growth readily in favourable conditions, but can also maintain their viability for prolonged periods of time in stasis.

Finally, I use *dormancy* to refer to an extreme case of persistence. These cells require special conditions to resume growth, and are the subpopulation of cells that is completely tolerant to antibiotic treatment during the Cornell model of latency (McCune *et al.*, 1966, Gomez and McKinney, 2004). Dormant cells cannot be cultured from tissues of mice immediately after the cessation of antibiotic treatment in the Cornell model, however they can lead to the reactivation of the infection at a later point in the life of the

mouse (McCune *et al.*, 1966). As defined here, dormancy can also be referred to as a "viable but nonculturable" state (Oliver, 1993). Cells in this state are considered physiologically alive but unable to undergo sustained cell division on solid media, therefore unable to form colonies (Oliver, 1993). The culturability of these cells can be re-established by using liquid media and the presence of resuscitation-promoting factors (RPF). This state has been described for mycobacteria *in vitro* (Shleeva *et al.*, 2002, Shleeva *et al.*, 2004), and it may play a role in infection given that *Mtb* lacking RPF were shown to be less virulent in mice (Downing *et al.*, 2005, Kana *et al.*, 2008).

1.3.1.2 Bacterial persisters and persistence

The phenomenon of population heterogeneity addressed by the "Special populations" hypothesis described in section 1.2.3 is not unique to *Mtb*. Antibiotic treatment of many bacterial populations reveals the presence of a slow-growing subpopulation of bacteria that are able to tolerate the presence of antibiotics (Keren *et al.*, 2004, Balaban *et al.*, 2004). The mechanism involved in tolerance is distinct from resistance, as descendents of tolerant cells retain their susceptibility to the antibiotic (Wiuff *et al.*, 2005). These cells are called persister cells in *Escherichia coli* (Lewis, 2010), and their phenotype is highly reminiscent of isoniazid and streptomycin tolerant *Mtb* cells in the clinic. It has therefore been proposed that these two represent similar physiological states that can arise in a variety of organisms with significant repercussions for antibiotic treatment (Lewis, 2007). The exact mechanism of persister formation remains to be determined, but it appears that the rate of formation is influenced by the overall activity of cellular metabolism (Lewis, 2010, see section 1.4.2).

1.3.2 The granuloma

In the classical understanding of tuberculosis, the formation of a granuloma is a host driven process paramount to the confinement and control of *Mtb* infection (Flynn and Chan, 2001). It is a key structure in the establishment and maintenance of latent

infection, representing a state of equilibrium (or perhaps a stalemate?) where the ability of *Mtb* to avoid being killed by the macrophage is exactly opposite to the ability of the immune system to clear the infection.

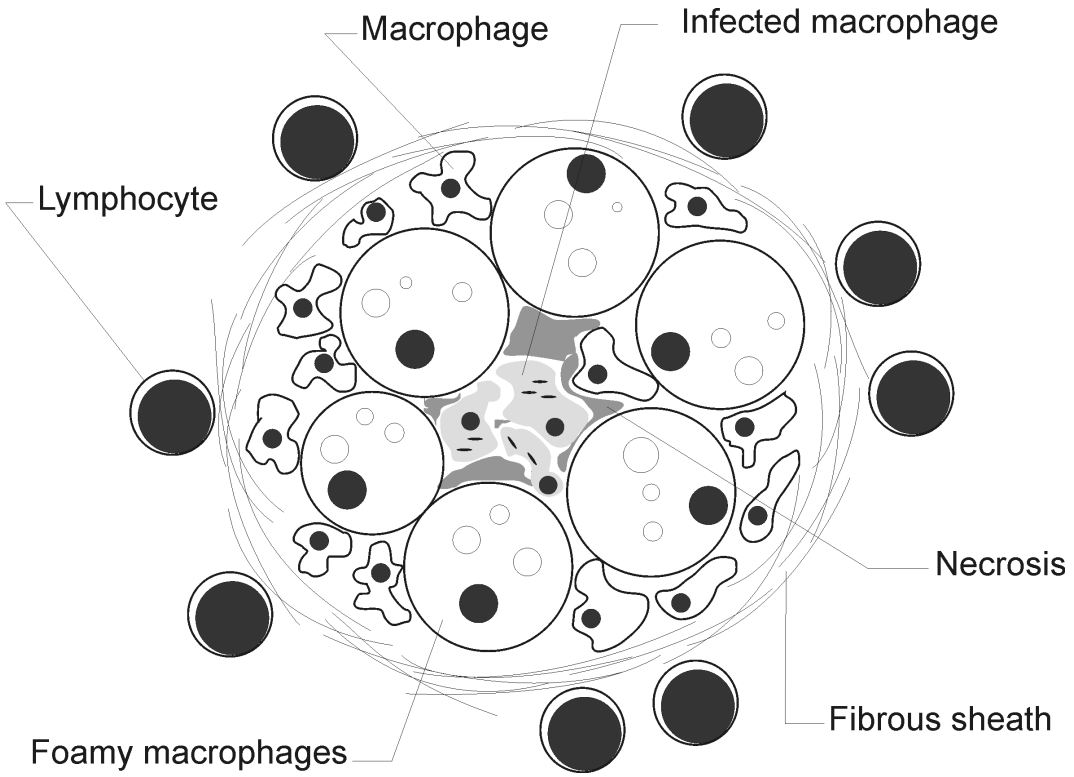


FIG. 1.3 The classic granuloma. Granulomas are highly organised immune structures. The core is formed by *Mtb*-infected macrophages surrounded by an inner layer of foamy macrophages and other phagocytic cells enclosed in a fibrous sheath. Lymphocytes can be found beyond the fibrous cuff. Necrosis can give rise to accumulation of cellular debris in the centre of the structure. Adapted from Russell (2007).

Mature granulomas have a highly organised structure consisting of a central core of caseous necrosis, surrounded by an inner layer of macrophages and an outer layer of lymphocytes, fibroblasts and extracellular matrix components (see Fig. 1.3). The bacilli are present within infected macrophages inside the granuloma. At the later stages when the caseum becomes completely acellular, *Mtb* is thought to exist at the edges of the necrotic material (Mitchison, 1992, Fenhalls *et al.*, 2002, Russell, 2007).

1.3.2.1 Granuloma formation and dynamics

Investigations using *Mycobacterium marinum* (*Mma*) infection of zebrafish as a model of latent mycobacterial infection show that the early aggregation of *Mma* containing macrophages occurs independently of adaptive immunity (Davis *et al.*, 2002). Furthermore, this aggregation already leads to changes in *Mma* gene expression that are thought to be specifically expressed in granulomas (Chan *et al.*, 2002, Davis *et al.*, 2002). Work done by the same group also provides evidence refuting the view that mycobacteria are unwilling captives in a granuloma. Davis and Ramakrishnan showed that *Mma* actively promotes the aggregation of macrophages, and that the recruitment of uninfected macrophages is a crucial aspect in the initial exponential expansion of the bacterial population (Davis and Ramakrishnan, 2009). Computer modelling of granuloma formation indicates that the ability of *Mtb* to induce macrophage apoptosis is crucial for the formation of granulomas and the survival of the bacteria within them (Ray *et al.*, 2009). In light of this evidence, the question posed by Russell "Who puts the tubercle in tuberculosis?" was very relevant (Russell, 2007). The answer seems to be a resounding – *Mtb*.

The above not withstanding, it would be wrong to think of the immune system as merely a puppet in the hands of *Mtb*. Its aim is to clear *Mtb*, not to establish latent infection. Increased understanding of many immunological, physiological and genetic aspects of *Mtb* and the host, combined with advances in imaging techniques point to the fact that the formation of a granuloma is not a stalemate position. It is one of the many possible dynamic equilibria on the continuum of disease presentation. These range from clearance of infection by sterilizing immunity to establishment of latent infection to fulminant active disease (recently reviewed by Young *et al.*, 2009, Barry *et al.*, 2009). It is the balance between bacterial and host factors that act in a pro- or anti-inflammatory manner that influence the presentation of disease (recently reviewed by Lin and Flynn, 2010).

1.3.2.2 Granuloma as an environmental niche

In view of the findings described above, we can claim that *Mtb* actively promotes the establishment of its ecological niche – the human granuloma.

Mtb usually colonises the phagosome of infected macrophages. For instance, while the pH of mature phagosomes normally reaches 4.5, *Mtb* is able to interfere with their maturation so that the pH of an *Mtb* containing phagosome is usually 6.4 (Russell, 2007, Russell *et al.*, 2010). Its main source of carbon is thought to be host lipids, with cholesterol playing a particularly important role (Russell *et al.*, 2010). Cholesterol utilisation was shown to be crucial for the establishment of persistence (Pandey and Sassetti, 2008), once inside a granuloma, *Mtb* upregulates genes involved in lipid sequestration and metabolism (Kim *et al.*, 2010).

Human granulomas were shown to be hypoxic (Via *et al.*, 2008). This poses an important challenge to *Mtb*, an obligate aerobe that requires oxygen for growth. Iron also appears to be limiting, with mutants in iron sequestration being attenuated in macrophage infection models (Timm *et al.*, 2003, Boelaert *et al.*, 2007, Siegrist *et al.*, 2009). Furthermore *Mtb* is exposed to bursts of reactive oxygen species (ROS) and reactive nitrogen species (RNS) while in the macrophage (Schnappinger *et al.*, 2003, Shi *et al.*, 2008, Russell *et al.*, 2009, VanderVen *et al.*, 2009). These cause significant damage the cell and need to be ameliorated if the cell is to survive (Boshoff *et al.*, 2003, Darwin *et al.*, 2003, Warner and Mizrahi, 2006).

1.3.3 Modelling latent tuberculosis

Overall granulomas do not provide a hospitable environment conducive to bacterial growth. There is a limited choice of readily available nutrients, with oxygen and iron in scarce supply. Furthermore, exposure to ROS and RNS pose additional challenges to the bacterium. Nonetheless *Mtb* is well adapted to survive in this milieu.

Understanding the ability of *Mtb* to withstand these conditions for prolonged periods of time require the establishment of suitable model systems. While there is still no definitive experimental model of latent *Mtb* infection, there are a plethora of *in vivo* and *in vitro* models that have been used to study specific aspects of mycobacterial infection and latency.

1.3.3.1 *In vivo* models

Mtb can infect a number of mammalian hosts. However, the disease symptoms do not always mimic that of humans. The mouse model has been invaluable for the study of *Mtb* immunology (North and Jung, 2004) and is used regularly to assess virulence during acute infection. Crucially, *Mtb* infection in mice does not lead to the development of hypoxic granulomas (Aly *et al.*, 2006), so their role as a model for latent tuberculosis is limited. However, work done in mice by McCune *et al.* led to the development of an interesting model of latent tuberculosis – the Cornell model. The model is based on the intravenous infection of mice followed by a course of anti-tuberculosis chemotherapy. Treatment leads to the clearance of infection and no viable cells can be recovered from tissues at this point. If chemotherapy is discontinued, then the majority of mice develop acute tuberculosis during their lifetime. Reactivation occurred significantly more rapidly in a higher proportion of mice if they were treated with immunosuppressants, indicating that *Mtb* were alive and held in check by the immune system in the mice (McCune *et al.*, 1966). The Cornell model of infection is technically demanding and yields highly variable results (Scanga *et al.*, 1999).

Alternative mammalian models of latent infection include the guinea pig, the rabbit and the macaque (Kashino *et al.*, 2008, Manabe *et al.*, 2008, Kesavan *et al.*, 2009, Lin *et al.*, 2009). *Mtb* infection in all of these was shown to give rise to hypoxic granulomas (Via *et al.*, 2008). However, due to the limited knowledge of the specific immunology of these animals, together with the significantly higher costs associated with keeping them, they

have not become widespread (Gomez and McKinney, 2004), leaving the mouse as the only accessible model in most cases.

An interesting alternative to mammalian models for the study of latency is provided by *Mma* infection of zebrafish and frogs (Chan *et al.*, 2002, Davis *et al.*, 2002). The studies using this model have proven particularly useful when studying early events in granuloma formation (Davis and Ramakrishnan, 2009). Similarly *Mma* infection of *Drosophila* spp. has been used to study signalling pathways during mycobacterial infection (Dionne *et al.*, 2003), while *Mma* infection of *Dictyosetlium discoideum* can be used to study intracellular events during macrophage infection (Solomon *et al.*, 2003).

1.3.3.2 *In vitro* models

In vitro models of latent tuberculosis are largely based on the observations made in the clinic and are designed to generate non-replicating, antibiotic tolerant bacilli whose morphological features (e.g. cell wall thickening, lipid body accumulation) resemble those of bacilli isolated from *in vivo* sources (Nyka, 1971, Nyka, 1974, Cunningham *et al.*, 1998, Garton *et al.*, 2008).

The main experimental strategies to induce the NRP state are based on the maintenance of stationary phase bacteria for prolonged periods of time in conditions of nutrient starvation (Nyka, 1974, Cunningham and Spreadbury, 1998, Smeulders *et al.*, 1999, Primm *et al.*, 2000, Betts *et al.*, 2002, Hampshire *et al.*, 2004, Archuletta *et al.*, 2005, Gengenbacher *et al.*, 2010), oxygen starvation (Wayne and Hayes, 1996, Boon and Dick, 2002, Voskuil *et al.*, 2003, Daniel *et al.*, 2004, Rustad *et al.*, 2008), or sometimes a combination of multiple stresses (Deb *et al.*, 2009). Although no single model is thought to encompass all the aspects of the NRP state *in vivo* (Schnappinger *et al.*, 2003, Shi *et al.*, 2005, Shi *et al.*, 2008, Deb *et al.*, 2009, Rustad *et al.*, 2009), combining the findings from different *in vitro* studies can yield information that are relevant to the context of infection (Timm *et al.*, 2003).

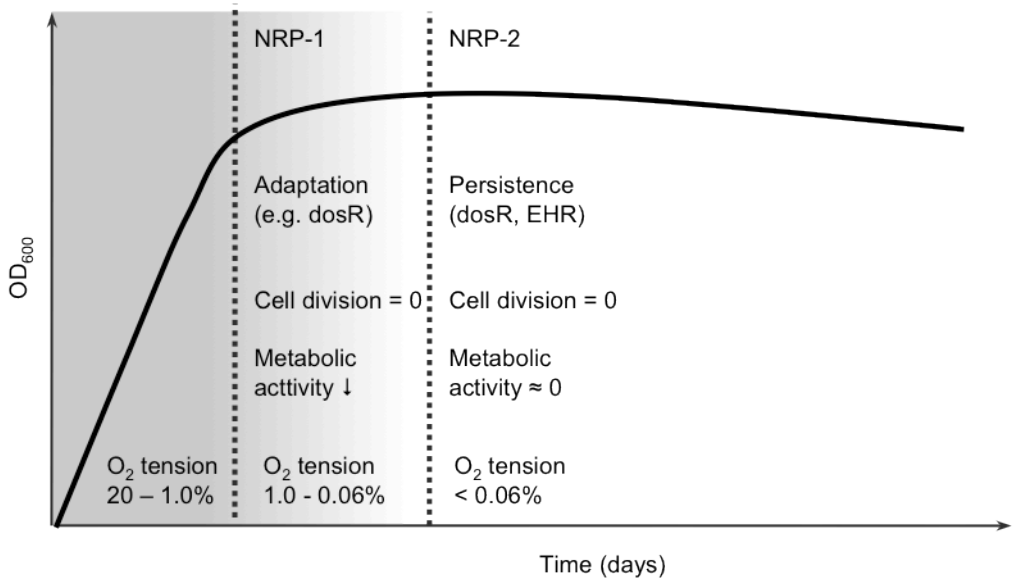


FIG. 1.4 The Wayne model of persistence. Cells grown in tightly sealed flasks gradually consume the available oxygen in the flask – the shading corresponds to methylene blue discolouration. When oxygen tension falls to less than 1% cells stop dividing and begin the adaptive phase called Non-replicating persistence 1 (NRP-1). When oxygen tension falls below 0.06% cells enter Non-replicating persistence 2 (NRP-2). Cells can survive for prolonged periods of time in NRP-2, without dividing and with very limited metabolic activity. Adapted from Wayne and Sohaskey (2001) and Boshoff and Barry (2005).

Perhaps the most commonly used model of persistence is one of gradual oxygen depletion, also known as the Wayne hypoxia model of persistence (Wayne and Hayes, 1996). In this model, cultures are grown in tightly sealed flasks and gradually consume the available oxygen as they grow. The rationale is to emulate the transition into a low oxygen environment found inside granulomas (Via *et al.*, 2008). Cell adaptation occurs in two stages (see Fig. 1.4). In the first stage, NRP-1, cells cease to divide, while adapting to the microaerophilic environment. Evidence shows that oxygen depletion needs to be gradual, pointing towards a highly regulated mechanism of adaptation involving transcriptional regulation and *ex novo* protein synthesis - an abrupt depletion of oxygen is lethal to the organism (Wayne and Hayes, 1996, Wayne and Sohaskey, 2001). Once the culture becomes hypoxic the cells enter the second stage, NRP-2 (Wayne and Sohaskey, 2001). I will refer to NRP-2 as persistence, as it resembles specific aspects of persistence *in vivo* (Wayne and Shoaskey, 2001, Rustad *et al.*, 2009), including lipid body

formation (Daniel *et al.*, 2004, Sirakova *et al.*, 2006, Reed *et al.*, 2007, Garton *et al.*, 2008) and metronidazole susceptibility (Wayne and Sramek, 1994, Via *et al.*, 2008). The Wayne hypoxia model has also been an important tool in testing the bactericidal activity of antibiotics against non-replicating bacteria (Wanye and Hayes, 1996, Paramasivan *et al.*, 2005, Iona *et al.*, 2007, Singh *et al.*, 2008, Rao *et al.*, 2008, Filippini *et al.*, 2010, Matteelli *et al.*, 2010).

An interesting recent variation on the classic batch culture approach to *in vitro* study of mycobacterial physiology is the use of chemostats. The use of defined media and controlled oxygen tension, is yielding important information regarding the physiological changes that are caused by a slow-down in metabolism (Beste *et al.*, 2005, Beste *et al.*, 2007, Berney and Cook, 2010). These studies have been successfully used in the identification of genes mediating growth-rate adjustments (Beste *et al.*, 2009).

There is an important distinction between chemostat and batch culture models – batch culture experiments provide information on NRP cells, while chemostat studies focus on bacteria that are still actively dividing, albeit at a slower rate.

1.3.3.3 Model organisms

Mtb is a challenging and labour-intensive organism to investigate. As a human pathogen, it is classed as a biosafety containment level 3 organism, which poses several limitations to its use in the context of a research laboratory. Since it has to be handled in dedicated facilities within biological containment cabinets, the physical constraints of this containment affect the sample sizes and the type of experiments that can be carried out with *Mtb* in the average laboratory. Furthermore, *Mtb* grows very slowly doubling approximately once every 24 hours, which lengthens the time of most experiments considerably.

Model organisms are used to overcome some of these limitations. For example, avirulent strains of slow-growing mycobacteria developed for vaccination programmes

such as *Mbo* BCG and auxotrophic mutants of *Mtb* (Larsen *et al.*, 2009) are used instead in the laboratory. These organisms do not pose a health and safety risk to the general population and they therefore require fewer containment measures. They are also genetically very similar to virulent *Mtb*, which makes them biologically very relevant. Nevertheless, their growth rate still poses limitations to the time scale on which experiments can be carried out.

An alternative model commonly used in the laboratory, particularly during the early stages of method development and biological investigations, is *Mycobacterium smegmatis* (*Msm*). *Msm* is a saprophytic fast growing mycobacterium, for which many genetic tools have been developed. It offers a convenient proxy for the study of *Mtb* physiology. However, *Msm* is genetically distinct from *Mtb*. This caused a significant debate in the tuberculosis community regarding its value as a model organism (Barry, 2001, Reyrat and Kahn, 2001, Tyagi and Sharma, 2002). Regardless, if used carefully, *Msm* can provide important information on specific aspects of *Mtb* physiology (Shiloh and DiGiuseppe Champion, 2010).

In addition, *Mma* infection of several hosts is proving particularly important in the study of early host-pathogen interactions (see section 1.3.3.1). Furthermore *Mycobacterium aurum* (*Mau*) is also emerging as a possible model organism (Gupta *et al.*, 2009).

1.4 The persistent mycobacterium

1.4.1 Physiological adaptations during persistence

As described in section 1.3.2.2, human granulomas impose important limitations on the optimal function of mycobacterial physiology. In order to be able to successfully re-emerge from the persistent state, mycobacteria require two key physiological adaptations that must endure through time. One is a stable and sufficient supply of

chemical energy. The other is a level of macromolecular integrity compatible with sufficient functionality to resume growth. Both adaptations lay at the core of the ability of any organism to stay alive. Depletion of the ATP pool will lead to cell death (Rao *et al.*, 2008), and so will the extensive degradation of cellular components (Davis *et al.*, 1986), or excessive damage to DNA – as exemplified by the bactericidal action of fluoroquinolone antibiotics (Filippini *et al.*, 2010).

If a cell is to survive and reinitiate growth it has two options. It can either generate sufficient energy for a constant turnover of biomolecules, or it can stabilise its components while ensuring sufficient energy to maintain the status quo. Based on the definition (1.3.1.1) of persistence mycobacteria seem to do the latter.

1.4.1.1 Energy generation

The main challenge faced by persistent bacilli is the limited availability of their usual terminal electron acceptor – oxygen. Early hypoxia can be thought of as an instance of reductive stress, where the generation of reducing equivalents exceeds the ability of the cell to deal with them, leading to an NAD^+:NADH imbalance. The maintenance of the NAD^+:NADH ratio and of steady ATP levels during persistence are still poorly understood (Boshoff and Barry, 2005). They are likely to involve the use of alternative electron donors and acceptors (see Fig. 1.5). Recent screens for future anti-tuberculosis chemotherapy have shown that ATP synthase and the type II NADH-dehydrogenase still play an active role and are good targets for intervention. Inhibition of both leads to bactericidal activity during both active growth and the Wayne model of persistence (Boshoff and Barry, 2005, Rao *et al.*, 2008, Diacon *et al.*, 2009, Matteelli *et al.*, 2010)

The end result of adaptation is a smaller but stable pool of ATP. Measurements of ATP levels during the Wayne model of persistence revealed a five fold reduction in the overall levels that could be maintained during NRP-2 (Wayne and Hayes, 1996, Starck *et al.*, 2004, Rao *et al.*, 2008).

ATP homeostasis is at least in part mediated by the action of genes in the *do*rmancy *s*urvival regulon induced by DosR (Park *et al.*, 2003, Voskuil *et al.*, 2004), as the DosR mutant in *Mtb* is unable to maintain wild type levels of ATP and NAD^+:NADH balance (Leistikow *et al.*, 2010). Importantly, DosR is known to be essential for hypoxic survival in many mycobacterial species, including *Mtb* (Leistikow *et al.*, 2010), *Mbo* BCG (Boon and Dick, 2002) and *Msm* (O'Toole *et al.*, 2003). The importance of the DosR regulon in ATP homeostasis is highlighted by DosR-dependent induction of many energy metabolism proteins required for survival in the persistent state both *in vivo* and *in vitro* (see Fig. 1.5).

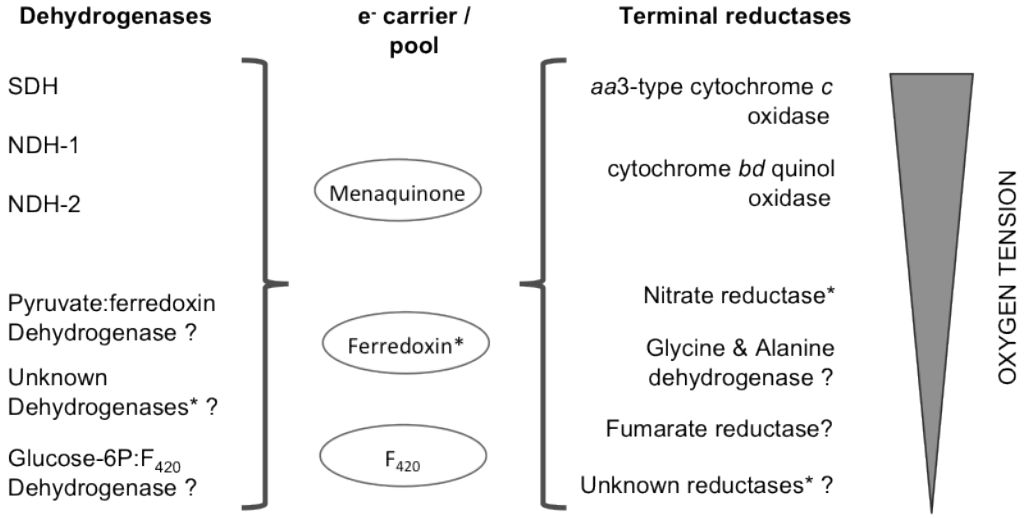


FIG. 1.5 The respiratory system of mycobacteria. SDH – succinate dehydrogenase, NDH-1 – NADH dehydrogenase type 1, NDH-2 – NADH dehydrogenase type 2, F_{420} – Coenzyme F_{420} (8-hydroxy-5-deazaflavin. Asterisk indicates members of the DosR regulon, the regulon includes putative dehydrogenases and oxidoreductases that may play a part in the respiratory system (Park *et al.*, 2003). Figure adapted from Boshoff and Barry (2005) and Kana *et al.* (2009).

1.4.1.2 Anabolic metabolism

Part of the definition of persistent cells includes a reduction in the level of metabolic activity. This is consistent with the decreased need for biosynthesis due to reduced replication, and it is also in line with a decrease in the available chemical energy.

It has been reported that *Mtb* does not incorporate detectable amounts of [^{35}S]-methionine once it has adapted to hypoxic conditions, unless stressed e.g. by heat shock (Hu *et al.*, 1998). Furthermore, a decrease in the incorporation of [^{3}H]-uridine was observed after growing *Mtb in vitro* under microaerophilic conditions for 100 days (Hu *et al.*, 2000). Overall it appears that *Mtb* adapts its physiology to a low energy environment by limiting biosynthesis, albeit not entirely abolishing it. In fact, antibiotics such as rifampicin (RNA polymerase inhibitor) and capreomycin (protein synthesis inhibitor) retain some activity against persistent *Mtb* (Wayne and Sohaskey, 2001, Heifets *et al.*, 2005, Rao *et al.*, 2008).

1.4.1.3 Stability

It is known that oxidative and nitrosative damage pose significant challenges to the stability of all cellular components (Halliwell and Gutteridge, 2007). Mycobacterial cells limit some of that damage by passive antioxidant defences such as mycothiol (Newton *et al.*, 2008) and ROS/RNS scavenging enzymes such as catalase, superoxide dismutase, alkyhydroperoxidases and thioredoxin (Gupta and Chatterji, 2005, Warner and Mizrahi, 2006).

In the event that damage does occur, the cell has three options: repair, replace or endure the consequences of the damage. In light of the limited resources available to mycobacteria during persistence, it would be very demanding for a cell to continuously replace cellular components by *ex novo* synthesis. The mechanisms by which the cell might ensure long-term stability of cellular components are largely unstudied. However, it is known that DNA integrity is actively maintained – DNA repair enzymes are needed for the establishment of infection and survival within macrophages (Boshoff *et al.*, 2003, Sassetti and Rubin, 2003, Schnappinger *et al.*, 2003, Warner and Mizrahi, 2006). Similarly, there is evidence to suggest that RNA turnover is substantially reduced during hypoxia *in vitro*, leading to a dramatic increase of RNA half-life in persistence (Rustad,

personal communication). The issue of RNA stability *in vivo*, on the other hand, is yet to be addressed. The same is true for other macromolecules such as the ribosome.

The question of how mycobacteria ensure that their cellular components remain functional for protracted periods of stasis is one that deserves investigation.

1.4.1.4 Sporulation

Many of the issues described above only pertain to mycobacteria when they are defined as non-sporulating organisms. However, there is a significant body of evidence in the literature that suggests that mycobacteria exist in a "spore-like" form when exposed to prolonged periods of stasis (Anuchin *et al.*, 2009, Salina *et al.*, 2010). Spores are immune to antibiotics, highly resistant to physical and chemical damage. Moreover, they offer an excellent protection mechanism for preserving the integrity of cellular components. In fact many organisms – including members of the same genus as Mycobacteriaceae – take advantage of this form of persistence to bridge periods of hostile environmental conditions. Crucially, the existence of spores could provide a very tempting explanation for the formidable ability of mycobacteria to persist for decades in the face of adversity both *in vitro* and *in vivo*. It could also explain the phenomenon of sterility in the Cornell model of infection, and perhaps even the high resistance to the antibacterial action of our own immune system.

Recently, Ghosh and co-workers published evidence of sporulation in *Mma* in a paper that immediately became highly controversial (Ghosh *et al.*, 2009). These findings were rapidly challenged by a number of researchers who failed to replicate the results obtained by Ghosh *et al.* and dismissed them as experimental artefacts (Traag *et al.*, 2010). However Ghosh and co-workers have continued their research and have presented evidence of sporulation in a strain of *Mma* expressing GFP (Singh *et al.*, 2010a). However, despite the tempting (and terrifying) proposition offered by the possibility of sporulation in *Mtb*, I know of none who have managed to successfully

replicate the experiments carried out by Ghosh *et al.*. This makes their findings very difficult to validate and accept. For the purpose of this dissertation I will therefore continue to hold the accepted view that mycobacteria do not form endospores.

1.4.2 Regulation of persistence

The development and characterisation of *in vitro* models (see section, 1.3.3.2) has led to the identification of several environmental cues that trigger persistence in mycobacteria, including nutrient availability, hypoxia and nitric oxide.

Mtb detects growth-limiting stimuli by direct sensing of the environment via two-component signalling systems including DosR/S/T (Voskuil *et al.*, 2003, Voskuil 2004, Kumar *et al.*, 2008), MprA/B (Zahrt and Deretic, 2001), RegX3/SenX3 (Rifat *et al.*, 2009). It also monitors the nutritional state of the cell via alarmone signalling (Dahl *et al.*, 2003) and possibly toxin-antitoxin systems (Balaban *et al.*, 2004, Gerdes *et al.*, 2005, Ramage *et al.*, 2009). Loss of any of these pathways, with the exception of individual toxin-antitoxin systems (Singh *et al.*, 2010b), leads to a marked decrease in the ability of mycobacteria to persist both *in vitro* and *in vivo*. Two of the best-studied regulatory systems in mycobacterial persistence are the dormancy survival response (DosR regulon) and the stringent response.

1.4.2.1 DosR regulon

Sherman *et al.* used low oxygen tension to study the expression of the α-crystallin gene (also known as HspX or 16.3 antigen) in *Mtb* (Sherman *et al.*, 2001). HspX was known to be highly expressed in the Wayne model of hypoxia (Wayne and Sramek, 1979, Desjardin *et al.*, 2001), and identified as an antigen during infection in humans (Friscia *et al.*, 1995). By carrying out expression studies they identified in excess of 100 genes that are differentially expressed during hypoxia – 48 of which were found to be up-regulated (Sherman *et al.*, 2001) and were later confirmed to be under the control of the

DosR transcriptional regulator (Park *et al.*, 2003, Voskuil *et al.*, 2003). DosR induction was found be controlled by two haem-containing sensor histidine kinases – DosS and DosT (Dasgupta *et al.*, 2000, Roberts *et al.*, 2004, Honaker *et al.*, 2009) responsive to redox potential, oxygen level, nitric oxide and carbon monoxide (Ioanoviciu *et al.*, 2007, Kumar *et al.*, 2007, Sousa *et al.*, 2007, Yukl *et al.*, 2007, Voskuil *et al.*, 2009). The DosR/S system is conserved in all sequenced mycobacteria (Kanehisa *et al.*, 2006), indicating that its function is not unique to latency in the context of infection, but rather may form part of an ancestral adaptation to oxygen limiting conditions (Voskuil *et al.*, 2009). The need for its activity in persistence is well established *in vitro* (Boon and Dick, 2002, Voskuil *et al.*, 2003, O'Toole *et al.*, 2003, Leistikow *et al.*, 2010), while remaining controversial *in vivo* (Rustad *et al.*, 2008, Rustad *et al.*, 2009, see section 1.4.2.2).

The mechanism by which DosR modulates persistence is multifactorial and remains to be fully established. It is likely to be involved in ATP homeostasis (Fig. 1.5, section 1.4.1.1), and it may be involved in stress resistance since 6 of the 10 universal stress proteins (USP) encoded in the genomes of *Mbo* BCG and *Mtb* are under the control of DosR (Park *et al.*, 2003, O'Toole and Williams, 2003, Hingley-Wilson *et al.*, 2010). USPs in *E. coli* are up-regulated in response to multiple stresses and stasis (Nystrom *et al.*, 1992, Nystrom *et al.*, 1994, Gustavsson *et al.*, 2002) and mutation of *uspA* in *E. coli* leads to premature death in stationary phase (Nachin *et al.*, 2005). The role of USPs in mycobacteria is less clear. Knocking out *Rv3134c* was reported to reduce *Mbo* BCG persistence *in vitro* (Sherman *et al.*, 2001) while *Msm* cells over-expressing *Rv2623* had a growth defect (Drumm *et al.*, 2009). However, knocking out individual USPs did not have an effect on hypoxic persistence in *Mtb* (Hingley-Wilson *et al.*, 2010).

The description of bacilli from the sputum of patients with active tuberculosis indicates the presence of TAG-rich lipid bodies (Garton *et al.*, 2002, Garton *et al.*, 2008). TAG accumulation was shown to be DosR dependent (Sirakova *et al.*, 2006) and was

observed to be important for antibiotic tolerance, persistence (Deb *et al.*, 2009) and reactivation upon exit from hypoxia (Low *et al.*, 2009).

In addition to these processes the DosR regulon may be involved in many other aspects of persistence that remain to be determined, since there are multiple genes in the regulon whose function is still unknown.

1.4.2.2 DosR regulon or Enduring Hypoxic Response

Rustad *et al.*, have recently challenged the view that DosR plays a key role during *in vivo* persistence and latent infection by arguing that 1) *dosR* mutants of *Mtb* do not show a decreased virulence in the mouse infection model, 2) the induction of the DosR regulon is too transient in nature to coordinate long-term hypoxic survival, 3) the loss of long-term viability of the *dosR* mutant under hypoxic conditions is too mild to justify the central role currently attributed to it, 4) the over-expression of DosR in the W-Beijing lineage (Reed *et al.*, 2007) of *Mtb* does not lead to an *in vitro* growth defect and 5) the delay between the loss of viability and the onset of hypoxia is too great to warrant direct involvement (Rustad *et al.*, 2008, Rustad *et al.*, 2009). They propose an alternative theory whereby *Mtb* establishes an "enduring hypoxic response", independent of DosR. They suggest the EHR encompasses approximately 230 genes that are stably up-regulated later in the course of hypoxia and are responsible for the coordination and maintenance of long-term survival under these conditions (Rustad *et al.*, 2008).

While it is true that studies of the DosR regulon alone have not yet given a clear understanding of the mechanisms underlying *Mtb* persistence, the rationale behind the dismissal of DosR as an important player may be flawed. Here I offer several possible issues. First, the mouse model of infection is not directly analogous to human chronic infection, as mice do not form hypoxic granulomas (Aly *et al.*, 2006, Tsai *et al.*, 2006). Animal models where hypoxic lesions do occur – e.g. guinea pig and rabbit (Via *et al.*, 2008) do offer a milieu where ΔdosR has a comparative disadvantage (Converse *et al.*,

2009). Second, although the spike of induction of the DosR regulon may be transient, however on average, the expression of the DosR regulon further into hypoxia remained approximately 3-fold higher than in log phase (Rustad *et al.*, 2008). Rustad *et al.* made no attempt to investigate the stability of the expressed proteins, which limits the ability to comment on their contribution to persistence. Crucially many of the genes encoding the enzymes that are believed to be important for energy generation during persistence (e.g. nitrate reductase, isocitrate lyase, glycine dehydrogenase, Wayne & Sohaskey 2001, Boshoff & Barry, 2005) were found to be down-regulated in the EHR (Rustad et al., 2008). Third, the drop in viability of the *dosR* mutant during their study was considerable – 99.7% after 35 days (Rustad *et al.*, 2008). Longer incubations lead to an even more pronounced effect in *Mtb* (Leistikow *et al.*, 2010). Fourth, over-expression of DosR during active normoxic growth was shown to cause a marked reduction in growth rate in *Mbo* BCG (Flores Valdez and Schoolnik, 2010). Fifth, ΔdosR mutants in *Mtb* have a reduced ability to adapt their rate of oxygen consumption to a decreasing supply of oxygen (Leistikow *et al.*, 2010). Similarly they are unable to fully adjust their metabolism to maintain a wild type NAD^+:NADH ratio and ATP level immediately after the onset of hypoxia (Leistikow *et al.*, 2010). These changes do not lead to an immediate loss of viability but rather do so only after weeks of hypoxia. The explanation for this may be internal energy reserves or perhaps the ability of other pathways to partially reduce the impact of the loss of DosR.

Overall, DosR is not the only regulator of persistence, but there is a wealth of experimental evidence that stresses its importance – perhaps best illustrated by Wayne and Hayes who have shown that the duration of NRP-1 determines the ability of cells to survive in NRP-2 (Wayne and Hayes, 1996). The DosR regulon is induced concurrently with entry into NRP-1 (Sherman *et al.*, 2001, Voskuil *et al.*, 2003, Rustad *et al.*, 2008) and its action is needed to couple oxygen consumption to oxygen availability hence extending the duration of the adaptive NRP-1 state (Leistikow *et al.*, 2010). DosR

therefore plays a dual role in persistence: it both enhances the ability of cells to adapt, as well as actively driving adaptation (e.g. ATP homeostasis, TAG biosynthesis). And both these roles are needed to maintain persistence in the long run.

1.4.2.3 Stringent response and persistence

Amino acid depletion leads to the reduced synthesis of amino-acyl:tRNA complexes, which serves as a trigger for (p)ppGpp synthesis by RelA. The stringent response is designed to rationalise the volume of the biosynthetic machinery and replenish the pool of amino acids by recycling and increased amino acid biosynthesis (Magnusson *et al.*, 2005).

RelA-mediated stringent response is essential for survival of *Mtb* during long-term carbon starvation (Primm *et al.*, 2000), but it appears to be dispensable for the survival in macrophages *ex vivo* (Primm *et al.*, 2000). ΔrelA was found to be able to proliferate as well as wild type *Mtb* during the early stages of infection, however unlike wild type, ΔrelA was not able to establish chronic infection (Dahl *et al.*, 2003). The same pattern of survival was seen for isocitrate lyase mutants (McKinney *et al.*, 2000) and cholesterol catabolism mutant Δmce4 (Pandey and Sassetti, 2008). Pandey and Sassetti suggested that this persistence defect stems from the inability of *Mtb* to use cholesterol as its only carbon source during infection – mce4 is required for the uptake of cholesterol (Pandey and Sassetti, 2008), while RelA drives the expression of mce4 (Dahl *et al.*, 2003). Isocitrate lyase on the other hand is needed for the utilisation (Munoz-Elias and McKinney, 2005) and detoxification of the propionate that results from the breakdown of cholesterol (Pandey and Sassetti, 2008).

1.4.2.4 Stringent response regulation of the ribosome

There are interesting parallels between starvation induced persistence and hypoxia induced persistence. Nutrient starved cells, as well as ΔrelA cells were found to have a

survival defect during hypoxia *in vitro* (Primm *et al.*, 2000, Gengenbacher *et al.*, 2010). One possibility is that the dual shock of nutrient and oxygen starvation leads to a depletion of ATP that is beyond the ability of the cell to cope – this explains why nutrient starved cells are less able to deal with hypoxia (Gengenbacher *et al.*, 2010). However it does not explain the effect on ΔrelA, which is unable to adapt to hypoxia even in rich medium (Primm *et al.*, 2000).

Consider the repercussions of RelA driven (p)ppGpp biosynthesis. (p)ppGpp interferes with RNA polymerase activity leading to an overall decrease in processivity (Vogel and Jensen, 1994) as well as the specific suppression of many biosynthetic genes including rRNAs (Magnusson *et al.*, 2005). The impact of (p)ppGpp on rRNA is thought to form part of the mechanism that couples growth rate and ribosomal synthesis in *E. coli* (Gourse *et al.*, 1996, Magnusson *et al.*, 2005, Potrykus and Cashel, 2008). Therefore (p)ppGpp leads to the accumulation of polyphosphate which triggers Lon protease mediated inhibition of translation by toxin-antitoxin systems (Gerdes *et al.*, 2005).

In mycobacteria RelA, in concert with CarD, regulates rRNA synthesis in response to starvation as well as oxidative and genotoxic stress (Stallings *et al.*, 2009). Furthermore carbon starvation was shown to lead to a down-regulation of rProtein genes (Betts *et al.*, 2002, Beste *et al.*, 2007, Berney and Cook, 2010) as well as an overall decrease in ribosomal levels in *Mbo* BCG grown in defined medium in chemostats (Beste *et al.*, 2005). It is therefore not surprising that ΔrelA cultures have five times more ribosomes during carbon starvation than wild type (Primm *et al.*, 2000). When shifted to hypoxia, the maintenance and activity of excess ribosomes is likely to impose a significant energetic burden on the cell and possibly leading to energy depletion and ultimately cell death.

The importance of the control of ribosomal levels is reflected in the physiological findings regarding bacteria from active infection sites. Lipid body laden *Mtb* cells from

the sputum of patients with active tuberculosis had a reduced expression of ribosomal genes when compared to actively growing cells or even NRP-2 cells (Garton *et al.*, 2008). This would indicate that cells adapt to lower availability of chemical energy by decreasing the size of the ribosomal population. However, degradation is not the only way by which cells can control the energy expenditure required for the maintenance of the ribosomal apparatus.

1.4.3 Ribosomal stability as a survival strategy

We usually associate an optimally functioning cell with the "mid-log" phase, however bacteria in nature rarely exist in a state of exponential growth with optimal activity (Kurland and Mikkola, 1993). Instead they need to adapt their metabolism to survive periods of "Fast and famine with rare feast" (Morita, 1993). So how do cells maintain their complement of functional macromolecules? Continuous biosynthesis is energetically unsustainable in most environments, and so it is probably unsustainable in the context of a human granuloma.

So far, most of the effort to understand the physiology of persistent mycobacteria was focused on determining their ability to replicate, change gene expression and modify different aspects of metabolism. However, there was no attempt made towards understanding the stability of their macromolecular complexes – with the notable exception of DNA (Davis and Forse, 2009)

It stands to reason that a metabolically quiescent organism, with limited biosynthetic activity, needs to ensure the stability of all cellular components to maintain viability and emerge from prolonged stasis. Consider the implications for the ribosome. The ribosome is a 2.5 MDa complex comprising 3 RNA molecules and over 50 proteins and is made at great energy expense to the cell. In mycobacteria, there would be "rational" scope for the stabilisation of ribosomes during prolonged stasis. This observation is reinforced by the fact that ribosomal genes are down-regulated

concomitantly with the cessation of growth (see 1.4.2.3), and there is limited chemical energy available to the cell during persistence (see 1.4.1.1). Studies of ribosomal stability during the transition from active growth to stasis have been done primarily in *E. coli*.

1.4.3.1 Ribosomal stability in *E. coli*

Loss of ribosomal function is incompatible with life – a fact that is very well illustrated by the number of antibiotics that act on the ribosome. The stability of ribosomes is therefore intimately linked with the ability of any organism to survive. Consider an actively growing *E. coli* cell. As much as 40% of its dry weight is made up of ribosomes (Nomura and Gourse, 1984), and at least 83% of its RNA consists of rRNA. When cells stop growing, part of the ribosomal population is degraded (Kaplan and Apirion, 1975, Davis *et al.*, 1986) while a proportion undergoes stabilisation leading to the formation of 100S ribosomal dimers (Wada *et al.*, 1990, Wada *et al.*, 2000, Wilson and Nierhaus, 2007). 100S ribosomes are not translationally active (Wada *et al.*, 1995, Ueta *et al.*, 2008), and when present in a cell have a protective role against heat and acid shock (Niven, 2004, El-Sharoud and Niven, 2005). The biological properties of 100S dimers led to the hypothesis that they are a storage form for the ribosome (Yoshida *et al.*, 2002).

The formation of 100S ribosomal dimers is dependent on the presence of two factors: ribosomal modulation factor – RMF and the hibernation promoting factor – HPF (Ueta *et al.*, 2008, Kato *et al.*, 2010). RMF is required for ribosomal dimerisation, while the association of HPF leads to the formation of the mature 100S dimer (Maki *et al.*, 2000, Ueta *et al.*, 2005). Ribosomal dimerisation is antagonised by translation initiation factor 3 (Yoshida *et al.*, 2009), as well as an HPF homologue – cold shock protein Y – YfiA (Ueta *et al.*, 2005). YfiA is produced when *E. coli* cells enter stationary phase (Maki *et al.*, 2000, Agafonov *et al.*, 2001) and in response to cold shock (Agafonov *et al.*, 2001). When bound to the ribosome it leads to translational inhibition by subunit association

(Agafonov *et al.*, 1999, Agafonov *et al.*, 2001, Vila-Sanjurjo *et al.*, 2004). Translation resumes readily when these ribosomal factors dissociate from the ribosome (Wilson and Nierhaus, 2007).

The common feature of ribosomal dimerisation and cold shock induced translational arrest is the stabilisation of the associated form of the ribosome (Vila-Sanjurjo *et al.*, 2004, Kato *et al.*, 2010). The biological relevance of this mechanism appears to lay in the increased physical stability of associated ribosomes (Zundel *et al.*, 2009). It is rationally appealing to consider reducing translational activity of a cell by a combination of associative stabilisation and degradation. Such an approach is energetically less costly than relying solely on ribosomal degradation and *ex novo* synthesis. Crucially, stabilising a proportion of the ribosomal population allows the cell rapid access to biosynthetic capacity when nutrients become available, thus allowing it to resume growth promptly.

There are no RMF homologues in mycobacteria, however HPF and YfiA homologues have been identified in *Mtb* (Ueta *et al.*, 2008). Studies on the function of RelA and CarD have indicated that controlling the level of ribosomal synthesis is very important for survival under stasis. However, protecting a fraction of the active ribosomes from degradation and stabilising them for future biosynthetic needs may be equally important.

1.5 The stressed persistent mycobacterium

1.5.1 Oxidative and nitrosative damage

So far we have considered the adaptation of *Mtb* to a limited supply of nutrients and chemical energy during persistence. However *Mtb* does not exist in an environment that is simply passively limiting – survival of *Mtb* during infection is also inhibited by macrophage-produced ROS and RNS. Hosts with an impaired ability to produce RNS,

particularly via the inducible nitric oxide synthase, are less able to control infection (Chan *et al.*, 1995, Cooper *et al.*, 2000, North and Jung, 2004, Lin and Flynn, 2010). Similarly *Mtb* with reduced antioxidant defences (Piddington *et al.*, 2001, Pym *et al.*, 2001, Ng *et al.*, 2004, Rengarajan *et al.*, 2005, Cirillo *et al.*, 2009, Colangeli *et al.*, 2009) or reduced ability of damage amelioration is less virulent (Boshoff *et al.*, 2003, Darwin *et al.*, 2003, Darwin and Nathan, 2005). The exact role of ROS on the other hand is still not fully established. Infection of NADPH oxidase deficient mice resulted in either a reduced ability to control initial infection (Cooper *et al.*, 2000) or no discernable increase in susceptibility (Adams *et al.*, 1997, Ng *et al.*, 2004). Recent work indicates that *Mtb* can actively reduce the levels of ROS in the phagosome by the action of KatG and NADH dehydrogenase type I, an activity that has an anti-apoptotic effect on the macrophage (Miller *et al.*, 2010). The same effect was observed for SodA (Hinchey *et al.*, 2007). Maintenance of anti-apoptotic mechanisms is required for virulence in macrophages (Hinchey *et al.*, 2007, Velmurugan *et al.*, 2007, Miller *et al.*, 2010). ROS have also been shown to be important for the action of other bactericidal agents, leading to an increase in the efficiency of killing by the phagosome (Halliwell and Gutteridge, 2007). Taken together, these findings indicate that anti-oxidant defence plays a crucial role during infection. They also indicate that RNS and particularly ROS may have roles during *Mtb* infection that reach beyond their bactericidal activity.

The importance of ROS and RNS during persistent infection is also not clear. Work done by VanderVen *et al.*, show that the oxidative burst, during which macrophages produce high levels of ROS and RNS, lasts for 20-25 minutes post phagocytosis (VanderVen *et al.*, 2009), therefore the time scale of the stress is not sufficient to influence survival of persistent bacteria. Similarly expression studies show that antioxidant defences are only up-regulated in the first three weeks of infection after which they are down-regulated (Shi *et al.*, 2008). This could indicate that ROS/RNS are only important during the early stages of infection. In contrast however, just as during

acute infection, *Mtb* strains deficient in antioxidant defences have been shown to be less able to sustain chronic infection as well (Li *et al.*, 1998, Cirillo *et al.*, 2009).

Consider the proposed shift of persistent bacilli towards ferredoxin as a low potential electron carrier (Boshoff and Barry, 2005). Reduced ferredoxin can donate e^- to O_2 to leading to the formation of superoxide (Halliwell and Gutteridge, 2007). If we think of latent tuberculosis as a dynamic state, then the environment of the persistent bacilli may occasionally be exposed to oxygen, which could lead to episodes of superoxide formation and oxidative stress.

Overall, the information at hand regarding the level of ROS/RNS induced damage to persistent bacteria is still not fully established and merits further investigation.

1.5.1.1 Sources of damage

Hydrogen peroxide, nitric oxide and superoxide are the principal species produced during infection. Nitric oxide is able to inhibit respiration (Voskuil *et al.*, 2009) but it causes only limited nitrosative damage by itself (Halliwell and Gutteridge, 2007). However it can readily diffuse across membranes and enter the cell where it can interact with other ROS and RNS (Halliwell and Gutteridge, 2007) to form more toxic species, key among which is peroxynitrate (see Fig. 1.6).

Like nitric oxide, superoxide can cause only limited damage on its own; not least because it cannot cross biological membranes (Halliwell and Gutteridge, 2007). However superoxide dismutation, both non-enzymatic and via superoxide dismutase, leads to the formation of hydrogen peroxide, which can cross biological membranes and cause oxidative damage intracellularly via the formation of the hydroxyl radical (see Fig. 1.6 and section 1.5.1.2). The intracellular formation of superoxide can lead to direct damage of Fe-S clusters in proteins, resulting in the leaching of Fe ions and the stimulation of hydroxyl radical formation by the Fenton reaction (see Fig. 1.7, see section 1.5.1.2).

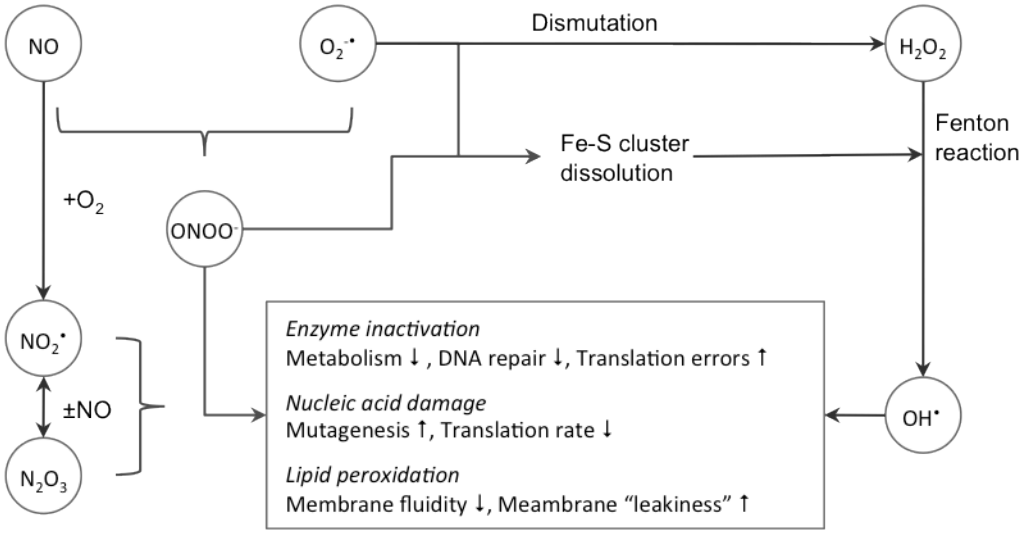


FIG. 1.6 Impact of biologically relevant ROS and RNS interactions.

1.5.1.2 Targets for damage

When discussing ROS and RNS damage *in vivo* it is perhaps easiest to consider the direct damage by two key species – peroxynitrate and the hydroxyl radical. Both are able to react with practically all biomolecules including carbohydrates, lipids, nucleic acids and proteins. The effects of this damage can result in lipid peroxidation, which can decrease membrane fluidity and increase membrane permeability to various ions. Oxidation, nitration, carbonylation and sulphonation of amino acid as well as dissolution of Fe-S clusters can occur in response to ROS and RNS, which can lead to a decrease in enzymatic function as well as stability of proteins. ROS and RNS damage to nucleic acids can lead double stranded DNA breaks, as well as chemical damage to nucleobases including nitration, deamination and oxidation. Examples include but are not limited to 8-hydroxyguanine, 8-hydroxyadenine, 5-hydroxyadenine, 5-hydroxycytosine, 5-hydroxyuracil and uracil. Many of these can be mutagenic as they can result in aberrant – non Watson-Crick base pairing (see Fig. 1.8), and are targeted by specific base excision DNA repair enzymes (see section 1.5.2.3).

In vivo measurements suggest that guanine is the most susceptible nucleobase (Halliwell and Gutteridge, 2007). Hydroxyl radical induced oxidation of guanine to 8-hydroxyguanine (see Fig. 1.7) is among the most common ROS induced lesions *in vivo* (Halliwell and Gutteridge, 2007).

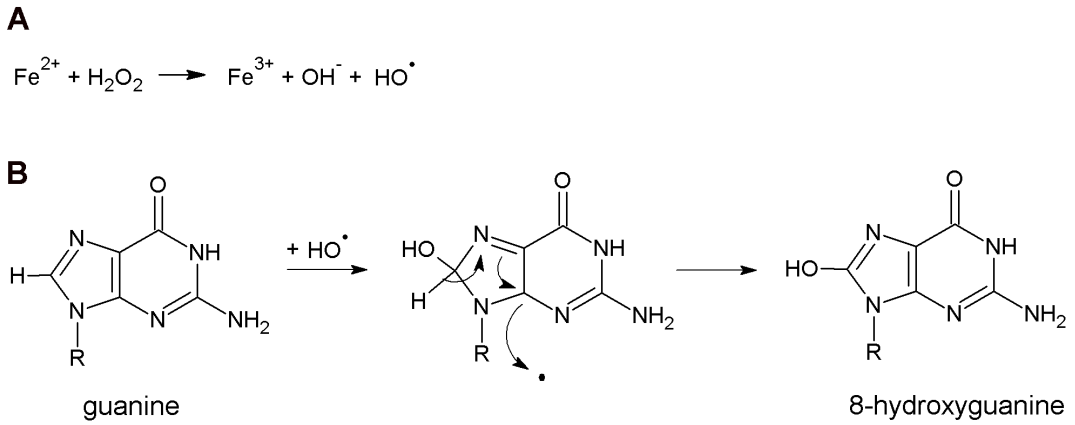


FIG. 1.7 The Fenton reaction (**A**) and the formation of 8-hydroxyguanine (**B**) via the oxidation of guanine by the hydroxyl radical.

1.5.1.3 General mitigation of damage

Given the widespread effects of ROS and RNS on cellular physiology cells go to significant lengths to limit the amount of damage that is incurred on them. A key mechanism is antioxidant defence, whose purpose is to reduce the overall concentration of ROS and RNS that can affect the cells. Mycobacteria achieve this by the expression of catalases, superoxide dismutases and alkyl hydropoeroxidases (Sherman *et al.*, 1995, Schnappinger *et al.*, 2003, Shi *et al.*, 2008, Miller *et al.*, 2010) as well as by synthesising considerable levels of radical scavenging mycothiol (den Hengst and Buttner, 2008, Newton *et al.*, 2008). Most organisms, including mycobacteria, respond to oxidative stress by changing the expression profile of a host of genes. Exposure to ROS and RNS leads to the induction of several heat shock proteins, which could act as sacrificial radical scavengers (Garbe *et al.*, 1996, Garbe *et al.*, 1999, Schnappinger *et al.*, 2003, Rhee *et al.*, 2005, Stewart *et al.*, 2005a). A further response is that of limiting free iron in the

cytosol, thus limiting the exacerbation of damage (Schanppinger *et al.*, 2003, Rodriguez and Smith, 2003) by Fenton chemistry.

1.5.2 Implications of damage

Despite the extensive network of damage mitigation mechanisms, ROS and RNS still cause considerable damage to the cell. What are the repercussions of this damage to the cell? Much of the ROS and RNS damage to biomolecules is considered irreversible, forcing the bacterium to recycle damaged components. For example, proteasome function is instrumental in the resistance of *Mtb* to nitrosative damage (Darwin *et al.*, 2003). Nonetheless, some damage can be reversed – DNA repair mechanisms are indispensable for resistance to oxidative damage (Boshoff *et al.*, 2003, Darwin and Nathan 2005, Jain *et al.*, 2007, Kurthkoti *et al.*, 2008, Davis and Forse, 2009).

1.5.2.1 Selective targeting

While in principle all biomolecules are likely to be targeted by ROS and RNS, it is not the case that all biomolecules accumulate the same amount of damage at steady state. In eukaryotic organisms, 8-hydroxyguanine accumulation is greater in RNA than DNA following hydrogen peroxide stress (Hofer *et al.*, 2005, Hofer *et al.*, 2006). The explanation for this phenomenon may lay in the chromatin-mediated protection of eukaryotic DNA or the wider distribution of RNA throughout the cell (Hofer *et al.*, 2006). Similarly, differences in 8-hydroxyguanine accumulation may reflect the specific repair of DNA damage or a disproportionate binding of unsequestered iron in the cytosol to RNA (Honda *et al.*, 2005). The presence of bound iron and other transition metals makes biomolecules particularly susceptible to oxidative damage, as Fenton reaction generated hydroxyl radicals (see Fig. 1.7) will interact with the first molecule they diffuse to (Halliwell and Gutteridge, 2007).

The level of oxidative damage to RNA in microorganisms is not known, as no studies have been carried out to date to investigate the relative levels of oxidative damage to different nucleic acids in bacteria.

1.5.2.2 Downstream effects of DNA and RNA damage

The implication of nucleic acid damage is determined by the nature of the damaged molecule. Damage to DNA is considered especially deleterious, as it is heritable. Oxidised nucleotides in DNA exhibit non-Watson-Crick (see Fig. 1.8) base pairing and can be mutagenic if unrepaired (Imlay and Linn, 1987, Jain *et al.*, 2007, Kurthkoti *et al.*, 2008, Halliwell and Gutteridge, 2007). Not all instances of oxidative damage are lethal. Damage to DNA can have positive consequences for the cell as well. It has recently emerged that treatment of *E. coli* with sublethal concentrations of antibiotic can lead to ROS generation *in vivo* (Kohanski *et al.*, 2007), which can result in multidrug resistance (Dwyer *et al.*, 2009, Kohanski *et al.*, 2010), possibly via the accumulation of ROS mediated mutations.

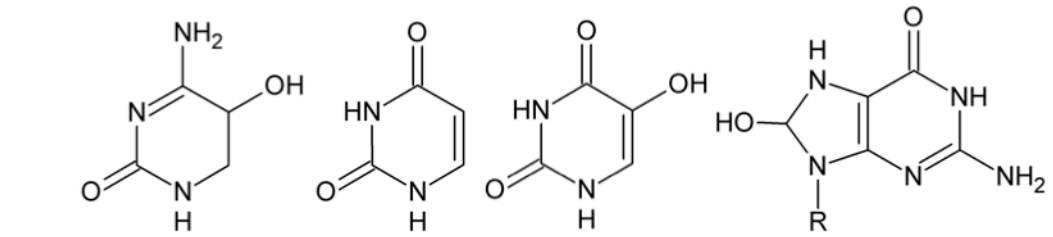
The effect of RNA oxidation on the other hand is not heritable. Its impact on the cell is considered to be limited, as damaged components can be readily replaced, therefore posing only a minor problem to the cell – provided of course that a sufficient proportion of the components remain intact. However, RNA oxidation is being recognised as an important driver of neurodegenerative disorders (Catellani *et al.*, 2008). Recent studies show that mRNA oxidation occurs early in the progression of disease (Shan *et al.*, 2003, Shan *et al.*, 2007, Chang *et al.*, 2008), as does rRNA oxidation (Honda *et al.*, 2005). Similarly, cellular RNA oxidation increases in ageing animals (Hofer *et al.*, 2008, Seo *et al.*, 2008, Xu *et al.*, 2008). Oxidative damage to rRNA and mRNA was shown to lead to a decrease in ribosomal processivity and fidelity, as well as increased number of strand cleavages (Ding *et al.*, 2005, Honda *et al.*, 2005, Tanaka *et al.*, 2007, Kong *et al.*, 2008, Moreira *et al.*, 2008, Ling and Soll, 2010).

The impact of the loss of translational processivity and fidelity can impose a multifactorial stress on the bacterial cell. The function of mistranslated proteins can be impaired leading to loss of cell integrity (Kohanski *et al.*, 2008) and mutagenesis (Al Mamun *et al.*, 2006). Mistranslated proteins are degraded by the cell, and lead to the induction of the heat shock response, which greatly increases the energy requirements of the cell (Dukan *et al.*, 2000, Ballesteros *et al.*, 2001, Fredriksson *et al.*, 2005, Fredriksson *et al.*, 2006, Fredriksson *et al.*, 2007). Overall, RNA oxidation can pose a greater threat to the cell than has been appreciated to date – understanding the full implications of it in the context of infection may give us important insights into potential unexploited vulnerabilities of bacterial physiology.

1.5.2.3 Repair of oxidative damage to DNA

Repair of oxidative damage to DNA occurs on two levels. On the one hand the cell ensures that it does not incorporate damaged nucleotides while on the other it removes damaged bases from the DNA.

The cell maintains a healthy dNTP pool by constantly santising it via the action of MutT/nudix hydrolases (Ito *et al.*, 2005). The function of MutT is to hydrolyse 8-hydroxyguanosine triphosphate and 8-hydroxy-2'-deoxyguanosine triphosphate thus preventing them from being incorporated into cellular RNA and DNA. There are four MutT homologues in *Mtb*, one of which was shown to have anti mutator activity as well as 8-hydroxy-2'-deoxyguanosine triphosphatase activity (Dos Vultos *et al.*, 2006).



	5-hydroxycytosine	Uracil	5-hydroxyuracil	8-hydroxyguanine
Source	Cytosine oxidation	Cytosine deamination	Uracil oxidation	Guanine oxidation
Pairing	G or A	A	A	A
Repair	Fpg/MutM Nei	Ung	Fpg/MutM Nei	Fpg/MutM Nth MutY*

FIG. 1.8 Modified nucleobases exhibit non Watson-Crick base pairing and are actively removed from DNA. Fpg Formamidopyrimidine-DNA glycosylase, Ung – uracil DNA glycosylase, Nei – endonuclease VIII, Nth – endonuclease III.

*MutY removes misincorporated adenine opposite 8-hydroxyguanine.

Oxidative damage to DNA can result in double stranded DNA breaks, which are repaired by SOS response enzymes (Boshoff *et al.*, 2003, Davis and Forse, 2009). Oxidative damage to nucleobases that affects nucleobase pairing is repaired by base excision and nucleotide excision repair (Darwin and Nathan, 2005, Jain *et al.*, 2007, Kurthkoti *et al.*, 2008, Davis and Forse 2009). These mechanisms are based on substrate specific glycosylases that recognise lesions that occur during oxidative damage. Formamidopyrimidine-DNA glycosylase (Fpg / MutM) removes 8-hydroxyguanine, 2,6-diamino-4-hydroxy-5-formamidopyrimidine (FAPyG), 5-hydroxycytosine and 5-hydroxyuracil from DNA. The latter two are the substrate for a related glycosylase – Nei. In addition to these lesions, the cell can remove mispaired adenines that have been inserted opposite 8-hydroxyguanine or cytosine by virtue of Adenine DNA glycosylase MutY. Oxidative damage can lead to the deamination of cytosine as well, which leads to the presence of uracil in DNA. These lesions are recognised and removed by Uracil DNA glycosylase (Ung). Homologues of all of these genes are present in most Mycobacterial species, with the exception of *Mycobacterium leprae*, which lack a Nei homologue (Davis

and Forse, 2009), and were shown to be up-regulated during infection and important for oxidative stress resistance and virulence (Sassetti and Rubin, 2003, Talaat *et al.*, 2004, Jain *et al.*, 2007, Kurthkoti *et al.*, 2008).

1.5.2.4 Repair of oxidative damage to RNA

In light of the profound consequences of oxidative RNA damage to the cell (see 1.5.2.2), it is conceivable that there is a mechanism to repair it. While there is rational scope for such a process, it remains to be demonstrated both *in vivo* and *in vitro*, as there is currently no experimental evidence to support its existence.

Nonetheless, there are important parallels between DNA repair strategies and RNA-related cellular processes. For example, MutT can hydrolyse 8-hydroxyguanosine triphosphate, therefore limiting the incorporation of damaged nucleotides into newly synthesised RNA (Ito *et al.*, 2005). Importantly, 8-hydroxyguanine containing RNA is recognised and sequestered by polynucleotide phosphorylase (Pnp) in *E. coli*, showing that bacterial cells can recognise oxidatively damaged RNA (Hayakawa *et al.*, 2001). Pnp is part of the RNA degradosome in bacteria (Carpousis *et al.*, 2007), so this binding is likely to target the RNA for degradation, however it may also serve as an initial step for the recruitment of other factors to the site of damage (Hayakawa *et al.*, 2001). Crucially, AlkB was shown to be able to repair alkylated RNA in *E. coli* (Aas *et al.*, 2003). Given that bacteria are probably no less likely to encounter oxidative damage than alkylating damage it is possible that they possess an RNA repair mechanism for oxidative damage as well as alkylating damage. If true it is not unreasonable to envisage that such a mechanism would have an important function in a nutrient starved persistent bacterium. However, before we can begin to look for evidence of RNA repair, we need to establish whether RNA stability is important for persistent mycobacteria, and whether oxidative damage to RNA is likely to occur and jeopardise the stability of RNA *in vivo*.

1.6 Summary of aims

The main aim of my project was to determine whether RNA stability plays a role in the survival of mycobacteria in the absence of growth. I chose to pursue this goal by investigating the fate of the ribosome during stasis and persistence.

As I was conscious of the many limitations of slow-growing bacteria (see 1.3.3.3 and 3.1) I chose to use the *Msm* model organism during the majority of my studies. In light of the availability of the ΔdosR strain of *Msm* I focused my work on the Wayne hypoxia model of persistence. I expected that the inability of this strain to survive prolonged hypoxia might inform us on the possible importance of ribosomal stability during the adaptation required for the establishment of persistence.

My hypothesis was the following: a persistent cell, with a limited source of chemical energy and reduced level of biosynthesis, would benefit from actively stabilising the ribosome. Stabilisation mechanisms should therefore exist to reduce the need for *ex novo* synthesis while the cell is in a limiting environment.

I planned to test this hypothesis by first determining whether RNA biosynthesis levels were compatible with a stable ribosomal population (Chapter 3). I then aimed to investigate the changes in the status of the ribosomal pool during different growth phases of mycobacteria, with a particular focus on stasis and the possible role of DosR during it (Chapter 4.3). I extended the time-frame of my investigations by focusing specifically on the stability of rRNA during the Wayne model of persistence and during prolonged carbon starvation, again examining the possible role of DosR (Chapter 4.4). I proceeded to probe the changes in the composition of the ribosome during stasis, using a quantitative proteomic approach, in an attempt to identify possible stabilising factors (Chapter 4.7). I was able to identify two putative ribosomal stabilising factors – MSMEG_3935 and MSMEG_1878 and test the importance of MSMEG_3935 for ribosomal stability (Chapter 4.8).

Finally, I hypothesise that ROS have a negative impact on the stability of RNA. Damaged RNA may therefore pose a significant challenge to persistent cells, increasing the cell's need for ribosomal stability. I addressed this hypothesis by testing whether RNA oxidation is a legitimate challenge to *Msm* viability, and attempt to outline an initial sketch of the mechanisms that determine the cellular response to it (Chapter 5).

2. Materials and Methods

2.1 General methods

2.1.1 Bacterial strains and growth media

All strains used during this study are listed in Table 2.1. The compositions of bacterial growth media are listed in Table 2.2. *Msm* and *E. coli* strains were routinely cultured at 37°C in LB medium – LB was supplemented with 0.05% (*v*/*v*) Tween 80 for the growth of *Msm*. For carbon starvation experiments the cells were grown in Hartmans-de Bont (HdB) medium supplemented with glycerol and Tween 80 to a final concentration of 0.04% (*v*/*v*) and 0.05% (*v/v*) respectively. *Mbo* BCG cells were cultured in 7H9 medium (Sigma), as described in Table 2.2. Cells cultured under hypoxic conditions were grown in 125 Erlenmeyer flasks (Croning) sealed with an air-tight rubber suba-seal (Sigma). Log phase cells were harvested when their optical density at 600 nm (OD_{600}) reached 0.5. Stationary phase cells and cells grown under hypoxic or carbon limiting conditions were harvested 48 hours post inoculation, unless stated otherwise. For culture on solid medium we used 7H10 medium (Sigma) or we added 2% (*w/v*) agar to LB prior to autoclaving.

TABLE 2.1 Bacterial strains used during this study.

Strain	*Genotype description*
M. smegmatis mc2 155	wild type
M. smegmatis mc2 155 ΔdosR	ΔdosR::hyg
M. smegmatis mc2 155 $\Delta dosR^{c}$	ΔdosR::hyg, $dosR^{Mtb}$::pRMV306
M. smegmatis mc2 155 ΔMSMEG_3935	ΔMSMEG_3935::hyg
M. bovis BCG	wild type
M. bovis BCG "ΔdosR" A-C	MycoMarT7 transposon insertion into *Mb3157c*
Escherichia coli MG1655	F^{-} λ^{-} $ilvG^{-}$ rfb-50 rph-1

TABLE 2.2 Growth media formulation.

Medium	*Components per l*
Luria-Bertani (LB) medium	5 g Yeast extract (Oxoid), 5 g NaCl, 10 g Tryptone (Oxoid)
Hartmans-de Bont (HdB) medium	0.01 g EDTA, 0.1 g $MgCl_2 \cdot 6H_2O$, 1 mg $CaCl_2 \cdot 2H_2O$, 0.2 mg $NaMoO_4 \cdot 2H_2O$, 0.4 mg $CoCl_2 \cdot 6H_2O$, 1 mg $MnCl_2 \cdot 2H_2O$, 2 mg $ZnSO_4 \cdot 7H_2O$, 5 mg $FeSO_4 \cdot 7H_2O$, 0.2 mg $CuSO_4 \cdot 5H_2O$, 1.55 g K_2HPO_4, 850 mg NaH_2PO_4, 2 g $(NH_4)_2SO_4$. The medium was supplemented with 0.05% Tween 80, and with 4 ml glycerol (full medium), or 400 µl glycerol (minimal medium).
7H9 medium	4.7 g Middlebrook 7H9 broth powder (Sigma), 2 ml glycerol, 0.05 % (*v/v*) Tween 80, make to 900 ml with dH_2O. 100 ml of sterile Middlebrook OADC supplement (BD) added after autoclaving.
7H10 medium	19.47 g Middlebrook 7H10 medium powder (Sigma), 2 ml glycerol, make to 900 ml with dH_2O. 100 ml of sterile Middlebrook OADC supplement (BD) added after autoclaving.

2.1.2 Viability determination

Bacterial viability was determined by plating serial dilutions onto solid media. Aliquots from cultures were vortexed and used for 10-fold dilution series. Four 20 µl samples were spotted for each dilution, incubated at 37˚C and enumerated after three days.

2.1.3 Toxicity assay

Cells were grown under oxygen limiting or carbon limiting conditions. All experiments were performed on early stationary phase cultures. Mitomycin C (Sigma) and H_2O_2 (Sigma) were added directly to the culture medium. Mitomycin C was added to a final concentration of 750 nM or 200 nM in carbon starved or oxygen starved cultures respectively, samples were taken every 90 min and serially diluted to determine the number of colony forming units (CFU) per ml of culture. H_2O_2 was added to the desired final concentration and samples were taken at the appropriate time. 10 µl of catalase (20 mg/ml, Roche) was added to each culture aliquot prior to dilution and LB agar

plates supplemented with catalase (final concentration of 0.01 mg/ml, Roche) were used for determining the CFU ml^{-1}. UV susceptibility experiments were performed by irradiating lawns of bacteria (200 µl of bacterial culture spread over an LB agar plate) for 3, 15, 30 and 60 s using a UVB handheld light emitting shortwave UV light. The irradiation of oxygen starved cultures was performed in an anaerobic cabinet, to ensure that exposure occurred in hypoxic conditions.

2.1.4 Methylene blue toxicity

Cultures were grown in full HdB medium to mid log phase (OD_{600} of 0.5), vortexed and 200 µl aliquots were dispensed into 24-well polycarbonate clear-bottom plates. None or 0.5 – 100 µg methylene blue (stock solution 0.5 mg ml^{-1}, Sigma) was added to each well and the volume of medium adjusted to 1 ml with sterile HdB. Plates were incubated at 37˚C on an orbital shaker and the viability was determined by plating on solid media.

2.1.4.1 Photo-oxidation with methylene blue

Plates were prepared as described and then incubated on a custom-made light-box with 24 red light emitting diodes. The diodes used had an emission maximum at λ = 635 nm, and emitted light with a luminous intensity of 16000 mcd at a viewing angle of 8˚ (RS components).

2.1.5 Biosynthesis determination

Cultures were grown at 37˚C, using either minimal HdB or LB medium, as described above.

2.1.5.1 Protein synthesis

Protein synthesis was assessed by adding L-[4,5-^{3}H]-leucine (Perkin Elmer) or L-[methyl-^{3}H]-methionine (Perkin Elmer) to a final concentration of 0.5 µCi ml^{-1}. Cells were harvested by centrifugation (6,000 × *g*, 10 min at 4˚C). The cell pellet was

resuspended in 400 μl lysis buffer (0.2% [*w/v*] n-laurylsarconate, 20 mM Tris-HCl [pH 7.5]), transferred to a 1.5 ml screw-top skirted eppendorf tube containing one third of acid-washed beads and lysed using a mini bead beater. The lysate was clarified by centrifugation (12,000 × *g*, 15 min at 4˚C), and the proteins precipitated as described in section 2.2.1. The pellet was resuspended in 200 μl of distilled water, 3 ml of UltimaGold scintillation liquid (Perkin Elmer) was added and the radioactivity measured using a Wallac scintillation counter (Perkin Elmer). Raw data were collected in duplicate over five minutes using the pre-set parameters for ^{3}H.

2.1.5.2 RNA synthesis

RNA synthesis was assessed by adding L-[5,6-^{3}H]-uracil (Perkin Elmer) to a final concentration of 0.5 μCi ml^{-1}. Cells were harvested by centrifugation (6,000 × *g*, 10 min at 4˚C). The cell pellet was resuspended in 700 μl of the Trizol reagent (Invitrogen), transferred to a 1.5 ml screw-top skirted eppendorf tube containing one third of acid-washed beads and lysed using a mini bead beater. RNA was isolated as described in section 2.2.4.2. The RNA pellet was resuspended in 200 μl of distilled water, and quantified spectrophotometrically (see section 2.2.4.3) prior to adding 3 ml of UltimaGold scintillation liquid (Perkin Elmer). Radioactivity was measured using a Wallac scintillation counter (Perkin Elmer) – 2 × 5 min.

2.2 Molecular biology techniques

2.2.1 Protein precipitation

1/100 (*v/v*) of 2% (*w/v*) Na-deoxycholate (Sigma) was added to each sample followed by vortexing and incubation at 4°C for 30 min. 1/10 (*v/v*) of TCA stock solution (13.5 M) was added and the mixture was vortexed and incubated overnight at 4°C. The samples were then centrifuged (15,000 ×*g*, 15 min at 4°C), the supernatant was discarded and

the pellet washed twice with ice-cold acetone. After the final wash the pellet was air-dried and resuspended in 20 µl 0.75 M Tris-HCl (pH 8.5).

TCA precipitation was not used for protein samples analysed by mass spectrometry; in those instances the proteins were precipitated by adding 6× sample volume of ice cold acetone (e.g. 1200 µl of acetone would be added to 200 µl of aqueous suspension) and incubated at -20˚C overnight. The proteins were pelleted by centrifugation (17,000 × *g*, 15 min at 4˚C) and resuspended in distilled water or "Dissolution Buffer" (see 2.5.2) prior to further analysis.

2.2.1.1 Colorimetric Protein Quantitation

Protein concentrations were determined by using the Coomassie Plus (Bradford) Protein Assay (Thermo). 3 µl of protein sample were mixed with 100 µl of the Coomassie Plus Reagent (Thermo) and allowed to equilibrate at room temperature for 10 min prior to measuring the absorbance at 595 nm. The samples were quantified by using a BSA standard curve as recommended by the manufacturer.

2.2.2 SDS-PAGE

5 µl of 6× sample loading buffer (Sigma) were added to 25 µl of protein sample and the mixture was boiled for 5 min prior to loading onto a 15% polyacrylamide-SDS gel. Gels were run at 150 V for 2 h and stained by using Imperial Blue (Thermo) overnight. Gels were developed by washing in distilled water (3 × 30 min).

2.2.3 Western blot analysis

Gels used for western blotting were not stained with Imperial Blue, and proteins were transferred by electroblotting to a PVDF membrane (Hybond P, GE healthcare) overnight (25 V at 4°C). Membranes were blocked (0.01% [*v/v*] Tween 20, 5% non-fat milk in PBS) and incubated for 4 hours at room temperature or overnight at 4°C with α-HspX mouse monoclonal antibody (1:100 dilution of antibody in 0.01% [*v/v*] Tween 20,

0.1% non-fat milk in PBS, Colorado State University, Colorado) or α-Rv1636 rabbit polyclonal antibody (1:2000 dilution of antibody in 0.01% [*v/v*] Tween 20, 0.1% non-fat milk in PBS). Bound antibody was detected using horseradish peroxidase-conjugated α-mouse or α-rabbit IgG from sheep (1:7500 dilution, GE healthcare). The ECL detection kit (GE healthcare) was used to reveal binding and the luminescence was detected using photographic film.

2.2.3.1 Densitometric analysis

Developed photographic films were digitalised at a resolution of 300 dpi, using a ScanJet 6200c scanner (Hewlett-Packard). The images were imported into ImageJ software (Abramoff *et al.*, 2004) and the intensity of the relevant bands quantified using the Analyze>Plot Profile>Integrate functionality of the software.

2.2.4 Nucleic acid isolation

2.2.4.1 Isolation of DNA

The protocol was adapted form Belisle and Sonnenberg, 1998. Genomic DNA was isolated from 20 ml of mid-log phase cultures (OD_{600} approximately 0.5). The cells were harvested by centrifugation (6,000 × *g*, 10 min at 4˚C) and resuspended in 1 ml of TE buffer (10 mM Tri-HCl [pH 8.0], 1 mM EDTA). An equal amount of chloroform : methanol (2:1) was added to the cell suspension and the mixture was rocked at room temperature for 5 minutes. The suspension was centrifuged (6,000 × *g*, 10 min at room temperature), both the aqueous and organic layers were removed, and the pellet was air dried for 3 h. The dry residue was resuspended in 800 μl of TE + 0.1 M Tris (pH 8.5) and transferred to a 1.5 ml screw top skirted eppendorf tube. Lysozyme was added to a final concentration of 100 μg ml^{-1} and the mixture was incubated at 37˚C overnight. The following day, 80 μl of 10% SDS was added together with proteinase K (final concentration 100 μg ml^{-1}) and the samples were incubated at 37˚C for 4 h. 800 μl of

phenol : chloroform (1:1) was added to the solution after the incubation, mixed well and rocked at room temperature for 30 min. The mixture was then centrifuged (12,000 × *g*, 15 min at 4˚C), the aqueous phase transferred to a new tube and the DNA precipitated by adding 50 µl of 3 M sodium acetate and 500 µl of isopropanol and centrifuged (17,000 × *g*, 30 min at 4˚C). The pellet was washed with ice-cold 70% ethanol, and pelleted by centrifugation (7,500 × *g*, 5 min at 4˚C). The pellet was air dried to remove traces of ethanol and resuspended in 100 µl of distilled water.

2.2.4.2 Isolation of RNA

All aqueous reagents used for RNA analysis were prepared with nuclease free, or diethylpyrocarbonate (DEPC)-treated water (Sambrook and Russell, 2001). RNA was isolated using the Trizol reagent (Invitrogen) according to the manufacturer's instructions. Briefly, 50 ml of culture were harvested by centrifugation (6,000 × *g*, 10 min at 4˚C). The cell pellet was resuspended in 700 µl Trizol and transferred to a screw top eppendorf tube containing one third of the volume of acid washed beads. The cells were lysed by bead beating for one minute followed by a 5 minute incubation on ice and another one minute of bead beating. 200 µl of chloroform was added to the lysate and the contents were mixed by vigorous shaking for 30 s. The mixture was left to stand at room temperature for 2 minutes prior to centrifugation (12,000 × *g*, 15 min at 4˚C). The aqueous phase was transferred to a fresh tube, making sure not to disturb the material at the interface of the two phases. The RNA was precipitated by adding an equal volume of ice cold isopropanol to the aqueous phase and incubating overnight at -80˚C. The RNA was pelleted by centrifugation (10,000 × *g*, 10 min at 4˚C). The pellet was washed with ice-cold 75% ethanol, collected by centrifugation (7,500 × *g*, 5 min at 4˚C), air dried to remove traces of ethanol and resuspended in 200 µl of nuclease free water. The sample were incubated at 65˚C for 2 min and then placed on ice to improve the dissolution of the RNA pellet in water.

2.2.4.3 Spectrophotometric analysis

Nucleic acids were quantified by measuring the absorbance of samples at 260 and 280 nm. An absorbance unit (1.0) at 260 nm was considered to be equivalent to 38 μg ml^{-1} of RNA and 50 μg ml^{-1} of DNA. The purity of the preparation was estimated by calculating the ratio of the absorbance at 260 nm and 280 nm. A value between 1.75 – 1.90 was considered appropriate.

2.2.4.4 Bioanalyzer analysis

RNA integrity was assayed using the Agilent RNA 6000 Nano Chip kit (Agilent) analysed by a 2100 Bioanalyzer instrument (Agilent). RNA samples were purified as described in 2.2.4.2 and prepared for analysis according to the manufacturer's instructions.

2.2.5 Polymerase chain reaction

Routine polymerase chain reaction (PCR) was performed using Go*Taq* polymerase (Promega) together with the provided reaction mix (1.5 mM $MgCl_2$ final), which was supplemented with 5% (*v/v*) DMSO, 1 mM dNTP mix and 1 μM of each primer (see Table. 2.3 for a complete list of primers used).

The routine PCR program consisted of an initial incubation at 95˚C for 2 min followed by the following steps repeated for 30 cycles: denaturation at 95˚C for 30 s, annealing at 55-68˚C depending on primer properties for 30 s, elongation at 72˚C for 1 min, or more, depending on the length of the product. A final incubation of 72˚C was performed to allow the enzyme to complete the elongation.

Pfu (Fermentas) and Phusion (Finnzyme) were used for the amplification of DNA products used for cloning and knockout applications (see Section 2.2.6).

2.2.5.1 Agarose gel electrophoresis

PCR products were analysed by agarose gel electrophoresis. Gels normally contained 1.5% (*w/v*) agarose, DNA was visualised using the SYBR safe (Invitrogen) dye. Images of the gels were obtained using a Gel Doc (Bio-Rad) system controlled by Quantity One (Bio-Rad) software. If needed, the gels were analysed densitometrically as described in 2.2.3.1.

2.2.5.2 Restriction enzyme digestion and ligation

Restriction enzyme digestions and ligations were carried out using Fermentas reagents according to manufacturer's instructions for the specific enzyme used. Digested fragments were purified using column based "PCR purification" kit (QIAGEN). Ligations were normally carried out at room temperature, and the products were either used directly for transformations (see section 2.2.7) or were purified using gel electrophoresis followed by column based "Gel extraction" kit purification (QIAGEN) when used for recombineering (see section 2.2.6).

2.2.6 Recombineering mutagenesis

Mutant *Msm* strains were obtained following the protocol established by van Kessel and Hatfull (2007). Briefly, a linear construct was generated such that it contained a hygromycin cassette flanked by approximately 500 bp of up- and downstream sequence of the gene of interest. Each of the components of the construct was amplified separately by using the following combination of primers (see Table 2.3):

- upstream (US) fragment: **Msm**_xxxX**RUS**[2] + **Msm**_xxxX**F1**,
- downstream (DS) fragment: **Msm**_xxxX**FDS** + **Msm**_xxxX**R2**
- hygromycin cassette (Hyg^R): **pSMT3_hygRR2** + **pSMT3_hygRF2**

[2] Name of the primer as presented in Table 2.3; xxxX refers to the gene of interest.

The components were digested using *Xba*I (upstream fragment, Hyg^R) and *Bgl*II (downstream fragment, Hyg^R) and then ligated to generate the desired construct. The construct was purified by gel electrophoresis followed by gel extraction, amplified by PCR and used for transforming electrocompetent *Msm* cells (see section 2.2.7.2) harbouring the pJV53 plasmid (see Table 2.4). pJV53 carries an acetamide inducible high efficiency recombinase which catalyses the integration of the linear fragment of DNA into the relevant genetic locus (van Kessel and Hatfull, 2007).

This method was used to attempt to generate mutants for: *ahpC* (MSMEG_4753), *alkB* (MSMEG_5451), *ideR* (MSMEG_2750), *katG* (MSMEG_6384), *mca* (MSMEG_5261), *mshA* (MSMEG_0933), *MSMEG_3935*, *sodA1* (MSMEG_6427), *sodA2* (MSMEG_6636), *soxR* (MSMEG_5450).

Putative mutants were positively selected on plates containing 20 μg ml^{-1} hygromycin. Individual colonies were picked and streaked onto new hygromycin containing plates. Genomic DNA was purified from potential mutants, as described in section 2.2.4.1 and the strains were assessed for the presence of the hygromycin cassette, as well as the insertion of Hyg^R into the correct genetic locus.

2.2.6.1 Complementation of ΔMSMEG_3935

Three separate approaches were used to generate a plasmid with which to attempt the complementation of ΔMSMEG_3935. MSMEG_3935 was amplified from genomic DNA of wild type *Msm* either including only the coding sequence – $MSMEG_3935^{Hsp60}$ (Msm_hraAF2 + Msm_hraAR2) and $MSMEG_3935^{TetO}$ (Msm_hraAFC3a + Msm_hraARC3) or including a putative DosR responsive element 82 bp upstream of the gene $MSMEG_3935^{DosR}$ (Msm_hraAFC4a + Msm_hraARC3). The primers were designed so that $MSMEG_3935^{Hsp60}$ contained terminal *Bam*HI sites while $MSMEG_3935^{TetO}$ and $MSMEG_3935^{DosR}$ contained a 5' *Nde*I site and a 3' *Pvu*II site. These restriction enzyme sites were used to attempt to ligate $MSMEG_3935^{Hsp60}$ into pSMT3, $MSMEG_3935^{TetO}$ into

pTetO and MSMEG_3935^{DosR} into the integrating plasmid pGiles (see Table 2.4). The digestion, ligation and transformation was carried out at least three times for each construct and over 50 colonies were screened (by colony PCR) in total for each plasmid.

TABLE 2.3 Primers used for PCR and *Msm* mutagenesis

Name of primer Primer sequence	Use of primer
MSMEG_3935 mutagenesis and complementation	
Msm_hraAF1 CGGCCATCCCCTCGACCA	Forward primer for *MSMEG_3935* mutagenesis
Msm_hraAFc TACCGGCGAAGCCCTCCC	Forward primer for *MSMEG_3935* knockout confirmation
Msm_hraAF2 ATAGGATCCCTAGCCGTCCG	Forward primer for *MSMEG_3935* native complementation *Bam*HI
Msm_hraAR2 ATAGGATCCAATGGACGTCGATGT	Reverse primer for *MSMEG_3935* native complementation *Bam*HI
Msm_hraAFC3a GGCAGCGAGATTACATATGATGATGAAGG	Forward primer for *MSMEG_3935* native complementation longer 5'
Msm_hraAFC4a GGCAGCGAGATTACATATGGACGTCGATG	Forward primer for *MSMEG_3935* Tet complementation longer 5'
Msm_hraAFDS GGGAGTCAGGCAACTATGGATGAAAGATCTGACCTCTGGTAGCCCTGTTC	*MSMEG_3935* knockout downstream
Msm_hraAR1 GGCTTTTCGCCGCCGAGT	Reverse primer for *MSMEG_3935* mutagenesis
Msm_hraARC3 TGTAATCAGCTGTGCTAGCCGTCCGCA	Reverse primer for *MSMEG_3935* complementation
Msm_hraARUS TGGCATCCTCGATCATCTCCTCTAGACAGTACAGCTAGCCAGTTGC	*MSMEG_3935* knockout upstream
Oxidative damage mutagenesis	
Msm_ahpCF1 CTGACCCGCCTGCGCATTCA	Forward primer for *ahpC* mutagenesis
Msm_ahpCFc TCACACGCGGCGATCACG	Forward primer for *ahpC* knockout confirmation
Msm_ahpCFDS GGGAGTCAGGCAACTATGGATGAAAGATCTCGCGTGACCTTCAGGTCTGT	*ahpC* knockout downstream
Msm_ahpCR1 CGTCGAGGGGGCTGTGGGTA	Reverse primer for *ahpC* mutagenesis
Msm_ahpCRUS TGGCATCCTCGATCATCTCCTCTAGAGCACAAGATCCCTTCTCGTC	*ahpC* knockout upstream
Msm_alkBFc ACGACGAGTCGCGGGTGA	Forward primer for *alkB* knockout confirmation

Msm_alkBFDS *alkB* knockout downstream
GGGAGTCAGGCAACTATGGATGAAAGATCTCGCACTTATCCCCGGACC

Msm_alkBRUS *alkB* knockout upstream
TGGCATCCTCGATCATCTCCTCTAGACCAGCTCCATGCGCGCGAG

Msm_ideRF1 Forward primer for *ideR* mutagenesis
GATCGCCCTGGCGTTGAC

Msm_ideRFDS *ideR* knockout downstream
GGGAGTCAGGCAACTATGGATGAAAGATCTTCATGCGCGCCTTCCCAGC

Msm_ideRR1 Reverse primer for *ideR* mutagenesis
ACGAGCGCGAGCAGCAG

Msm_ideRRUS *ideR* knockout upstream
TGGCATCCTCGATCATCTCCTCTAGAGGTCGAGAAGGTCTGATCC

Msm_katGF1 Forward primer for *katG* mutagenesis
CACCCGCACGCCGATAC

Msm_katGFDS *katG* knockout downstream
GGGAGTCAGGCAACTATGGATGAAAGATCTGCTTCGACGTCGCCTGACA

Msm_katGR1 Reverse primer for *katG* mutagenesis
TCGGCGTCACCCAGCAGA

Msm_katGRUS *katG* knockout upstream
TGGCATCCTCGATCATCTCCTCTAGAATGCATTTCCTTTCGGGAGT

Msm_mcaF1 Forward primer for *mca* mutagenesis
TCTCCGGGGTGCTGTCCG

Msm_mcaFc Forward primer for *mca* knockout confirmation
CACCAGTGACAGGCGGCG

Msm_mcaFDS *mca* knockout downstream
GGGAGTCAGGCAACTATGGATGAAAGATCTTCACTCATTTCGTTCCATCT

Msm_mcaR1 Reverse primer for *mca* mutagenesis
GTGCGCGGACGATGCAGA

Msm_mcaRUS *mca* knockout upstream
TGGCATCCTCGATCATCTCCTCTAGACGAGCCATGATCGACACCT

Msm_mshAF1 Forward primer for *mshA* mutagenesis
CGTGCCTGCCGAAGGTCC

Msm_mshAFc Forward primer for *mshA* knockout confirmation
GTGAGCGACGAGGCCGTG

Msm_mshAFDS *mshA* knockout downstream
GGGAGTCAGGCAACTATGGATGAAAGATCTGAGTACGCACGTGAATGTCA

Msm_mshAR1 Reverse primer for *mshA* mutagenesis
CGAGACCCGCCACTCCCA

Msm_mshARUS *mshA* knockout upstream
TGGCATCCTCGATCATCTCCTCTAGATAGACGCACATCGTCATGTC

Msm_sodAF1 Forward primer for *sodA* I mutagenesis
GGCGGGATGGTGGGGCTA

Msm_sodAF2 Forward primer for *sodA* II mutagenesis
CCCGGTTCGGGGCTGGTA

Msm_sodAFDS1 *sodA* I knockout downstream
GGGAGTCAGGCAACTATGGATGAAAGATCTCTTCGGCTGATCCGCTCACA

Msm_sodAFDS2 *sodA* II knockout downstream
GGGAGTCAGGCAACTATGGATGAAAGATCTATGGGTATCCTCTCGCGCTTG

Msm_sodAR1 Reverse primer for *sodA* I mutagenesis
TGCGGTTCATCCGGCAGC

Msm_sodAR2 Reverse primer for *sodA* II mutagenesis
GGGCCACCACCCGGAGAA

Msm_sodARUS1 *sodA* I knockout upstream
TGGCATCCTCGATCATCTCCTCTAGACACGAGATTCCTTCCTCAT

Msm_sodARUS2 *sodA* II knockout upstream
TGGCATCCTCGATCATCTCCTCTAGATCTGAGCGGCACAGTCGGC

Msm_soxRF1 Forward primer for *soxR* mutagenesis
TGCATGCGGCGCACAAGA

Msm_soxRF2 Forward primer for *alkB* mutagenesis
CCGTCGCACATCCGGCAA

Msm_soxRFc Forward primer for *soxR* knockout confirmation
CTGGTTTCGCGTGCGGGT

Msm_soxRFDS *soxR* knockout downstream
GGGAGTCAGGCAACTATGGATGAAAGATCTCTCTGACACATCGAACGTGT

Msm_soxRR1 Reverse primer for *soxR* mutagenesis
TCGCGCCCAGACTCACGA

Msm_soxRR2 Reverse primer for *soxR-alkB* mutagenesis
GTTCGAGCCCGCCGACTG

Msm_soxRRUS *soxR* knockout upstream
TGGCATCCTCGATCATCTCCTCTAGATCGTGCATGTCCATGACACC

pSMT3_hygRF Forward primer for hygromycin cassette in pSMT3
GGAGATGATCGAGGATGCCA

pSMT3_hygRF2 Higher T_m forward primer for hygromycin cassette in pSMT3 + 5' *Xba*I site
TCTAGAGGAGATGATCGAGGATGCCA

pSMT3_hygRF_XbaI Forward primer for hyg amplification + 5' *Xba*I site
TCTAGAGGAGATGATCGAG

pSMT3_hygRR Reverse primer for hygromycin cassette from pSMT3
TTCATCCATAGTTGCCTGACTCCC

pSMT3_hygRR2 Higher T_m reverse primer for hygromycin cassette in pSMT3 + 3' *Bgl*II site
AGATCTTTCATCCATAGTTGCCTGACTC

pSMT3_hygRR_BglII Reverse primer for hyg amplification + 3' *Bgl*II site
AGATCTTTCATCCATAGTTGC

pSMT3_hygRR_EcoRV Reverse primer for hyg amplification + 3' *Eco*RV site
GATATCTTCATCCATAGTTGC

TABLE 2.4 Plasmids used during this study

Name	*Properties*	*Source*
pJV53	Kan^R, OriE, OriM, Acetamidase promoter - Che9c genes 60-61 *Recombineering mutagenesis*	Van Kessel and Hatfull, 2007
pGiles	Zeo^R, OriE, attP, integrase *ΔMSMEG_3935 complementation integrating*	M. Chao (unpublished)
pSMT3	Hyg^R, OriE, OriM, Hsp60 promoter- Hsp60-VP6 *ΔMSMEG_3935 complementation Hsp60 promoter*	G. Joyce (Unpublished)
pTetO	Zeo^R, TetO promoter-RipA *ΔMSMEG_3935 complementation TetO promoter*	M. Chao (unpublished)

NB. Zeo – Zeocin, Kan – Kanamycin, Hyg - Hygromycin

2.2.7 Transformation

Chemically competent *E. coli* cells were prepared as described in Sambrook and Russell (2001), while electrocompetent cells were generated as described by van Kessel and Hatfull (2007).

2.2.7.1 Transformation of *E. coli*

100 ng of plasmid DNA prepared using "Mini Prep" kits (QIAGEN) or ligation products were added to 50 μl of high-efficiency chemically competent cells and the mixture was incubated on ice for 20 min. The cells were heat shocked at 42˚C for 45 s, returned to ice for a further 2 min and then allowed to recover in 1 ml of LB medium at 37˚C for 1.5 hours. After the recovery period, 200 μl of the cell suspension was spread onto plates with an appropriate selection marker (e.g. hygromycin for pSMT3, see table 2.4) and incubated at 37˚C overnight. Colonies were screened for the presence of the desired plasmid using colony PCR – same protocol as described in section 2.2.5, with the initial incubation at 95˚C extended to 10 min.

2.2.7.2 Transformation of *Msm*

100 μl of electrocompetent *Msm* cells were mixed with 100 ng of DNA (either plasmid or linear construct, see section 2.2.6) and transferred to a prechilled 0.2 cm electrocuvette. The cells were electroporated using a Gene Pulser instrument (BioRad) set to 2.5 kV and 25 μF and the pulse controller set to 1000 Ω. The cells were allowed to recover in 1 ml of 7H9 medium for 4 hours prior to plating 500 μl of the transformation suspension onto antibiotic selection 7H10 plates. Plates were incubated at 37˚C for 4 days. Individual colonies were picked and re-streaked on fresh antibiotic containing plates prior to further work.

2.3 Ribosomal profiling

2.3.1 Cell lysis

Cells were grown in 2.5 l glass conical flasks (Pyrex) containing either 1 l of HdB, LB or 7H9 medium depending on the organism cultured and the desired conditions. Hypoxic cultures were obtained by inocculating 1.7 l of LB medium in a flask and sealing it with a tight-fitting rubber bung, which has been perforated and modified to fit a 33 mm SubaSeal air-tight rubber septum (Sigma). Each bung was further sealed with silicone grease (Dow Corning) and wrapped in a layer of parafilm to minimise the diffusion of oxygen across the seal.

At least 6 l of culture were harvested by centrifugation (10,000 × *g*, 15 min at 4˚C), and the pellet was resuspended in ribosomal buffer (10 mM Tris-HCl [pH 7.4], 70 mM KCl, 10 mM $MgCl_2$) at the concentration of 1.0 g wet weight ml^{-1} lysed by a single passage through a French press. After cell breakage the samples were clarified by centrifugation (30,000 × *g*, 30 min at 4°C) to remove cellular debris and unbroken cells. The supernatant was kept for further analysis.

2.3.2 Ribosomal profiling

Clarified cell extract was centrifuged through a sucrose cushion (1.1 M sucrose, 50 mM Tris-HCl [pH 7.4], 25 mM KCl, 10 mM $MgCl_2$) for 2.5 h at 31,000 rpm and 4 °C, in a Beckman MLS-50 rotor (Beckman-Coulter) using an Optima Max tabletop ultracentrifuge (Beckman-Coulter). The washed ribosomal pellet was resuspended in ribosomal buffer (10 mM Tris-HCl [pH 7.4], 70 mM KCl, 10 mM $MgCl_2$) and loaded onto a sucrose linear gradient (15-40%) and centrifuged (5 h, 35,000 rpm at 4 °C) in a SW 41-Ti Rotor (Beckman-Coulter) using an Optima L-100 XP ultracentrifuge (Beckman-Coulter). After the centrifugation the gradients were fractionated by piercing the bottom of the tube with a needle (40 × 11 mm, BD) and collecting approximately 400 µl (7 drops) samples into clean eppendorf tubes. The absorbance at 254 nm, 260 nm and 280 nm was measured for each fraction using a DU640 spectrophotometer (Beckman-Coulter). The refraction in each fraction was measured using an Abbe 60 refractometer (Bellingham and Stanley). The values obtained were compared those of the prepared stock solutions.

If necessary the proteins were precipitated from gradient fraction using either TCA or acetone precipitation (see 2.2.1). The former was used for SDS-PAGE (see 2.2.2) and western blot analysis (see 2.2.3) while the latter was used for mass spectrometric analysis (see 2.5).

2.3.3 Sucrose gradient preparation

Sucrose gradients were prepared by layering 5.5 ml of a 15% sucrose solution (15% sucrose [*w*/*v*], 50 mM Tris-HCl [pH 7.4], 25 mM KCl, 10 mM $MgCl_2$) on top of 5.5 ml of a 40% sucrose solution (40% sucrose [*w*/*v*], 50 mM Tris-HCl [pH 7.4], 25 mM KCl, 10 mM $MgCl_2$) in Polyallomer thin walled ultracentrifuge tubes (Beckman-Coulter). The tubes were sealed with parafilm, gently tipped on the side and left at room temperature for 3 h

to allow the gradient to form by diffusion. After this time the tubes were gently put back into the vertical position and used for ribosomal profiling.

2.4 Fast protein liquid chromatography (FPLC) of ribosomes

2.4.1 Fast protein liquid chromatography

All FPLC was performed on an AKTA-FPLC liquid chromatography system (GE healthcare) using a 0.6 ml mixer unit, and either a 100 µl or a 5 ml sample loop. The chromatographic matrix used for most experiments were two Quaternary Amine Convective Interaction Media (QA) monolithic discs (BIA separations) encased within a polyoxymehylene casing (BIA separations). In some cases Diethylaminoethyl Covective Interaction Media (DEAE) monolithic discs (BIA separations) were used in place of QA. The programmes were performed with a flow of 2 ml min^{-1} and the mobile phase consisted of (10 mM Tris-HCl [pH 7.4], 70 mM KCl, 10 mM $MgCl_2$) – Buffer A and (10 mM Tris-HCl [pH 7.4], 70 mM KCl, 10 mM $MgCl_2$, 1 M NH_4Cl) – Buffer B – N.B. 1 M NaCl was used instead of 1 M NH_4Cl when samples were intended to be used for iTRAQ labelling. Four different chromatographic programmes were used: Linear, Step, Profiling I and Profiling II (see Fig. 4.28). The "Linear" program consisted of an initial 2 column volume (CV) buffer A wash, followed by a linear gradient of 0-100% Buffer B over 20 CV, and a final column wash at 100% Buffer B for 2 CV. The "Profiling I" chromatographic program consisted of a 2 column volume (CV) Buffer A wash after sample loading, followed by a linear gradient of 0-40% Buffer B over 8 CV, then a linear gradient of 40-54% Buffer B over 10.5 CV and then a linear gradient 54-100% Buffer B over 9.2 CV, a final wash with 5 CV of Buffer B was then performed. "Profiling II" was carried out in a similar fashion to "Profiling I" but using a stepwise gradient, with an increment of 2% every 1.5CV (40-54% Buffer B), instead of the linear 40-54% gradient.

The program used for isolating ribosomes "Step" started with a 2 CV Buffer A wash after loading the sample, followed by a step increase 0 to 38% Buffer B for 4 CV, a step

increase 38 to 46% Buffer B and a step increase 46 to 100% Buffer B, a final wash with 5 CV of Buffer B was performed at the end.

All samples were filtered through a 0.2 μm syringe filter (Pall corporation) prior to injecting into the system. In some cases 1 μg of DNAse I (Invitrogen) was added sample aliquots (100 μl) and left to incubate at room temperature for 1 hour prior to loading. Eluting species were recorded using an in-line UV detector.

Proteins were precipitated from the chromatographic fractions using either TCA or acetone precipitation (see 2.2.1). The former was used for SDS-PAGE (see 2.2.2) and while the latter was used for mass spectrometric analysis (see 2.5).

2.4.2 Coupled transcription-translation assay

The assay was based on the commercially available "*E. coli* S30 Extract System for Circular DNA" kit (Promega). The standard protocol specified by the manufacturer was modified for the coupled transcription-translation in the following way: ribosomes from the S30 extract were pelleted by centrifugation - 2 h at 31,000 rpm at 4 °C, in a Beckman MLS-50 rotor (Beckman-Coulter) using an Optima Max tabletop ultracentrifuge (Beckman-Coulter). The supernatant was carefully removed (S100 extract) and added to FPLC purified ribosomes. Two types of purified ribosome preparations were used: we either used an aliquot of the ribosome containing fraction eluted from the QA column, or we concentrated the eluted ribosomes by centrifugation - 2 h at 31,000 rpm at 4 °C, in a Beckman MLS-50 rotor (Beckman-Coulter) using an Optima Max tabletop ultracentrifuge (Beckman-Coulter) and resuspended them in ribosomal buffer prior to the assay. Purified ribosomes were supplemented with a complete amino acid mix, the appropriate amount of the "Premix" supplied with the kit and an appropriate amount of the S100 extract. Their ability to produce firefly luciferase was compared to that of the luciferase control, which was synthesised as specified by the manufacturer.

Bioluminescence of the synthesised firefly luciferase was measured by adding 20µl of Luciferase Assay Reagent (Promega) to the assay mixtures that have been adjusted to a final volume of 1 ml in phosphate-buffered saline. Raw data were collected in duplicate over a period of 30 s using a Berthold AutoLumat LB953 tube luminometer.

2.4.3 [^{3}H]-erythromycin binding assay

The assay was carried using a modification of the protocol described by Maguire *et al.* (2008). Briefly, FPLC purified ribosomes were concentrated by using 3,000 Da molecular size cut-off centrifugation filters (Amicon) to a final volume of 100 µl. The ribosomes were resuspended in 10 ml of ribosomal buffer (see 2.3.1) and concentrated again using the size exclusion filter to 100 µl. 10 µl aliquots of ribosomes were incubated for 15 minutes with 1, 0.5, 0.2 or 0.1 µCi of [N-methyl-^{3}H]-erythromycin (American Radiolabelled Chemicals). After the incubation the reaction mixture was filtered onto a glass fibre disc (GF/C, ϕ13 mm, Millipore). Unbound [^{3}H]-erythromycin was washed off with 5 ml of ethanol. The ribosome bound radiolabel was determined by transferring the washed filter into a scintillation vial with 3 ml of UltimaGold scintillation liquid (Perkin-Elmer) and measured using a Wallac scintillation counter (Perkin-Elmer). Raw data were collected in duplicate over a period of 5 min using the pre-set parameters for ^{3}H.

2.5 Mass spectrometric analysis of peptides

2.5.1 Trypsin digestion

Protein samples were concentrated using acetone precipitation (see 2.2.1) and resuspended in dH_2O. A fraction of the suspension was used to determine the concentration of proteins in the sample (see 2.2.1.1). TPCK Trypsin (Applied Biosystems) was added so that it corresponded to 1/40 of the protein present (for

example 2.5 μg of trypsin added to 100 μg of protein). The mixture was incubated at 37˚C overnight (12-16 h). The digest was used for HPLC-MS analysis.

2.5.2 iTRAQ labelling

Protein content was quantified prior to acetone precipitation and 100 μg of protein was precipitated and resuspended in 20 μl of dissolution buffer provided in the iTRAQ labelling kit (Applied Biosystems). The samples were labelled with the isobaric 8plex iTRAQ reagent (Applied Biosystems) according to the manufacturer's protocol. Briefly, protein samples were reduced with tris-(2-carboxyethyl) phosphine, cysteine-blocked with methyl methanethiosulfonate and digested with trypsin overnight at 37˚C. The content of one iTRAQ reagent vial was added to each sample, allowed to react and all samples were combined after labelling. In total we analysed ribosomal peptides isolated from four FPLC purifications and three sucrose gradient ultracentrifugations for method comparison (see 4.6.2). Two FPLC-purified samples were analysed for each of the following conditions during the compositional analysis (see 4.7): wild type *Msm* log phase, wild type carbon starvation, wild type hypoxia, ΔdosR hypoxia.

2.5.2.1 Sample cleanup

Peptides were purified using an iCAT Cation Exchange Cartridge (Applied Biosystems) to remove chemicals that may interfere with mass spectrometry. The eluent was vacuum-dried in a SpeedVac, resuspended in 100 μl of distilled water and used for mass spectrometric analysis.

Solid phase supports based on octadecyl reversed phase (C18) chemistry such as C18 ZipTip (Millipore) and C18 SepPak (Waters) were assessed as possible alternatives to ion exchange chemistry for sample cleanup. The materials were used on peptide samples following the manufacturer's protocol.

2.5.3 HPLC of peptides

Samples were loaded on a Zorbax SB-C18 5 μm, 35 × 0.5 mm (Agilent) trap column and washed for 60 min using 96.7% water: 3% acetonitrile: 0.3% formic acid; the extended wash was to remove residual KCl remaining from the ion exchange purification step (introduced in the elution buffer used – provided by the manufacturer). Peptides were separated using a Zorbax 300SB-C18 5 μm, 150 × 0.3 mm capillary column (Agilent) at a flow rate of 5 μl min^{-1} using an Agilent 1100 HPLC system. Buffer C (94.9% water: 5% acetonitrile: 0.1% formic acid) and Buffer D (94.9% acetonitrile: 5% water: 0.1% formic acid) were used for the elution of peptides according to the following program: gradient 0-30% Buffer D over 90 min, gradient 30-90% Buffer D over 10 min, 90% Buffer D for 10 min, gradient 90-100% Buffer D over 1 min and 100% Buffer D for 10 min.

2.5.4 Mass spectrometric analysis

Eluted peptides were analysed using an AB2000Q-TRAP mass spectrometer (Applied Biosystems) equipped with a Turbo Spray Ion source at 150˚C and controlled using Analyst software (version 1.5.1, Applied Biosystems). Data were collected with an IDA method consisting of a survey scan (350 m/z to 1200 m/z), an enhanced resolution scan and four enhanced product ion scans (100 m/z to 1500 m/z). Dynamic background subtraction was used prior to ion selection; the four most abundant doubly or triply charged ions were selected for the product ion scans.

2.5.4.1 Mass windows

To increase the depth of sample coverage we divided the mass range of the initial survey scan into distinct mass windows. The same sample was run multiple times with different mass ranges for the survey scan for each sample. The mass ranges used were: 325-400, 400-500, 500-550, 550-600, 600-650, 650-700, 700-800, 800-900, 900-1200 m/z. The survey scan was followed by an enhanced resolution scan and four enhanced

product ion scans. As for the full IDA method we used dynamic background subtraction prior to ion selection; the four most abundant doubly or triply charged ions were selected for the product ion scans.

2.5.4.2 Data analysis

The resulting spectra were analysed and quantified by ProteinPilot software (version 2.0.1 revision 67476, Applied Biosystems/MDS SCIEX). Specifically, spectra were assigned with the Paragon algorithm (default parameters) using a custom FASTA protein database containing all predicted proteins encoded by the *Msm* genome (downloaded from cmr.jcvi.org), and a collection of common contaminants (database released on 11/07/2007 by Applied Biosystems). Proteins were identified and quantified using the ProGroup algorithm (Unused ProtScore of less than 1.3 – 95% confidence), the quoted significance values were obtained with the inbuilt statistical analysis tool.

ProteinPilot calculated ratios of label abundance for the measured peptides were used to plot the distribution of peptides from the 30S and the 50S ribosomal subunits (see 4.6.1.3 and 4.7.2.1). The significance of the difference of the distributions was calculated using a two-tailed, unpaired, Student T-test.

2.5.5 Multiple reaction monitoring approach to specific protein detection

To enhance the sensitivity of detection for specific peptides derived from MSMEG_1878, MSMEG_3935 and ribosomal proteins S2 and L7/12 we modified the detection method by implementing a multiple reaction monitoring (MRM) approach. In this approach the survey scan is performed as normal, and is followed by an MRM acquisition method based on the detection of specific mother ion → daughter ion transitions (see Table 2.5). We tested six peptides identified *in silico* as possible candidates for MRM analysis. Three peptides with good signal intensity and well-defined chromatography were used for

analysis – shown in bold in table 2.5. Only ions with ion transitions corresponding to these peptides were recorded.

TABLE 2.5 Peptides used for MRM analysis

MSMEG_1878[a]

Retention time	*Peptide*	*Parent ion m/z*	*Daughter m/z*
25.1 min	**DPLAGLDVSR**	521.8	717.5, 646.4, 830.6, 589.3
21.1 min	**TPVSLAEATAK**	544.5	790.4, 889.6, 703.6, 590.5
21.6 min	**NVEVPDHFR**	556.8	671.5, 899.5, 770.6, 459.4
	TMVVEDDR	482.2	
	YNDGVAEHEPGR	672.3	
	TIYLFDVELDHER	825.4	

MSMEG_3935[a]

Retention time	*Peptide*	*Parent ion m/z*	*Daughter m/z*
13.0 min	**GGVPAEAGR**	407.2	600.4, 503.3, 432.0, 303.4
13.9 min	**AQVEGVNAR**	472.2	744.5, 645.4, 516.4, 459.4
24.8 min	**YDGHYGLITPADG**	689.8	359.3, 460.0, 1020.6, 919.6
	GTGFAAVLYK	513.8	
	RPGYFFPRPPEER	750.9	
	LGLLGLPFLFYIDAAEGR	983.0	

Ribosomal proteins S2 and L7/12[a]

Retention time	*Peptide*	*Parent ion m/z*	*Daughter m/z*
24.9 min	**VIASAVAEGLQAR** (S2)	642.9	673.4, 744.4, 843.4, 544.4
	VPSAVNVVDTNK	657.9	
35.5 min	**LSTEELLDAFK** (L7/12)	633.3	706.4, 835.5, 964.5, 1065.6
	DLVDSAPKPLLEK	712.9	

[a] Peptides used for detecting the proteins in samples are shown in bold.

2.6 Nucleoside analysis

2.6.1 induction of oxidative stress

Bacteria were grown under hypoxic or normoxic conditions as described above. Oxidative stress was induced by the addition of the appropriate amount of H_2O_2. For the *in vitro* oxidation of purified nucleic acids we incubated tRNA in the presence of 100 μM H_2O_2, 1 μM Fe^{2+} and 10 μM ascorbic acid at 37°C for 1 h. tRNA was precipitated by the addition of sodium acetate (final concentration 300 mM) and ice-cold ethanol (2.5-fold total volume). RNA was retrieved by centrifugation (12,000 × *g*, 10 min at 4°C) and washed with ice-cold 70% ethanol.

Methylene blue photo-oxidation prior to nucleoside analysis was performed as follows: methylene blue was added to 250 ml of *Msm* culture (OD_{600} of 0.1) to a final concentration of 2 μg ml-1 (6.25 μM). The cultures were grown for 7.5 hours at 37°C on an orbital shaker (200 rpm) while exposed to a wall mounted neon light – the inbuilt light of the incubator room was used.

2.6.2 Nucleic acid extraction

Nucleic acids used for nucleoside analysis were extracted from suitably treated cultures by resuspending the harvested cells in 500μl of GLT buffer (3 M guanidine thiocyanate, 0.2% [*w/v*] n-laurylsarconate, 20 mM Tris-HCl [pH 7.5], 10 mM deferoxamine mesylate). The suspension was transferred to a 1.5 ml screw-cap tube containing 1/3 acid washed silica beads (0.1 mm, Sigma). The cells were lysed by bead-beating (2 × 1 min), using a mini beadbeater (Biospec products). After cell lysis 500 μl of phenol : chloroform : isoamyl alcohol (25:24:1, Fluka) was added and the suspension was kept on ice for 10 min with occasional vortexing. The suspension was then centrifuged (12,000 × *g*, 15 min at 4°C) the aqueous phase was collected and washed with 500 μl chloroform : isoamyl alcohol (24:1, Fluka) and centrifuged again (12,000 × *g*, 15 min at 4°C). Nucleic acids were precipitated by adding 500 μl of ice-cold isopropanol to the aqueous phase and incubating at -80°C for 1 h followed by a centrifugation (10,000 × *g*, 10 min at 4°C). The pellet was washed with ice-cold 70% ethanol and centrifuged again (7,500 × *g*, 5 min at 4°C). The pellet was air-dried and resuspended in 25μl of DEPC-treated water.

2.6.3 nucleic acid digestion

Nucleic acids were quantified spectrophotometrically (see 2.2.4.3) and an equal amount was used for each experiment. The volume of each sample was adjusted to 85 μl. 10 μl of Nuclease P1 (0.4 U/μl, MP Biomedicals) and 5 μl of shrimp alkaline phosphatase (1 U/μl, Promega) were added to each sample and hydrolysis was carried out at 50°C for 60 min.

The samples were then spun briefly and transferred to a Micropure-EZ filter (Millipore) and centrifuged at 16,000 × *g*, until most of the liquid was collected (approximately 15 min).

2.6.4 HPLC

All nucleosides used as chromatographic standard were obtained from Sigma, with the exception of 8-hydroxyguanosine, which was obtained from Berry and Associates.

2.6.4.1 HPLC prior to mass spectrometry

Samples were separated on a Gemini 3 μm C6-phenyl 150 × 3 mm (Phenomenex) column at a flow rate of 0.2 ml min^{-1} using an Agilent 1100 HPLC system. The chromatography was performed in isocratic mode using a mobile phase consisting of 94.9% water: 5% methanol: 0.1% formic acid. The eluent was analysed using a diode array UV detector (Agilent) and a AB2000Q-TRAP mass spectrometer (Applied Biosystems) – see section 2.6.5.

2.6.4.2 HPLC prior to electrochemical detection

Samples were separated on a Pursuit 3 μm pentafluorophenyl (PFP) 150 × 4.6 mm (Varian) column with a Pursuit 3 μm PFP metaguard column (Varian) at a flow rate of 0.3 ml min^{-1} using a Dionex Ultimate 3000 HPLC system. The chromatography was performed in isocratic mode using a mobile phase consisting of 92% 50 mM sodium acetate (pH 5.3) : 8% methanol. The eluent was analysed using a variable wavelength UV detector set to 260 nm (Dionex) and a Coulochem III electrochemical detector (ESA Inc) – see section 2.6.6.

In addition to the Gemini C6-phenyl and the Pursuit PFP columns we also tested the chromatography using an Acclaim 120 3 μm octadecyl (C18) 150 × 4.6 mm (Dionex) column. This column was used in isocratic mode with a mobile phase consisting of either

94.9% water: 5% methanol: 0.1% formic acid or 92% 50 mM sodium acetate (pH 5.3) : 8% methanol.

2.6.5 Tandem mass spectrometry

The chromatographic eluent was analysed on an Applied Biosystems Q-TRAP mass spectrometer (Applied Biosystems) using a turbo spray source. All ions were detected in positive mode using a multiple reaction monitoring (MRM) method. The investigated transitions and collision energies are listed in table 2.6. Sensitivity was increased by prolonging the dwell time for transitions corresponding to 8-hydroxyguanosine and 8-hydroxy-2'-deoxyguanosine (250 ms and 100 ms respectively rather than 20 ms).

TABLE 2.6 m/z transitions and collision energies for nucleoside analysis

Nucleoside	*Mother ion (m/z)*	*Daughter ions (m/z)*	*Collision energy (eV)*
Adenosine	268.1	136.0	40
2'-deoxyadenosine	252.0	136.0	45
2'-deoxyguanoinse	268.1	135.0	45
		152.0	19
Guanosine	284.1	135.0	49
		152.0	21
8-hydroxy-2'deoxyguanosine	284.2	140.0	39
		168.0	19
8-hydroxyguanosine	300.1	140.0	43
		168.0	21
Pseudouridine	245.1	125.0	21
		209.1	15

2.6.6 Electrochemical detection

The chromatographic eluent was analysed using a Coulochem III electrochemical detector with a coulometric direct current analytical cell. The range of the detector was adjusted according to the abundance of the species that was analysed. The filter value was set to 5.0 s and the signal output was set to 1.0 V. A guard cell was installed online and set to +900 mV to pacify the mobile phase.

2.6.6.1 Hydrodynamic voltammograms

Hydrodynamic voltammograms (HDV) were used to determine the correct potential to be used for the identification and quantitation of analytes. HDVs were acquired by setting the cell to a range of potentials from 0 to +900 mV. The potential was increased in 50 mV increments after each injection, the amount of sample was constant (approximately 100 ng on column).

2.6.6.2 Nucleoside detection

A coulometric cell has two glassy carbon electrodes; the first was set to a potential of + 400 mV and the second to a potential of + 800 mV. The majority of nucleosides in the sample cannot be analysed with electrochemical detection, however 8-hydroxyguanosine and 8-hydroxy-2'-deoxyguanosine are readily oxidised at + 400 mV, while guanosine and 2'-deoxyguanosine can be oxidised at + 800 mV.

2.6.7 Sample quantification

Samples were quantified by first establishing standard curves for each nucleoside of interest. Standard curves were obtained by using a dilution series (2-fold) of a mixture of chromatographic standards whose relative abundance reflected that of biological samples. The abundance of unmodified nucleosides exceeds that of 8-hydroxylated nucleosides approximately 10^5-fold, therefore the two types of nucleosides have to be

analysed in two separate runs to ensure that the analytes are within the dynamic range of the instrument.

Unmodified nucleosides (adenosine, guanosine, 2'-deoxyguanosine) were quantified using UV absorbance at 260 nm. 8-hydroxylated nucleosides were quantified using mass spectrometry (see Table 2.6) or electrochemical detection. These two detection methods were also used on unmodified nucleosides to confirm their identity.

2.7 Trash experiment

2.7.1 Phage stock preparation

For the initial preparation a single plaque of ϕMycoMarT7 was picked and resuspended 100 μl of MP buffer (50 mM Tris-HCl [pH 7.5], 150 mM NaCl, 10 mM $MgSO_4$, 2 mM $CaCl_2$). 500 μl of normoxic stationary phase *Msm* cells were harvested and washed in MP buffer, and resuspended in 200 μl of MP buffer. The phage suspension was mixed with 200 μl of *Msm* cell suspension and 3.5 ml of molten (42˚C) 0.6% agarose prior to plating on LB plates. The plates were incubated at 30˚C for two days. Phage was harvested by inundating the plate with 5 ml of MP buffer and incubating on a rocking platform at 4˚C for 4 h. The buffer, now containing phage, was collected and filtered through a 0.2 μm syringe filter (Sartorius). The amount of phage titrated by spotting 10 μl 10-fold serial dilutions onto a lawn of *Msm*. Lawns were prepared by resuspending 200 μl of MP washed cells in molten (42˚C) 0.6% agarose and pouring the mixture onto LB plates.

The final stock was prepared by setting up several plates using sufficient phage to obtain "lacy" lawns of *Msm* (Murry *et al.*, 2008). The titre of the stock was usually approximately 10^{10} plaque forming units (pfu) ml^{-1}.

2.7.2 Transposon mutant library construction

The protocol used for the generation of an extensive transposon mutant library was adapted from Murry *et al.*, (2008). *Msm* cells were grown at 37˚C until mid- to late log phase (OD_{600} 0.8-1.0). 50 ml of culture was harvested by centrifugation (6,000 × *g*, 10 min at room temperature) and the cells washed in warm (42˚C) MP buffer twice. Finally the cells were resuspended in 5 ml of warm (42˚C) MP buffer and approximately 10^{11} pfu of ϕMycoMarT7 were added to the cells. The mixture was incubated at 42˚C for 4 h, and the transductants were frozen in multiple aliquots. Prior to freezing a sample was taken and used to determine the number of transductants by spotting 4 x 10 μl of a serial dilution onto plates containing 20 μg ml^{-1} of kanamycin.

3. Persistent Physiology

3.1 Introduction

Both oxygen and nutrient starvation can be used to investigate the mechanisms involved in the establishment of the NRP state (Wayne and Hayes, 1996, Primm *et al.*, 2000, Hampshire *et al.*, 2004). Wild type *Mycobacterium smegmatis* (*Msm*) cells were shown to be able to survive prolonged periods of oxygen (O'Toole *et al.*, 2003) and nutrient starvation (Smeulders *et al.*, 1999) and are therefore able to maintain an intact and functional complement of macromolecules even when not actively growing. Importantly, ΔdosR *Msm* was shown to have a survival defect during hypoxic stasis, but not during carbon-starved stasis (O'Toole *et al.*, 2003) a fact that could be exploited to tease out information regarding the mechanisms by which macromolecular stability is achieved during hypoxia.

We chose to work with *Msm* because it offers a number of advantages as an experimental organism when compared to *Mtb* and *Mbo* BCG. There are fewer biological safety considerations – *Msm* is a Biological Safety Class I organism (*Mbo* BCG is a Class II while *Mtb* is a Class III organism). It has a considerably shorter generation time – 3 h (24 h in case of *Mbo* BCG and *Mtb*), while still offering a reasonable degree of physiological similarity (O'Toole *et al.*, 2003). Importantly, all the relevant strains - ΔdosR and the complemented strain were available within the laboratory. Overall, *Msm* is well suited for the development of experimental approaches, whose implementation can provide the foundations on which to base future work on *Mbo* BCG and *Mtb*.

The aim of this chapter was to gain an understanding of stationary phase physiology of *Msm* so that we would be able to interpret future experiments investigating ribosomal stability. We started by assessing the long-term viability of hypoxic and carbon starved *Msm* cultures (section 3.2), and their ability to withstand nucleic acid damage (section 3.3). We also investigated the level of biosynthesis that occurs in the energy-starved context of hypoxic stasis (section 3.4), as knowledge of the

biosynthetic activity would be instrumental in assessing the importance of macromolecular stability during stasis.

3.2 Stationary phase survival

3.2.1 Long-term viability of Msm

We started our experimentation by determining the viability of *Msm* during prolonged hypoxic and carbon-starved stasis.

3.2.1.1 Persistence model parameters

In the Wayne hypoxia model, cells are grown in tightly sealed vessels with a headspace ratio of 0.5[3] and constant stirring. The rate of equilibration between the gas and liquid phases can be controlled to ensure a gradual depletion of oxygen – necessary to maintain viability during prolonged hypoxic stasis (Wayne and Hayes, 1996). We used a slightly modified Wayne model where we grew the cultures in a shaking incubator, rather than in stirred tubes. We used a slower shaking speed (150rpm) to counter the negative effects of rapid oxygen depletion (Wayne and Hayes, 1996). By using these modifications we were able to establish oxygen-starved cultures whose growth stopped when they reached an optical density (OD_{600}) of 0.35 - 0.40, corresponding to approximately 4.5×10^7 colony forming units (cfu ml^{-1}). On average we observed that viability decreased at a rate of $1.4\times10^6 \pm 7.6\times10^5$ cfu day^{-1} in wild type *Msm* during hypoxia (see Fig. 3.1), which usually corresponded to a 10-fold decrease in cfu over a period of 35 days. The rate of loss of viability during our version of the Wayne hypoxia model was less than that observed by O'Toole *et al.* (2003) and less than that reported for *Mtb* by Wayne and Hayes (1996). We therefore concluded that the depletion of

[3] Headspace ratio of 0.5 refers to the fact that the air in the sealed vessels occupies half of the volume of the medium ie a third of the total volume of the vessel.

oxygen under these conditions occurred slowly enough to allow cells to adapt in a way that was compatible with prolonged survival in hypoxic stasis.

We induced carbon-starved stasis by growing cells in defined Hartmans-de Bont's medium supplemented with 0.04% glycerol (*w*/*v*). This concentration of glycerol was used because it was shown to limit growth by carbon starvation in *Msm* in previous studies (Smeulders *et al.*, 1999). We observed that cultures usually reached stationary phase at an OD_{600} of 1.0 (approximately 1.0×10^{9} cfu ml^{-1}). On average we observed that there was a more contained loss of viability when compared to hypoxic cultures decreasing at a rate of $1.7\times10^{7} \pm 1.6\times10^{6}$ cfu day^{-1} (see Fig. 3.1). This rate of loss lead to a 3-fold reduction in overall number of cfu over 35 days, which was less than that reported previously (Smeulders, 1998).

3.2.1.2 Stationary phase survival of ΔdosR *Msm*

We proceeded by determining the viability of wild type, ΔdosR and ΔdosR complemented with DosR from *Mtb* ($DosR^{c}$) strains of *Msm* during prolonged hypoxia (See Fig. 3.1). Wild type and $DosR^{c}$ were found to undergo a gradual, but steady, decrease in viability during hypoxia. ΔdosR showed a severe and significant survival defect in hypoxic conditions when compared to wild type and $DosR^{c}$ ($p < 0.05$) *Msm*. We also observed an apparent increase in cfu for ΔdosR after four weeks of stasis, so that the number of cfu ml^{-1} at the end of the experiment was comparable to wild type. This effect was reported before and was shown not to occur due to the acquisition of suppressor mutations (O'Toole *et al.*, 2003), and may arise as a result of a transient establishment of dormancy (Shleeva *et al.*, 2004). Furthermore it is likely to be specific to *Msm*, as it was not observed during the studies of ΔdosR mutants in *Mbo* BCG (Boon and Dick, 2002) or *Mtb* (Leistikow *et al.*, 2010).

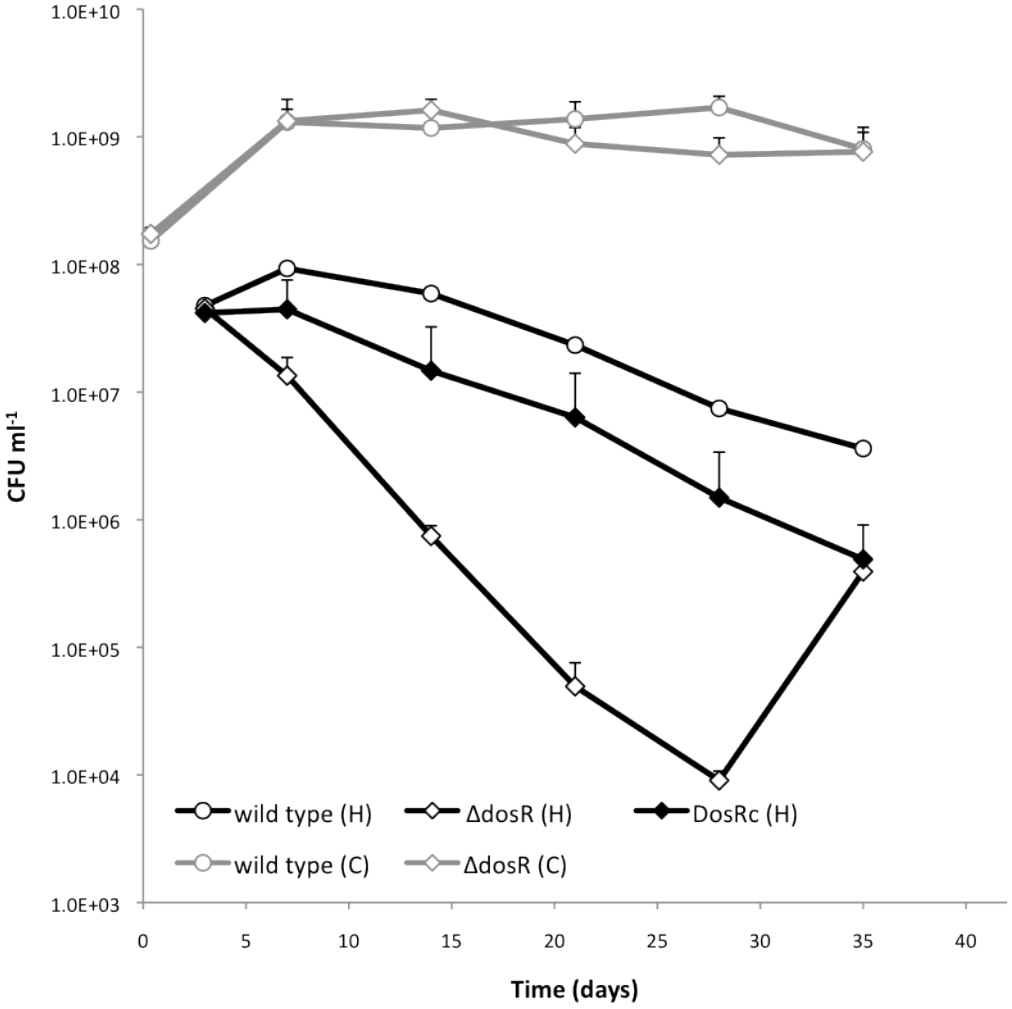


FIG. 3.1 The viability of ΔdosR *Msm* is compromised during prolonged hypoxic stasis, but not prolonged carbon starvation. Strains of wild type (○) ΔdosR (◇) and complemented ΔdosR – DosR^{c} (◆) of *Msm* were grown to stationary phase and maintained in prolonged hypoxia (H) or carbon starvation (C). The viability was determined at specific time points by plating serial dilutions and enumerating the colonies formed. Hypoxic cultures were sampled through the airtight septum using a needle, thus preserving the hypoxic nature of the cultures.

All curves represent three independent cultures that were measured in triplicate. Error bars correspond to the standard deviation (N=9).

As stated in 3.2.1.1 the decrease in cfu ml^{-1} was much less during carbon starvation than during hypoxia. Importantly the survival of ΔdosR was not significantly less than wild type under these conditions.

3.2.2 Mbo BCG ΔdosR mutant

We contacted Prof Thomas Dick in order to obtain the ΔdosR mutant strain of *Mbo* BCG constructed in his laboratory (Boon and Dick, 2002). However, we were unable to confirm the identity of the received strain as ΔdosR *Mbo* BCG. We also attempted to construct the strain by collaborating with Professor Nico Callewaert at the University of Gent. They have successfully constructed an ordered transposon mutant library in *Mbo* BCG using the MycoMarT7 phasmid (Batni *et al.*, 2009), and were able to identify three separate putative ΔdosR transposon insertion mutants. They used DNA sequencing to identify the transposon insertion site in the mutants and were able to confirm the locus for two mutants. One, which we designated "ΔdosR" B, had an insertion 41 bp upstream of the DosR gene possibly disrupting the normal expression of DosR. The second mutant, which we designated "ΔdosR" C, was found to have an insertion 550 bp downstream of the start codon which may have disrupted the DNA binding domain of DosR (see Fig. 3.2A). The insertion site for "ΔdosR" A had not been determined.

We tested the three strains using the Wayne hypoxia model. We assessed DosR activity by monitoring the expression of HspX, a major DosR regulated protein (Boon *et al.*, 2001, Desjardin *et al.*, 2001, Park *et al.*, 2003). We were able to detect HspX expression after 10 and 30 days of hypoxia in all three putative mutant strains (see Fig. 3.2B), which lead us to conclude that DosR was active in all three strains. More importantly there were no differences in viability between the mutants and the wild type strain during these experiments (data not shown).

While we did observe variation in expression levels, these were not consistent between time points, so that a decreased activity of DosR in any strain was also unlikely. The observed differences can be explained by differences in loading of SDS-PAGE. We did not pursue the construction of ΔdosR *Mbo* BCG strains any further and focused all our subsequent work on *Msm*.

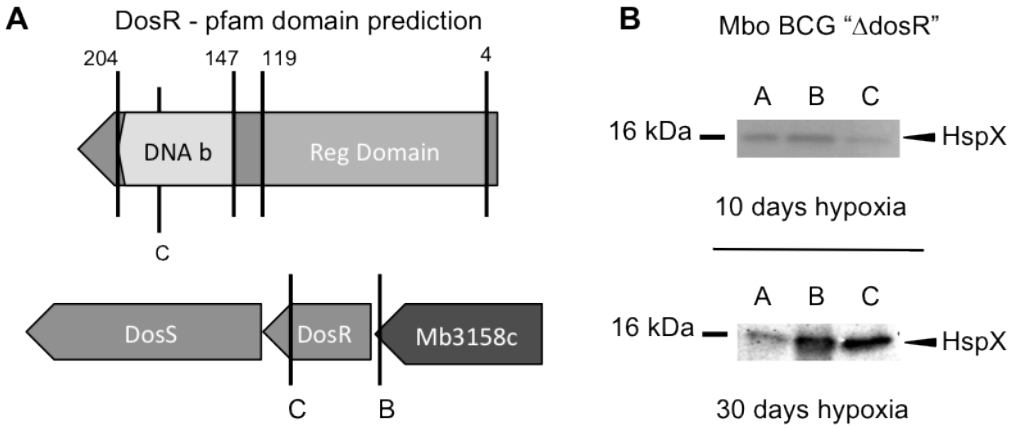


FIG. 3.2 *Mbo* BCG putative *dosR* mutants harbour active DosR. (**A**) The location of the MycoMarT7 transposon insertions in "ΔdosR" strains. The domain structure of *Mbo* BCG DosR (*Mb3157c*) as predicted by Pfam (Finn *et al.*, 2010), shows the insertion site for *Mbo* BCG "ΔdosR" C is in the predicted DNA binding domain (DNA b). The insertion site for *Mbo* BCG "ΔdosR" B is 42 bp upstream of the gene, while the insertion site for *Mbo* BCG "ΔdosR" A was not determined successfully. (**B**) Western blot analysis using α-HspX of crude cell extracts of *Mbo* BCG "ΔdosR" strains grown under hypoxic conditions for 10 and 30 days.

3.3 Toxicity studies

3.3.1 Effect of H_2O_2 on Msm growth

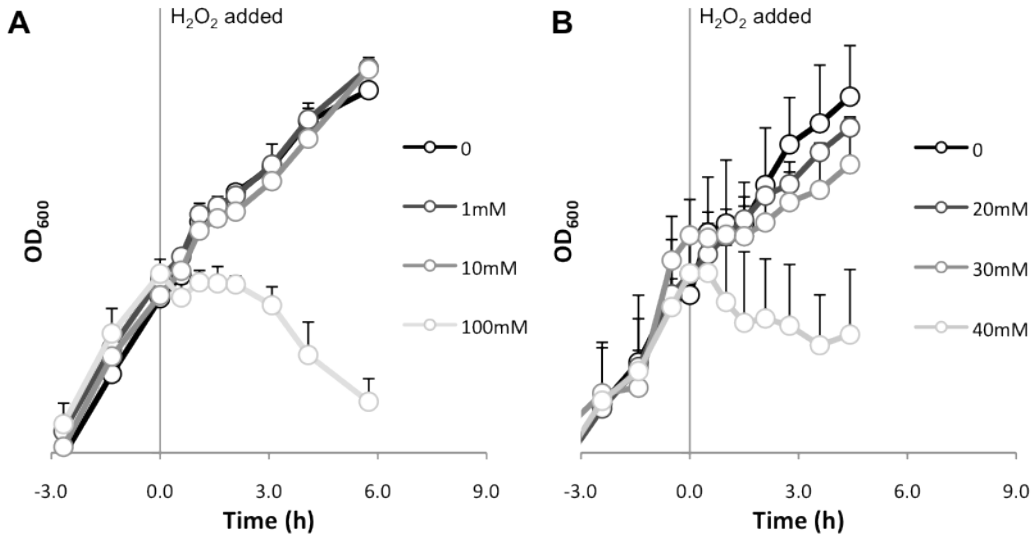


FIG. 3.3 H_2O_2 has a concentration-dependent effect on active growth of *Msm*. The growth of wild type *Msm* cultures exposed to varying concentrations of H_2O_2 1, 10 and 100 mM (**A**) 20, 30 and 40 mM (**B**) was monitored by OD_{600}.

Three independent cultures were used for each experiment. Error bars correspond to the standard deviation (N = 3).

There are a variety of different H_2O_2 concentrations in the literature that have been used to assess the ability of *Msm* to resist oxidative stress, ranging from 0.5 mM (Kurthkoti *et al.*, 2007) to 36 mM (Smeulders *et al.*, 1999). We therefore examined the exponential growth of wild type *Msm* in the presence of increasing concentrations of H_2O_2 (see Fig. 3.3). When monitoring growth by following OD_{600} alone we found that concentrations of up to 10 mM H_2O_2 did not have a discernable effect on cell growth when added to mid-exponential phase cultures at an OD_{600} of 0.4 (see Fig. 3.3). The addition of 20 mM and 30 mM H_2O_2 seemed to decrease the growth rate in a concentration dependent manner, however the overall impact on viability was limited when measured by plating (data not shown). Concentrations of 40 mM of H_2O_2 and above were found to lead to an apparent decrease of OD_{600}, due to the formation of cell clumps. The formation of clumps coincided with a large drop in viability (data not shown).

3.3.2 Susceptibility of static Msm to nucleic acid damaging agents

The ability of ΔdosR *Msm* to survive in hypoxia does not decrease immediately upon entry into hypoxic stasis – ΔdosR viability is comparable to wild type after approximately 2 days in hypoxic stasis (see Fig. 3.1). This period offers a convenient window during which the contribution of DosR to hypoxic survival can be studied. It has been reported previously that ΔdosR *Msm* strains are no more susceptible to UV induced damage than wild type during hypoxic stasis (O'Toole *et al.*, 2003). We wanted to expand on this observation and assess whether hypoxic ΔdosR cultures are any more susceptible to other nucleic acid damaging agents such as H_2O_2 or Mitomycin C. Both these agents lead to a higher level of RNA damage than DNA damage (Hofer *et al.*, 2005, Kato *et al.*, 1970), which may have important repercussions for macromolecular stability during stasis.

The experiments were carried out in the following way, we induced growth arrest by carbon starvation or hypoxia and exposed early stationary phase cultures of wild type

and Δ*dosR* and DosR^{c} *Msm* to nucleic acid damaging agents. We assessed the effect of damage on viability by using plating to determine the number of cfu ml^{-1}.

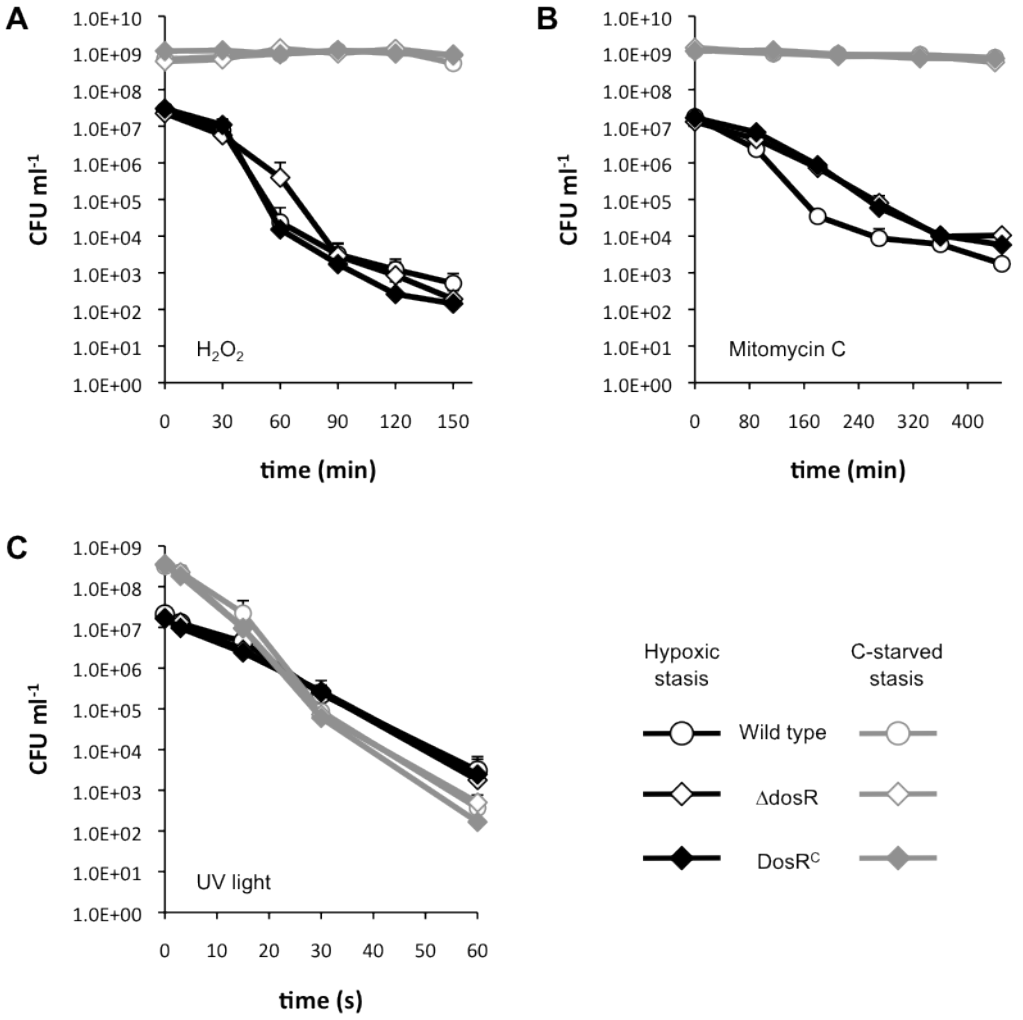


FIG. 3.4 DosR does not play a role in the resistance to nucleic acid damaging agents during stasis. Cultures of wild type (○) ΔdosR (◇) and DosR^{c} (◆) *Msm* were grown to hypoxic stasis (black) or carbon-starved stasis (grey); genotoxic stress was induced 2 days after the establishment of stationary phase by adding (**A**) 13 mM H_2O_2, (**B**) 750 or 200 nM Mitomycin C (C-starved and hypoxia respectively) and (**C**) exposing the cells to UV light. Viability was determined at specific time points by plating serial dilutions and enumerating the colonies formed. Hypoxic cultures were sampled through the airtight septum using a needle, thus preserving the hypoxic nature of the cultures. Needles were used to add H_2O_2 and Mitomycin C to the cultures. UV light stress was performed by plating cells prior to irradiation. NB Mitomycin C stress to hypoxic wild type cultures was performed using a fresh batch of Mitomycin C.

All curves represent three independent cultures that were measured in triplicate. Error bars correspond to the standard deviation (N=9).

We found that all strains were more resistant to H_2O_2 and Mitomycin C stress during C-starved stasis when compared to hypoxic stasis. The opposite appeared to be true for UV light induced stress. We did not observe any significant differences between the viability of the tested strains under carbon-starved conditions, since DosR is not involved in the physiological response to carbon starvation. There appeared to be no significant difference in the susceptibility of strains under hypoxic conditions either. Differences in survival were only observed during the exposure of hypoxic cultures to Mitomycin C (Fig. 3.4B). This is probably an artefact as a fresh batch of Mitomycin C was used for the experiment with wild type *Msm*.

3.4 Biosynthesis

3.4.1 Measuring biosynthesis by [^{3}H]-label incorporation

We were interested in the level of protein and RNA biosynthesis as proxy measures for ribosomal biosynthesis during prolonged stasis. We chose to measure biosynthesis by monitoring the level of tritium incorporation into cellular RNA and protein during prolonged stasis in order to limit the amount of radioactivity used during our experiments.

3.4.1.1 Amino acid incorporation

Protein synthesis in mycobacteria is usually measured by using [^{35}S]-methionine (Blokpoel *et al.*, 2005, Hu *et al.*, 1998). However protein synthesis has been successfully measured using [^{3}H]-leucine in environmental bacterial communities (Azam and Simon, 1989). We therefore compared the rate of incorporation of [^{3}H]-methionine and [^{3}H]-leucine into proteins precipitated by TCA (see Fig. 3.5A).

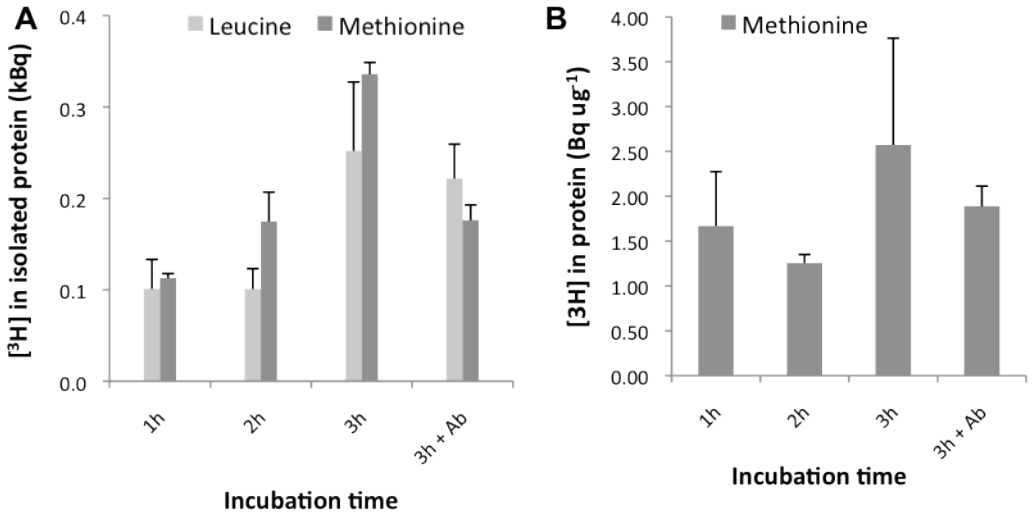


FIG. 3.5 [^{3}H]-label from [4,5-^{3}H]-leucine and [methyl-^{3}H]-methionine is poorly incorporated into proteins by *Msm*. (**A**) 37 kBq of [^{3}H]-labelled amino acids were added to early log cultures (OD_{600} ~0.2) of *Msm* wild type either in the presence or absence of streptomycin (5 μg ml^{-1}). Cellular proteins were extracted by TCA precipitation and the incorporated [^{3}H] measured by liquid scintillation. (**B**) The amount of incorporated [^{3}H]-methionine (shown in A) per μg of protein isolated.

All graphs represent three independent cultures that were measured in duplicate. Error bars correspond to the standard deviation (N=6).

Based on our data the rate of amino acid incorporation was calculated to be 16 pmol h^{-1} for [^{3}H]-leucine and 40.9 pmol h^{-1} for [^{3}H]-methionine. If we assume that the cellular composition of actively growing *Msm* is comparable to that of *Mbo* BCG (Beste *et al.*, 2005) then we would expect the rate of incorporation to be considerably higher in a 50ml culture than that observed during our experiment – namely 40.5 and 8.1 nmol h^{-1} for leucine and methionine respectively[4]. The rate of amino acid incorporation was only modestly, albeit significantly (T-test, $p < 0.05$), affected by the presence of streptomycin after three hours of incubation. However, when the level of [^{3}H]-methionine incorporation was adjusted for the overall amount of protein isolated, we found that the level of incorporation was no longer significantly different between antibiotic treated and untreated cells after 3h of incubation (T-test, $p = 0.15$). The reason for such a

[4] Assuming that the content of protein per cell increases by 24 fg h^{-1} (72.07 fg increase per doubling, divided by 3h); with leucine composing 10.16% and methionine 2.27% of total protein mass. The total number of cells at the point of addition was assumed to be 5.0×10^8 – 10^7 cfu ml^{-1} in 50 ml of culture. All parameters were taken from Beste *et al.*, 2005.

modest incorporation of [^{3}H]-labelled amino acids into protein may lay in the fact that cells were grown in LB within which unlabelled amino acids in the form of oligo peptides are abundant and could directly outcompete the incorporation of tritiated amino acids. A further possibility is that amino acids that are taken up from the medium are not used directly for incorporation into proteins, but rather enter the pool of cytosolic metabolites. This effect may be less obvious when [^{35}S]-methionine is used (Hu *et al.*, 1998, Blokpoel *et al.*, 2005) as labelled sulphur may eventually end up in proteins irrespective of the fate of the C-backbone of methionine (Tsukamura *et al.*, 1964). Based on the data presented here we decided not to use tritiated amino acids as a measure of protein synthesis during stasis.

3.4.1.2 Uracil incorporation

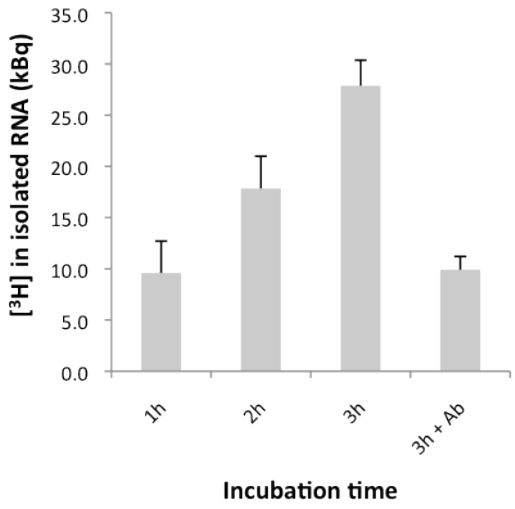


FIG. 3.6 [^{3}H]-label from [5,6-^{3}H]-uracil is incorporated readily into cellular RNA in *Msm*. 37 kBq of [^{3}H]-uracil was added to early log cultures (OD_{600} ~0.2) of *Msm* wild type either in the presence or absence of rifampicin (0.1 μg ml^{-1}). Cellular RNA was extracted with the TRIzol reagent and the incorporated [^{3}H] measured by liquid scintillation.

All graphs represent three independent cultures that were measured in duplicate. Error bars correspond to the standard deviation (N=6).

RNA biosynthesis could provide a better proxy for ribosomal biosynthesis, as 83% of cellular RNA is believed to be composed of ribosomal RNA (Cox, 2004, Beste *et al.*, 2005). We added [^{3}H]-uracil to actively growing cells and measured the amount of radioactivity incorporated into cellular RNA isolated with Trizol (see Fig. 3.6).

Using the acquired data we calculated the rate of [^{3}H]-uracil incorporation to be 8.3 nmol h^{-1}. Using similar assumptions[5] to those in section 3.4.1.1 we estimated the expected rate of incorporation to be 3.97 nmol h^{-1}. Our calculated value was higher than expected, which may be indicative a higher level of RNA and possibly protein biosynthesis level in *Msm* when compared to *Mbo* BCG. Nonetheless our observations revealed a highly linear correlation between label incorporation and time (R^2 = 0.99), which points to the fact that uracil incorporation, would provide a good method for measuring ribosomal biosynthesis.

3.4.2 RNA biosynthesis during stasis

3.4.2.1 Hypoxia

We interrogated the biosynthetic activity of wild type, ΔdosR and DosR^c strains of *Msm* during hypoxic stasis. We found that the level of [^{3}H]-uracil incorporation into RNA decreased by 99.25% ± 0.28%, immediately after the onset of hypoxic stasis when compared to actively growing cells. The levels of incorporation thereafter were several orders of magnitude smaller than during active growth (see Fig. 3.7A). The metabolic activity of the culture as a whole is therefore very low, consistent with previous observations for *Mtb* (Hu *et al.*, 2000). Importantly, the level of incorporation is not zero, suggesting that a very low but steady level of RNA biosynthesis may occur during hypoxic stasis. Interestingly the levels of label incorporation per cell in the ΔdosR strain

[5] Assuming that the RNA content per cell increases by 3.32 fg h^{-1} (9.96 fg increase per doubling, divided by 3h); with UMP composing 16.37% of total RNA mass. The total number of cells at the point of addition was assumed to be 22.5×10^8 – 4.5×10^7 cfu ml^{-1} in 50 ml of culture. All parameters were taken from Beste *et al.*, 2005.

were significantly (T-test, $p < 0.05$) higher than wild type or DosR^c (see Fig. 3.7B) after 7, 14, 28 and 35 days of hypoxia. There were no significant differences between wild type and DosR^c samples.

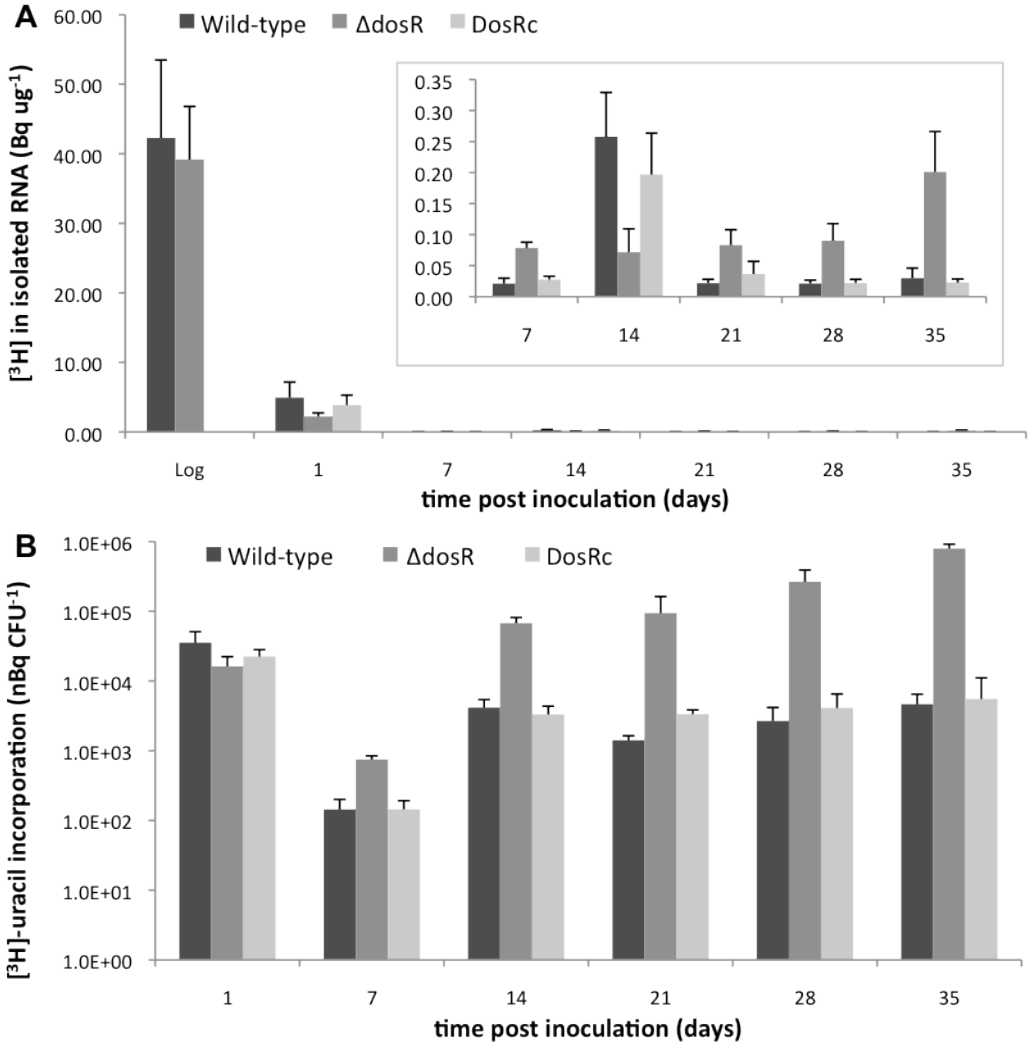


FIG. 3.7 RNA biosynthesis is reduced to a lesser extent in ΔdosR than wild type during prolonged hypoxia. (**A**) Wild type, ΔdosR and DosR^c *Msm* were grown to hypoxic stasis. At the indicated time post inoculation, 37 kBq of [^{3}H]-uracil were injected through the septum, without disturbing the hypoxic state of the culture. [^{3}H]-uracil incorporation was performed for 24 h, after which the cultures were harvested sacrificially. Cellular RNA was isolated using the Trizol reagent and the incorporation determined by scintillation counting. Cells entered NRP-1 1 day post inoculation. (**B**) The amount of [^{3}H]-uracil incorporation was adjusted to the number of CFU determined by plating. Possible dormant cells (see 3.2.1.2) were not included in the total number of cells.

All graphs represent three independent cultures that were measured in duplicate. Error bars correspond to the standard deviation (N=6).

3.4.2.2 C-starvation

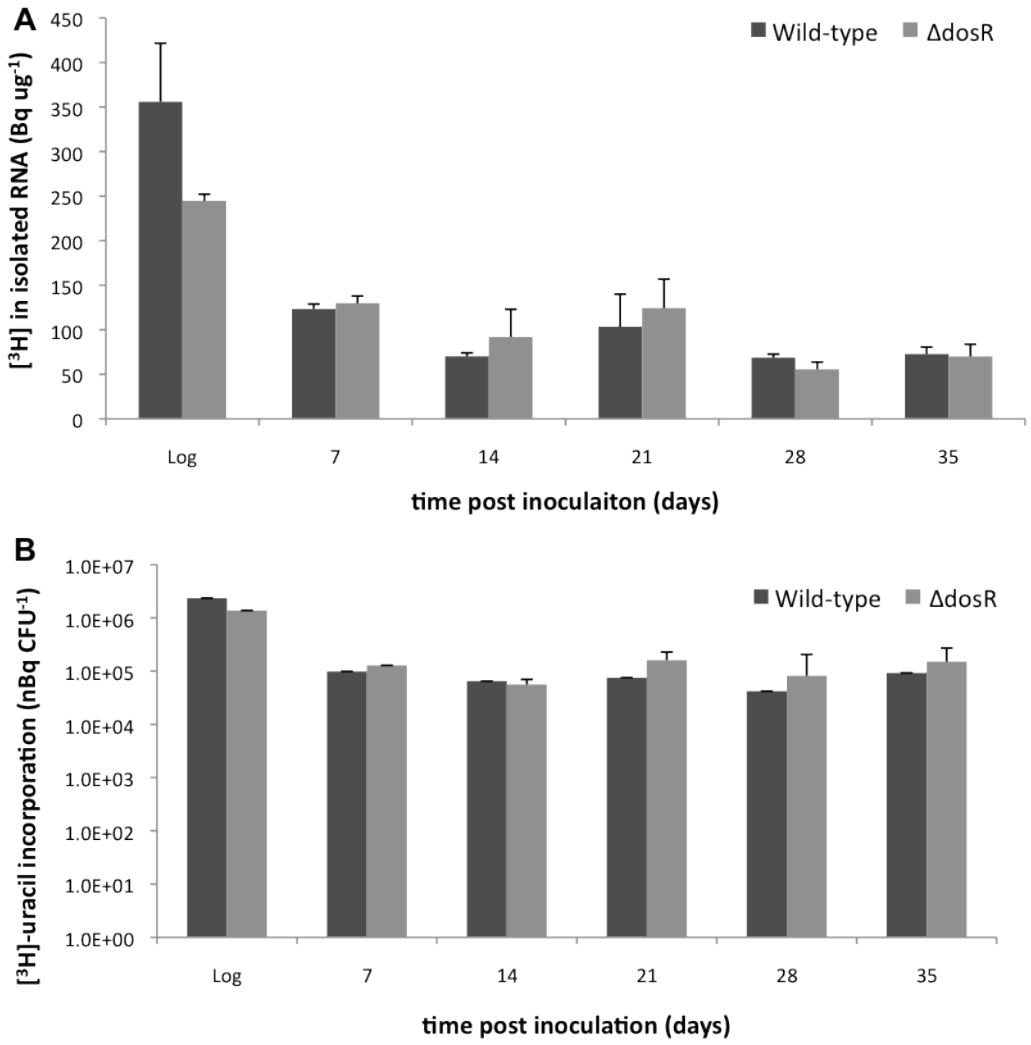


FIG. 3.8 [^{3}H]-uracil incorporation into RNA during prolonged carbon starvation. (**A**) Wild type and ΔdosR *Msm* were grown to carbon starved stasis in large cultures. An aliquot of the main culture was transferred to sterile flask at the indicated time post inoculation and 37 kBq of [^{3}H]-uracil was added. [^{3}H]-uracil incorporation was performed for 2 h, after which the cultures were harvested sacrificially. Cellular RNA was isolated using the TRIzol reagent and the incorporation determined by scintillation counting. Timepoint 0 corresponds to [^{3}H] incorporation into actively growing cells. (**B**) The amount of [^{3}H]-uracil incorporation was adjusted to the number of CFU determined by plating. Possible dormant cells (see 3.2.1.2) were not included in the total number of cells.

All graphs represent three independent cultures that were measured in duplicate. Error bars correspond to the standard deviation (N=6).

We repeated the same experiment using C-starved stationary phase cultures. Due to possibility that uracil might serve as a source of carbon for C-starved cells (Loh *et al.*, 2006) we first performed an experiment where we added 1 mM uracil to C-starved

stationary phase cultures and monitored OD_{600} to determine whether such an addition could support bacterial growth. We found no differences in the OD_{600} even after 24h incubation with 1 mM uracil (data not shown). We therefore concluded that uracil is not a carbon source that could sustain *Msm* outgrowth from stasis, so we used it to determine the level of RNA biosynthesis during C-starved stasis (see Fig. 3.8). We used wild type and ΔdosR strains during these experiments.

We found that the level of [^{3}H]-uracil incorporation into cellular RNA during active growth (time point 0) was higher when cells were grown in Hartmans-de Bont medium than when cells were grown in LB. This might be a reflection of substrate competition in LB leading to an apparently lower level of RNA biosynthesis.

Like in hypoxic stasis, the level of [^{3}H]-uracil incorporation during C-starved stasis was found to be significantly lower (T-test, $p < 0.05$) than during active growth. In contrast to hypoxic stasis, [^{3}H]-uracil incorporation was only 10-fold lower in C-starved stasis when compared to active growth (see Fig. 3.8). The difference in hypoxic cultures was between 100- and 1000-fold. There were no significant differences in the incorporation rates of wild type and ΔdosR cultures.

It is important to note that we did not observe any increase in OD_{600} after the addition of uracil to C-starved cultures, and the majority of the [^{3}H]-uracil remained in the culture supernatant even after 24h of incubation (data not shown). The high rate of [^{3}H]-label incorporation would indicate that there is significant turnover of RNA during carbon starvation, however we cannot exclude the possibility that the increased incorporation is due to the presence of [^{3}H]-uracil as a nutrient source for RNA biosynthesis. This measurement problem limits our ability to interpret these data biologically.

3.5 Discussion

3.5.1 Biosynthesis in the Wayne model of persistence

Having established that we could model persistence *in vitro*, we were able to investigate the extent to which *ex novo* RNA synthesis occurred in persistent *Msm* cells. The biosynthetic activity of *Msm* in prolonged hypoxic or C-starved stasis has been only partially addressed in the literature. The level of protein biosynthesis, measured by the incorporation of [^{35}S]-methionine, was found to be very low in *Msm* cultures during prolonged C-starved stasis (Blokpoel *et al.*, 2005). There are no records to our knowledge regarding protein synthesis during hypoxia in *Msm*. Protein biosynthesis in *Mtb*, as measured by [^{35}S]-methionine incorporation, is negligible in unperturbed hypoxic stationary phase cultures of *Mtb* (Hu *et al.*, 1998). Translation was induced when NRP cells were exposed to heat shock or oxygenation (Hu *et al.*, 1998). Work done by the same group, using [^{3}H]-uridine, suggests that RNA biosynthesis is also negligible during hypoxic stasis in *Mtb* (Hu *et al.*, 2000). It is important to point out that Hu *et al.* did not measure the rate of incorporation in hypoxia *per se*, but rather the rate of incorporation in hypoxia adapted cells that were taken out of their hypoxic environment (Hu *et al.*, 2000). This experimental design measures the capacity of cells emerging from prolonged hypoxic stasis to synthesise RNA rather than the *de facto* level of biosynthesis during hypoxia. The experimental design was different in our case. We added [^{3}H]-uracil directly to hypoxic cells without introducing any air into the culture, which should allow us to measure incorporation that occurs with minimal perturbations to the environment of the cells.

We found that the overall amount of [^{3}H]-uracil incorporated into 1 μg of RNA falls by approximately 99% concomitantly with the onset of hypoxia (24 h post-inoculation). The level of incorporation per μg of RNA then stabilises at approximately 0.01% of active growth levels. However, if we consider the amount of incorporation per

CFU, we found that the average stable level of incorporation per CFU was approximately 0.2% that of active growth for wild type and DosR^{c} strains. This rate of biosynthesis is consistent with the observation that the half-life of mRNA is significantly higher in *Mtb* during hypoxic stasis (>4h) when compared to active growth (15 min, Rustad, personal communication), lessening the need for *ex novo* synthesis.

Overall our findings regarding the physiological state of wild type cells are not surprising and are consistent with the reports in the literature. Unlike the data in the literature however, we were able to obtain a quantitative measure for a process that has been addressed only qualitatively until now.

3.5.2 ΔdosR in hypoxia

Our initial interest in the ΔdosR strain was spurred by its inability to survive during prolonged hypoxic stasis, while being able to cope with C-starved stasis.

An interesting physiological feature of the *Msm* ΔdosR mutant in hypoxia is its apparent re-growth approximately 4 weeks after the onset of stasis (see Fig. 3.1). The mechanism governing this effect has not yet been elucidated (O'Toole *et al.*, 2003, Shleeva *et al.*, 2004). Studies using the fluorescent dye carboxyfluorescin diacetate succinidimyl ester[6], which followed the proliferation of *Msm* during hypoxia, have suggested that the apparent increase in the number of viable cells is not a result of cell division (Smeulders, Emerson and Williams, unpublished data). This observation is consistent with the possibility that ΔdosR mutants are viable during hypoxia, however they are less able to form colonies on solid media than wild type, i.e. they become dormant (Shleeva *et al.*, 2004). If true the apparent drop in viability is therefore a side

[6] Carboxyfluorescin diacetate succinidimyl ester is converted to carboxyfluorescin succinidimyl ester by cellular esterases. This product is fluorescent, membrane impermeable and highly stable within the cytosol. The fluorescent intensity of each cell approximately halves at each cell division, therefore the dye can be used for following cell proliferation (Weston and Parish, 1990).

effect of the scoring method rather than a reflection of the physiological state of the mutant.

A further factor that may play a role in the apparent re-growth of ΔdosR is the presence of a second DosR homologue in *Msm*. The ΔdosR strain we used during these experiments was a knockout in MSMEG_5422 (O'Toole *et al.*, 2003). This gene was chosen because it had the highest homology to *Mtb* DosR ($e = 7.0 \times 10^{-80}$) and its genomic locus resembled that of DosR with an adjacent DosS homologue (MSMEG_5241, $e = 10^{-168}$) and two universal stress proteins homologous to Rv3134c (O'Toole *et al.*, 2003). However a bioinformatic search reveals that MSMEG_3944 also has a high homology to *Mtb* DosR ($e = 2.0 \times 10^{-70}$) and like MSMEG_5422 there is a GAF domain containing DosS homologue (MSMEG_3941, $e = 7.0 \times 10^{-67}$) and a universal stress protein in the same locus. MSMEG_5244 and MSMEG_3944 are both annotated as "DevR" and they are, together with many of the genes adjacent to them, up-regulated at low oxygen tensions (Berney and Cook, 2010). It is therefore possible that MSMEG_3944 could partially complement ΔdosR (ΔMSMEG_5244), albeit inefficiently, so that its effect can be seen only later in hypoxic stasis – approximately four weeks in our case. The fact that *Mbo* BCG and *Mtb* lack this second locus may help to explain why we do not see the same apparent increase in viability in these two strains even after prolonged hypoxic stasis.

Given that *dosR* from *Mtb* can complement ΔMSMEG_5422 it points to the fact that their activity is the same in the two organisms. This poses an important question, what role does MSMEG_3944 play during hypoxia? This is an interesting question that is worth addressing in the future, as it may help us understand *Msm* physiology during hypoxia better.

Independently of the exact mechanism behind the loss of viability of the ΔdosR strain during hypoxia, it is apparent that the physiological state of the mutant is not as

well suited to deal with hypoxia as that of the wild type (see 1.4.2.1). Surprisingly ΔdosR cultures were found to have a higher rate of [^{3}H]-uracil incorporation when compared to wild type cells. Furthermore the rate of incorporation per cell increased with time, the longer cells stayed in hypoxia (see Fig. 3.7B). This finding was counterintuitive, especially when we consider the fact that ΔdosR cells are not able to maintain stable ATP levels (Leistikow *et al.*, 2010). It is possible that these two findings are linked – an increased level of RNA biosynthesis would require additional energy, which may lead to energy depletion and eventually cell death. Does it then follow that the RNA of ΔdosR is inherently less stable?

To elaborate on the role of DosR in RNA stability during hypoxic stasis we exposed cultures to nucleic acid damaging agents – H_2O_2, UV light and Mitomycin C. We found no evidence that DosR played a role in the immediate response to nucleic acid damaging agents during hypoxic stasis. Similarly, *Mtb* ΔdosR was not found to be any more susceptible than wild type when exposed to different antibiotics, including rifampicin, during hypoxia (Bartek *et al.*, 2009). The only indication that components of ΔdosR cells may be less stable than wild type during hypoxia came from the observation that ΔdosR *Msm* was more susceptible than wild type to heat shock during hypoxic stasis (O'Toole *et al.*, 2003). Increased susceptibility to heat shock may point to decreased ability of the cell to deal with heat shock, either by a reduced activity of chaperones – the DosR regulon encodes for several chaperones including HspX and universal stress proteins that might play a role in heat shock protection (Ohara *et al.*, 1997, Tabira *et al.*, 1998, Park *et al.*, 2003, O'Toole *et al.*, 2003). It can also indicate a decreased ability of the cytosol to limit heat shock – one of the DosR regulon genes encodes for a trehalose phosphatase (Park *et al.*, 2003). A slightly more speculative explanation that would take into consideration the higher level of RNA biosynthesis in hypoxia is that perhaps ribosomes are less stable in ΔdosR mutants. There is very little evidence for this claim, however our knowledge regarding macromolecular stability

during mycobacterial persistence is very limited. We believe that addressing this gap in our knowledge may lead to interesting insights into mycobacterial physiology.

4. Ribosomal Stability in Stasis

4.1 Introduction and aims

The aim of the work presented in this chapter was to investigate the status of mycobacterial ribosomes during stasis. In it I describe the development and the implementation of analytical tools, used to address biological questions regarding the stability of ribosomes in the absence of growth.

I started by asking a simple question – what happens to the ribosome when mycobacteria enter the NRP state? The field of stationary phase ribosomal stability is best understood in *E. coli* (see section 1.4.3). Upon the cessation of growth *E. coli* degrades a significant proportion of its ribosomes (Kaplan and Apirion, 1975, Davis *et al.*, 1986, Zundel *et al.*, 2009) while stabilising the rest by way of dimerisation (Wada *et al.*, 1990, Wada *et al.*, 2000). I used a combination of ribosomal and rRNA profiling (sections 4.2-4.4) to determine whether the changes observed in *E. coli* occur also in *Msm*. Given the importance of DosR in NRP survival (see section 1.4.2.1, 3.2) I extended the investigation to testing whether there exists a correlation between DosR function and the ribosomal population of a cell in hypoxia.

I then turned my attention to the identification of the players involved in the stability of the ribosome during stasis. This included the development of a new method for purifying ribosomes (see section 4.5), combining this method with quantitative proteomics (see section 4.6), which paved the way to a global compositional analysis of the mycobacterial ribosome during active growth and stasis (see section 4.7).

Finally I describe the initial work done to characterise the putative stabilisation factors identified during the compositional analyses of ribosomes (see section 4.8).

4.2 Ribosomal profiling (method development)

The most direct way to study ribosomal populations is by ribosomal profiling. This technique relies on separating cellular components on the basis of their density, and has

been used successfully to purify mycobacterial ribosomes since the 1960s (Youmans and Youmans 1968, Baker 1972). In short, a crude cellular lysate is loaded onto a linear sucrose gradient and separated by ultra-centrifugation. After ultracentrifugation the gradients are fractionated and the presence of nucleic acids/ribosomes is detected by monitoring the absorbance at 254nm (Davies and Abe, 1995).

There was no experience with ribosomal profiling in the laboratory so we had to implement and optimise the method anew. In order to obtain biologically relevant information from our experiments we needed to make sure that we were able to generate ribosomal profiles in a reproducible manner. We focused on several parameters during the method development stages, before finally being able to achieve our goal.

4.2.1 Ribosomal profiling – sample preparation

The amount of starting material and the lysis method, influence the success of the profiling protocol. We initially attempted to obtain profiles by harvesting cells from 50ml cultures and disrupting them by bead-beating. We clarified the extract by two separate rounds of centrifugation and used the resulting lysate for profiling. The measured absorbance was very low (see Fig. 4.1A), pointing to the need for a more concentrated extract. We therefore began to use larger volumes of culture, ranging from four to seven litres, which increased the retrieved cell pellet (at least 2 g wet weight). A larger cell pellet posed the question of the optimal method for cell lysis. We compared bead beating, sonication and French press lysis. Profiles obtained using samples passed through the French press gave the highest overall signal intensity, as measured by absorbance (data not shown). High-pressure disruption was identified in a recent study to be the most efficient way to release cellular components (Rezwan *et al.*, 2007). Despite being able to load sufficient sample onto the sucrose gradient, we were unable

to resolve ribosomal subunits in our profiles (Fig 4.1B). We hypothesised that the reason for this was the composition of the lysis buffer.

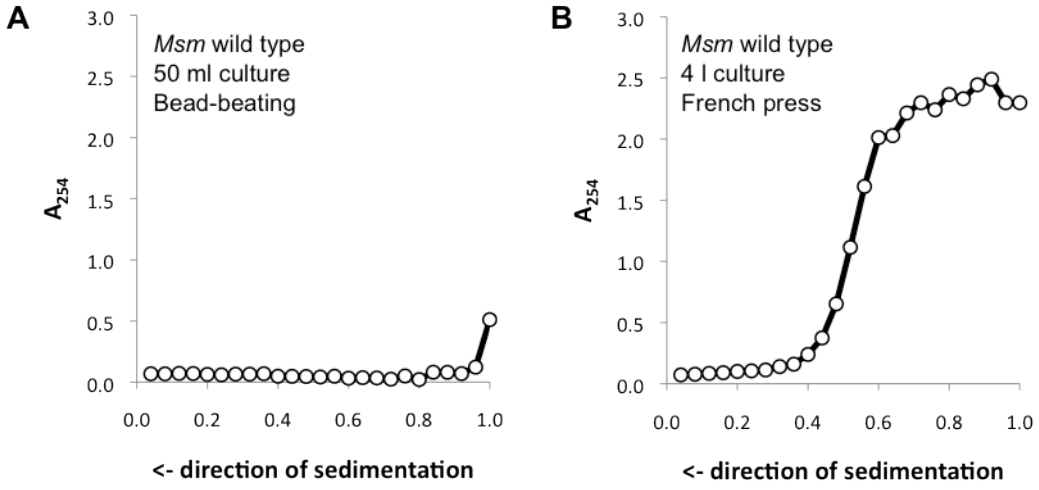


FIG. 4.1. Mycobacterial cells are lysed more efficiently by passage through the French press. *Msm* wild type cells in normoxic stasis were harvested by centrifugation and lysed by (**A**) bead beating or (**B**) French press. The extract was clarified to remove cellular debris and unbroken cells and loaded on a linear sucrose gradient (15-40%) prior to ultracentrifugation. Gradients were fractionated manually and the absorbance at 254 (A_{254}), 260 and 280 nm was determined for each fraction. Fractions are plotted as a proportion of the total number of fractions (e.g. fraction 10 of 20 corresponds to 0.5 on the plot). This was done to allow for easier comparison between experiments.

4.2.2 Ribosomal profiling – buffer composition

The lysis buffer we used initially, while commonly utilised in the laboratory for protein extraction, was not suitable to maintain intact the isolated ribosomes. An important difference between the lysis buffer used during this study and those used in reports in the literature (Baker *et al.*, 1972, Davies and Abe, 1995, Sato *et al.*, 2005) is the concentration of Mg^{2+} as well as that of Tris-HCl. While we did not use either in the formulation of the lysis buffer, Davies and Abe suggest using between 10-25 mM $MgCl_2$ and 50-200 mM Tris-HCl (pH 8.5) for the preparation of polysomes. Baker *et al.* (1972) have used 10 mM $MgCl_2$ and 10 mM Tris-HCl (pH 7.4) during their isolation of *Msm* 70S ribosomes. The concentration of $MgCl_2$ was reduced to 1 mM for the isolation of the large ribosomal subunits.

We therefore repeated the profiling experiment by resuspending the cell pellet in a ribosomal buffer adapted from Baker *et al.* (1972), containing either 10 mM $MgCl_2$ or 1 mM $MgCl_2$. We reasoned that such experimental design would allow us to interpret the obtained profiles, since ribosomal dissociation should be favoured at lower [$MgCl_2$], while 70S ribosomes should be prevalent at higher [$MgCl_2$]. We harvested exponentially growing cells, split the pellet into two parts and resuspended each in a different buffer prior to lysis with the French press. The extracts were then treated with DNAse I prior to profiling (See Fig. 4.2).

Note that all the profiles are plotted in such a way that the X-axis is in the range of 0-1, with the direction of sedimentation indicated with an arrow. This value was obtained by dividing the sequential number of each fraction by the total number of fractions collected. We chose to present our data in this format because the manual fractionation led to variation in the number of collected fractions. Over the course of our experiments the number of fractions was in the range of 23 and 31 with the median being 27. This variation was sometimes intentional, as we decreased the volume of the collected fractions, and in some cases arose due to temperature-induced changes in viscosity of the liquid, leading to an involuntary variation of fraction volume. By plotting the profiles in this way we were able to compare profiles obtained over the span of this project.

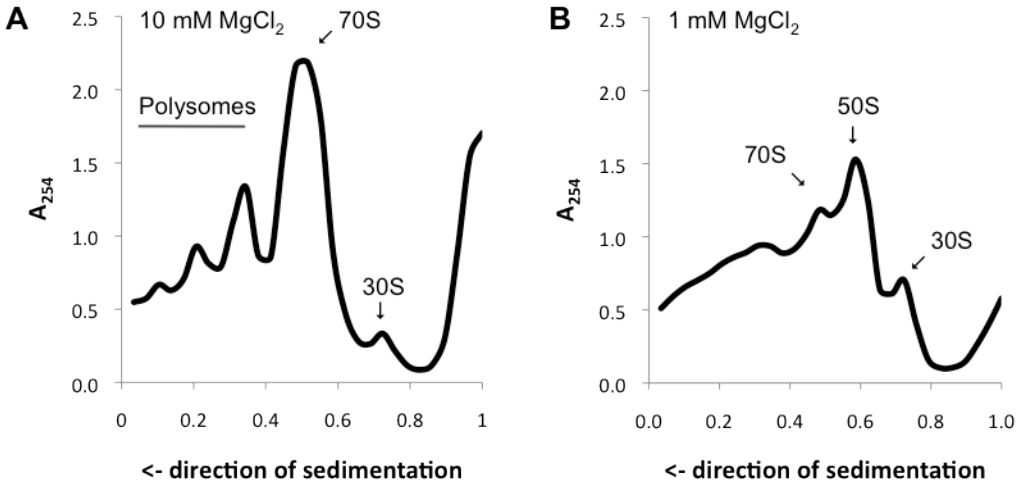


FIG. 4.2 Polysomes, intact ribosomes and ribosomal subunits form part of the ribosomal population of *Msm* during active growth. Actively growing *Msm* wild type cells were harvested by centrifugation and lysed by passage through the French press in ribosomal buffer containing (**A**) 10 mM $MgCl_2$ (favours ribosomal association) or (**B**) 1 mM $MgCl_2$ (favours ribosomal dissociation). The extracts were clarified to remove cellular debris and unbroken cells. Ribosomes were pelleted by centrifugation through a 1.1 M sucrose cushion and treated with RNAase-free DNAse prior to loading on a linear sucrose gradient (15-40%) and ultracentrifugation. Gradients were fractionated manually and the A_{254} was determined for each fraction.

Peaks in the lower 40% of the gradient were insensitive to DNAse treatment, and are therefore not due to cellular DNA. However they appeared to dissociate into two peaks of lower density in low $MgCl_2$ conditions. We concluded that the peak at the 50% mark is made up of 70S ribosomes, peaks in earlier fractions are due to the presence of polysomes, while peaks in later fractions correspond to 50S and 30S ribosomal subunits migrating at 60% and 70% of the gradient respectively.

4.2.3 Ribosomal profiling – Ultracentrifugation parameters

Once we established all the parameters for sample preparation, we turned our attention to improving the resolution of the profiles. After ultra-centrifugation we routinely measured the refraction of several fractions to confirm that our sucrose gradients did indeed follow a linear concentration gradient. An example of such a result is shown in Fig. 4.3.

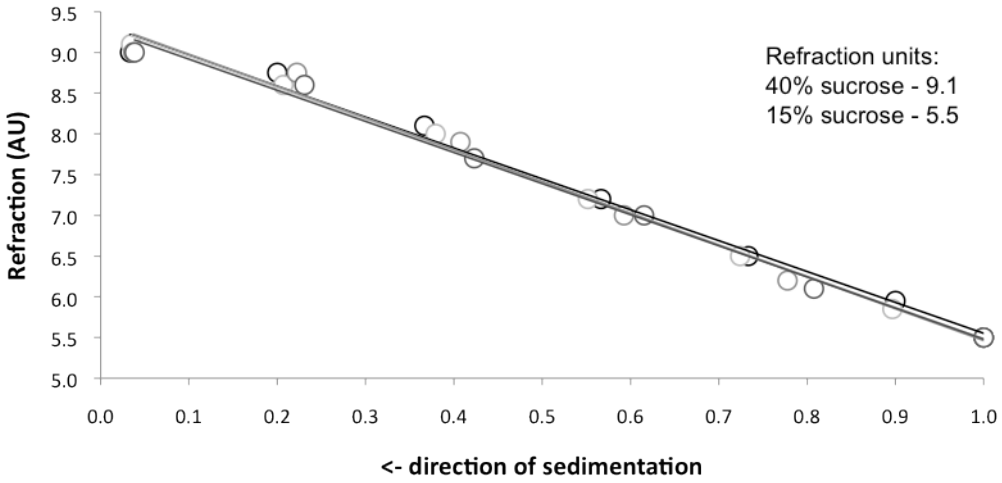


FIG. 4.3 Sucrose concentration gradients were linear. The refraction of sucrose gradient fractions was determined using a refractometer. Three representative gradients are shown. 9.1 refraction units correspond to a 40% sucrose solution, 5.5 refraction units correspond to a 15% sucrose solution.

We found that resolution was significantly improved when we introduced an additional "pre-spin" step to the profiling protocol. This step consisted of pelleting ribosomes from a crude extract through a 40% sucrose cushion. By doing so we were able to remove many of the cytosolic proteins – as illustrated by the decrease in the overall A_{254} signal in the fractions from the top of the gradient (Fig. 4.4).

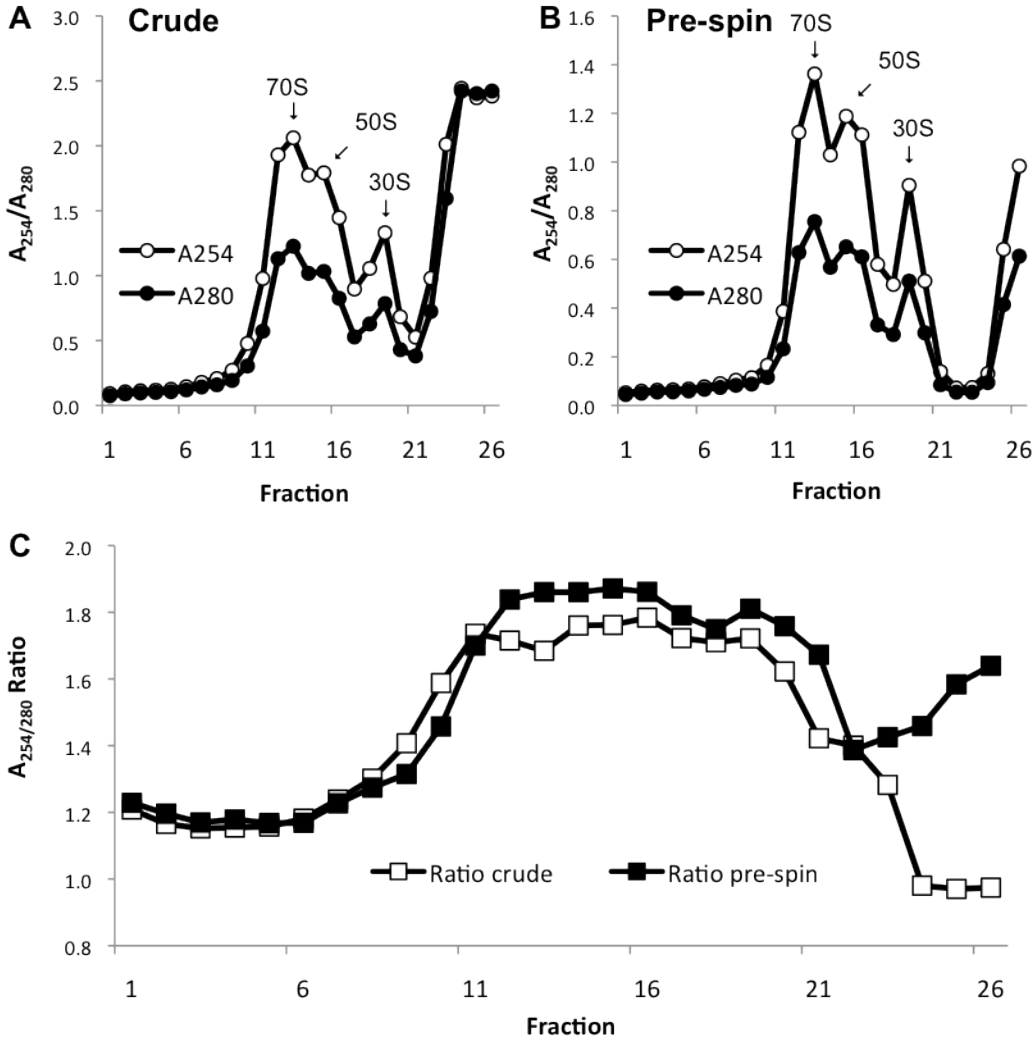


FIG. 4.4 Pre-spin improves the resolution of ribosomal profiles and removes cytosolic proteins. Actively growing *Mbo* BCG wild type cells were harvested by centrifugation and lysed by passage through the French press. The extract was clarified to remove cellular debris and unbroken cells. The extract was either (**A**) loaded directly or (**B**) the ribosomes were pelleted through a 1.1 M sucrose cushion prior to loading onto a linear sucrose gradient (15-40%) and ultracentrifugation. Gradients were fractionated manually and the absorbance at 254, 260 and 280 nm was determined for each fraction. (**C**) The ratio of absorbances at 254 and 280 nm was calculated for each sample and plotted.

As can be observed from Figs. 4.2 and 4.4 we were not able to achieve the complete separation of the different ribosomal species (30S, 50S and 70S). We attempted to improve the separation by using different concentrations of sucrose gradients (10-25%, 10-30%, 15-40%) as well as varying the time of centrifugation (3.5h and 5h respectively). We found that a shallower gradient did increase the separation between subunits, albeit at the expense of peak broadening (data not shown). We

attempted to compensate for the peak broadening effect by decreasing the time of centrifugation. However, by doing so we did not improve the resolution of the profiles (Fig. 4.5). We therefore decided to proceed with 15-40% gradients as used in initially. A summary of the final method is shown in Fig. 4.6.

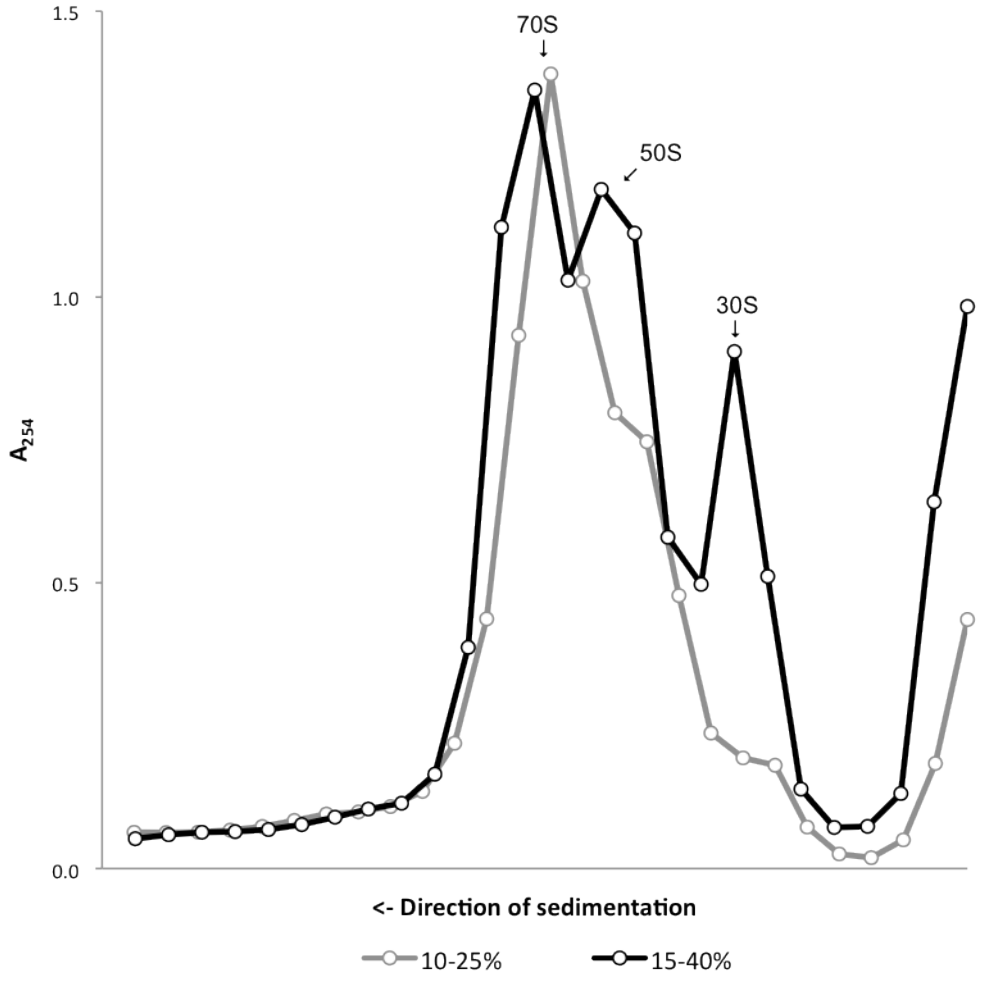


FIG. 4.5 Resolution is comparable when different combination of gradient range and spin times are used. Pre-spun ribosomal extracts were loaded on linear sucrose gradient 10-25% or 15-40% and centrifuged for 3.5 h and 5 h respectively. Gradients were fractionated manually and the absorbance at 254, 260 and 280 nm was determined for each fraction.

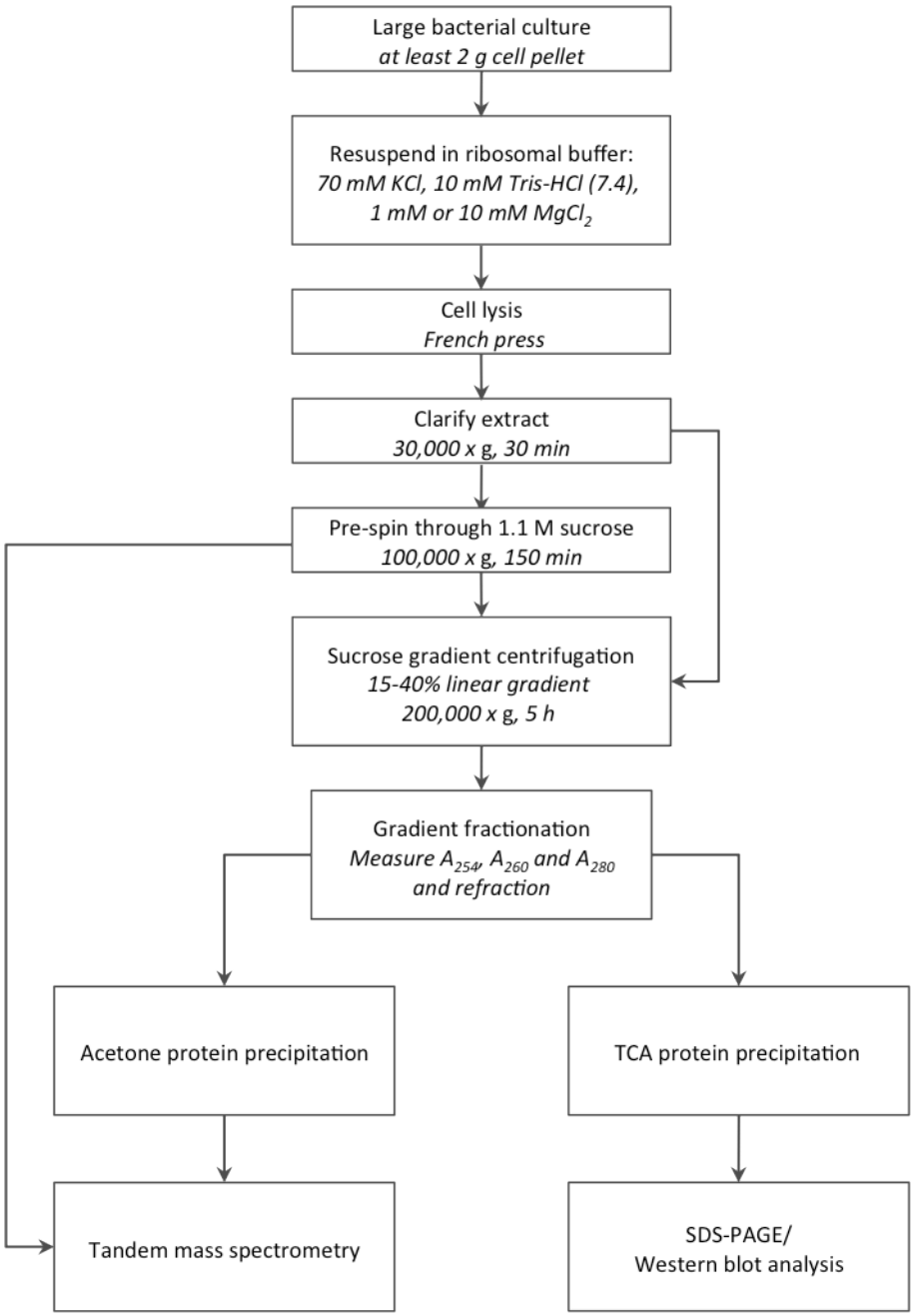


FIG. 4.6 Summary flow chart of the ribosomal profiling protocol.

4.3 Ribosomal profiling (results)

4.3.1 The mycobacterial ribosome during growth and stasis

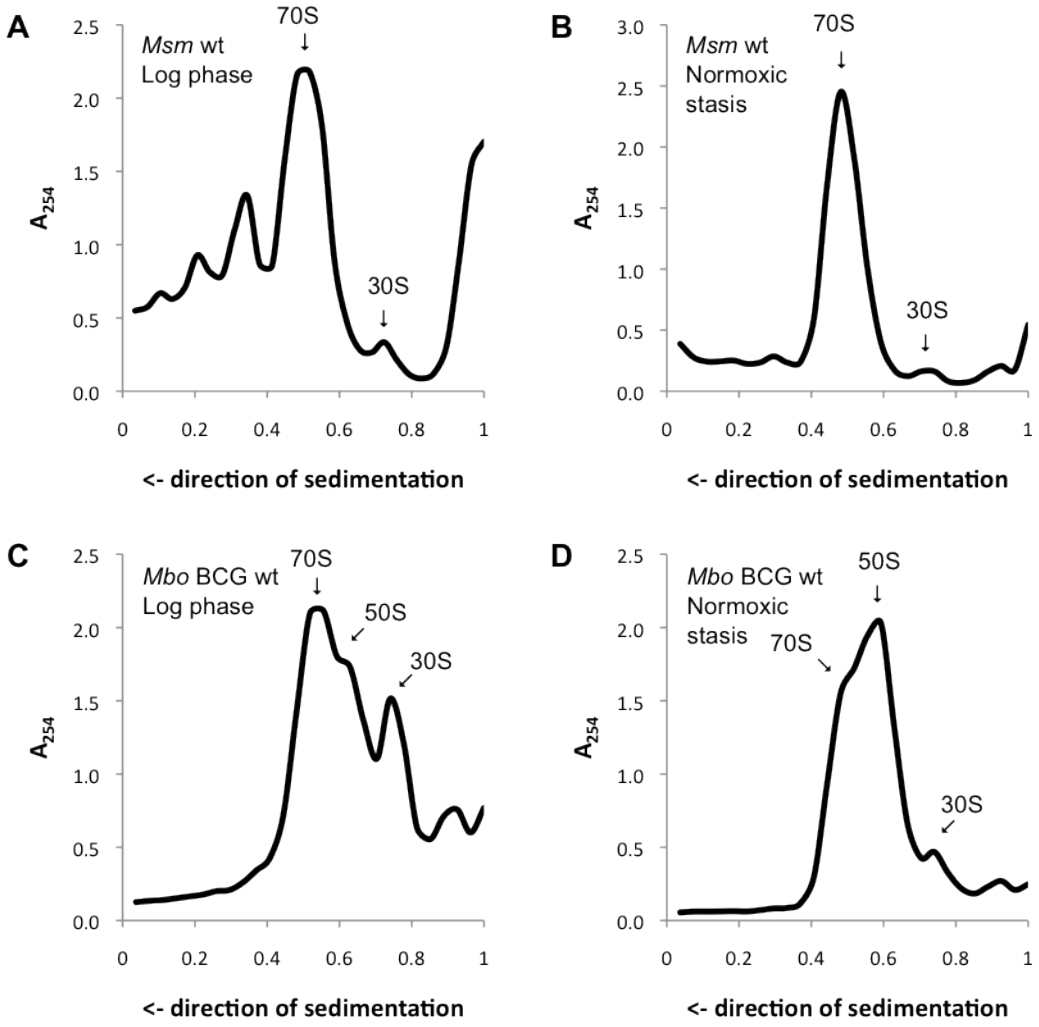


FIG. 4.7 Ribosomal profiles of actively growing and stationary phase bacteria during normoxia. (**A**) Actively growing *Msm* wild type (**B**) *Msm* wild type normoxic stationary phase (**C**) actively growing *Mbo* BCG wild type and (**D**) *Mbo* BCG wild type normoxic stationary phase cells were harvested and lysed by passage through the French press. The extract was clarified to remove cellular debris and unbroken cells, treated with RNAse-free DNAse, and the ribosomes were pelleted through a 1.1 M sucrose cushion. Pre-spun ribosomes were loaded onto a linear sucrose gradient (15-40%) prior to ultracentrifugation. Gradients were fractionated manually and A_{254} was determined for each fraction.

Each experiment was repeated at least three times, and representative profiles are shown.

In *E. coli* the transition from growth to stasis is characterised by the appearance of 100S ribosome dimers. Wada *et al.* (1990) were able to determine that entry into stasis and

ribosomal dimerisation occurs simultaneously using ribosomal profiling. The generation times of *E. coli* and even the fast growing *Msm* are significantly different – 40 min compared to 3 h. Therefore we cannot assume that the mechanism of ribosomal stabilisation is comparable in the two organisms.

Given that nothing is known about ribosomal stability during stasis in mycobacteria we chose to start our investigations by making the basic comparison of ribosomal profiles of actively growing and static cells. We carried out our analysis in *Msm* and *Mbo* BCG in order to be able to observe differences in the ribosomes of fast- and slow-growing mycobacteria (Fig. 4.7).

The population of ribosomes in exponentially growing *Msm* cells was made up predominantly of 70S ribosomes and polysomes, with almost no free 50S or 30S subunits (Fig. 4.7A). No polysomes were observed during stationary phase – ribosomes were found to be almost exclusively in the associated 70S form (Fig. 4.7B). In contrast to profiles from *Msm*, no polysomes were observed in the samples of exponentially growing *Mbo* BCG cells (Fig. 4.7C). Furthermore, there was a significant pool of dissociated ribosomal subunits, both during exponential growth and stationary phase (Fig. 4.7D), not observed in *Msm*. It is perhaps interesting to note that the level of 30S subunits is higher in the exponential pool compared to the stationary phase pool in *Mbo* BCG.

Crucially, we did not observe any evidence of higher order ribosomal structures reminiscent of 100S ribosomal dimers known from *E. coli*. Therefore if a ribosomal stabilisation mechanism exists in mycobacteria it is independent of dimerisation.

4.3.2 Ribosomal stability during hypoxia – a role for DosR?

The adaptation of mycobacteria to oxygen starvation *in vitro* provides us with an important window into the physiological adaptations that are likely to be important during infection (Wayne and Sohaskey, 2001, Rustad *et al.*, 2009, see 1.3.3.2). The NRP state, induced during hypoxia, is characterised by a cessation of growth and a shift down in metabolism and is effectively a form of energy starvation – reduced levels of terminal electron acceptor. We were interested whether mycobacteria bridge periods of energy starvation by forming specialised stable ribosomal structures rather than controlling their turnover. Previous work in the lab, using quantitative RT-PCR, showed that ΔdosR strains had significantly less 16S rRNA (constituent of 30S subunit) than wild-type strains during hypoxia (Hingley-Wilson, unpublished). This led us to hypothesise that DosR might play a role in the overall stability of the ribosome.

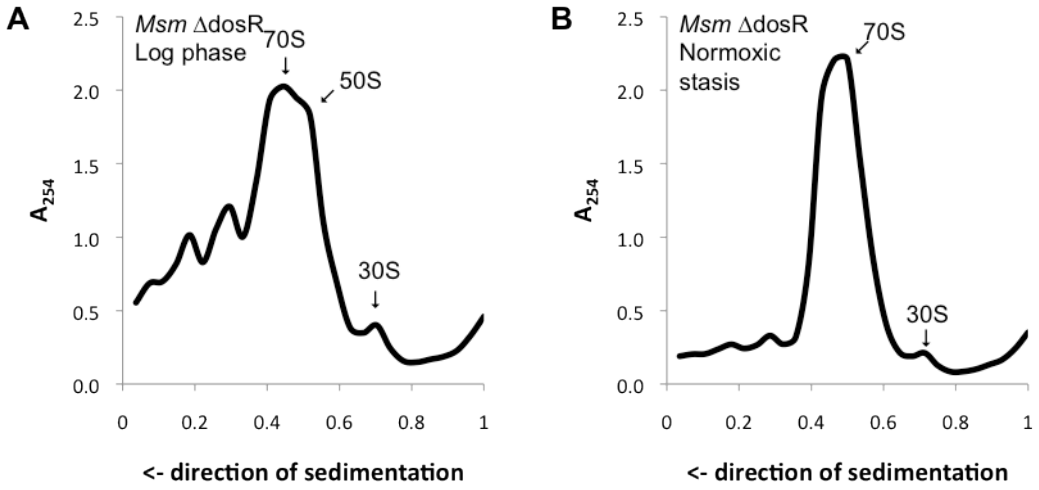


FIG. 4.8 Ribosomal profiles of actively growing and stationary phase *Msm* ΔdosR during normoxia. Ribosomes were prepared from (**A**) actively growing *Msm* ΔdosR and (**B**) *Msm* ΔdosR cells in normoxic stationary phase as described in Fig. 4.7.

Each experiment was repeated at least three times; representative profiles are shown.

We did not have access to a ΔdosR mutant of *Mbo* BCG (see 3.2.2); we therefore carried out our experiments in *Msm* for which the ΔdosR strain was available (O'Toole *et*

al., 2003). We started by confirming that the ribosomal population of the ΔdosR strain behaves in a similar fashion to wild type during normoxic conditions (See Fig. 4.8).

We then focused on changes to the ribosomal profiles during hypoxia. We grew the cultures in tightly sealed 2 l Pyrex conical flasks with a 1:2 headspace to medium ratio and harvested them 3 days into hypoxic stasis.

The ribosomal profile of hypoxic *Msm* wild type cultures was similar to those of normoxic stationary phase cultures (Fig. 4.9). There was no indication of any higher order organisation of ribosomes, and the majority of the ribosomes were found to be in the associated 70S form. Unlike during normoxic stasis, we were able to detect a small proportion of dissociated ribosomal subunits, however these were not as abundant as observed in *Mbo* BCG stasis. In contrast, the ΔdosR strain had a markedly different profile when compared to wild type. Notably, the level of associated 70S ribosomes was much lower in the mutant strain, with the 50S subunit being the dominant species. Interestingly, the levels of the 30S subunit were very low and did not match the apparent rise in the level of the 50S subunit. This effect is probably not simply due to a dissociation of the ribosomes, but may reflect a loss of stability of the 30S ribosomal subunit in ΔdosR during hypoxia.

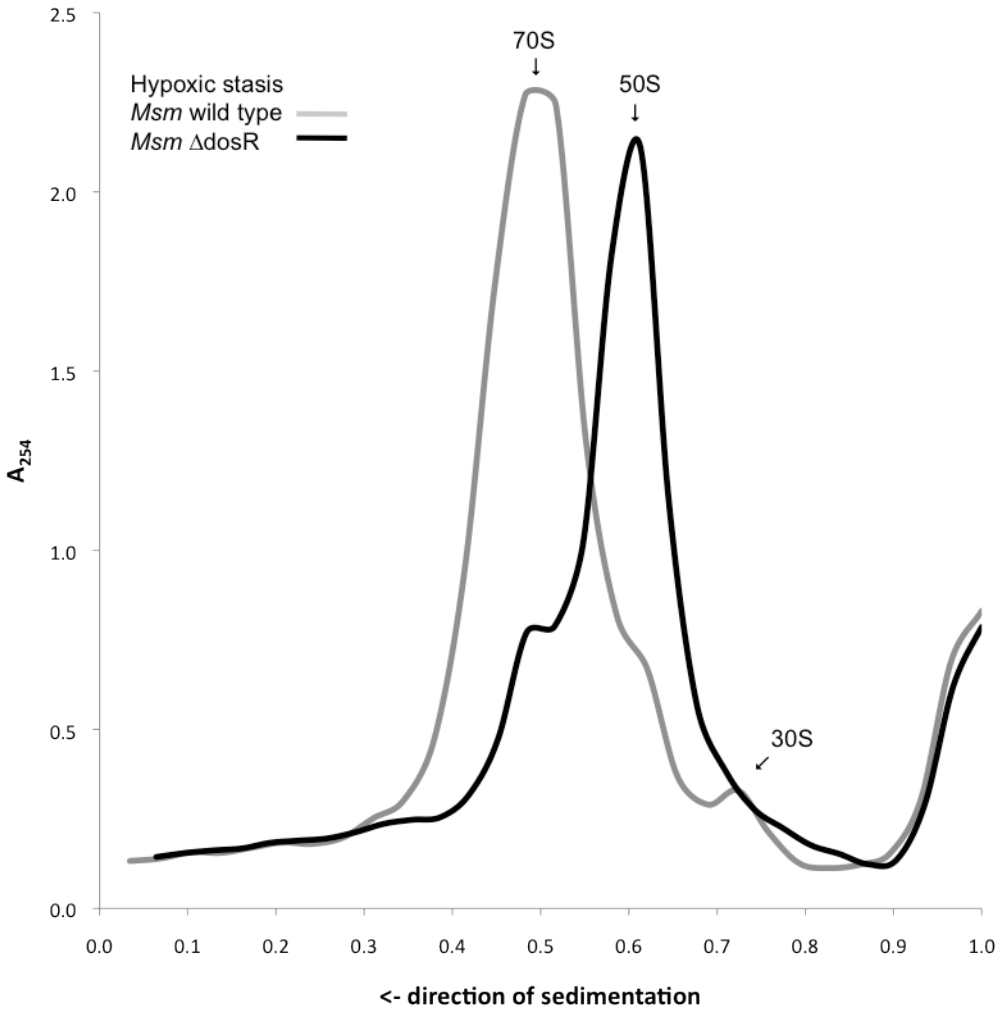


FIG. 4.9 *Msm* ΔdosR ribosomes are destabilised during hypoxic stasis. Ribosomes were prepared from 3-day-old hypoxic cultures of *Msm* ΔdosR (black line) and *Msm* wild type (grey line) as described in Fig. 4.7.

Each experiment was repeated at least three times; representative profiles are shown.

The striking ΔdosR ribosomal phenotype made us consider the possibility that the ribosome undergoes gross rearrangements or loss of rProteins. To address this possibility we prepared ribosomal extracts from hypoxic ΔdosR cultures using a low magnesium buffer. As is evident from Fig. 4.10 the size of the isolated subunits and the associated ribosome aligns well with that of dissociated ribosomes of actively growing wild type *Msm*.

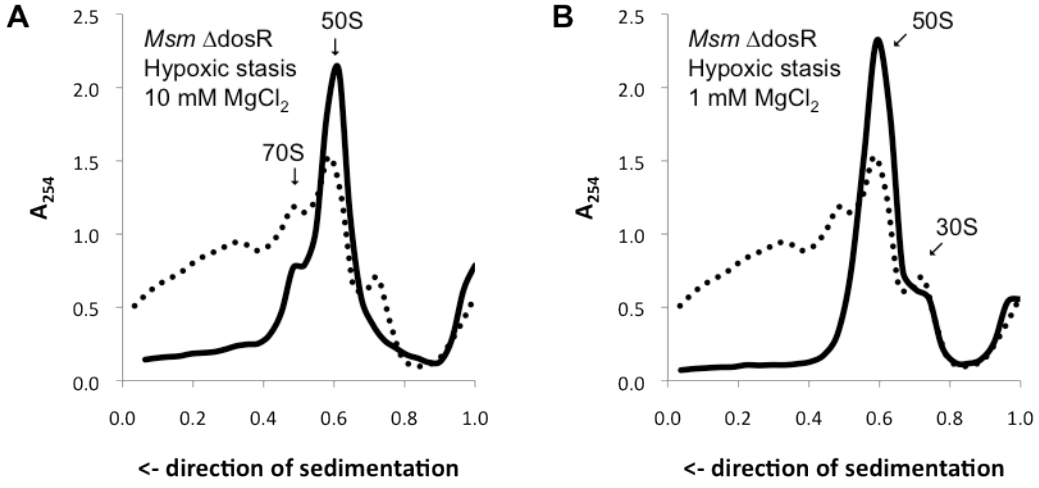


FIG. 4.10 *Msm* ΔdosR ribosomes during hypoxia are the same as wild type ribosomes. 3-day-old hypoxic cultures of *Msm* ΔdosR were harvested by centrifugation and lysed by passage through the French press in ribosomal buffer containing (**A**) 10 mM $MgCl_2$ (favours ribosomal association) or (**B**) 1 mM $MgCl_2$ (favours ribosomal dissociation). Ribosomal profiles were obtained as described in Fig. 4.7.

Profiles of dissociated ribosomes from actively growing *Msm* wild type cells are shown as reference (dotted line).

In our experience it was very important to harvest the cultures 3 days after the onset of hypoxic stasis. When we harvested the cells 4 days after the onset of hypoxic stasis the overall level of ribosomes in the culture fell dramatically (see Fig. 4.11). It is interesting to note that the profile of wild type cultures 4 days into hypoxia (Fig. 4.11 A&C) phenocopies the ΔdosR profiles harvested a day earlier – as the most abundant species becomes the 50S ribosomal subunit rather than 70S ribosomes. However it is evident that ribosomal levels are decreased even further in ΔdosR after 4 days of hypoxic stasis (Fig. 4.11 B&D). Importantly we are still able to detect 70S ribosomes in wild type extracts at this time point, while almost none could be detected in ΔdosR extracts.

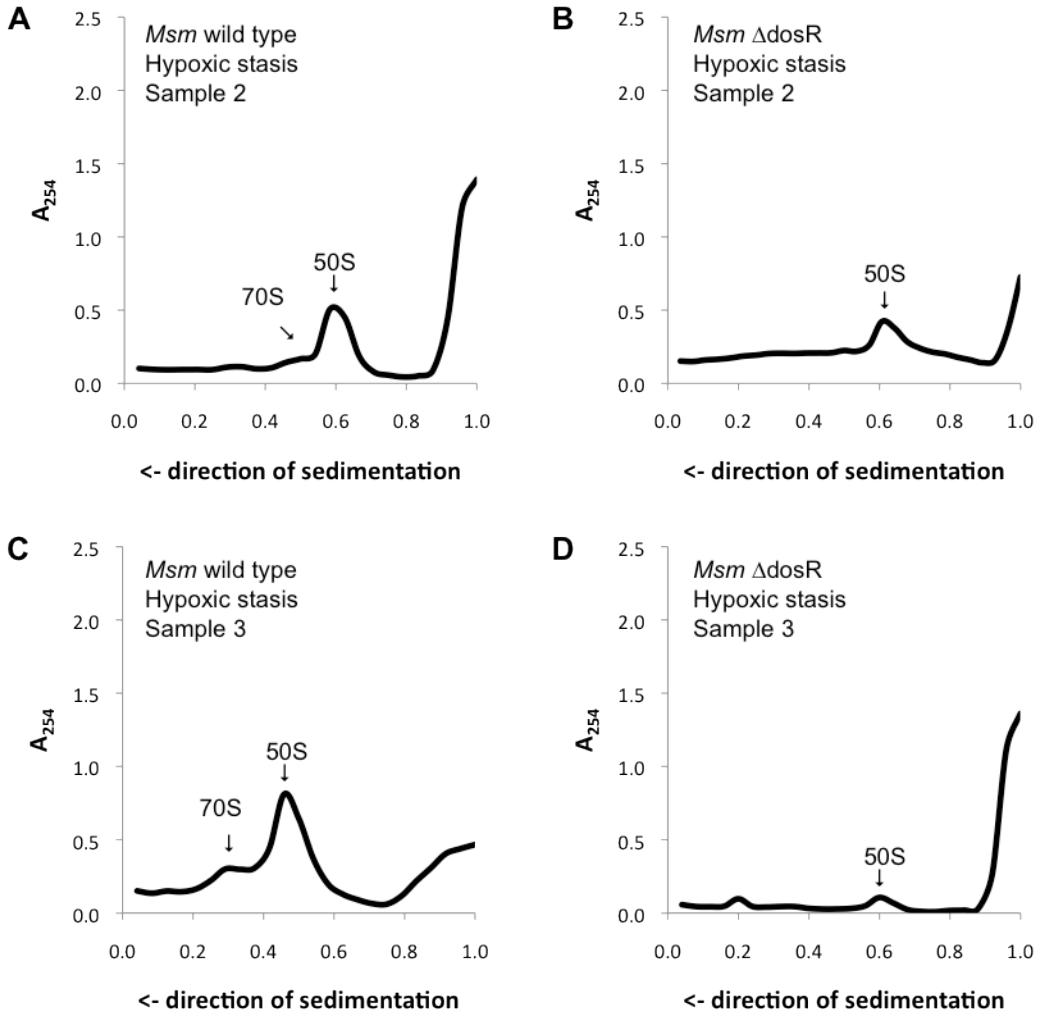


FIG. 4.11 Ribosomal profiles of 4-day-old hypoxic cultures of *Msm*. Ribosomes were obtained from (**A,C**) 4-day-old hypoxic *Msm* wild type and (**B,D**) 4-day-old hypoxic *Msm* ΔdosR as described in Fig. 4.7. Ribosomal profiles shown in separate panels represent independent experiments.

4.3.3 Ribosomal stability during carbon starvation

So far we were unable to detect any changes to the ribosomal population that would be reminiscent of 100S ribosomal dimers. It is clear from our observations of hypoxic stasis that there is a process by which ribosomal levels are regulated – at least early in hypoxia. Crucially, it appears that DosR may mediate this process. However, mycobacteria would require stabilisation of their ribosomes in contexts where DosR is not induced. One such example is carbon starvation. Like hypoxia, carbon starvation could also be regarded as energy starvation and may therefore pose a similar kind of

challenge from the point of view of ribosomal stability. We have therefore carried out ribosomal profiling of carbon-starved cultures. The obtained profile is almost identical to that obtained after 3 days of hypoxic stasis (Fig. 4.12). *Msm* ΔdosR has the same profile as wild type (data not shown).

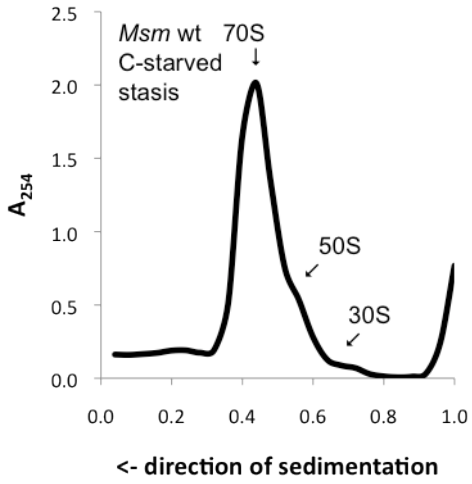


FIG. 4.12 Ribosomal profiles during carbon starvation. Ribosomes were prepared from 3-day-old carbon-starved cultures of *Msm* wild type as described in Fig. 4.7.

Profiling experiments were repeated at least four times; a representative profile is shown.

4.3.4 DosR regulon in ribosomal stability

The effect of the *dosR* mutation on the ribosomal profile could be explained as the loss of a stabilising interaction between the ribosome and an associated protein. There are at least two types of potential candidates for such a stabilisation within the DosR regulon. On one hand the highly induced member of the DosR regulon, α-crystallin (HspX) was reported to associate to the ribosome under hypoxic conditions (Tabira *et al.*, 1998). On the other hand USPs (six of which are DosR-regulated in *Mtb*) could play a role in ribosomal stability since they possess GTPase activity, which is often linked to ribosome physiology (see 4.3.4.2).

4.3.4.1 HspX

The evidence regarding the ribosomal association of HspX in *Mbo* BCG presented by Tabira *et al.*, was ambiguous, as the authors did not fully investigate the possibility of the association of HspX with cell membranes. This is particularly important as membranes would not be fully excluded from the ribosomal fraction during the fractionation method that they used. We therefore decided to readdress this interaction; the HspX-specific antibodies available in the laboratory were raised against *Mtb* HspX and were observed to have almost no cross-activity to the *Msm* protein, while they did cross-react with the *Mbo* BCG homologue (data not shown). We therefore carried out the analysis of HspX interaction using *Mbo* BCG.

We prepared ribosomes from cultures of *Mbo* BCG grown under hypoxic conditions for 12 days, and washed them with ribosomal buffer alone or ribosomal buffer supplemented with either 1 M ammonium chloride or 0.5% (*v/v*) Tween 80. We chose these treatments to exclude loosely bound factors (ribosomal buffer wash), tightly bound factors ("salt washing" with 1M ammonium chloride) and membranes from ribosomal preparations. We used Tween 80 rather than any other detergent, because it was shown not to affect ribosomal stability (Body and Brownstein, 1978). We analysed proteins obtained from ribosomal profiling fractions using SDS-PAGE and western blotting.

Ribosomal populations isolated from hypoxic cultures of *Mbo* BCG had a similar profile to that of *Mbo* BCG during normoxic stasis (Fig. 4.13A and Fig. 4.7D). In both cases there appeared to be a pool of dissociated ribosomal subunits as well as a sizeable proportion of associated ribosomes. Unfortunately the resolution of the profiles used for SDS-PAGE/western blot analysis were not high enough to discern between 50S subunits and intact ribosomes. Nonetheless the resolution was sufficient to be able to comment on the ribosomal association of HspX.

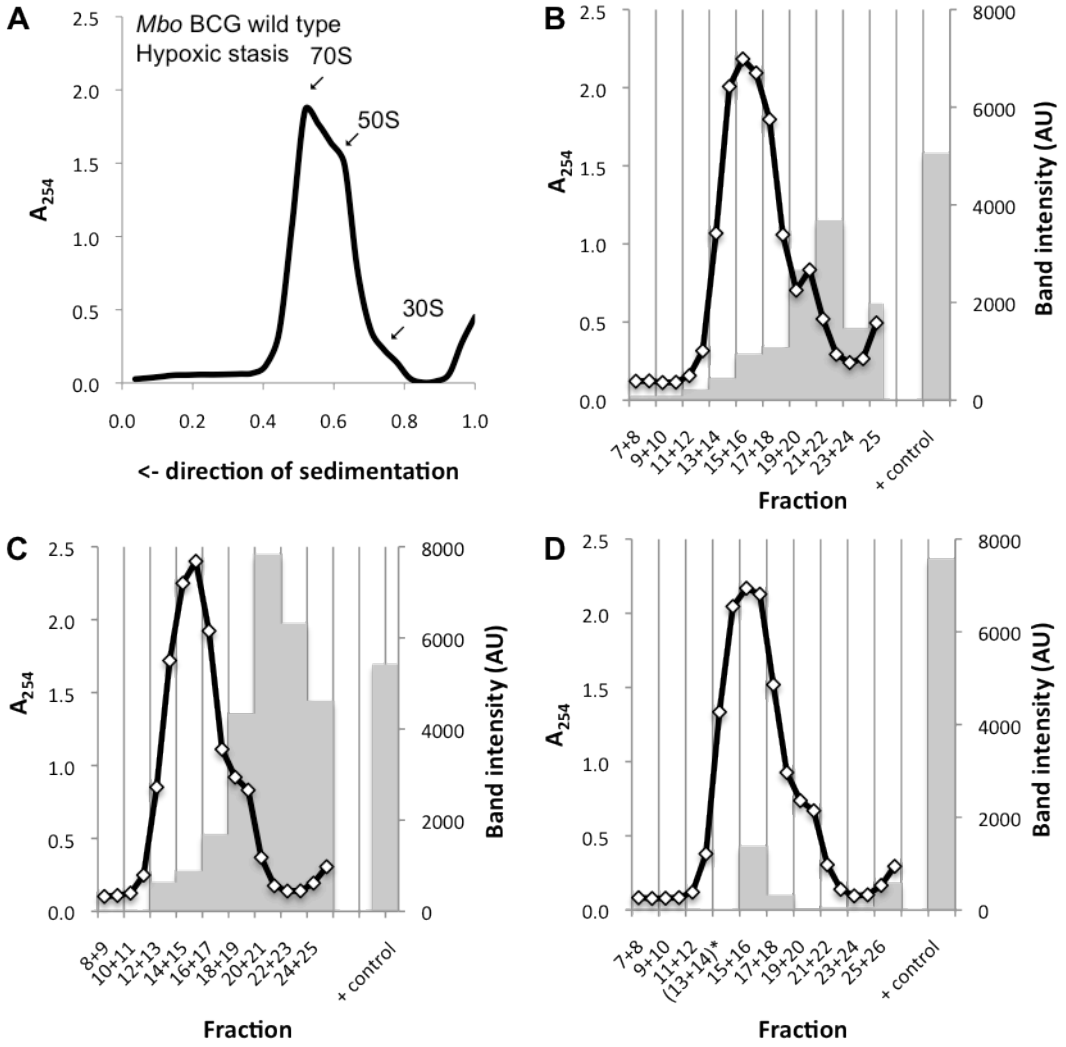


FIG. 4.13 α-crystallin does not associate exclusively to the ribosome in *Mbo* BCG. (**A**) Ribosomal profile was obtained for hypoxic *Mbo* BCG wild type cultures as described in Fig. 4.7. Pre-spun ribosomes were washed in ribosomal buffer (**B**) supplemented with 1M ammonium chloride (**C**) or 0.5% (*v/v*) Tween 80 (**D**) prior to profiling using linear (15-40%) sucrose gradients (◇).

Proteins were precipitated from pooled fractions with TCA and separated by SDS-PAGE. Western blotting using monoclonal antibodies specific for *Mtb* α-crystallin (See Fig. 4.14). The intensity of each band was determined by electronic densitometry using ImageJ software (Abramoff, 2004) and plotted on top of the ribosomal profiles. Vertical lines indicate the pooled fractions.

Western blotting of the profiling fractions (Fig. 4.14) revealed that the distribution of HspX through the gradient does not match that of ribosomes (Fig. 4.13B and 4.13C) unless the ribosomal pellet is washed with 0.5% Tween 80 (Fig. 4.13D). Furthermore the level of HspX in the wash after we pelleted the ribosomes was highest in the wash containing Tween 80 (data not shown). Therefore HspX can be said to

associate with *Mbo* BCG ribosomes during hypoxia, however this interaction encompasses only a small fraction of the overall HspX present in the cell, and is therefore unlikely to be the primary role of HspX during hypoxia.

This result is partially consistent with the published view that HspX associates with ribosomes, however it also points towards an association with cellular lipids. Lipid association is consistent with the observation that the ability to isolate HspX by centrifugation is Tween 80 dependent (Tabira *et al.*, 1998). Moreover, the association between HspX and cellular lipids could explain the distribution of the protein in the sucrose gradient – maximum signal was found to be present in fractions that are removed from both: the top of the gradient and ribosomal fractions.

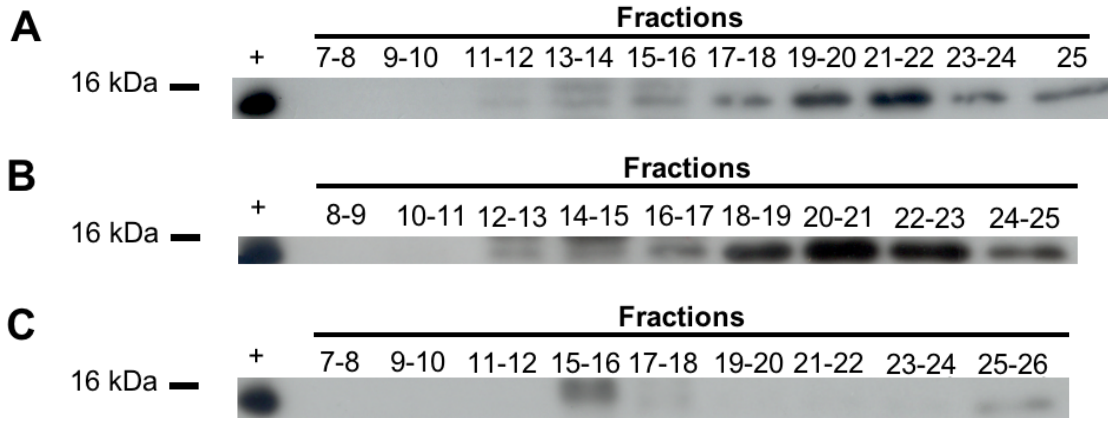


FIG. 4.14 Western blots used for the quantitation of HspX association shown in Fig. 4.13. Proteins were precipitated from fractions of profiles of pre-spun ribosomes, which were washed with ribosomal buffer (**A**), ribosomal buffer + 1M NH4Cl (**B**) or ribosomal buffer + 0.5% Tween 80 (**C**) prior to ribosomal profiling.

4.3.4.2 USPs

USPs have a degree of GTPase activity (Leiva Poveda, Bradley, Williams, unpublished) and GTPases are known to interact with ribosomes and modulate their assembly/function (Sato *et al.*, 2005, Wout *et al.*, 2004, Uicker *et al.*, 2007). Furthermore six USPs are regulated by DosR in *Mtb* (Park *et al.*, 2003). We were therefore interested in the possibility that this class of proteins mediates the DosR effect on ribosomal stability. Unfortunately we did not have access to antibodies specific for DosR-regulated

USPs, however previous work in the lab resulted in the generation of polyclonal antibodies against a recombinant USP from *Mtb* - His_6-Rv1636. Rv1636 is not a member of the DosR regulon, and unlike the DosR-regulated USPs which all have tandem USP domains, Rv1636 has a single USP domain. However, there are several USPs in most mycobacterial genomes, with at least partial functionally redundancy (Hingley-Wilson *et al.*, 2010), and Rv1636 is up-regulated together with the DosR regulon in the presence of nucleic acid damaging agents such as UV light, Mitomycin C and H_2O_2. We therefore reasoned that if DosR-regulated USPs interact with the ribosome, Rv1636 and its homologues in *Msm* and *Mbo* BCG may also be found to associate with the ribosome.

We first addressed the possibility of interaction between the ribosome and one of the *Msm* homologues of Rv1636, MSMEG_3811 or MSMEG_3308. We started by testing the cross-reactivity of α-His_6-Rv1636 to *Msm* USPs by performing western blot analysis on cellular extracts from exponential and stationary phase wild type and *dosR* mutant cells. We were able to observe that α-His_6-Rv1636 does cross-react with an *Msm* protein of appropriate size, albeit with much lower specificity (Fig. 4.15). We attempted to use ribosomal profiling and western blotting to investigate the association of USPs to the ribosome in *Msm*; unfortunately the lower specificity of α-His_6-Rv1636 for *Msm* USPs impeded us from getting a meaningful result (data not shown).

α-His_6-Rv1636 was shown to cross-react well with the *Mbo* BCG homologue of Rv1636 - Mb1662 (Fig. 4.15), we therefore repeated the profiling experiment in *Mbo* BCG. As with *Msm* we were unable to detect any Mb1662 associated to the ribosome (data not shown). We found no evidence that single USP domain proteins from either *Msm* or *Mbo* BCG would associate to the ribosome. Single domain USPs are therefore unlikely to play a direct role in ribosomal stability.

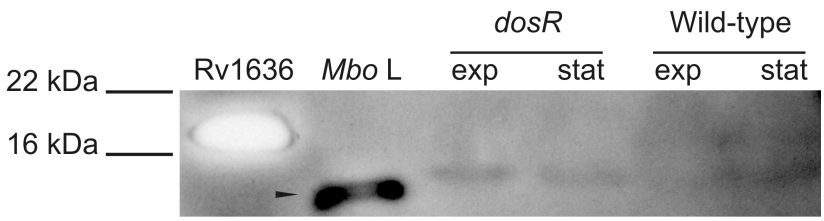


FIG. 4.15 Anti-His_6-Rv1636 antibodies cross-react with *Msm* cellular extracts. Clarified cellular lysates were separated by 15% SDS-PAGE, Rv1636 was detected by western blotting using α-His_6-Rv1636 rabbit polyclonal antibody. Lysates of *Msm* wild type and *dosR* mutant cells were obtained from exponential (exp) and stationary (stat) phase cultures. "Rv1636" – recombinant His_6-Rv1636, "*Mbo* L" – lysate of stationary phase *Mbo* BCG. Arrowhead indicates *Mbo* BCG homologue of Rv1636 (Mb1662).

Taken together our findings regarding ribosomal stability in mycobacteria can be summarised as follows: *Msm* and *Mbo* BCG do not form 100S ribosomal dimers upon entry into stasis (1). Ribosomes of *Msm* are found predominantly in the associated (70S) form during stasis (2). The ribosomal profiles of normoxic stasis, hypoxic stasis and carbon-starvation induced stasis are very similar (3). Dissociation of the 70S ribosome may lead to ribosomal degradation, as shown in hypoxic cultures (4). DosR might play a role in the stability of the ribosome during hypoxia, and this activity is independent of HspX or USPs (5).

4.4 rRNA stability

Ribosomal profiling using large cultures proved to be unsuitable for the study of ribosomal stability during prolonged periods of stasis. As described in section 4.3.2 the profiling experiment was limited to 4 days after the entry into hypoxic stasis – longer incubations led to a decrease in the ribosomal signal that made meaningful analysis impossible. It would not be feasible to increase culture volume further to counter the limitations imposed by lower ribosomal levels using the equipment available in the laboratory.

We tried to improve the sensitivity of the profiling methodology by turning to the analysis of rRNA species in the cell instead of the ribosomes. Such analysis would not be able to inform us on any higher-order structure of ribosomes, however, given that we

established already that no such structures were formed in mycobacteria at the time of entry into stasis, we did not perceive that to be a potential limitation.

4.4.1 Explanation of the approach

There are multiple approaches to studying rRNA levels and integrity, including denaturing gel electrophoresis (Sambrook and Russell, 2001), quantitative RT-PCR (Gong *et al.*, 2006), CsCl/sucrose gradient ultracentrifugation (Glisin *et al.*, 1974) and capillary electrophoresis – "lab-on-a-chip". We chose to use the latter as it enabled us to measure a large number of samples quickly, effectively and in digitised form, thus simplifying data manipulation and analysis.

The Agilent Bioanalyzer 2100 RNA 6000 Nano chip uses capillary electrophoresis to separate molecules on the basis of their size. Smaller molecules migrate faster than larger ones and are therefore recorded earlier. RNA 6000 Nano chips are used primarily to estimate RNA integrity prior to transcriptomic experiments (Bustin *et al.*, 2004), however we adapted the same meter to measure the stability of rRNA molecules during prolonged stasis. We isolated rRNA using guanidium thiocyanate – acidic phenol extraction (Trizol reagent) prior to measuring the composition using the Bioanalyzer. Given that Bioanalyzer results give us analogous data to ribosomal profiling, we call the resulting traces rRNA profiles – an example from exponentially growing *Msm* cells is shown in Fig. 4.16.

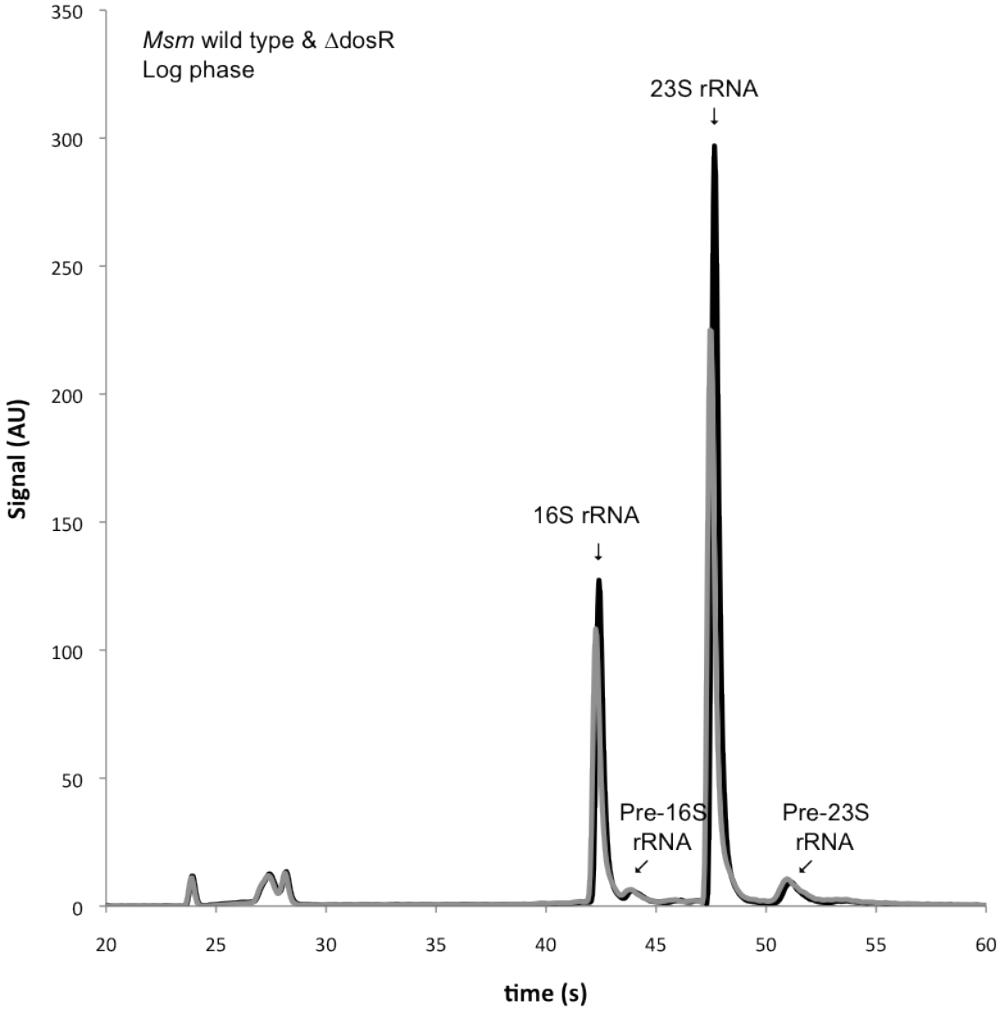


FIG. 4.16 Ribosomal RNA profiles of actively growing *Msm* cells. RNA was extracted for actively growing *Msm* wild type (black line) and *Msm* ΔdosR (gray line) cells using the Trizol reagent. Purified RNA was analysed on an Agilent 2100 Bioanalyzer instrument using a RNA 6000 Nano chip kit.

The experiment was repeated at least three times; representative profiles shown.

The two main peaks correspond to 16S and 23S rRNA molecules, which are constituent of the 30S and 50S ribosomal subunits respectively. The apparent higher abundance of 23S rRNA compared to 16S rRNA reflects the chemical properties of the dye and is consistent with sample data provided by the manufacturer.

Analysis of rRNA using the Bioanalyzer proved itself to be very versatile as illustrated by the fact that, we were routinely able to observe RNA species adjacent to the main rRNA peaks in extracts of exponentially growing cells. These molecules are

larger than rRNAs and we believe them to be the immature pre-16S and pre-23S rRNA, which have been synthesised but not yet incorporated into ribosomes and fully processed. No such peaks were observed in static cultures, as the level of ribosomal biosynthesis is negligible during stasis (see Figs. 4.18 & 4.19).

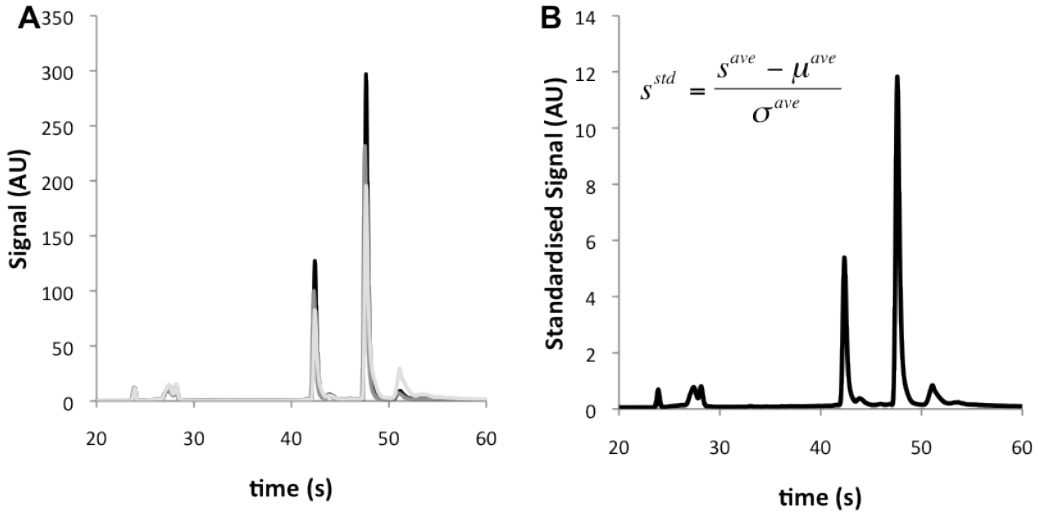


FIG. 4.17 Ribosomal RNA profiles – data processing. (**A**) multiple rRNA profiles were obtained for RNA purified from independent samples for each condition – in this case three samples from actively growing *Msm* wild type. (**B**) The average signal intensity (s^{ave}) was calculated and standardised (s^{std}) by subtracting the mean of the averaged signals (μ^{ave}) from s^{ave} and dividing the difference by the standard deviation of the averaged signals (σ^{ave}) – see formula. Standardised signal intensities were then plotted against time.

In our experience rRNA profiles obtained with the Bioanalyzer were highly reproducible – we were always able to superimpose all samples ran on the same day. However, there was a slight variation due to an occasional shift in the migration of rRNA species between measurements made on different days. In addition, the nature of our samples, which were obtained from different stages of growth, introduced a further level of variability. We chose not to normalise the amount of rRNA loaded onto the chip, as we wanted rRNA profiles to reflect the levels and state of rRNA in the cultures. We therefore present each rRNA profile as the average of three independent cultures; to facilitate the comparison of samples with different amounts of rRNA we standardised all

our averaged profiles. The effect of our processing on the resulting rRNA profiles is shown in Fig. 4.17.

4.4.2 rRNA stability during hypoxia

We have already determined that there is very little RNA turnover during hypoxia (see 3.4.2.1), suggesting that mycobacteria have to rely on ribosomal stability in order to be able to emerge from stasis with a functional translational apparatus. Ribosomal profiling revealed that no higher order ribosomal structures appear during stasis, pointing to the 70S ribosome as the stable form. We were also able to identify DosR as a potential player in ribosomal stability. However we were unable to draw any more conclusions from our profiling experiments. Our aim with rRNA profiling was to obtain a more comprehensive time-course, which would complement our ribosomal profiling findings, and hopefully shed some light on the mechanisms that govern ribosomal stability during prolonged hypoxia. We set up hypoxic cultures of *Msm* wild type, ΔdosR and DosR^{c}, sacrificed three independent cultures at each time-point and isolated the RNA from the culture prior to rRNA profiling (Fig. 4.18).

Prolonged hypoxia led to a progressive deterioration of the rRNA pool in the wild type and DosR^{c} strains, characterised by the appearance of multiple intermediate peaks (not observed during active growth, see Fig. 4.16). It is tempting to speculate that these peaks are indicative of discrete rRNA cleavage events. Specific stepwise breakdown of rRNA is well documented in enteric bacteria, and may occur as a result of the dissociation of the 70S ribosome (Zundel *et al.*, 2009). It is therefore possible that mycobacteria degrade their ribosomes using a related mechanism.

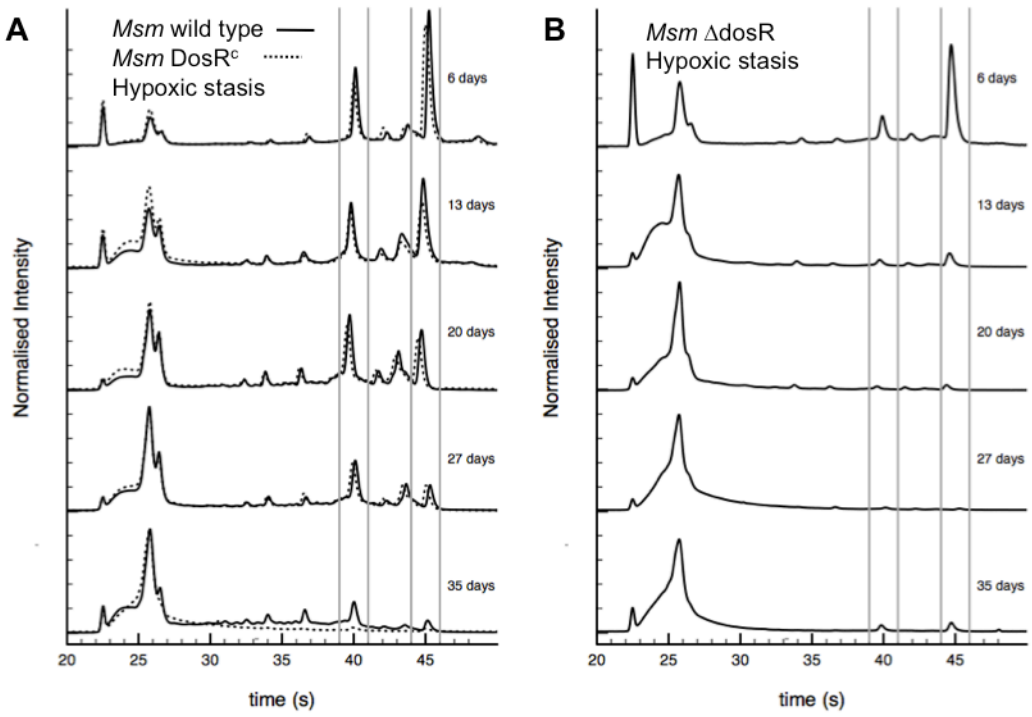


FIG. 4.18 rRNA stability during prolonged hypoxic stasis. RNA was purified from (**A**) *Msm* wild type (solid line), *Msm* DosR^c (dashed line) and (**B**) *Msm* ΔdosR cultures 6, 13, 20, 27 and 35 days after the onset of hypoxic stasis. 16S rRNA eluted at approximately 40 s while 23S rRNA elutes at approximately 45 s.

Each profile represents three independent cultures as described in Fig. 4.17.

As observed with ribosomal profiling, the degradation of rRNA in the ΔdosR strain occurred more rapidly than in the wild type. While the profiles were similar after 6 days of hypoxia, the majority of the rRNA was gone within the first two weeks of hypoxia in the mutant but not in the wild type or the complemented strain. In contrast to ribosomal profiling, there was no evidence of the bias towards the 50S subunit in ΔdosR during hypoxia. However, it is important to note that cleavage products of the larger 23S rRNA could have the same size as 16S rRNA. The existence of such fragments is supported by rRNA profiles of wild type and DosR^c cultures after 20-35 days of hypoxia, where the normally larger 23S peak (Fig. 4.18), becomes smaller than 16S. This observation could be due to the 16S rRNA peak being obscured by a degradation product of 23S (a similar result was obtained by Zundel *et al.*, 2009).

4.4.3 rRNA stability during carbon starvation

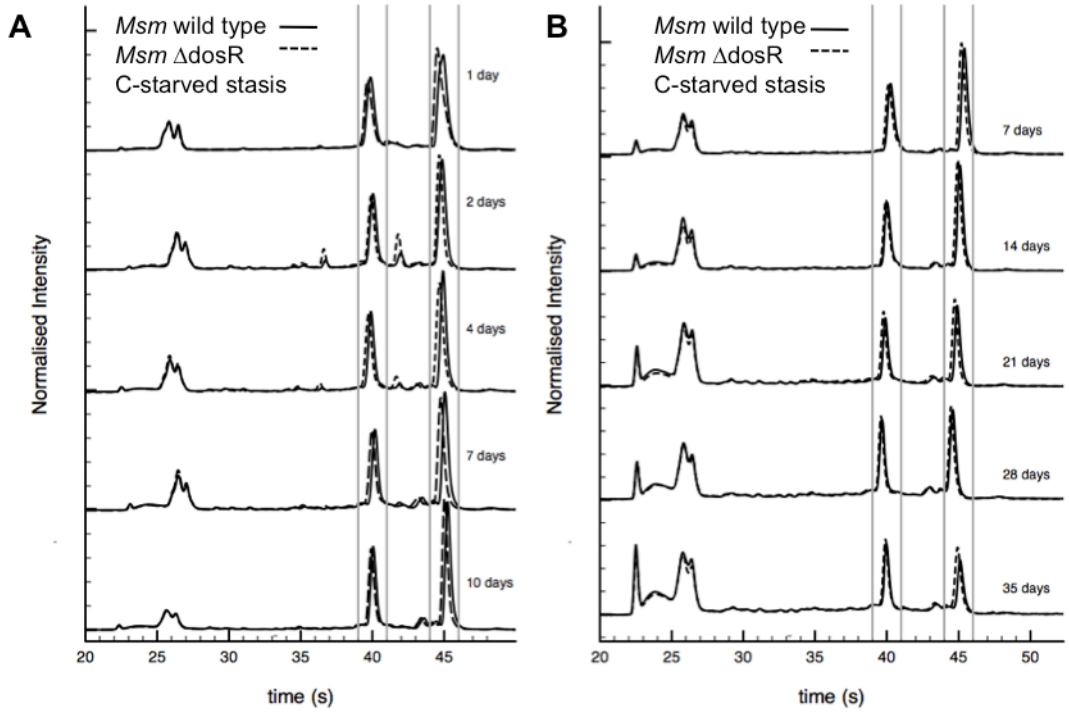


FIG. 4.19 rRNA stability during prolonged carbon-starved stasis. RNA was purified from *Msm* wild type (solid line) and *Msm* ΔdosR (dashed line) cells after (**A**) 1, 2, 4, 7 and 10 days and (**B**) 7, 14, 21, 28 and 35 days after the onset of carbon-starved stasis. 16S rRNA eluted at approximately 40 s while 23S rRNA elutes at approximately 45 s.

Each profile represents three independent cultures as described in Fig. 4.17.

Ribosomal profiles of carbon starved and early hypoxic cultures were comparable. We were interested whether rRNA stability and degradation are also similar during carbon starvation and hypoxia. Repeating the rRNA stability experiment in a context where DosR does not act would allow us to test whether the hypoxic rRNA stability phenotype is specific related to the action of DosR or a more general side-effect.

The population of rRNA molecules during carbon starvation, in the wild type and the dosR mutant, was remarkably more stable than during hypoxia. The progressive deterioration of the rRNA pool was much reduced and there were also far fewer intermediate peaks present in the rRNA profiles. Taken together these observations point to a higher stability of ribosomes during carbon starvation than during hypoxia.

By comparing the viability of *Msm* during prolonged hypoxia and prolonged carbon starvation (see 3.2.1.2) we observed that the number of culturable cells remained almost constant during the latter, while decreasing (particularly dramatically for ΔdosR) during the former. It can therefore be said that there is a correlation between viability and rRNA stability. This correlation presents the possibility that the ΔdosR ribosomal phenotype can be explained by a simple effect on viability. To test this hypothesis we exposed stationary phase cultures to the protonophore CCCP to simulate the kind of energy depletion conditions that are likely to occur during hypoxia.

4.4.4 rRNA stability during CCCP-induced energy starvation

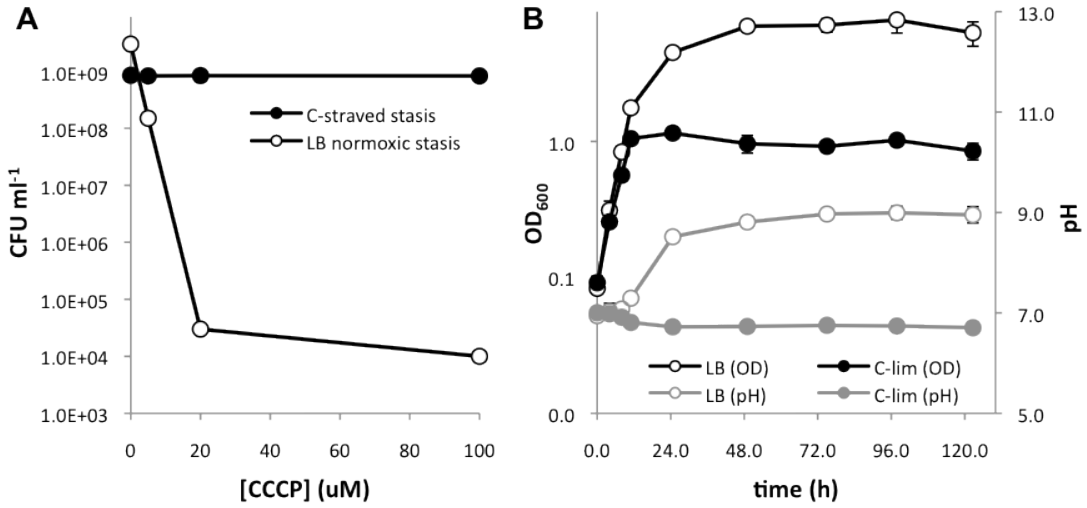


FIG. 4.20 Wild type *Msm* is more susceptible to CCCP when grown to normoxic stationary phase in rich medium. (**A**) The viability of 3-day-old normoxic stationary phase *Msm* wild type grown in LB (○) or carbon limited Hartmans–de Bont medium (●) when exposed to different concentrations of CCCP. (**B**) Growth curve (OD_{600}) for *Msm* wild type grown in LB (○) or carbon limited Hartmans-de Bont medium (C-lim, ●). The change in pH was followed for growth in LB (○) and carbon limited Hartmans-de Bont (C-lim, ●).

All curves represent three independent cultures. Viability was measured in triplicate, while single measurements of OD_{600} and pH were taken for each culture. Error bars correspond to the standard deviation (N=9 for viability and N=3 for OD_{600} and pH).

We postulated that if energy starvation leading to the loss of viability is the primary mediator of rRNA degradation then a carbon starved culture of *Msm* wild type should be more susceptible to CCCP treatment than a normoxic static culture in rich medium, as

the latter is more likely to have a higher intracellular [ATP] and therefore more able to withstand CCCP induced damage.

Contrary to our expectations we found that carbon starved cultures were much more resilient to CCCP treatment than normoxic static cultures in LB (see Fig. 4.20A). The stability of their rRNA follows the same pattern, providing further proof that viability and ribosomal stability are directly correlated (see Fig. 4.21).

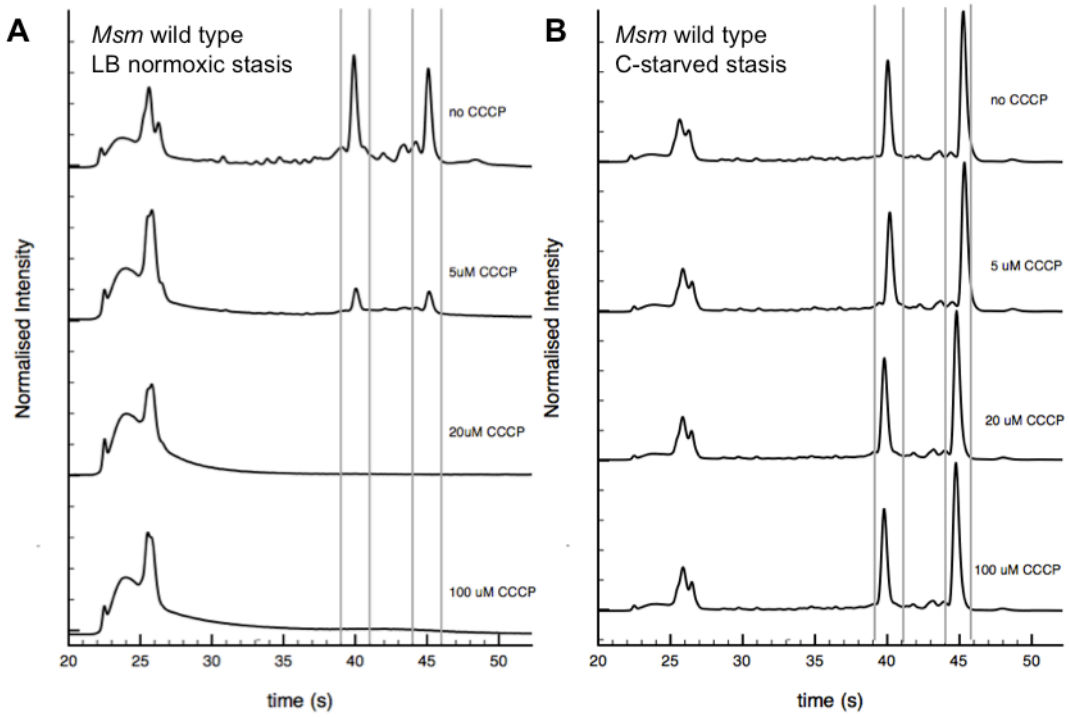


FIG. 4.21 rRNA stability of cultures exposed to CCCP. RNA was purified from *Msm* wild type cultures grown to (**A**) normoxic stasis in LB or (**B**) normoxic stasis in Hartmans-de Bont medium and exposed to 0, 5, 20 and 100 μM of CCCP. 16S rRNA eluted at approximately 40 s while 23S rRNA elutes at approximately 45 s.

Each profile represents three independent cultures as described in Fig. 4.17.

There is a striking similarity between hypoxic cultures of ΔdosR and CCCP-treated wild type static cultures in rich medium, suggesting that loss of viability alone can account for the rRNA phenotype we observed with ΔdosR. Interestingly CCCP seemed to have absolutely no effect on carbon starved cultures of *Msm*. A possible explanation for this effect could be a pH differential between the cell and the culture

medium (see Fig. 4.20B) the pH of static cultures in LB is very alkaline while that of carbon starved cultures hardly changes during different stages of growth.

The evidence at hand strongly supported an indirect role for DosR in ribosomal stability – mediated by a general loss of viability. However we were still unable to completely exclude a more specific and direct stabilising interaction with the data. In order to be able to do so we needed to ascertain that ribosomes isolated from hypoxic ΔdosR cultures were exactly the same in composition as those of wild type cells.

4.5 Compositional analysis of ribosomes

Compositional analysis of hypoxic ribosomes would allow us to answer a number of questions: firstly, are there any proteins that associate with the ribosome specifically during stasis? Are there any changes in the levels of individual rProteins in ΔdosR ribosomes? In the absence of any compositional differences, hypoxic ΔdosR ribosomes could provide us with information regarding ribosomal catabolism. It is evident from our ribosomal profiling experiments that ribosomal degradation during hypoxia proceeds in a similar fashion in both ΔdosR and wild type hypoxic cultures – albeit progresses more rapidly in the mutant. Therefore comparing ribosomes from the two sources might help us to shed some light on the underlying mechanism of ribosomal degradation.

4.5.1 Proteomic analysis of "Pre-spin" ribosomal pellets

It became clear earlier (see section 4.3.4) that a targeted approach using SDS-PAGE and western blot analysis was not suitable for the study of ribosomal stability at this stage of the project. An approach was needed that would allow a more global analysis of the ribosome. We chose to use mass spectrometry as a tool for proteomic analysis.

Our first step was to determine the appropriate method to prepare our samples prior to analysis. Our goals were to detect as many ribosomal proteins as possible whilst

excluding from the preparation proteins that were unlikely to associate to the ribosome. As indicated in section 4.2.3 pelleting ribosomes from crude extracts through a sucrose cushion improved the resolution of ribosomal profiles. This may have occurred by removing many of the cytosolic proteins (present at the top of the sucrose gradient) that were probably not associated with the ribosome. We obtained "Pre-spin" ribosomes from exponentially growing *Msm* wild type cultures. The ribosomal pellet was analysed by tandem mass spectrometry as described in section 2.5. We were able to identify 204 proteins (see Fig. 4.22). In order to gauge the purity of our sample we determined the subcellular localisation of each protein based on their function[7], or the predicted presence of transmembrane helices[8]. Proteins for which we were unable to predict a function (either based on experimental evidence in the literature or on homology) or the presence of transmembrane regions were classified as "unknown".

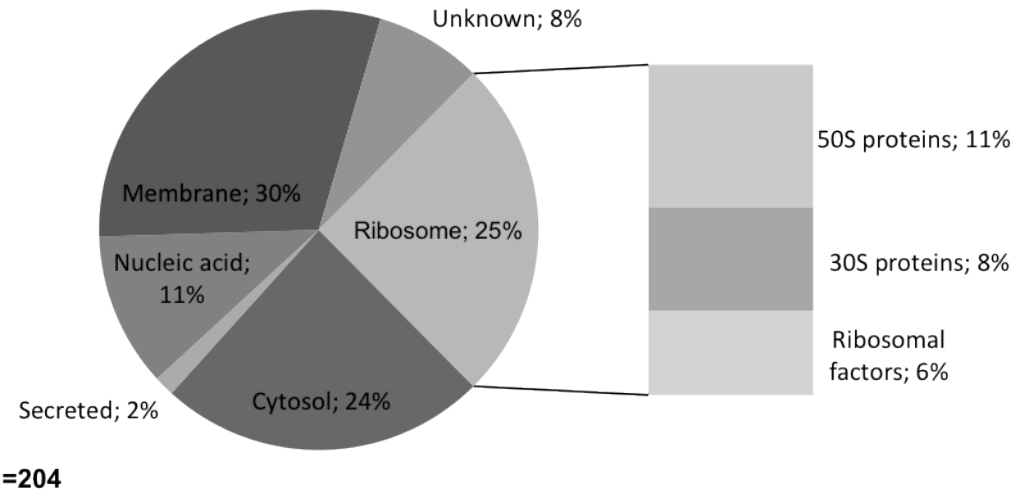


FIG. 4.22 "Pre-spin" ribosomal preparations contain proteins from all cellular compartments. Ribosomes were pelleted through sucrose cushions from clarified cell extracts of *Msm* wild type cultures. The pellets were resuspended and digested with trypsin prior to analysis by HPLC-MS. Spectra were interpreted using ProteinPilot software.

NB For the sake of clarity the details of the proteomic dataset have been omitted from this figure. The complete summary of the data presented here is included in "SupTab1.xls", which can be found on the attached data CD.

[7] Function was determined using the KEGG and TBDB databases (Kanehisa *et al.*, 2006, Reddy *et al.*, 2009).
[8] The presence of transmembrane helices was predicted using the Dense Alignment Surface method (Cserzo *et al.*, 1997).

"Pre-spin" ribosomal preparations contain proteins that are associated to most cellular compartments. We were able to confirm the presence of large membrane bound complexes such as ATP synthase and members of the electron transfer chain including components of cytochrome c oxidase and NADH dehydrogenase. The presence of nucleic acids in the preparation was evident by the identification of the entire RNA polymerase holoenzyme, as well as DNA polymerase I, and a number of transcriptional regulators. Nonetheless we were also able to identify 37 rProteins and 13 proteins that are known to interact with the ribosome (see table 4.1). Overall this method allowed us to identify 22 large subunit rProteins and 15 small subunit proteins, which represents 68.5% of the total number of expected rProteins - 64.7% of 50S rProteins and 75.5% of 30S rProteins.

TABLE 4.1 rProteins and ribosome-associated proteins in "Pre-spin" ribosomal preparations as identified by ProteinPilot[a].

DETECTED			NOT-DETECTED	
50S	*30S*	*Associated factors*	*50S*	*30S*
L2	S1	IF-1	L1	S10
L3	S2	IF-2	L4	S12
L5	S3	IF-3	L7/12	S14
L6	S4	EF-G	L15	S17
L9	S5	EF-Tu	L21	S20
L10	S6	EF-Ts	L23	
L11	S7	Trigger factor	L30	
L13	S8	Signal recognition particle	L31	
L14	S9	RimM	L32	
L16	S11	RbfA	L33	
L17	S13	DeaD-box RNA helicase	L34	
L18	S15	Obg	L36	
L19	S16	rRNA methyltransferase		
L20	S18			
L22	S19			
L24				
L25				
L27				
L28				
L29				
L35				

[a] The details of % sequence coverage and the number of peptides included for the analysis of each protein are listed in SupTab1.xls, SupTab2.xls and SupTab3.xls – see included data CD.

It is interesting to note that the proteomic data are consistent with the fact that these ribosomes came from actively growing cells. We were able to detect a number of ribosomal factors associated with active translation (IF1-3, EF-Tu, EF-Ts, EF-G, Signal recognition particle, trigger factor) as well as with ribosome maturation and biosynthesis (RimM, RbfA, rRNA methyltransferase). However we did not detect the full complement of ribosomal proteins. The most likely reason for this does not lay in the absence of these proteins from the preparation, but rather in the intrinsic bias of tandem mass spectrometers. The number of species that can be analysed by a tandem mass spectrometer at any one time is finite and fixed by the user, to accommodate for the fact that the detector needs to be exposed to a sufficiently large number of ions, in order to record interpretable spectra. The requirement for a minimal "dwell time" for each mother ion poses a problem when there is a large number of different ions that enter the mass spectrometer simultaneously. The standard approach to solving this problem is to program the mass spectrometer in such a way to focus its time on the most abundant species present. The main drawback of this solution is the masking of less abundant species by more abundant ones. There are several approaches that can be used to improve the breadth of detection including improving the chromatography and experimental design (see section 4.6.1.3). However, the simplest solution is to reduce the complexity of the starting material.

With this in mind we set out to develop a method for purifying ribosomes that would be simple, robust, fast and yield ribosomes with minimal contamination from proteins that are not associated to them.

4.5.2 Chromatographic purification of ribosomes

The methodology for purifying ribosomes can be divided broadly into three categories: centrifugation, ammonium sulphate precipitation and chromatographic separation

(Spedding, 1990). Each has its advantages, but the main disadvantage shared by all of them is that they are either labour intensive or lengthy, and in some cases both.

Sucrose purification is the gold standard for ribosomal purification. However, obtaining purified ribosomal proteins from sucrose gradients takes at least 3-4 days, before they can be processed further prior to mass spectrometric analysis, e.g. digestion with trypsin, label with iTRAQ (for quantitative proteomics). Chromatography, which has recently become the focus of renewed interest, offers an appealing alternative to sucrose purification of ribosomes (Maguire *et al.*, 2008, Simons *et al.*, 2009). Its major advantage lays in its simplicity. However, up until now the speed of separation has been severely limited due to the architecture of the columns. Using beads, as the chromatographic matrix, is poorly suited for the separation of large molecules. The fundamental problem is a rapid build up of backpressure as the macromolecules fill the space between tightly packed beads, which significantly limits the maximum flow through the column (Barut *et al.*, 2008). Most chromatographic approaches therefore rely on slow gravitational flow as a result of which separation takes in excess of 10h (Jelenc 1980, LeGoffic *et al.*, 1974, Maguire *et al.* 2008). A method that would circumvent this limitation would present an important methodological improvement.

Monolith columns are a novel class of chromatographic supports, whose architecture is designed to bypass the problem of high backpressures. In contrast to conventional chromatography columns packed with semi-porous beads, the monolithic column is a single piece of highly cross-linked porous polymer of uninterrupted and interconnected channels. The sample is transported through the column via convection leading to rapid mass transfer between the mobile and stationary phase even for large biomolecules (Barut *et al.*, 2008). The absence of matrix packing leads to low backpressures allowing high flow rates to be achieved, therefore facilitating rapid separations of very large biomolecules such as protein complexes, immunoglobulins and viruses (Bencina *et al.*, 2004, Brne *et al.*, 2007, Kramberger *et al.*, 2007, Smrekar *et al.*,

2008). Consequently, we decided to investigate whether monolithic chromatography would be suitable for rapid purification of mycobacterial ribosomes.

4.5.2.1 Cell fractionation using monolith chromatography

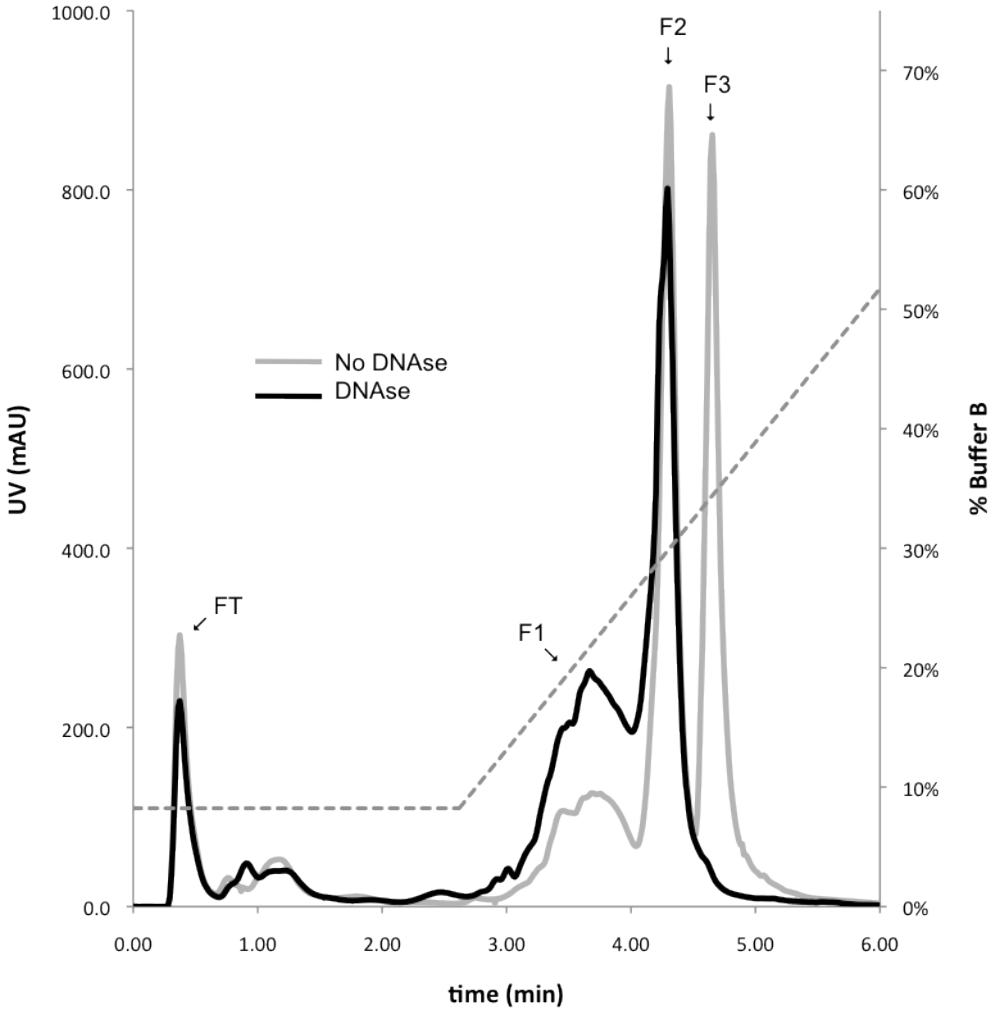


FIG. 4.23 Fractionation of *Msm* cell extracts on DEAE monolithic columns. Clarified cell extracts of *Msm* wild type were either treated with RNAse-free DNAse (black line) or loaded directly (grey line) onto a DEAE monolithic column. Bound material was eluted with a linear gradient of ribosomal buffer (10 mM Tris-HCl [pH 7.4], 70 mM KCl, 10 mM $MgCl_2$) containing 2 M NaCl (dashed line). The main fractions are labelled FT (flow through) and F1-3. Eluting species were recorded using an in-line UV detector

Our first choice regarded the chemistry of the chromatographic support. An inspection of the crystal structure of the ribosome (Selmer *et al.*, 2006) reveals that there are large areas of exposed rRNA on the surface of the ribosome. We hypothesised that the negatively charged phosphate backbone would interact with anion exchange column

chemistry. We chose to start our investigation by using two different anion exchangers – diethylaminoethyl (DEAE, see Fig. 4.23) and quaternary amine (QA, see Fig. 4.24). Given our experience with ribosomal integrity we performed the chromatography using the same ribosomal buffer we used during our profiling experiments, supplementing the buffer with 2M NaCl to elute the bound material.

Our initial attempts, using a linear NaCl gradient to elute the bound material, revealed that bacterial cell lysates could be fractioned very rapidly (less than 6 minutes) into three main components (F1-3). Given that DNA was reported to elute from monolithic columns at 0.6 – 0.8 M NaCl (Bencina *et al.*, 2004), we tested the possibility that genomic DNA elutes as a single fraction by pre-treating lysates with RNAse-free DNAse. We were thus able to identity fraction F3 as genomic DNA (Fig. 4.23).

We were interested in whether, analogously to DNA, ribosomes also elute as a single fraction. We collected the main fractions, pelleted the material by ultracentrifugation and analysed it by ribosomal profiling. We were successful in identifying 50S and 30S ribosomal subunits exclusively in fraction F2 (see Fig. 4.24).

We proceeded by precipitating the proteins from FT and F1-3 and analysing them by SDS-PAGE. The gels revealed that there were no proteins in FT and F3 (data not shown), while we were able to detect proteins in both F1 and F2. Importantly, a similar complement of proteins as those present in sucrose purified 70S ribosomes was observed in F2 (Fig. 4.25), providing additional evidence for the possiblity that ribosomes are the main component of F2.

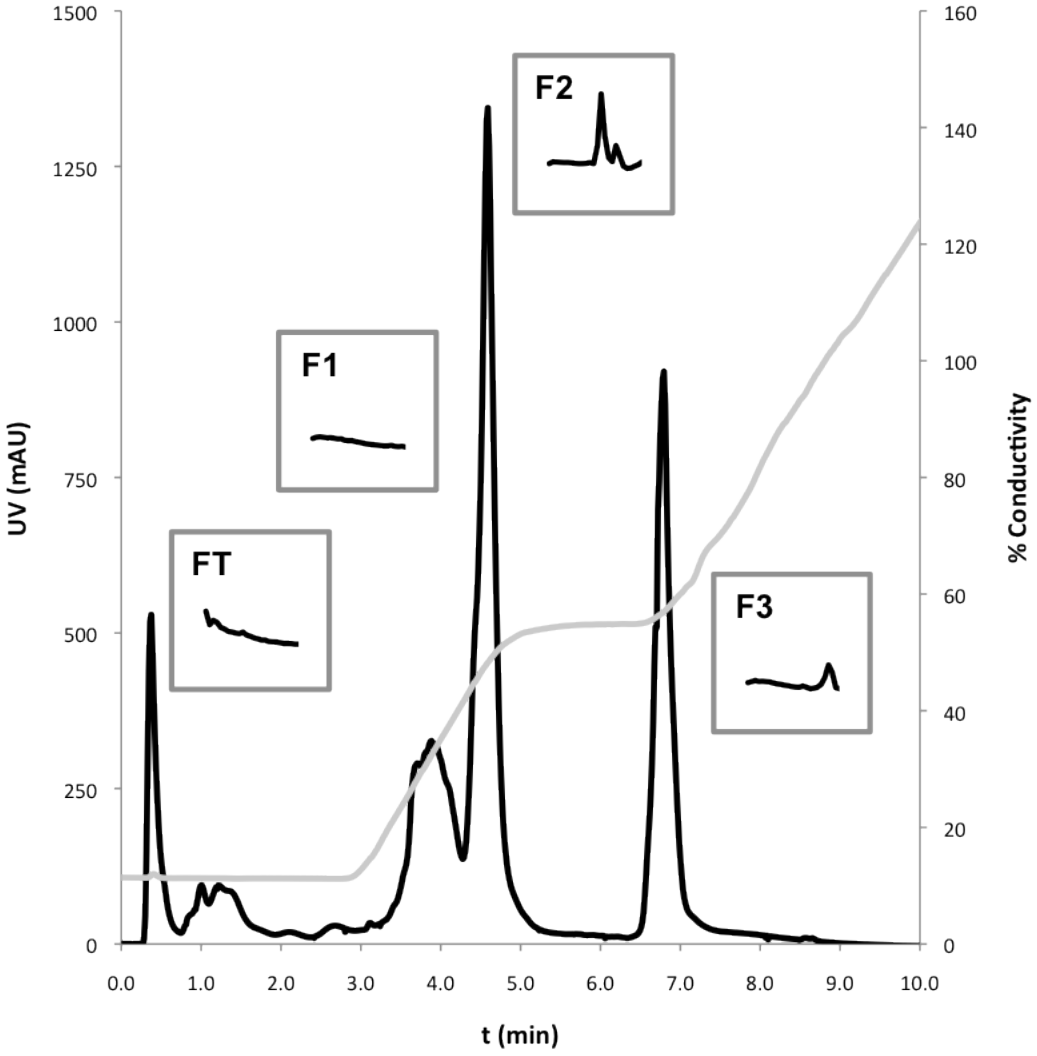


FIG. 4.24 Monolith-FPLC fraction F2 alone contains ribosomal subunits. Clarified cell extract from normoxic stationary phase *Msm* wild type cultures was loaded onto a QA monolithic column and eluted using ribosomal buffer containing 1 M NaCl. The same main fractions were obtained as with DEAE columns (labelled as in Fig. 4.23). Individual fractions were collected, ultracentrifuged to pellet ribosomes and used for ribosomal profiling (see insets). F2 shows evidence of 30S and 50S ribosomal subunits.

Eluting species were recorded using an in-line UV detector. % Conductivity (grey line) corresponds to the increase in the concentration of elution buffer.

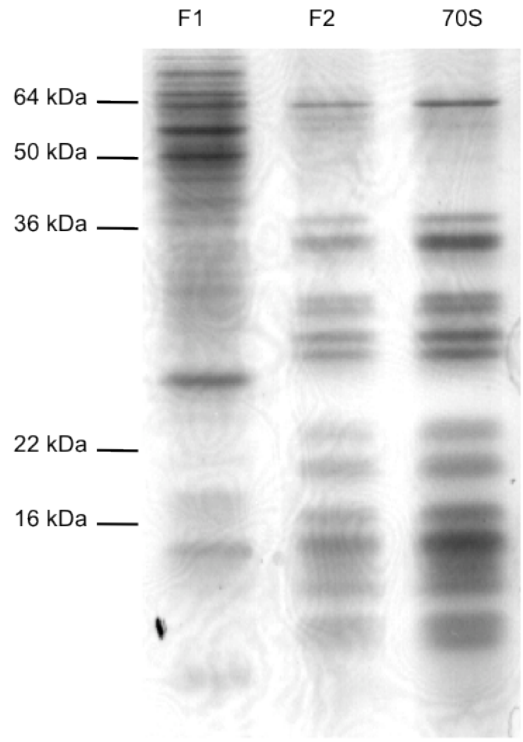


FIG. 4.25 The composition of chromatographic fraction F2 (see Fig. 4.24) and sucrose-purified ribosomes is comparable. Proteins from FPLC fractions F1, F2, and ribosome containing sucrose gradient fractions were precipitated with TCA and analysed by 15% SDS-PAGE. Gels were stained with Imperial Blue (Thermo) and developed by washing in dH_2O.

Having determined that the two main fractions are most likely to contain ribosomes (F2) and DNA (F3), we hypothesised that fraction F1 is likely to contain most other soluble cellular proteins. We precipitated proteins from all fractions, digested them with trypsin and performed a cursory analysis by mass spectrometry (data not shown). In accordance with SDS-PAGE analysis we were unable to identify any proteins in the flow through fraction and the DNA (F3) fraction. Fraction F1 contained many soluble proteins (enolase, adenylate kinase, pyruvate kinase, chaperones, superoxide dismutase), as well as some membrane and cell wall associated proteins (e.g Div IVA, fumarate reductase, ATP synthase). Fraction F2 on the other hand contained a large number of different ribosomal proteins as well as a few ribosome-associated proteins (e.g. EF-Tu, trigger factor) and some cytosolic proteins such as enolase, glycerol kinase. The scope of this set of mass spectrometric measurements was not to generate an

exhaustive catalogue of the proteins present in each fraction, but rather an exploratory glance, which would allow us to gain an appreciation of the likely components of each fraction. We revisited the composition of F2 later on (see Sections 4.6 and 4.7) using quantitative proteomics (iTRAQ).

4.5.2.2 Ribosomal profiling using chromatography

Eluting ribosomes in 2 M NaCl causes them to dissociate into their cognate subunits (see Fig. 4.24). This observation raised an interesting possibility – given that the overall amount of exposed negative charge on the two subunits as well as on the intact ribosome are likely to be different we were interested to see whether modifying the chromatographic program would allow us to separate these species and therefore maybe develop an alternative method of ribosomal profiling.

We first assessed the impact of different elution buffers on the chromatography. Maguire *et al.* (2008) reported that both ammonium chloride and ammonium sulphate can be used to elute ribosomes. They observed that by using ammonium chloride they were able to detect both dissociated subunits as well as associated ribosomes. We compared the cellular fractionation by adding NaCl, NH_4Cl and $(NH_4)_2SO_4$ to the elution buffer. We found that NaCl and NH_4Cl gave rise to comparable chromatography, while $(NH_4)_2SO_4$ had a detrimental effect, and we were unable to separate any fractions using this salt (Fig. 4.26A). To assess whether the ribosomes were still intact when eluted with NH_4Cl, we collected the chromatographic fractions and analysed them by ribosomal profiling. In accordance to the data obtained by Maguire *et al.* (2008) we were also able to isolate associated ribosomes directly after chromatographic separation (see Fig. 4.26B).

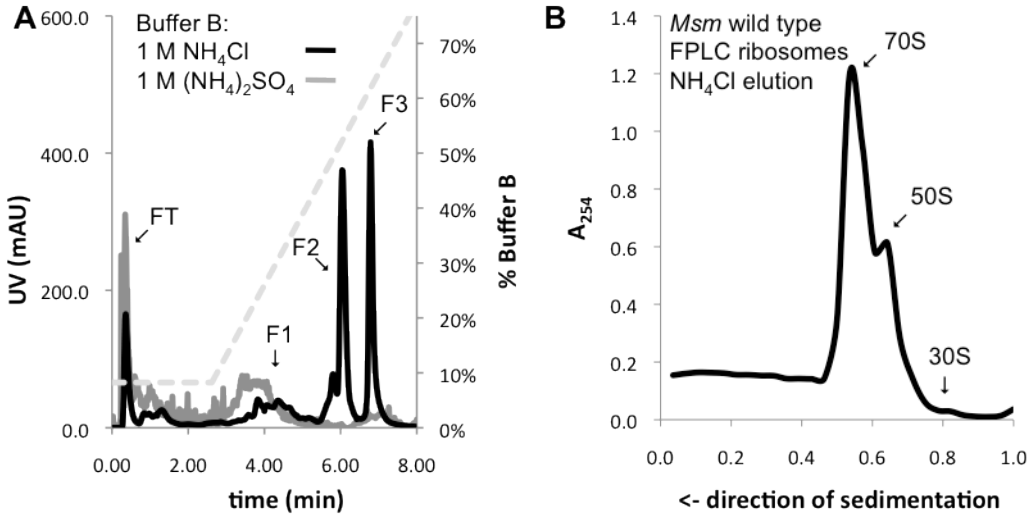


FIG. 4.26 Eluting ribosomes with NH_4Cl preserves associated ribosomes. (**A**) Clarified cell extract from normoxic stationary phase *Msm* wild type cultures was loaded onto an Akta-FPLC with an in-line QA monolithic column and eluted using ribosomal buffer containing either 1 M NH_4Cl (black line) or 1 M $(NH_4)_2SO_4$ (grey line). Fractions are labelled as in Fig. 4.23. Eluting species were recorded using an in-line UV detector. (**B**) Fraction F2 eluted with NH_4Cl was collected, ultracentrifuged to pellet ribosomes and used for ribosomal profiling.

Once we determined that we could elute associated ribosomes from the columns we were interested to see whether there are any differences in chromatography if we modify the concentration of Mg^{2+} ions in the chromatographic buffer in such a way to favour ribosomal dissociation (see Fig. 4.2). We used stationary phase *Msm* cultures for this analysis due to the simple ribosomal profile composed mostly of 70S ribosomes (see Fig. 4.7B) and split the cell pellet into two equal parts, one part was extracted using dissociative (1 mM $MgCl_2$) ribosomal buffer while the other was resuspended in normal (10 mM $MgCl_2$) ribosomal buffer. We then separated these extracts by chromatography using a linear elution gradient with ribosomal buffer + 1M NH_4Cl as the elution buffer (See Fig. 4.27).

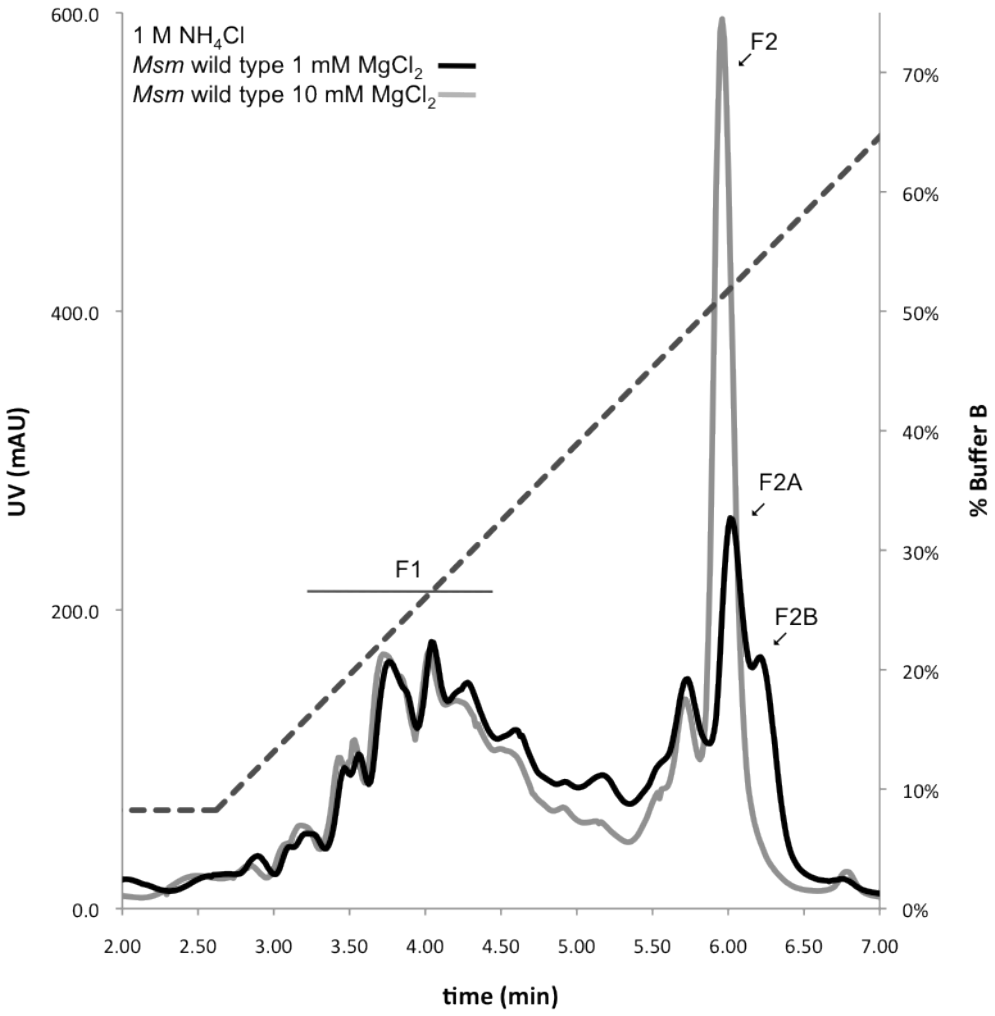


FIG. 4.27 Chromatographic profiling of *Msm* cell extracts. Stationary phase *Msm* wild type cells were lysed by passage through the French press in ribosomal buffer containing 10 mM $MgCl_2$ (favours ribosomal association) or 1 mM $MgCl_2$ (favours ribosomal dissociation). Extracts were loaded onto a QA monolithic column. Bound material was eluted with a linear gradient of ribosomal buffer containing 10mM $MgCl_2$ (grey line) or 1 mM $MgCl_2$ (black line) and 1 M NH_4Cl. Eluting species were recorded using an in-line UV detector.

Fractions F2A and F2B derived from F2 during the elution in buffer containing 1 mM $MgCl_2$ are indicated on the chromatogram.

Using this approach we were able separate additional species (F2A and F2B) under dissociative conditions, apparently arising from the ribosomal fraction (F2). This result could be indicative of the fact that we were able to separate 30S and 50S ribosomal subunits by chromatography. We were encouraged to pursue ribosomal profiling by chromatography further. We compared the separation using different anion

exchange column chemistry, but we found no significant differences in the separation using QA or DEAE columns (data not shown).

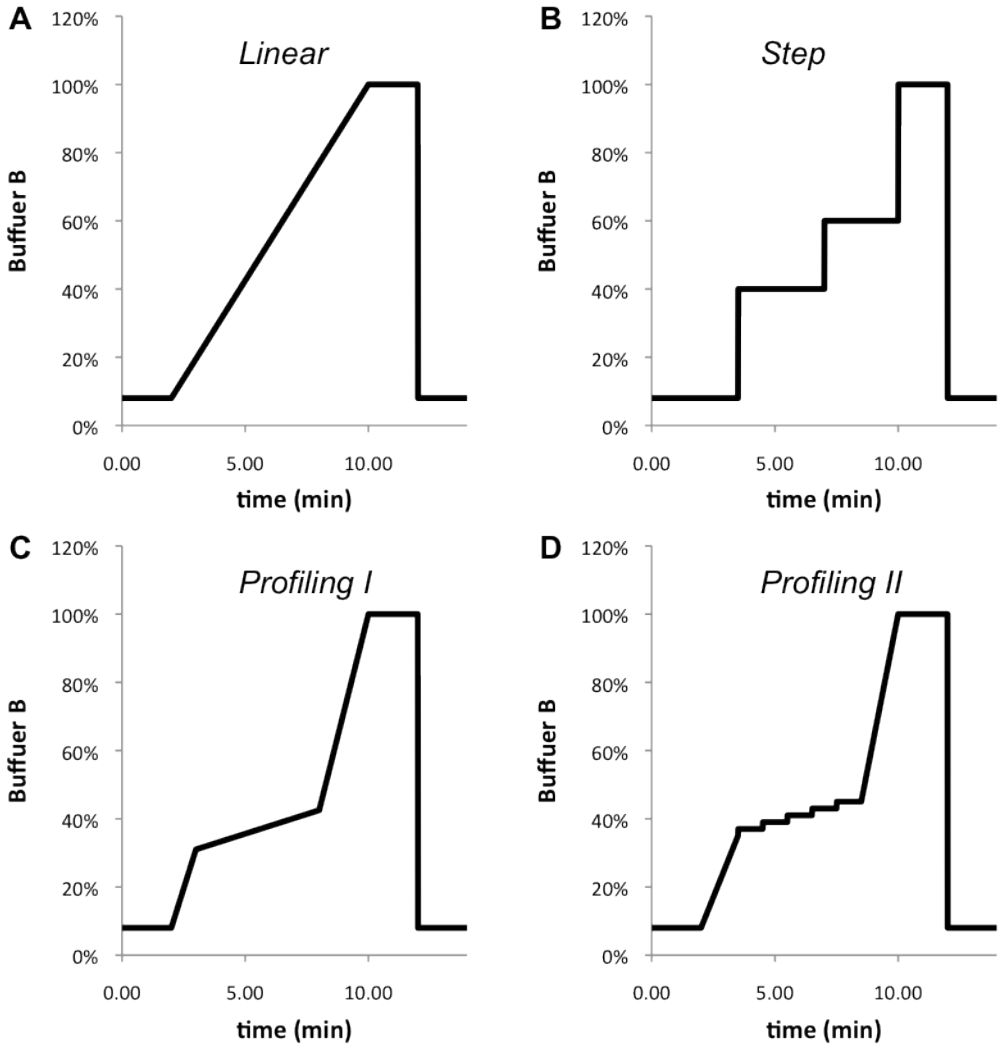


FIG. 4.28 Outline of chromatographic gradients used for the elution of ribosomal fractions during FPLC analysis.

Our next step was to modify the chromatographic program in an attempt to improve the separation between F2A and F2B. This was necessary in order to determine whether they correspond to the individual ribosomal subunits. We reasoned that by making the gradient shallower at the point where F2 elutes, we would be able to increase the separation at the expense of peak broadening. To this end we chose two chromatographic gradient, one that relied on a shallower linear gradient (Fig. 4.28C)

and one where the shallower linear gradient was replaced by multiple shallow step increases in elution buffer concentration (Fig. 4.28D).

Despite multiple attempts and our best efforts we were unable to devise a reproducible method for the separation of F2A and F2B (data not shown). The main limitation was that under the conditions used, the two fractions have very similar chromatographic properties. This meant that, to separate them we had to rely on the FPLC system to maintain a uniform flow and perfect elution buffer delivery. Any fluctuation in the concentration of elution buffer, due to imperfect mixing, or the flow, due to pump strokes, would affect the elution of the two species. The instrument in our laboratory – AKTA FPLC, was designed for preparative purposes and was not suitable for high precision work. As a result it was unable to maintain perfect buffer mixing and constant flow, therefore making it impossible to validate the use of monolith chromatography for ribosomal profiling.

4.5.2.3 Optimal isolation of ribosomes from crude extracts

Even though we were unable to develop a profiling method based on monolith chromatography, we became very familiar with the approach during the development stages, and were therefore able to understand how to manipulate the system to our advantage. Using our knowledge we adapted the chromatographic method to yield a single well-separated ribosomal fraction (Fig. 4.29).

The separation method was based on the stepwise increase in elution buffer concentration (see Fig. 4.28B). Using discrete steps, we minimised the negative effects of fluctuations in flow and elution buffer concentration, which hindered our attempts to use monolith chromatography for ribosomal profiling. The resulting chromatogram is consistent with our original fractionation and shows four distinct fractions – flow through, F1-3. As determined in 4.5.2.1 F1 contained mostly cellular proteins, while F2 and F3 contained ribosomes and DNA.

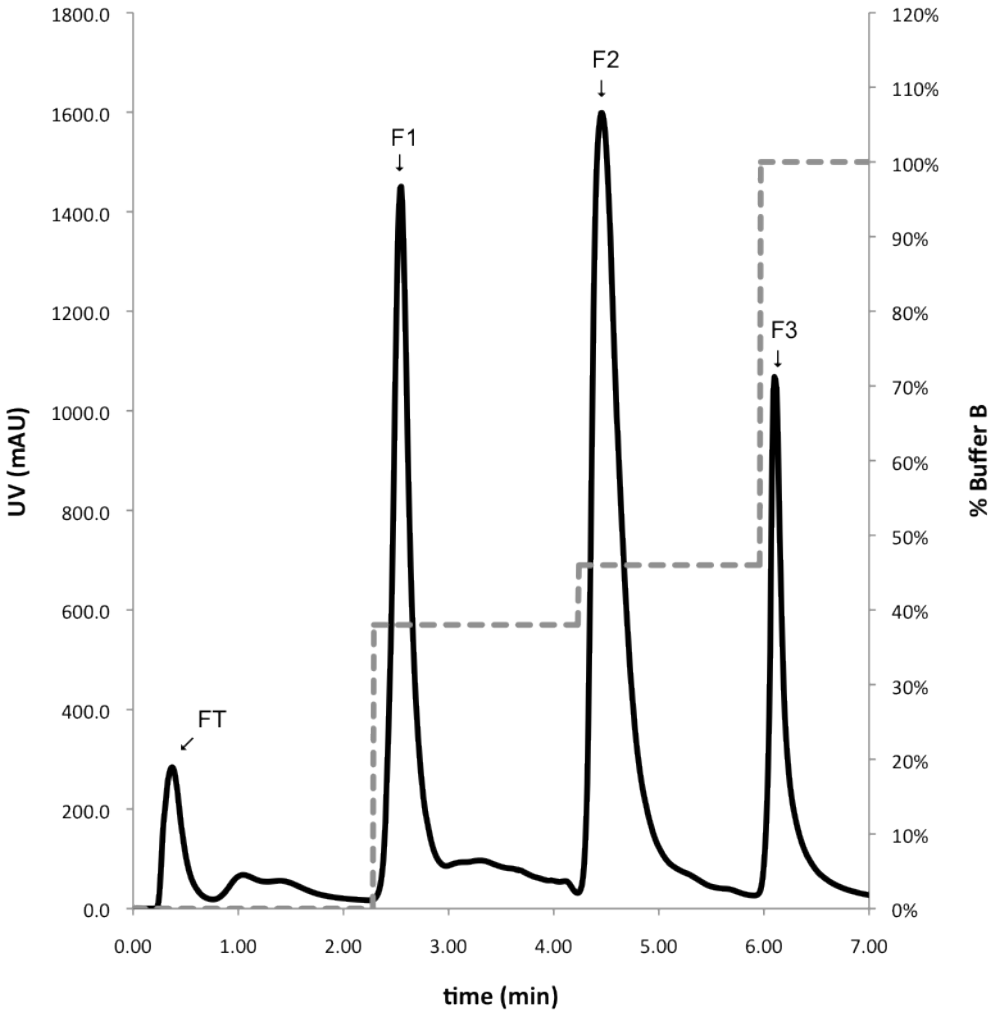


FIG. 4.29 Purification of *Msm* ribosomes using monolithic QA columns. *Msm* wild type cell extracts were loaded onto a QA monolithic column and eluted following a stepwise elution. The absorbance (black line) and the proportion of Buffer B (dashed line) are shown and the flow-through (FT) as well as fractions F1-3 are annotated.

4.5.2.4 Function of chromatography purified ribosomes

Given that we were able to purify ribosomes we were interested whether thus isolated ribosomes were also translationally active. Activity was not paramount for the success of this project; however if the isolated ribosomes were also active then we could obtain additional biological information regarding the biosynthetic potential of cultures in varying phases of growth.

We collected the ribosomal fractions and tested the activity of the eluted ribosomes using a coupled transcription-translation assay and [^{3}H]-erythromycin binding assay. We used a commercial *in vitro* transcription-translation kit, which we depleted of ribosomes by centrifugation. We then supplemented the kit with ribosomes purified from log phase *E. coli* cultures. The ribosomes were used either as eluted from the column (Fig. 4.30A "FPLC") or concentrated by ultracentrifugation prior to the addition to the reaction mixture (Fig. 4.30A "FPLC +"). We measured translational activity by recording the production of a bacterial luciferase enzyme.

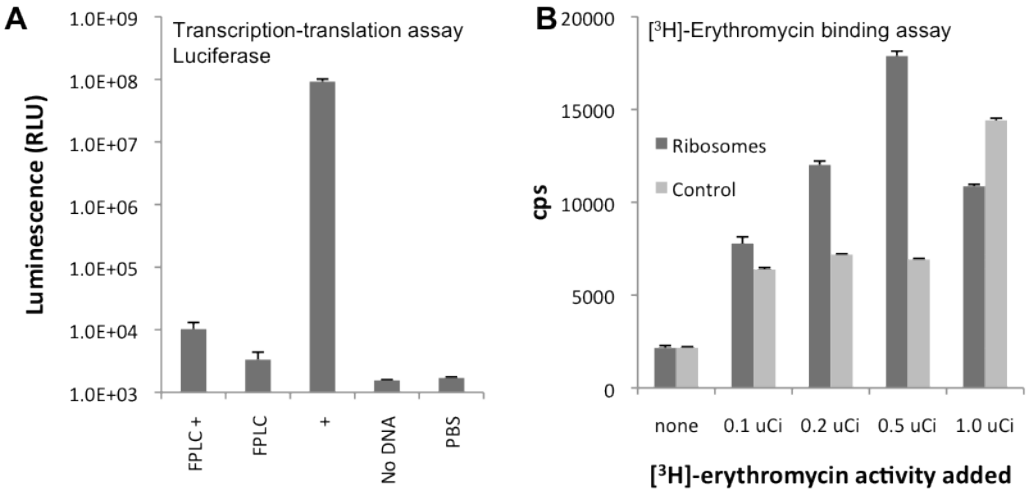


FIG. 4.30 Monolith-FPLC purified ribosomes show modest biological activity. (**A**) Ribosomes from actively growing *E. coli* were isolated by monolith-FPLC and used for coupled transcription-translation (T-T) assay expressing firefly luciferase. "FPLC+" ribosomes isolated by FPLC and concentrated by ultracentrifugation, "FPLC" ribosomes isolated by chromatography, "+" unaltered T-T kit activity, "No DNA" unaltered kit without template, "PBS" dilution buffer alone. (**B**) Binding of [^{3}H]-erythromycin by FPLC purified *Msm* wild type ribosomes that were concentrated using centrifuge filtration. Control experiments were performed in the absence of ribosomes (to assess the efficiency of the wash step to remove unbound antibiotic from filters).

T-T: histograms represent the average of 10 readings; error bars correspond to the standard deviation (N=10). [^{3}H]-erythromycin binding: histograms represent the average of two readings; error bars correspond to the standard deviation (N=2)

Our second approach was based on the observation that erythromycin binding can be used as proxy of ribosomal activity (Maguire *et al.*, 2008). We therefore measured the level of [^{3}H]-erythromycin binding to purified ribosomes prepared from

actively growing cells. Unlike for the transcription-translation assay, ribosomes were concentrated by filtration instead of centrifugation and incubated in the presence of tritiated erythromycin. The mixture was then loaded onto a glass fibre filter, washed with ethanol to remove unbound erythromycin and scored using a scintillation counter.

In both cases we were able to measure very modest levels of ribosomal activity. Showing that under the conditions used purified ribosomes were predominantly not translationally active. However, previous attempts to purify ribosomes by chromatography were successful in isolating active ribosomes, so it is probably possible to modify the protocol so that it would allow ribosomal activity to be maintained. We would expect that reducing the salt concentration in the buffer would improve the activity; a more concentrated ribosome preparation is also likely to yield higher measurable activity. However, we felt that ribosomal activity was not a sufficiently important priority for this project and have therefore decided not to pursue it further, focusing instead on evaluating our new method as a potential tool for the compositional analysis of mycobacterial ribosomes.

4.6 Evaluation of FPLC as a tool for compositional analysis

Having developed a rapid and reliable way to isolate ribosomes we turned to testing the method as a tool for compositional analysis. We were concerned with the possibility that by washing the ribosomes with relatively high concentrations of salt (both NaCl and NH_4Cl), we might wash off rProteins and therefore limit the scope of this approach for meaningful biological analysis. Given that such an effect is unlikely to be absolute we wanted to use a quantitative approach to compare ribosomes purified by FPLC to those purified by sucrose gradient ultracentrifugation. We chose an approach based on isobaric Tag for Relative and Absolute Quantitation (iTRAQ), which would allow us to identify the missing ribosomal proteins as well as determine the extent to which this

loss occurred. In addition we would also be able to compare how the complement of associated factors differs between the two purification methods.

4.6.1 Quantitative proteomics using iTRAQ – method implementation

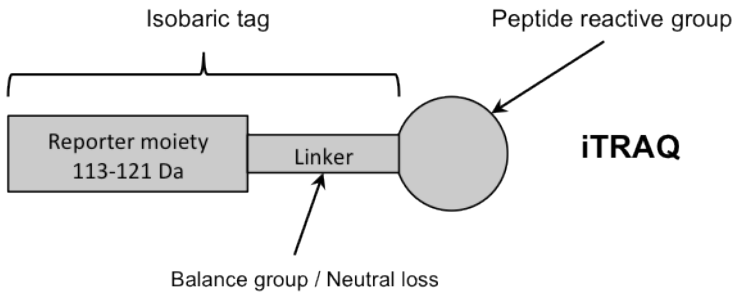


FIG. 4.31 Schematic representation of the iTRAQ tag. The relative abundance of peptides is determined by quantifying the abundance of the reporter moiety (113-121 Da for 8-plex labels).

The iTRAQ method is based on the use of up to eight isobaric (of same mass) labels to tag peptides obtained from separate samples (Fig. 4.31). All samples are pooled after labelling and the spectra of the constituent peptides acquired. Given that the labels are isobaric and have been developed to have a minimal impact on chromatography, the tagged peptides elute simultaneously and appear as the same species during the mother ion selection stage of the MS/MS experiment. The structure of each label is such that upon fragmentation during an MS/MS experiment it yields a diagnostic ion of specific size (114-119 or 121 Da) whose intensity is proportional to that of the tagged peptide. It is therefore possible to determine the relative abundance of each peptide in the different samples – as long as it is present. Protein quantitation is improved by measuring multiple peptides from a single protein.

The experiment itself can be divided into four distinct steps:

1. *sample preparation*: purified proteins are first reduced with *tris*(2-carboxyehtyl)phosphine (TCEP) and the free sulfhydryl groups are then blocked by methylation with methyl methanethiosulfonate (MMTS). Thus modified proteins are then digested with trypsin,

2. *covalent labelling of peptides*: iTRAQ binds covalently to free amino groups on peptides (both N-terminal and side chain). The reaction occurs under alkaline conditions in triethylamine bicarbonate (TEAB),
3. *purification of labelled peptides*: many of the reagents used are incompatible with HPLC-MSMS and must therefore be removed from the sample prior to analysis. Strong cation exchange (SCEX) chromatography is often used to purify labelled peptides,
4. *HPLC-MSMS analysis*.

4.6.1.1 Troubleshooting of iTRAQ implementation

In our first iTRAQ experiment we prepared four ribosomal samples by FPLC and four by sucrose gradient ultracentrifugation. We processed each sample according to the manufacturer's instructions prior to analysis by HPLC-MSMS. However we were only able to detect a very small number of peptides, both labelled and unlabelled. As can be seen from the chromatogram there is a limited number of species eluting every early in the separation (Fig. 4.32). It is important to note that the clustering of peptides early in the chromatogram indicates that they interact poorly with the reverse phase column used for the separation and are therefore most probably charged peptides. Taken together, these observations are indicative of a loss of sample, most probably during the SCEX purification of labelled peptides.

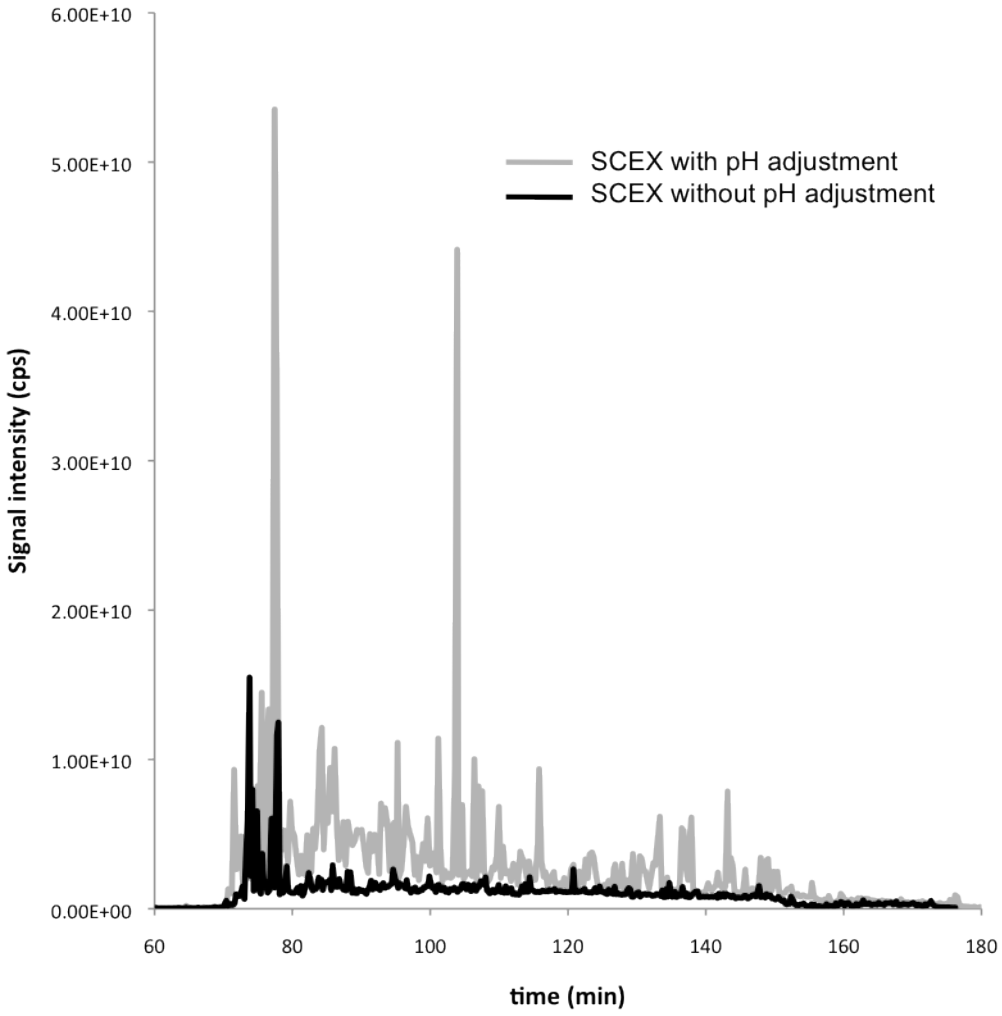


FIG. 4.32 The pH of iTRAQ labelled peptides needs to be adjusted prior to SCEX cleanup of the samples. Tryptic peptides from ribosomal fractions isolated by FPLC (4) and sucrose gradient ultracentrifugation (4) were labelled with different iTRAQ tags and pooled. Reagents that could interfere with mass spectrometry were removed from the peptide mixture by SCEX prior to HPLC-MS analysis. Signal intensity expressed as counts per second (cps) are shown for samples whose pH has (grey line) or has not (black line) been adjusted prior to SCEX.

It is important that peptides have an overall positive charge in order to be retained on the SCEX column. The pKa of most α-carboxylic groups of amino acids is less than 2.5 (Stryer, 2007) therefore making sure that the pH of the sample is low enough (around 2) prior to loading onto the SCEX column is very important, as full protonation would be required in order for peptides to bind the SCEX column. During our experiment we kept the flow-through from the SCEX column after loading the sample, which would contain all the peptides that did not bind to the SCEX column. When we

measured the pH of the flow-through we found it to be alkaline. Most carboxylic groups on peptides would be deprotonated under alkaline conditions and would therefore interact only poorly with a cation exchange column, explaining why we only saw a small number of peptides during our initial analysis, most of which charged. We therefore adjusted the pH of the flow through to 2 with HCl and performed the peptide purification step again. We then analysed these samples again by HPLC-MSMS, and were able to identify a number of labelled and unlabelled peptides – including ribosomal peptides (Fig. 4.32). Closer inspection however showed that labelled peptides were mostly derived from sucrose-purified samples, while almost none of the iTRAQ labels used for FPLC purified ribosomal preparations could be detected, making comparison impossible. To illustrate this point we extracted the signal from two iTRAQ labels: 114 Da was used for an FPLC sample, while 119 Da was used for a sucrose-purified sample (Fig. 4.33).

The chemistry of the iTRAQ label was developed to bind to free amino groups peptides. We therefore hypothesised that the lack of labelled peptides form FPLC purified ribosomes, may reflect the presence of residual NH_4Cl, from the elution buffer, in the sample. Initially we did not expect that carry over of NH_4Cl would be a problem, since proteins were precipitated with acetone and washed prior to further processing. However, the absence of labelled FPLC derived peptides is consistent with the possibility that residual NH_4Cl did react with most of the iTRAQ label added. We substituted NaCl for NH_4Cl in the elution buffer formulation, as it was obvious that if we were to successfully label ribosomal peptides from FPLC fractions then we could not use NH_4Cl in the elution buffer. To ensure that the FPLC purification did not interfere with iTRAQ labelling of peptides we purified bovine serum albumin using the same reagents used for ribosome purification. We then processed the eluted protein in the same manner as we would ribosomal samples, including labelling its peptides with iTRAQ and analysed them by HPLC-MSMS. We were able to prove that we did label peptides from

BSA and we managed to identify 42 labelled peptides covering 39.0% of the sequence (data not shown).

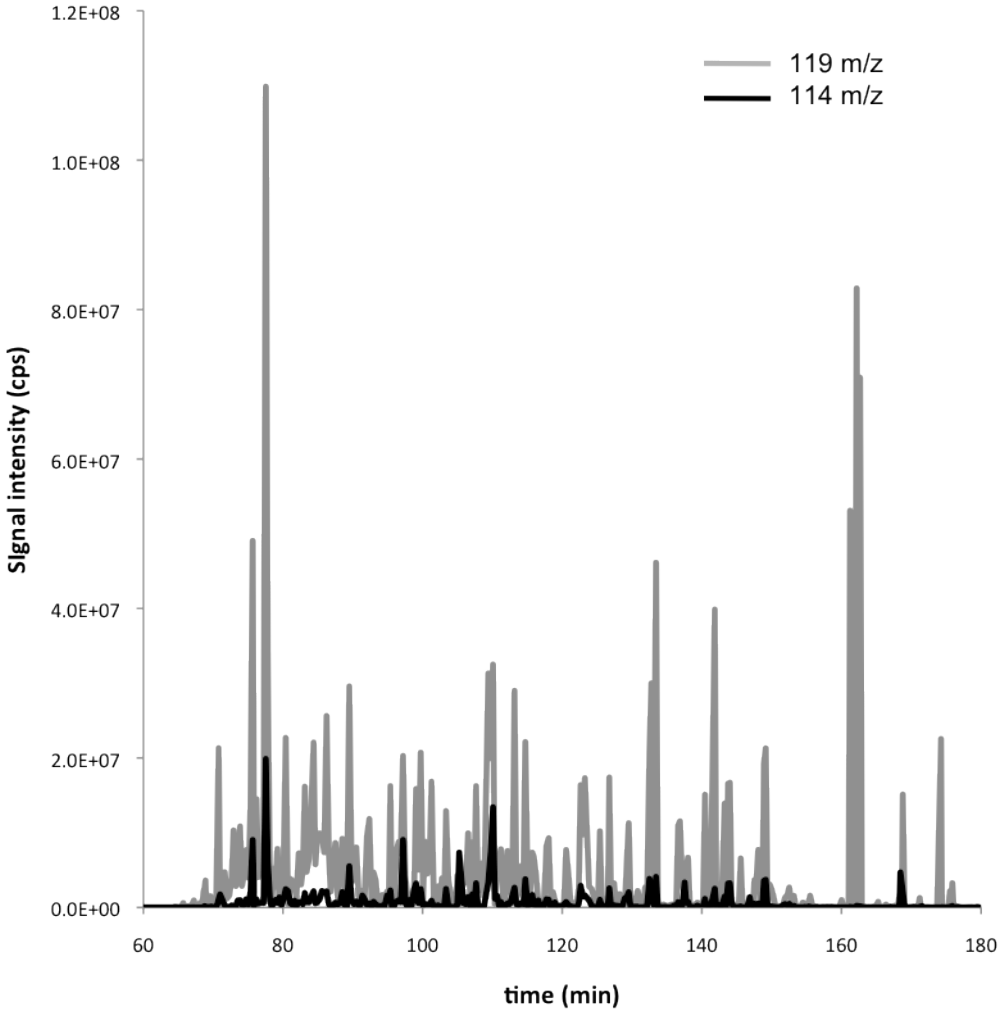


FIG. 4.33 Monolith-FPLC purified ribosomal preparations cannot be labelled with iTRAQ if eluted with 1 M NH_4Cl. The signal intensity for ions with an m/z of 114 corresponding to the tag used for a monolith-FPLC purified sample (black line) and ions with m/z of 119 corresponding to the tag used for a sucrose-purified sample (grey line) were extracted from the spectra shown in Fig. 4.32.

4.6.1.2 Optimisation of iTRAQ - labelled peptide purification

The use of SCEX chromatography prior to sample analysis is well suited for the removal of reagents that could interfere with HPLC-MSMS analysis – triethylamine, TCEP, MMTS; however the peptides are eluted using 300 mM salt, which can cause significant ion suppression in the mass spectrometer. There is therefore a need to "desalt" the samples

prior to separating the samples by HPLC. This can be done in two ways: the samples can either be desalted offline using solid phase octadecyl (C_{18}) cartridges (e.g. Waters SepPak or Millipore ZipTip), or online using a C_{18} trap column and an extensive wash.

We compared the complexity of samples that were desalted offline to those desalted online and found that the introduction of additional C_{18} purification steps leads to a small loss of sample complexity (data not shown). This finding led us to conclude that additional offline desalting was unnecessary and online desalting was sufficient to obtain good quality spectra. A summary of the iTRAQ labelling protocol is shown in Fig. 4.34 below.

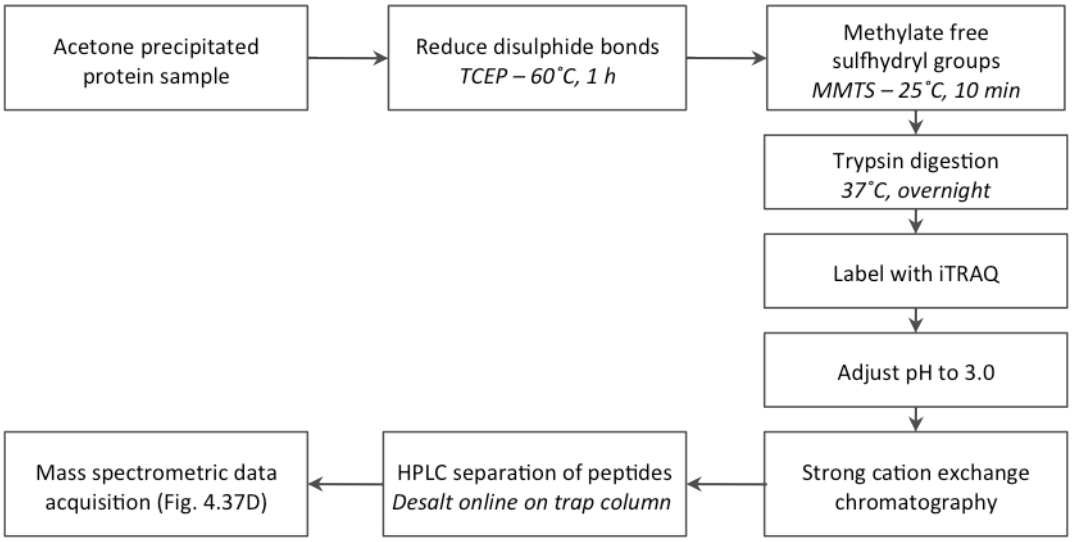


FIG. 4.34 Summary flow chart for iTRAQ labelling of tryptic peptides.

4.6.1.3 Optimisation of iTRAQ – data acquisition

As pointed out in section 4.5.1 there is a limit to the number of ions that can be analysed simultaneously by tandem mass spectrometry. We have so far described the steps taken to reduce the complexity of the sample, namely the development of a novel method for purifying ribosomes. It is evident from Fig. 4.32 that the chromatographic program used during HPLC prior to mass spectrometric analysis allows the elution of peptides over the entire course of the separation. While the chromatography could be improved by

adding a dimension to the separation (ie adding a column of different chemistry), we felt that the level of separation was sufficient for our needs.

Having reduced the complexity of the sample and decreased the number of peptides (ions) that enter the mass spectrometer simultaneously we turned to one more parameter that could be optimised further – the acquisition method. In all the runs so far we used the full information-dependent acquisition method (full IDA). The full IDA experiment relies on the mass spectrometer to cycle between enhanced MS (EMS) survey scan to determine what are the four most abundant ions at a particular time point; followed by an enhanced resolution (ER) scan to select these ions and use them for enhanced product ion analysis (EPI) – ie MSMS. Each cycle takes from 6-650ms depending on the amount of sample present.

The main problem with full IDA is that only four peptides can be analysed at any point, due to the minimum amount of time that the detector needs to spend on each ion. It is possible to improve the overall number of analytes by running each sample multiple times, but limiting the number of ions that the detector analyses during each run. There are two main strategies to achieve this, one based on "m/z windows" and one on the generation of a precursor ion exclusion list. In the "m/z windows" approach the user limits the mass to charge (m/z) range of mother ions that the mass spectrometer selects for further analysis. By giving the mass spectrometer an interval of m/z we artificially decrease the complexity of the sample. Using multiple m/z intervals, which cover the entire dynamic range of the detector and collating all the resulting data, would allow us to measure a larger population of peptides, than measuring the samples using full IDA alone.

An alternative approach would be to use a full IDA method, and generate a list of ions to be excluded from the next round of analysis. By running successive rounds of

analyses, each time excluding all the ions that were measured previously, we should be able to obtain a comprehensive list of peptides present in the sample.

We compared these two approaches on a new set of iTRAQ labelled ribosomal peptides obtained from FPLC (N=4) and sucrose gradient (N=3) purified preparations. An initial full IDA HPLC-MSMS analysis of the new sample revealed that we had successfully labelled peptides from both sources. Moreover we had sufficient sample for multiple injections, allowing us to investigate the different approaches to data acquisition and its impact on quantitation.

During the initial full IDA analysis of the sample, we detected 1822 ions. We used this result to create an exclusion list and to inform us regarding the distribution of detected ion masses, so that we could choose mass intervals that would generate windows of comparable sample size (Fig. 4.35).

When we ran a full IDA again using the result of the previous experiment as the exclusion list we were able to measure 1596 ions. This result was encouraging, since none of these ions appeared to be detected in the original sample. However, when we used the two full IDA results as separate sources of spectra for analysis with ProteinPilot, we identified the there was a significant overlap in the identified peptides (data not shown). The most likely explanation for this result is that the detector measured most of the same ions as during the initial full IDA. This can occur if the m/z accuracy of the instrument is less than the cut-off range for each excluded ion. For example, if an ion has an experimental m/z of 845.0707 while the theoretical m/z is 844.9916 then the ion was measured to an accuracy of ±0.0791 m/z. If the cut-off for the exclusion list is set to less than that value, then the ion could still be detected and analysed. Given that peptides have a very similar range of masses, then it is in the interest of the researcher to keep the cut-off for the exclusion as close to the actual ion as possible. Q-TRAP instruments, like the one used in these experiments, are known to

suffer from lower m/z accuracy when compared to quadrupole/time-of-flight (QTOF) instruments (Hager, 2004). An improved method is by using dynamic exclusion list (Wang and Li, 2008). In this approach the ion exclusion is coupled to a retention time window to improve the result. A dynamic exclusion list requires the chromatographic separation to be highly reproducible, which was not the case in our methodology (data not shown). Overall, we conclude that the exclusion list approach to increasing sample coverage is not appropriate for use in our analyses.

To assess the feasibility of using m/z windows as a way to improve data acquisition we split the 1822 ions detected during the first full IDA into m/z bins containing a comparable number of ions (Fig. 4.35A). By doing so we obtained nine m/z windows ranging from 325 m/z – 1200 m/z, containing approximately 150 ions each. We assumed that the distribution of m/z in the total sample would reflect that of the portion of the sample that we measured. We proceeded by loading the sample again 9 times limiting the detection span of the detector so that it corresponded to the m/z window. By using this approach we were able to detect 10824 ions (an average of 1203 ± 93 peptides per sample) - a 5.9 fold increase compared to full IDA alone.

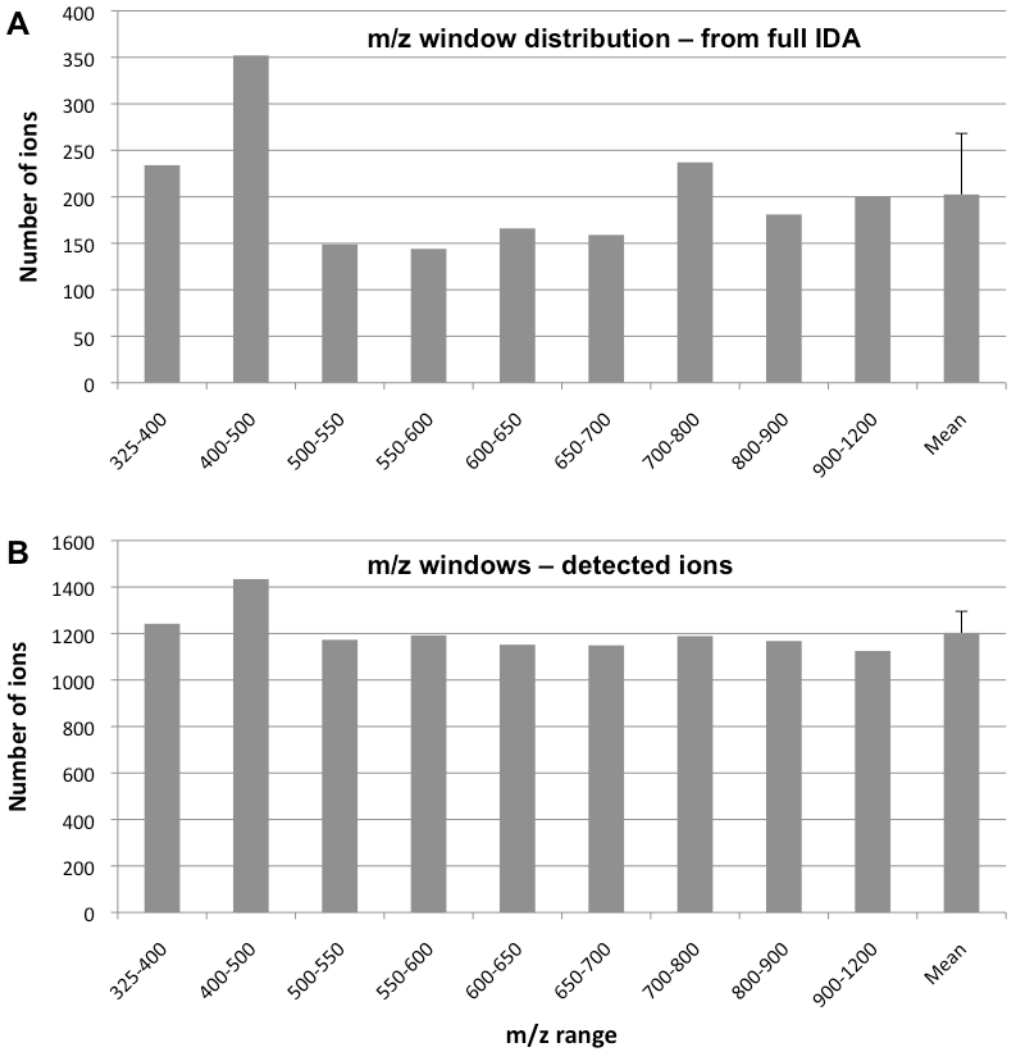


FIG. 4.35 Increasing the depth of analysis by setting up m/z windows for mass spectrometric analysis. Tryptic peptides from ribosomal fractions isolated by FPLC (N=4) and sucrose gradient ultracentrifugation (N=3) were labelled with different iTRAQ tags and analysed using a Full IDA mass spectrometric method as well as using distinct m/z windows. (**A**) The ions detected by full IDA could be split into bins of similar size based on their m/z (m/z windows). (**B**) A similar number of ions could be obtained from each analysis using the selected m/z windows. Spectra were analysed using ProteinPilot software.

We used the spectra from the full IDA, m/z windows and a collation of the two sets of spectra and analysed them using protein pilot. The software was able to attribute 1822 spectra from the full IDA experiment, 4591 from the m/z windows experiment and 6814 spectra in the collated data set. Since the number of peptides identified in the combined data set was much lower than the sum of the two constituent data sets we

were interested to see how the acquisition method affected the complement of detected peptides (Fig. 4.36)

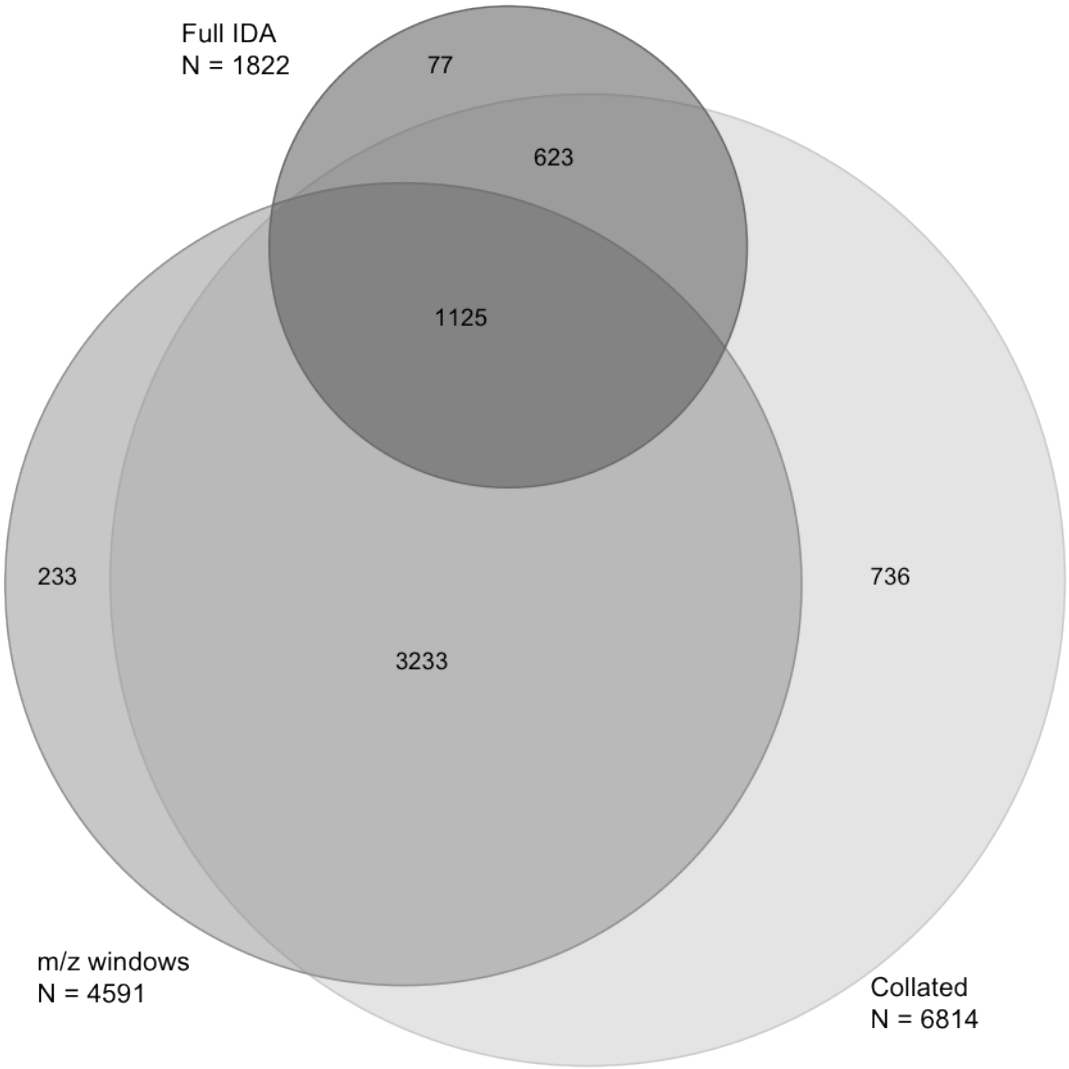


FIG. 4.36 A combination of acquisition methods yields a higher depth of analysis. Tryptic peptides from ribosomal fractions isolated by FPLC (4) and sucrose gradient ultracentrifugation (3) were labelled with different iTRAQ tags and analysed using a Full IDA mass spectrometric method and 8 m/z windows. Three different data sets were used as input for analysis by ProteinPilot software – full IDA alone, m/z windows alone as well as the two combined.

It is interesting to note that, even though we collated the spectra form m/z windows and the full IDA data sets prior to submission into ProteinPilot, there were still peptides that were only identified in the "full IDA" (77) or "m/z windows" (233) data sets. On the other hand there were 736 peptides that were identified in the collated data set alone. We cannot comment on this observation, and we assumed that this result

reflects the nature of the algorithms, thresholds and cut-offs used by ProteinPilot, the discussion of which is beyond the scope of our project.

When attributing the detected peptides to proteins with ProteinPilot, we were able to identify 58 distinct proteins from the full IDA data set, 69 proteins from the m/z windows data set and 74 proteins from the collated data set (Fig. 4.37A). Unlike with the peptides, there were no proteins that were identified exclusively in the m/z windows or full IDA data set, while collating the spectra did allow us to tease out additional information about proteins that would not be identified by either approach alone. While we expected that proteins identified from full IDA spectra would form a subset of those identified by m/z windows, we found that not to be the case despite the larger overall number of proteins identified from m/z windows data. For example, there were three ribosomal proteins, which could be identified from full IDA data but not m/z windows data (Fig. 4.37A-B).

Interestingly the median sequence coverage for the m/z windows dataset was 29.2% while that of full IDA was 37.8% and that of the combined dataset was 38.7%. This shows that using m/z windows does not improve the overall sequence coverage of proteins, however it does increase the pool of peptides and therefore increasing the confidence of identifying less abundant proteins (Fig. 4.37C). It is possible that many of the spectra acquired are of poorer quality or reflect impurities present in the sample, explaining why ProteinPilot only managed to assign a peptide to 42.4% of the total ions detected.

Overall we found that using a combination of the full IDA and the m/z windows acquisition methods allows us to increase the overall number of proteins that we were able to detect, while also improving the sequence coverage. This is particularly important for the quantitation of our results: since the significance of protein

quantitation is increased dramatically when multiple labelled peptides are quantified for each protein.

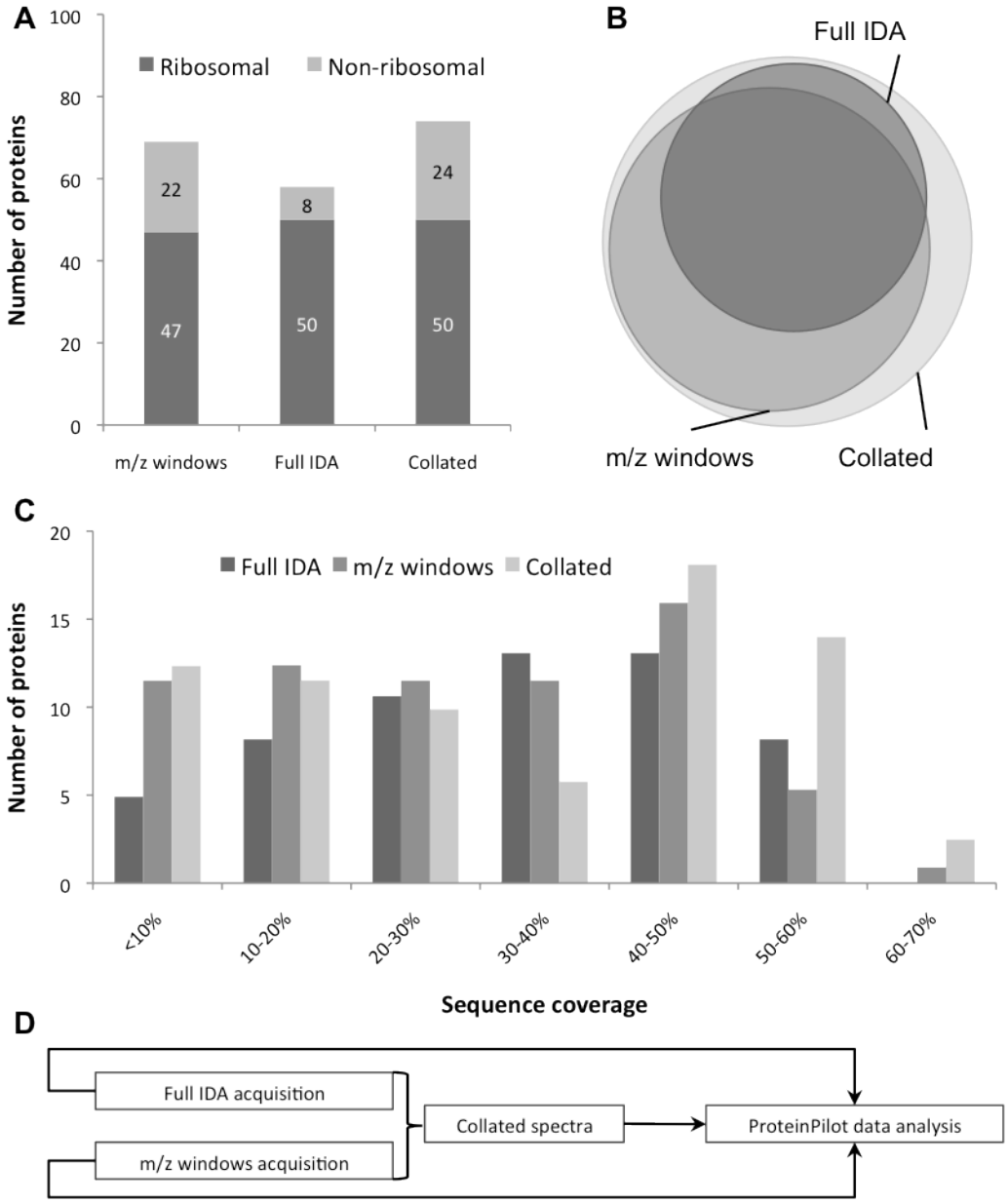


FIG. 4.37 The total number of proteins identified and the sequence coverage of each protein is improved by combining acquisition methods. (**A**) Number of identified proteins using each approach. (**B**) Venn diagram of identified proteins using each approach. (**C**) Sequence coverage of identified proteins using each approach. Spectra were analysed using ProteinPilot software. (**D**) Summary of data analysis approach.

Once we established that the acquisition method was improved allowing the identification of 16 additional proteins when compared to full IDA alone, we were interested to see how the quantitation ratios (e.g. ratio of label 115 over label 113, Fig.

4.38A) were distributed. We used the quantification data and plotted the distribution of peptide ratios. We expected a distribution centred around 1, since both these labels were used to label ribosomal proteins purified by sucrose gradient ultracentrifugation (see Fig. 4.38B).

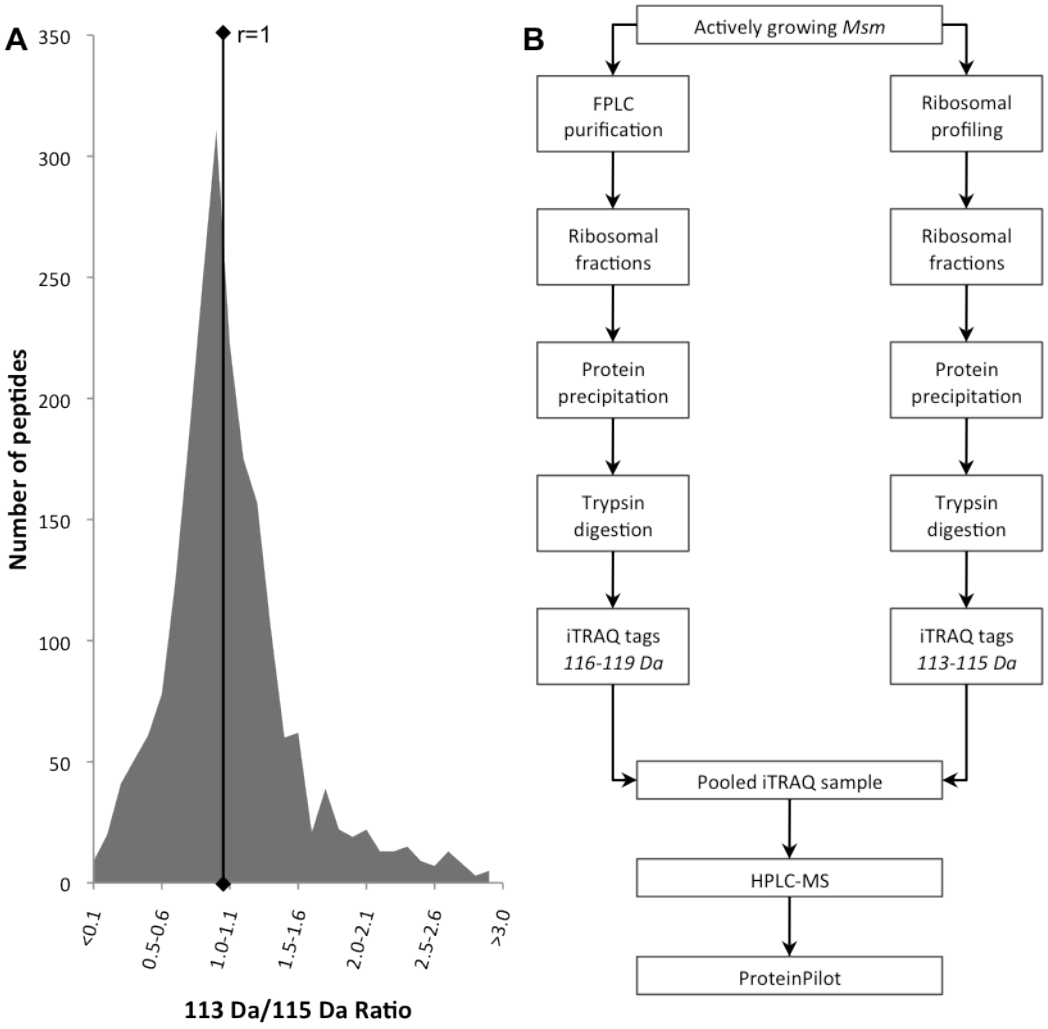


FIG. 4.38 Equivalent samples are comparable when labelled with different iTRAQ tags. Tryptic peptides from ribosomal fractions isolated by FPLC (4) and sucrose gradient ultracentrifugation (3) were labelled with different iTRAQ tags and analysed by HPLC-MS. (**A**) The ratios of intensities for iTRAQ labels 113 over 115 (both corresponding to sucrose purified samples) were calculated for all the identified peptides (confidence score of at least 95% in ProteinPilot). The data were split into 30 bins each corresponding to a ratio interval of 0.1. The number of peptides in each bin was plotted against the range of the ratios covered. (**B**) A flow chart illustrating the sample processing for the iTRAQ experiment used to compare the composition of ribosomes isolated by FPLC to those purified by sucrose ultracentrifugation.

4.6.2 iTRAQ compositional analysis – FPLC purification scrutiny

We used the optimised iTRAQ method to compare the protein composition of ribosomes isolated by FPLC-monolith chromatography to those isolated by sucrose gradient ultracentrifugation. We labelled sucrose-purified ribosomal samples with iTRAQ labels 113-115, while FPLC samples were labelled with iTRAQ labels 116-119 (see Fig. 4.38B). Label 121 was used to confirm the labelling of BSA (See section 4.6.1.1).

TABLE 4.2 Comparative iTRAQ analysis of *M. smegmatis* ribosomal fractions by mass spectrometry

Large Subunit Proteins[a]	L1, L2, L3, L4, **L5**[b], L6, **L7/12**[c], **L9**[b], L10, **L11**[b], L13, L14, L15, L16, L17, L18, L19, L20, L21, **L22**[b], L23, L24, L25, L27, **L28**[b], L29, L30, L32, L33, L36
Small Subunit Proteins[a]	S1, S2, S3, S4, S5, S6, S7, S8, S9, S10, S11, S12, S13, S14, S15, S16, S17, S18, S19, S20
Ribosome associated proteins[a]	EF–Tu, Trigger factor[c]
Non-ribosomal Proteins[a]	Enolase[c], RNA polymerase[c], Glutamine synthase[c], Glycerol kinase[c], Acyl carrier protein[c], trypsin

[a] The details of % sequence coverage, the number of peptides included for the analysis of each protein, the specific label ratios and significance values are listed in SupTab4.xls, SupTab5.xls and SupTab6.xls – see included data CD.

[b] significantly ($p < 0.05$) more abundant in sucrose purified ribosomal fractions

[c] significantly ($p < 0.05$) more abundant in FPLC purified ribosomal fractions

We successfully detected 50 out of the 53 different ribosomal proteins encoded in the *Msm* genome (Kanehisa *et al.*, 2006) in ribosomes isolated by monolith chromatography and sucrose gradient purification. The abundance of the vast majority of ribosomal proteins was found to be comparable in both preparations. The exceptions to this are highlighted in Table 4.2, most notable of which (2.2 fold difference) were ribosomal proteins L9 and L7/12. L9 was found to be more abundant in sucrose-purified fractions, while L7/12 was more abundant in chromatographically purified fractions. Furthermore, no significant differences were observed when comparing repeat FPLC runs and/or repeat samples, pointing to the high reproducibility of our

technique (data not shown). It is important to note that ribosomal proteins L31, L34 and L35 were not detected during our analyses of either chromatographically or sucrose purified ribosomes. We believe that the lack of these proteins in our dataset does not reflect their absence from isolated ribosomes, but points to the technical limitation of the mass spectrometer in detecting these particular proteins (Iost *et al.*, 2008).

We conclude that the protein composition of monolith chromatography purified ribosomes is qualitatively and quantitatively similar to sucrose–gradient purified ribosomes. In addition to ribosomal proteins we were able to identify a number of proteins that do not form an integral part of the ribosome. These could be divided into two groups, proteins that are known to associate to the ribosome (EF-Tu, Trigger factor) and those that are not (Glycerol kinase, Glutamate synthase). More proteins that are not normally considered to be ribosome-associated were present in the monolith chromatography preparations. As some of these proteins have been found to be present in ribosomal fractions during previous studies (Iost *et al.*, 2008, Simons *et al.*, 2009) it may suggest that chromatographically isolated ribosomes are less pure, and the presence of certain proteins just reflects their relative abundance in the cytosol. Alternatively, the co-purification of these enzymes may reflect similar chromatographic properties to those to ribosomes.

Despite these differences, overall the data indicate that ribosomes obtained by the two approaches are comparable and we believe that rapid FPLC purification of ribosomes is a suitable tool to address question of compositional analysis of ribosomes.

4.7 Compositional analysis of ribosomes during stasis

We developed a new toolkit that would enabled us to ask questions regarding the composition of mycobacterial ribosomes, with the hope that we would be able to detect growth-phase dependent changes in the complement of ribosomal proteins and their associated factors.

4.7.1 Choice of samples

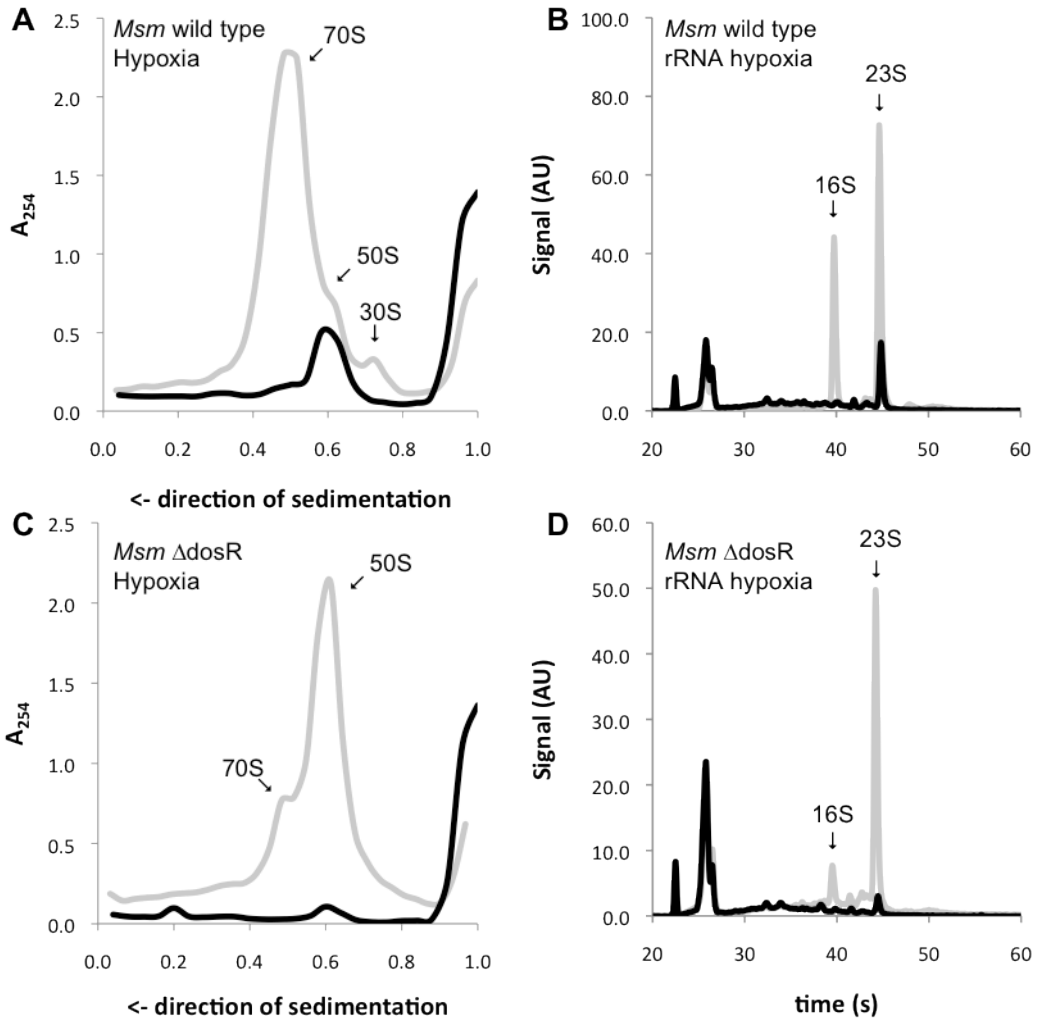
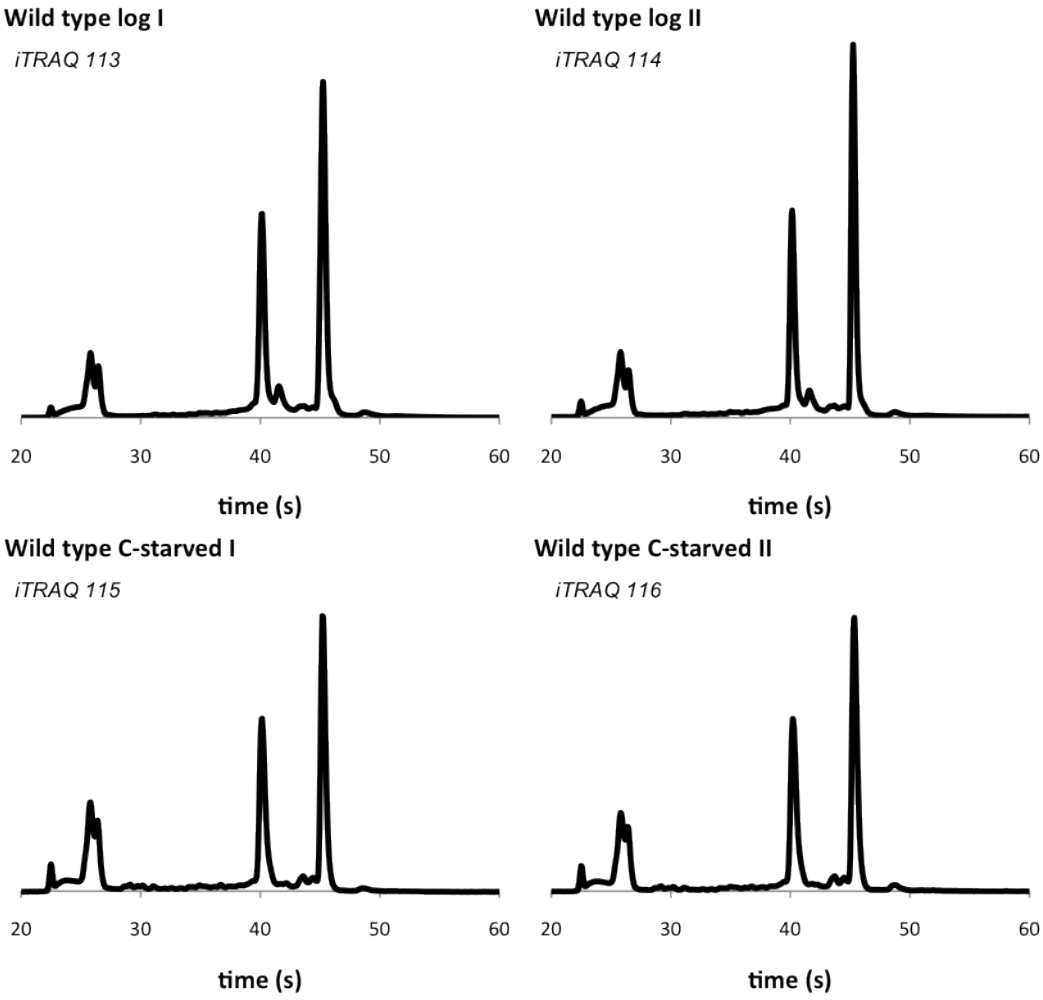


FIG. 4.39 rRNA profiles reflect the status of the ribosomal population. Crude extracts from hypoxic cultures of *Msm* wild type (**A**,**B**) and *Msm* ΔdosR (**C**,**D**) were analysed by ribosomal and rRNA profiling. Results from both analyses are shown for two samples of each strain. RNA was extracted directly from the crude lysate.

During our ribosomal profiling experiments (see section 4.3.2) we noticed that the there was only a limited window of time during hypoxic stasis where we could isolate sufficient ribosomes to be able to carry out compositional analysis. This was particularly true of samples from ΔdosR hypoxic cultures (Fig. 4.9-11). In our opinion, arbitrarily choosing samples to analyse further would constitute cherry picking and potentially introduce a bias into our analysis. As a result, we tried to use rRNA profiling as a quality control measure to select samples that we could use for compositional analysis.

We started by measuring the rRNA profiles of samples whose ribosomal profiles we have already determined. We observed that the results obtained by rRNA profiling correlated very well with ribosomal profiles. In Fig. 4.39 we show the ribosomal profiles of two *Msm* wild type hypoxic samples and two *Msm* ΔdosR hypoxic samples. The samples in grey have been harvested three days after entry into hypoxic stationary phase, while samples shown in black were harvested four days after entry into hypoxic stationary phase. We can see that the overall levels of ribosomes measured in the profile are reflected in the signal intensity of rRNA in the bioanalyser trace. Furthermore the levels of 16S rRNA, as detected with the bioanalyser, change depending on the amount of 70S ribosomes in the sample.



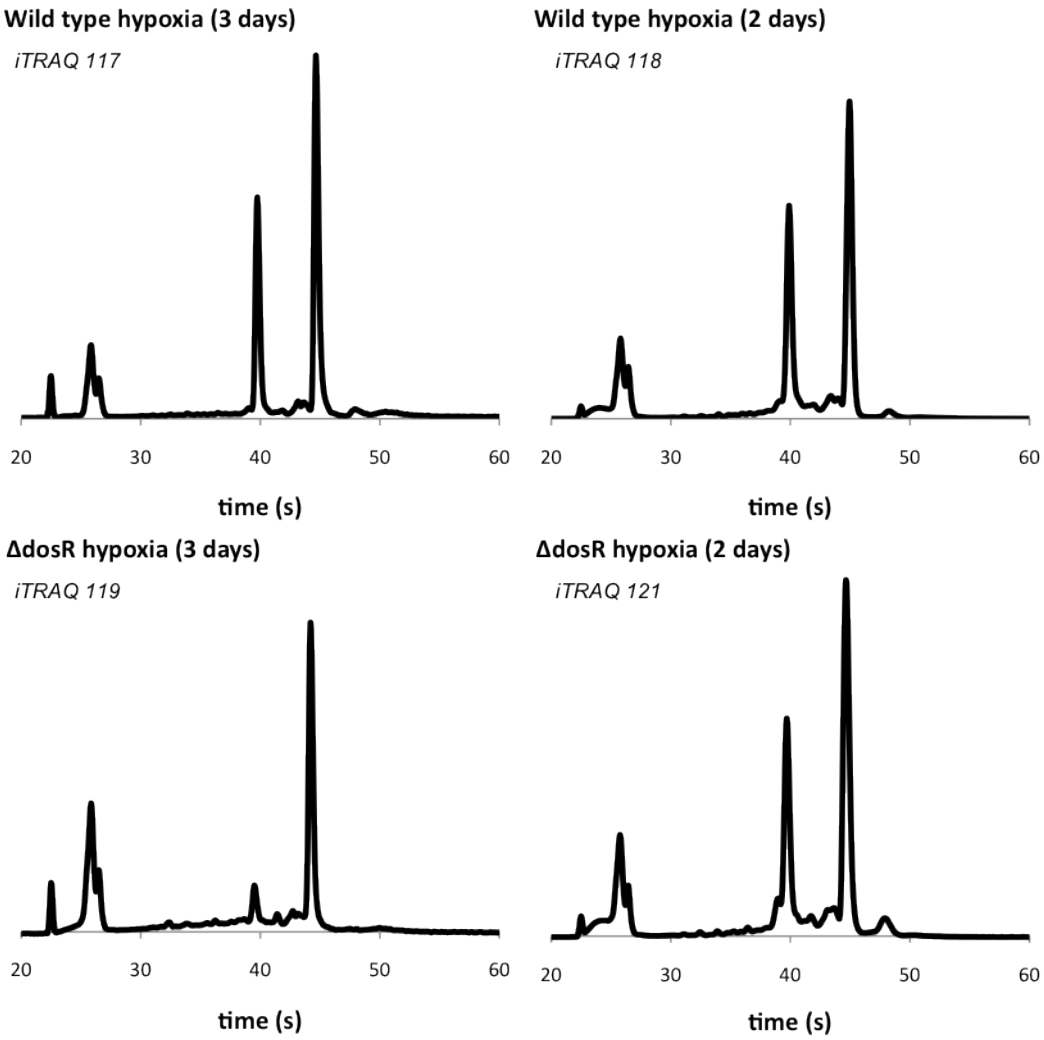


FIG. 4.40 rRNA profiles of samples used for iTRAQ. *Msm* wild type and *Msm* ΔdosR samples that were chose for compositional analysis. Culture conditions and iTRAQ label used are indicated for each sample.

Based on these observations we concluded that rRNA profiles could be used to assess the quality of samples prior to compositional analysis. With the help of this approach we compiled a collection of 8 samples: two log phase *Msm* wild type cultures, two *Msm* wild type carbon starved cultures, two *Msm* wild type hypoxic cultures and two *Msm* ΔdosR hypoxic cultures. We chose to analyse one hypoxic culture harvested two days after entry into hypoxic stasis and one three days after entry into stationary phase. Our decision was made based on the observation that the rRNA profile of hypoxic cultures of ΔdosR two days after entry into stationary phase were indistinguishable form wild type – unlike profiles later on in hypoxia (see Fig. 4.40). We hypothesised that

comparing these two time points would be well suited to identifying stabilising interactions.

4.7.2 iTRAQ of ribosomal samples

We used monolith-FPLC to purify ribosomes. Each sample was labelled with a different iTRAQ label (see Fig. 4.40) prior to HPLC-MSMS analysis. We used a combination of full IDA and m/z windows to acquire the spectra (see Fig. 4.38D). Overall we were able to identify and quantify 91 proteins, including 51 ribosomal proteins.

4.7.2.1 Ribosomal proteins

We were able to detect and quantify all but two ribosomal proteins during this study – L31 and L34. Importantly all ribosomal proteins were detected in all samples, indicating that complete loss of ribosomal proteins during stasis was unlikely.

The main trend in our samples was an increase in the relative abundance of large subunit proteins during hypoxic stasis when compared to active growth. Similarly, the relative levels of small subunit proteins were found to be lower during carbon starvation. To assess the significance of this finding, we compared the ratios of stationary phase samples (treatment/log) to those of the control set (log/log). We included peptides that were identified with at least 95% confidence and were found to come from either 50S or 30S ribosomal subunits. By doing so we were able to determine that 50S subunit peptides were significantly more abundant in all hypoxic samples (T-test, $p < 0.01$). In the case of ribosomes from ΔdosR cultures harvested three days after the onset of hypoxic stasis we were able to detect a significant decrease (2-fold) of 30S ribosomal peptides as well (T-test, $p < 0.01$). Taken together, these observations pointed to a stasis-induced bias towards 50S subunits, which occurs more slowly in wild type cultures than in the ΔdosR mutant. To illustrate this effect we plotted the distribution of

the labelled peptide ratios – treatment/log (See Fig. 4.41) – we expected the ratios to be normally distributed, with the distribution centred on r=1.

Of particular interest is the time dependent progressive increase in the ratio of 50S peptides (a ratio of 1 indicates no difference), which orders hypoxic samples as follows:

r=1 < wild type (2 days of hypoxia) < wild type (3 days of hypoxia) < ΔdosR (2 days of hypoxia) < ΔdosR (3 days of hypoxia) < r=2.1

In the case of ΔdosR the differences between the two sampling times used for hypoxic cultures give rise to a bimodal distribution of the ratios for both 50S and 30S peptides. Wild type ribosomal proteins harvested two or three days after the onset of hypoxia do not show the same bimodal distribution, however it is possible to see a 50S bias, which we would expect to increase later in hypoxia (see Fig. 4.11). We did not observe any ratio drift in ribosomes during carbon-starved stasis.

It is interesting to note that the only exception to the trend of increasing relative abundance of large subunit proteins was protein L9, which was significantly underrepresented in all samples from hypoxic stasis ($p < 0.01$). It can be observed in Fig. 4.41 as a small cluster of peptides whose distribution is centred on 0.4-0.6.

Overall, iTRAQ analysis of ribosomes obtained from hypoxic stationary phase cells confirmed the 50S bias observed during ribosomal profiling of hypoxic cultures (Fig. 4.9 and Fig. 4.11). It also confirmed the observation that ribosomal subunits isolated from hypoxic ΔdosR cultures are likely to contain most of the rProteins normally found within them (Fig. 4.10). However, it emerged from our analysis that stationary phase ribosomes are partially depleted of large subunit protein L9 – the possible biological relevance of this observation will be discussed later (see 4.9.1).

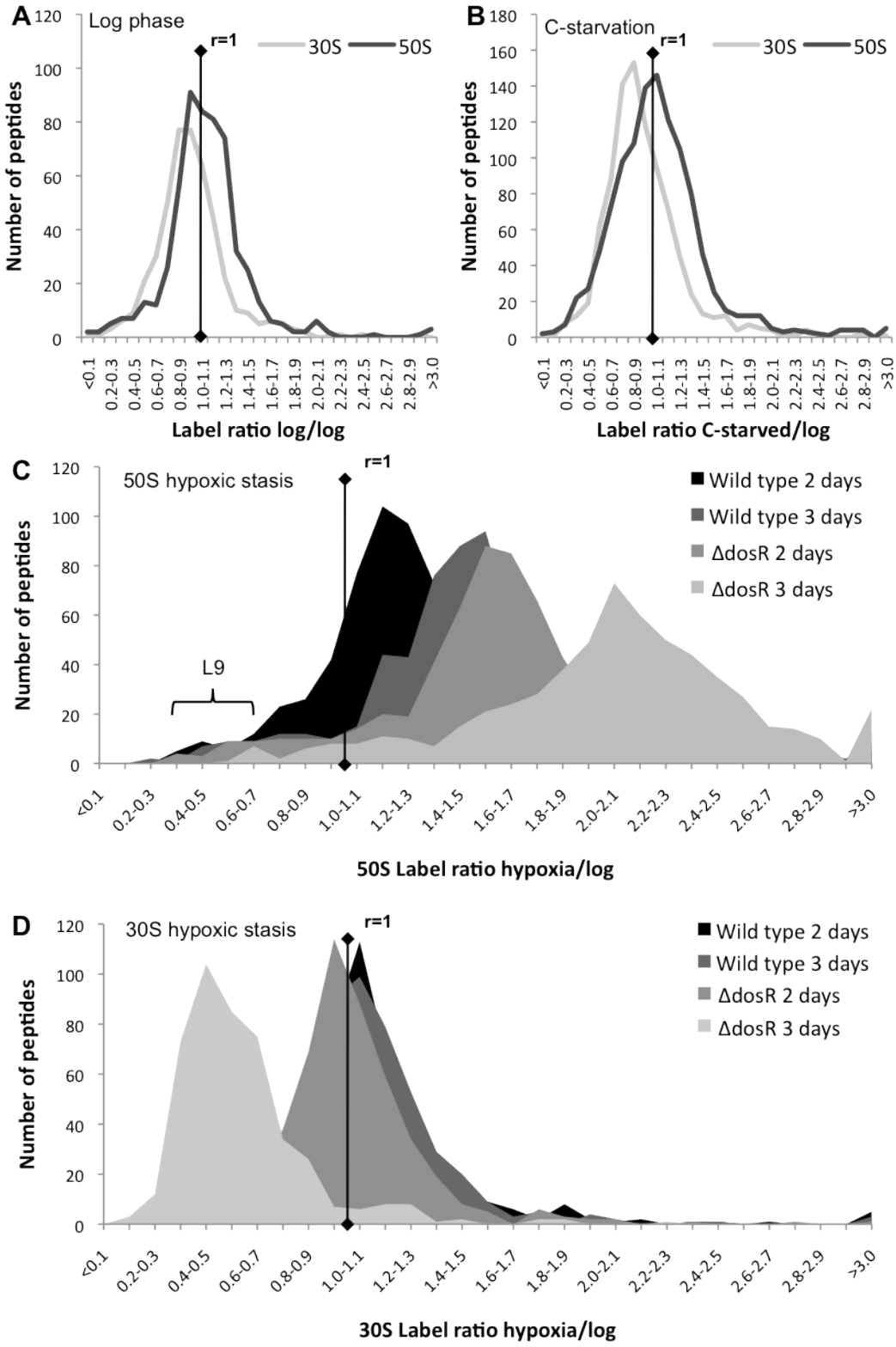


FIG. 4.41 Hypoxic stasis results in the progressive degradation of the ribosome, manifested by an imbalance in the 30S/50S ratio. The distribution of ratios was obtained as described in Fig. 4.38, using only ribosomal peptides. (**A**) Comparison of ribosomal peptides from actively growing cells, (**B**) C-starved ribosomes against log, (**C**) hypoxic stasis against – 50S peptides, (**D**) hypoxic stasis against log – 30S

FIG. 4.41 (continued) The ratios plotted on the abscissa were calculated for peptides identified with a confidence of 95% using ProteinPilot software. The software determines these ratios by dividing the intensity of the signal derived from the reporter moieties (see Fig. 4.31) for the samples chosen by the user. For example, in panel B we plotted the ratios for C-starved/log for 30S and 50S subunits. This means that we collated the ratios calculated for C-starved samples divided by log samples i.e. 115/113, 115/114, 116/113 and 116/114 (see Fig. 4.40), which gave us a normal distribution of ratios. We divided these values into bins of discrete size (0.1) and counted the number of peptides whose ratios fall into each bin. The number of peptides in each bin was plotted against the range of the ratios.

4.7.2.2 Non-ribosomal proteins

TABLE 4.3 Proteins detected during iTRAQ analysis of *M. smegmatis* ribosomal fractions

Ribosomal Proteins[a]	L1, L2, L3, L4, L5, L6, L7/12, L9, L10, L11, L13, L14, L15, L16, L17, L18, L19, L20, L21, L22, L23, L24, L25, L27, L28, L29, L30, L31, L32, L33, L36, S1, S2, S3, S4, S5, S6, S7, S8, S9, S10, S11, S12, S13, S14, S15, S16, S17, S18, S19, S20
Ribosome associated proteins[a]	EF–Tu, Trigger factor, MSMEG_1878[b], MSMEG_3935[b]
Cytosolic Proteins[a]	Enolase, Glycerol kinase, Glycerol-3-phosphate dehydrogenase, RNA polymerase, Glutamine synthase, Hsp10, Hsp60, Alcohol dehydrogenase, Aldehyde dehydrogenase, Adenosylhomocysteinase, Glycine cleavage system protein H, Methyltransferase, Proline dehydrogenase, Catalase, Ferredoxin, Superoxide dismutase, Alkyl hydroperoxide reductase, Heparin binding haemagglutinin
Membrane associated (and lipid metabolism) proteins[a]	ATP synthase, NADH dehydrogenase, Acyl carrier protein, Fatty acid synthase, Polyketide synthase, 3-ketoacyl-CoA thiolase, Acyl-CoA dehydrogenase, DoxX family protein, Putative ABC transporter
Proteins of unknown function[a,c]	MSMEG_0372, MSMEG_0643, MSMEG_1030, MSMEG_2261

[a] The details of % sequence coverage, the number of peptides included for the analysis of each protein, the label ratios and significance values are listed in SupTab7.xls, SupTab8.xls and SupTab9.xls – see included data CD.

[b] contain S30AE domain, S30AE domain proteins are associated to the ribosome in *E. coli*.

[c] Proteins annontated as (in order) oxidoreductase, extracellular solute binding protein, monooxygenase and unknown hypothetical protein.

In addition to 51 ribosomal proteins we identified a further 40 proteins in our samples (See Table 4.3). These include most of the non-ribosomal cytosolic proteins detected during our assessment of the FPLC method (Table 4.2) as well as membrane associated proteins and proteins involved in lipid metabolism. We also detected proteins associated to nucleic acids, such as RNA polymerase and polyribonucleotide

nucleotidyltransferase (Pnp). The latter can interact with RNase E and enolase (also detected) to form the bacterial RNA degradosome (Carpousis, 2007, see 1.5.2.4).

4.7.2.3 Ribosome-associated proteins

TABLE 4.4 Comparative levels of detected ribosome-associated proteins during *Msm* stasis.

			Wild type (C-starved)		*Wild type (hypoxia)*		*ΔdosR (hypoxia)*	
Protein	*%sequence coverage*	*Nº of used peptides*	Δ[a]	*p*[b]	Δ[a]	*p*[b]	Δ[a]	*p*[b]
EF-Tu	34.85%	25	- 1.11	0.32	-4.95	2.8×10^{-10}	-2.40	7.6×10^{-9}
Trigger	21.75%	15	- 2.76	0.17	-2.87	2.5×10^{-6}	-3.91	8.0×10^{-5}
MSMEG_3935	12.02%	4	1.39	0.14	1.66	0.20	-1.65	0.29
MSMEG_1878	12.17%	2	5.28	0.25	2.37	0.44	1.54	0.59

[a] change in protein level compared to active growth. Negative value indicates a decrease.
[b] p-value for null hypothesis that the peptide ratio is 1 and that the observed ratio is different from1 by chance.

Of the 40 non-ribosomal proteins we were able to detect, we believe that only four are associated to the ribosome. EF-Tu and trigger factor are known to be associated to the ribosome and we found that they were both significantly ($p<0.05$) less abundant in ΔdosR hypoxic samples (2.40-fold and 3.91-fold, respectively) when compared to log phase cultures (see Table 4.4). The same was true for wild type hypoxic samples where EF-Tu and trigger factor were significantly ($p<0.05$) less abundant (4.95-fold and 2.87-fold, respectively) when compared to active growth (see Table 4.4). The levels of Trigger factor and EF-Tu during carbon starvation were not found to be significantly different than during active growth.

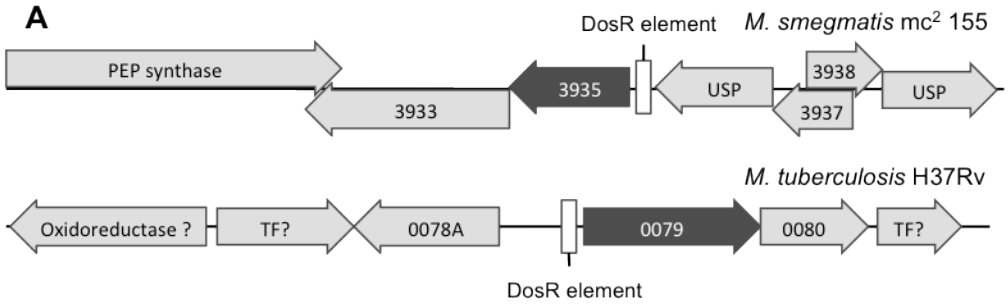
In addition to EF-Tu and trigger factor, we hypothesised that MSMEG_1878 and MSMEG_3935 are also associated to the ribosome because they are predicted to contain a S30AE domain, which is found in ribosome-associated proteins of *E. coli* (see section 4.8). There is no experimental evidence in the literature to link either of these proteins to ribosomes in mycobacteria; however the *Mtb* homologue of MSMEG_3935 – Rv0079,

was recently predicted to be a "likely cytoplasmic translation factor" using a bioinformatic approach (Mishra, 2009).

The abundance of MSMEG_1878 and MSMEG_3935 were not found to be significantly different during stasis when compared with active growth in our dataset (see Table 4.4). The p-value calculated by ProteinPilot is used to test the null hypothesis that "the ratio of peptides is 1 and the observed ratio is different from 1 by chance". The exact method by which it is calculated is beyond the scope of this thesis, however it is important to point out that the statistical test used follows a t-distribution. It takes into account the overall number of contributing peptides, the weighted average of peptide ratios (thus accounting for the quality of the spectra), the possibility of unequal loading and labelling (i.e. sample bias) as well as the weighted standard deviation of the peptide ratios, therefore controlling for the consistency of the data. The statistic test was devised to avoid strong statements in situations where a paucity of peptide data or a limited quality of the spectra is an issue, therefore limiting the number of false positive (and negative) results. Such a conservative stance is important in proteomics as much as in any other high-throughput experimental approach to prevent the generation of false leads and erroneous correlations.

While the results are not statistically significant, the discrepancy of the result obtained for MSMEG_3935 from wild type and ΔdosR hypoxic samples may be biologically very relevant. The *Mtb* homologue of MSMEG_3935, Rv0079, is a member of the DosR regulon. MSMEG_3935 is also likely to be regulated by DosR and therefore not expressed in the ΔdosR mutant. The result we obtained by iTRAQ was consistent with MSMEG_3935 not being present. To confirm this hypothesis we inspected the upstream region of MSMEG_3935 and we found a putative DosR binding site 82 bp upstream of the start codon (see Fig. 4.42), which is very similar to that of Rv0079 found 87 bp upstream of the start codon (Park *et al.*, 2003). We believe that these are strong indications that DosR regulates the expression of MSMEG_3935.

Assuming that MSMEG_3935 is part of the DosR regulon, then loss of DosR could have a direct impact on ribosomal stability. This correlation would require MSMEG_3935 to be associated to the ribosome and play a role that is analogous to that of its homologues in *E. coli*.



B

Rv0079 – DosR element[1]	CATGG GACTT TCGGC CCTGT	S = C/G
MSMEG_3935 – DosR element	GAGGT GACTT TCGGC CCTGT	W = A/T
Consensus[1]	TTSGG GACTW WAGTC CCSAA	[1]Park *et al.*, 2003

FIG. 4.42 MSMEG_3935 has a putative DosR responsive element upstream of its start codon. (**A**) Genetic context of MSMEG_3935 and Rv0079. PEP synthase – phosphoenolpyruvate synthase, TF – transcription factor, USP – universal stress protein. Numbers indicate the standard annotation of genes whose function is unknown. Figure not drawn to scale. (**B**) DosR responsive element of MSMEG_3935 has a high sequence identity to that of Rv0079 (underlined). Letters in bold indicate agreement with the consensus determined by Park *et al.*, 2003.

In light of our findings, we returned to the hypothesis put forward in section 4.3.2, which postulated that based on the ribosomal profiling data, DosR is likely to play a role in ribosomal stability. We amended the hypothesis by positing that DosR plays a specific role in ribosomal stability mediated by MSMEG_3935. The loss of this effect leads to a premature degradation of the ribosome during hypoxic stasis. In order to test this hypothesis we first needed to confirm that MSMEG_3935 is associated to the ribosome and that its expression is DosR dependent. Once this was done we could assess the impact MSMEG_3935 may have on ribosomal stability and consequently survival during prolonged hypoxia.

4.8 S30AE domain proteins of *Msm*

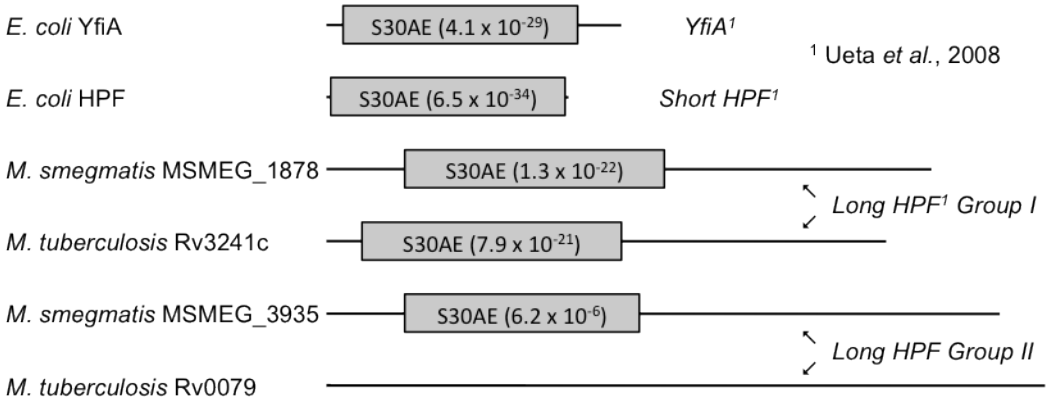


FIG. 4.43 S30AE proteins of *E. coli*, *Msm* and *Mtb*. Predicted S30AE domain location is indicated, value in brackets represents the E-value calculated by Pfam (Finn *et al.*, 2010). The classification of S30AE domain proteins as suggested by Ueta *et al.* (2008).

In silico analysis reveals that MSMEG_1878 and MSMEG_3935 are both predicted to contain an S30AE (Ribosomal protein S30Ae/Sigma 54 modulation protein) domain (Fig. 4.43). The domain was predicted by Pfam (Finn *et al.*, 2010) to be present between residues 32-131 (E value of 1.3×10^{-22}) in MSMEG_1878 and between residues 12-99 (E value: 6.2×10^{-6}) in MSMEG_3935. These are the only two S30AE proteins encoded by the *Msm* genome. Homologues of MSMEG_1878 can be found in all mycobacterial genomes sequenced to date. There is at least one MSMEG_3935 homologue in most sequenced mycobacterial genomes with the exception of *M. abscessus, M. avium* and *M. leprae* (Kanehisa *et al.*, 2006). Plotting the phylogenetic tree of mycobacterial S30AE proteins points to the presence of two groups of S30AE proteins (Fig. 4.44). Group I contains MSMEG_1878 and Rv3241c and its members are more closely related to S30AE domain proteins from other bacteria. Group II contains MSMEG_3935 and Rv0079 and the sequences of its members are less conserved outside of mycobacteria, apart from some firmicutes.

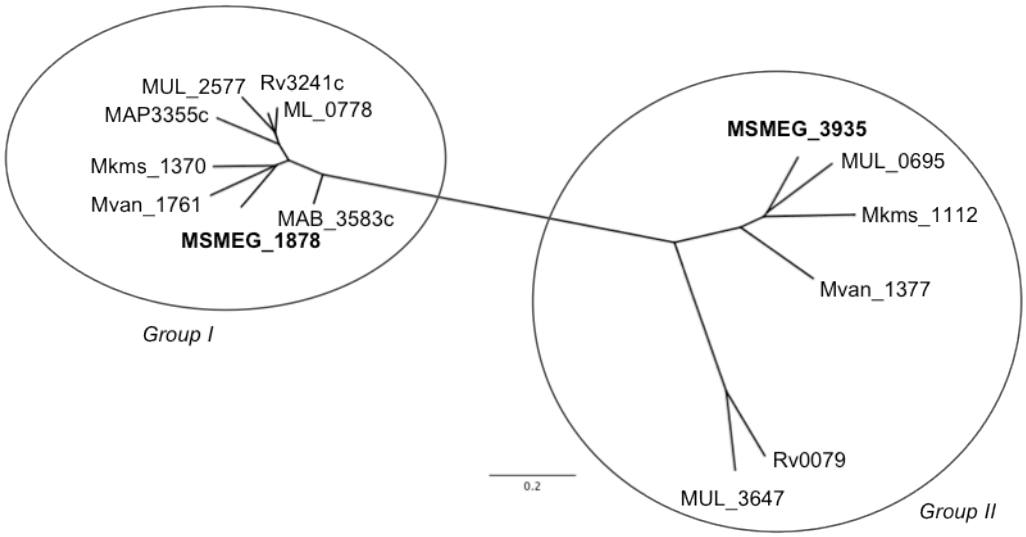


FIG. 4.44 Phylogenetic tree of selected mycobacterial S30AE proteins. MAB_3583c – *M. abscessus*, MAP3355c – *M. avium*, Mkms_1112 and Mkms_1370 – *Mycobacterium sp.* KMS, ML_0778 – *M. leprae*, MSMEG_1878 and MSMEG_3935 – *Msm*, MUL_0695, MUL_2577, MUL_3647 – *M. ulcerans*, Mvan_1377 and Mvan_1761 – *M. vanbaalenii*, Rv0079 and Rv3241c – *Mtb*.

S30AE domain proteins are best studied in *E. coli* where they are involved in ribosomal function and stability (See section 1.4.3.1). The two S30AE domain proteins of *E. coli* are cold shock protein Y whose induction interferes with the ribosome cycle and stabilises the 70S ribosome (Vila-Sanjurjo *et al.*, 2004) and Hibernation promoting factor which is essential for the maturation of 90S ribosomal particles to 100S dimers during stasis (Ueta *et al.*, 2008). The action of both *E. coli* S30AE proteins is to promote the associated form of the ribosome, which was found to be inherently more stable (Zundel *et al.*, 2009), hence they can be thought of as ribosome stabilising factors.

For mycobacterial S30AE proteins to play the same role as their *E. coli* homologues, they need to associate to the ribosome. While we did identify MSMEG_1878 and MSMEG_3935 in our FPLC purified ribosomal preparations, we felt that it would be appropriate to confirm this association using a complementary method. We therefore returned to ribosomal profiling, and used mass spectrometry to measure the presence of MSMEG_1878 and MSMEG_3935 in the ribosome containing fractions.

4.8.1 MSMEG_3935 and MSMEG_1878 interact with the ribosome

The signal intensity for S30AE proteins during the iTRAQ analysis was very low. We therefore resorted to using a multiple reaction monitoring (MRM) mass spectrometric experiment. The superior sensitivity of this method would allow us to reliably detect S30AE proteins in sucrose gradient purified ribosomes. During an MRM experiment a mass spectrometer detects user-determined ions of a specific m/z and uses them for tandem MS. Furthermore, the instrument only records ions, whose daughter ions also match a user-determined m/z. By doing so the user can effectively dictate to the mass spectrometer what peptides to analyse. The exclusive nature of the experimental design allows the overall sensitivity to be increased, as the detector only needs to focus on a very small number of peptides. This approach is often used for quantification purposes, as using a labelled standard peptide allows the analyst to quantify the absolute levels of a peptide of interest. However, we were not interested in the absolute levels of S30AE proteins at this point, but rather whether the protein of interest is present or absent from sucrose-purified ribosomes.

In order to be able to configure the mass spectrometer to monitor the correct transitions (mother ion / daughter ion combinations) we first needed to select the most suitable peptides for the analysis. We assessed six peptides for MSMEG_1878 and MSMEG_3935 (Table 2.5). To select the most appropriate peptides for analysis, we ran an HPLC-MSMS experiment using an EPI acquisition program. Our aim was to select peptides with suitable chromatography (well defined single peak) and whose transitions gave a single identifiable signal. We were able to select three such peptides for each protein (Table 4.5). We monitored several transitions for each peptide to ensure that we identified the right ion. In addition to MSMEG_1878 and MSMEG_3935 we also monitored the presence of ribosomal proteins S2 and L7/12 whose transitions we obtained from the global protein machine.

TABLE 4.5 MSMEG_1878 and MSMEG_3935 peptides used for MRM analysis

MSMEG_1878		
Peptide	*Parent ion m/z*	*Daughter m/z*
DPLAGLDVSR	521.8	717.5, 646.4, 830.6, 589.3
TPVSLAEATAK	544.5	790.4, 889.6, 703.6, 590.5
NVEVPDHFR	556.8	671.5, 899.5, 770.6, 459.4
MSMEG_3935		
Peptide	*Parent ion m/z*	*Daughter m/z*
GGVPAEAGR	407.2	600.4, 503.3, 432.0, 303.4
AQVEGVNAR	472.2	744.5, 645.4, 516.4, 459.4
YDGHYGLITPADG	689.8	359.3, 460.0, 1020.6, 919.6

Once we established the MRM parameters we analysed the presence of MSMEG_1878 and MSMEG_3935 in ribosomal sucrose gradient fractions from log, carbon starved and hypoxic (wild type and ΔdosR) cultures. We were able to detect S30AE proteins in a subset of the ribosomal fractions tested, thus confirming our hypothesis that S30AE proteins associate to ribosomes in mycobacteria. Moreover, we were able to detect S30AE proteins only in static cultures. MSMEG_1878 was present in both hypoxic and carbon-starved stasis. MSMEG_3935 on the other hand was present exclusively in wild type hypoxic samples (Fig. 4.45A). The absence of MSMEG_3935 from carbon starved cultures (data not shown) and ΔdosR cultures (Fig. 4.45B), is a strong indication that DosR controls the expression of MSMEG_3935 in *Msm* as well as Rv0079 *Mtb* (Park *et al.*, 2003).

In light of our observations regarding the ribosomal association of MSMEG_3935 and the correlation between the presence of MSMEG_3935 and DosR we turned to the role of MSMEG_3935 during hypoxia. We therefore decided to attempt to knock out MSMEG_3935 to assess the impact of such a mutation on ribosomal stability and hypoxic survival.

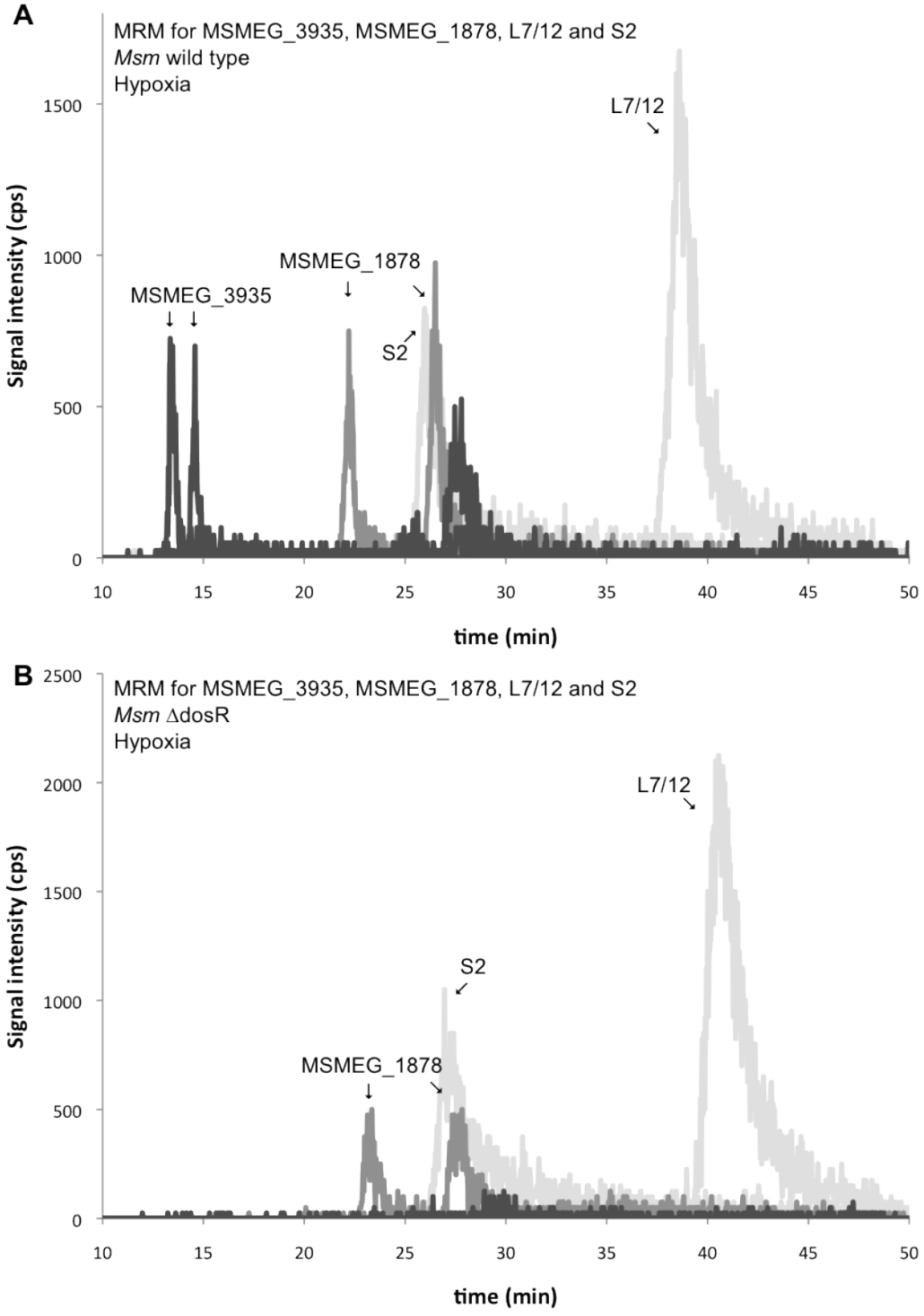


FIG. 4.45 MSMEG_3935 is absent from hypoxic *Msm* ΔdosR cultures. Ribosomal samples from hypoxic stationary phase cultures of (**A**) *Msm* wild type and (**B**) *Msm* ΔdosR were analysed using the multiple reaction monitoring acquisition method. Two peptides were detected for MSMEG_3935 and MSMEG_1878, and one peptide for each of the ribosomal proteins. The transitions used are listed in Table 4.5.

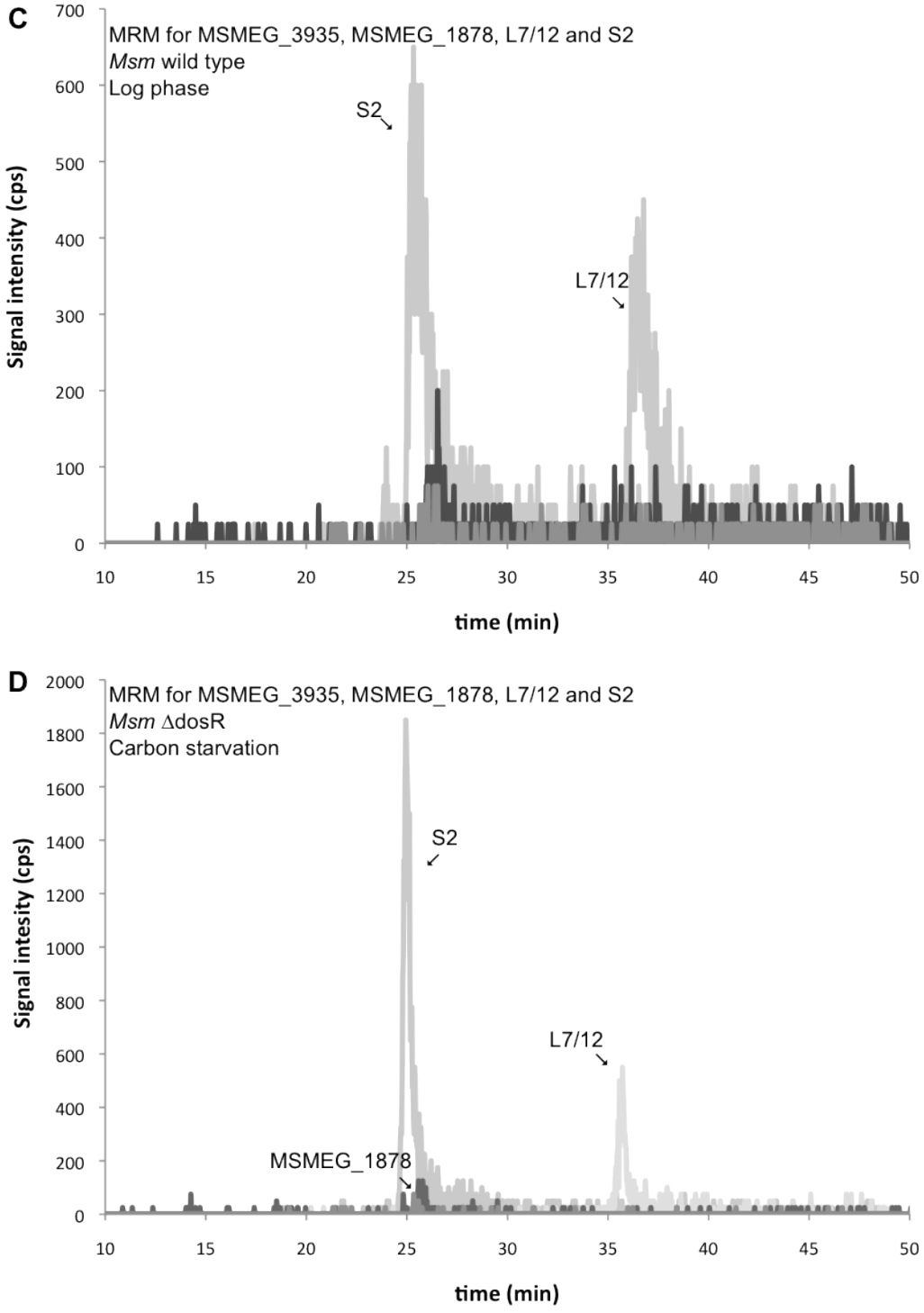


FIG. 4.45 (continued) Ribosomal samples from *Msm* wild type cultures in (**C**) Log phase and (**D**) during carbon-starved stasis were analysed using the multiple reaction monitoring acquisition method. Two peptides were detected for MSMEG_3935 and MSMEG_1878, and one peptide for each of the ribosomal proteins. The transitions used are listed in Table 4.5.

4.8.2 MSMEG_3935 mutagenesis and complementation

We used a recombineering method (van Kessel and Hatfull, 2007), to attempt to knock out MSMEG_3935. We first created a construct so that we flanked a hygromycin resistance cassette (amplified from pSMT3) with 462-bp of the sequence upstream and 445-bp of the sequence downstream from MSMEG_3935 (Fig. 4.46A). We electroporated the construct into wild type *Msm* cells and selected for growth on hygromycin. We screened 15 colonies for the insert by PCR (using primers P1 and P4, see Fig. 4.46A), tested the identity of the PCR product by digesting it with *Xba*I and *Bgl*II and selected 2 clones for further confirmation (Fig. 4.46B). We validated our mutants by using PCR (Primers P5 and P6, Fig. 4.46A).

We also attempted to generate plasmids for the genetic complementation of ΔMSMEG_3935. We amplified MSMEG_3935 either including its putative DosR promoter (MSMEG_3935^{DosR}) or without a promoter – in order to be able to drive its from a DosR independent promoter (MSMEG_3935^{TetO}, MSMEG_3935^{Hsp60}). The aim of the latter construct was to attempt to partially complement ΔdosR to assess the relative contribution of MSMEG_3935 to the overall hypoxia phenotype of ΔdosR.

Despite multiple attempts to clone MSMEG_3935^{DosR}, MSMEG_3935^{Hsp60} and MSMEG_3935^{TetO} into the pGiles, pSMT3 and pTetO respectively, we were unable to make either plasmid construct. We were therefore unable to complement the MSMEG_3935 mutation *in vivo*.

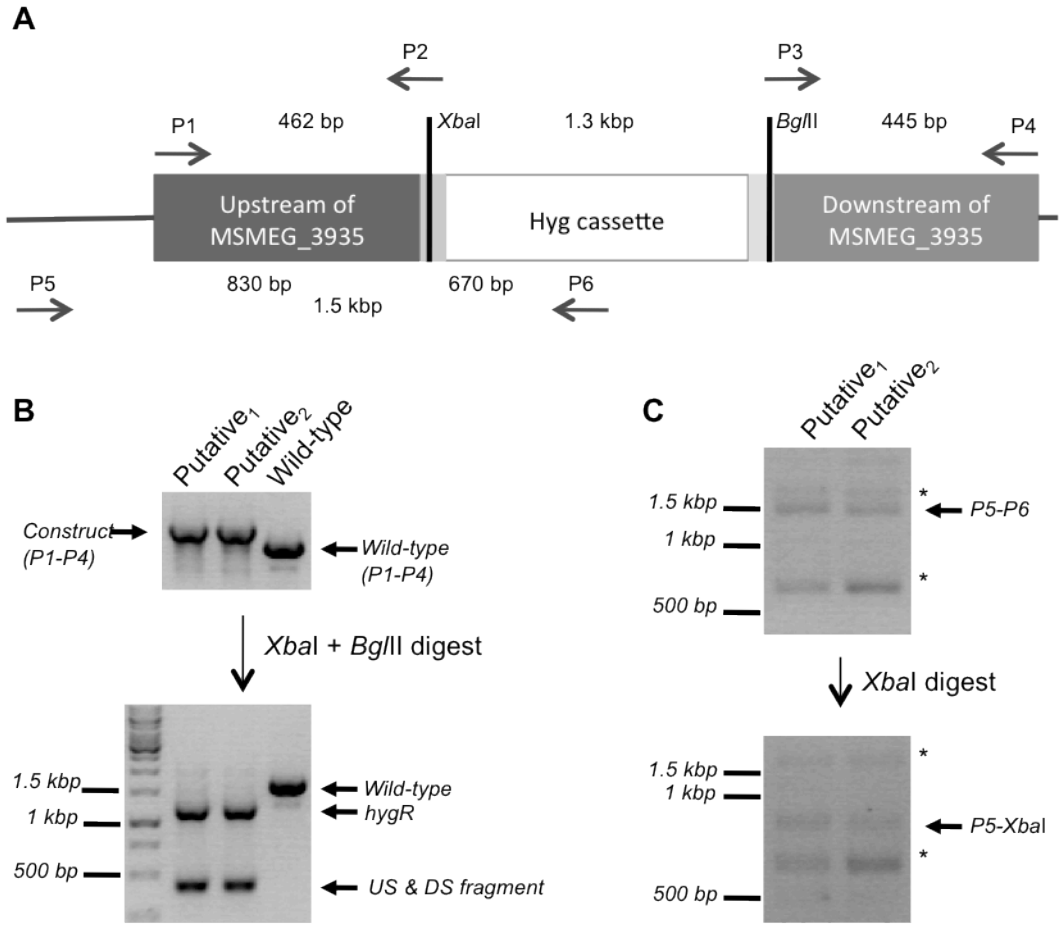


FIG. 4.46 Knocking out MSMEG_3935. (**A**) Diagram of the linear construct used for knocking out MSMEG_3935. (**B**) Confirmation of construct insertion into genomic DNA. DNA was isolated from fifteen putative MSMEG_3935 mutants and used as template to amplify the MSMEG_3935 locus. Two positive mutants were arbitrarily chosen and digested with *Xba*I and *Bgl*II to confirm that the source of the product was the construct in panel A. (**C**) A primer intrinsic to the hygromycin cassette (P6) and a primer exogenous to the construct (P5) were used to test the insertion of the construct in the putative mutants. * non-specific PCR bands.

4.8.3 ΔMSMEG_3935 viability and rRNA stability during hypoxia

Since we were unable to generate a MSMEG_3935 complemented strain, we used two independent ΔMSMEG_3935 mutants to test the effect of the mutation on viability and rRNA stability during hypoxia. Obtaining a consistent result with two independent mutants would allow us to have a greater confidence in our findings.

We set up four independent hypoxic cultures of *Msm* wild type, ΔdosR, DosR^c, ΔMSMEG_3935$_1$ and ΔMSMEG_3935$_2$. We sampled the cultures 9, 13 and 20 days after inoculation to determine the viability of the strains (see Fig. 4.47).

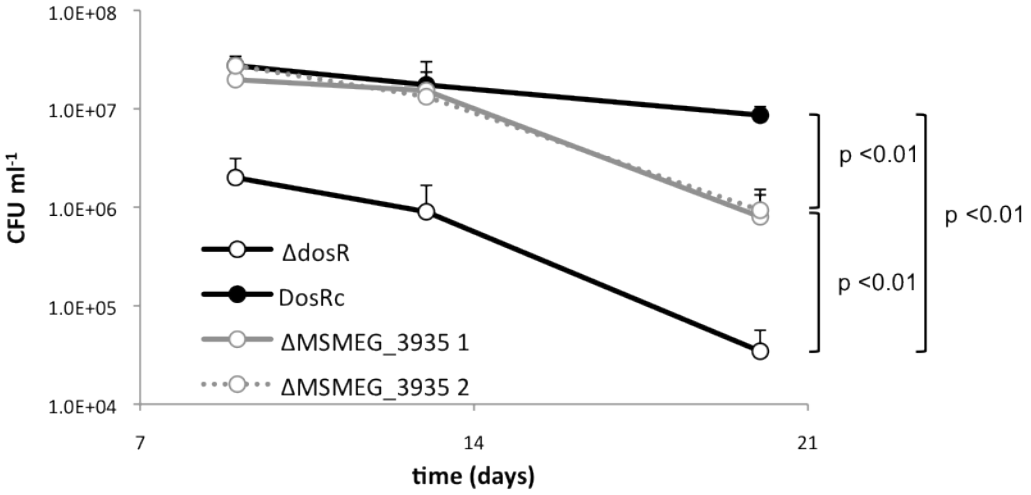


FIG. 4.47 The viability of ΔMSMEG_3935 *Msm* is compromised during prolonged hypoxic stasis, but but to a lesser extent than that of ΔdosR. Cultures of DosR^c (○), ΔdosR (●) and two ΔMSMEG_3935 (○) of *Msm* were grown to hypoxic stationary phase. Viability was determined at specific time points by plating serial dilutions and enumerating the colonies formed. Cultures were sampled through the airtight septum using a needle, thus preserving the hypoxic nature of the cultures.

All curves represent four independent cultures that were measured in triplicate. Error bars correspond to the standard deviation (N=12). The p-values indicated were calculated for the samples after 20 days of incubation using an unpaired two tailed student T-test.

The effect of hypoxia on the viability of DosR^c and ΔdosR was consistent with our previous observations (see 3.2.1.2). We did not detect any significant differences between the viability of either ΔMSMEG_3935$_1$ or ΔMSMEG_3935$_2$ and DosR^c 9 and 13 days after inoculation. However, there was a significant decrease in the viability of ΔMSMEG_3935 after 20 days of hypoxic stasis when compared to DosR^c. The viability of ΔMSMEG_3935 was significantly higher than that of ΔdosR throughout the experiment. Taken together these findings point to the fact that loss of MSMEG_3935 contributes to the ΔdosR hypoxic viability phenotype. It is important to note that the results from the two ΔMSMEG_3935 strains were very consistent throughout the experiment.

After 28 days of hypoxia we harvested the cultures and extracted the total RNA. By looking at the individual RNA profiles we noticed that data obtained for DosR^c and wild type *Msm* were very similar so we pooled the traces during the data analysis (see section 4.4.1). Similarly, the RNA profiles of MSMEG_3935$_1$ and MSMEG_3935$_2$ were also found to be highly comparable and we decided to combine these traces during the data analysis as well.

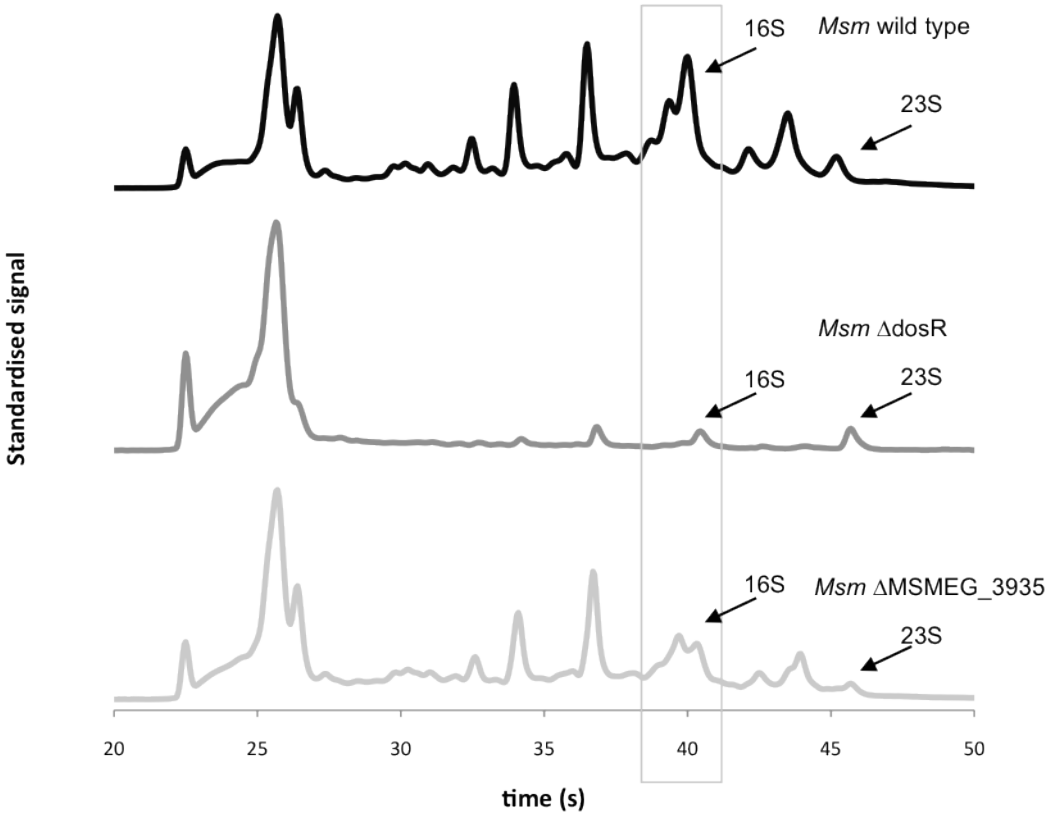


FIG. 4.48 rRNA stability of ΔMSMEG_3935 is compromised during prolonged hypoxic stasis. RNA was purified from (**A**) *Msm* wild type and *Msm* DosR^c, (**B**) *Msm* ΔdosR and (**C**) ΔMESMEG_3935 cultures 28 days after the onset of hypoxic stasis. 16S rRNA eluted at approximately 40 s while 23S rRNA elutes at approximately 45 s.

Wild type profiles represent six independent cultures (three wild type and three DosR^c), ΔdosR represents three independent cultures, ΔMSMEG_3935 represents six independent cultures (three for each putative mutant) as described in Fig. 4.17.

The comparison of thus collated data, revealed that the levels of 16S and 23S rRNA were lower in the ΔMSMEG_3935 mutant when compared to wild type strains. As with viability, the ΔMSMEG_3935 phenotype was not as severe as that of ΔdosR, suggesting that MSMEG_3935 is not solely responsible for the decrease in the levels of rRNA during hypoxia in ΔdosR strains.

4.9 Discussion

4.9.1 Mycobacterial ribosomes – stabilised by association?

The most obvious difference between non-growing mycobacteria and stationary phase *E. coli* is the presence of ribosomal dimers in the latter but not the former. Does that mean that *Msm* does not have a mechanism of ribosomal stabilisation? Not necessarily – consider why dimerisation should stabilise the ribosome. 100S dimers appear to have the same intrinsic stability as 70S particles: they dissociate into 30S and 50S subunits in a normal [$MgCl_2$]-dependent manner (Wada *et al.*, 1995) and they have comparable thermal properties to 70S ribosomes (Niven, 2004). And while the dimerisation mediator, RMF, does play a role in cell survival during heat shock and acid stress in stationary phase the activity may not due to ribosomal dimerisation (Niven, 2004, El-Sharoud and Niven, 2007). Perhaps the most crucial aspect of 100S ribosomal dimers is that they are not dynamic structures and they are not translationally active (Wada *et al.*, 1995, Kato *et al.*, 2010). The relative importance of association for ribosomal stability has been well characterised during a recent study by Zundel *et al.* (2009). They propose that ribosomal degradation is a spontaneous cellular process regulated by the availability of dissociated ribosomal subunits. They support their claims by showing that ribosomal stability in the presence of cell extract (lysate) is dependent on [$MgCl_2$]. Furthermore, they observe that carbon starvation induced ribosomal degradation is reduced by the activity of neomycin *in vivo*. Neomycin is an aminoglycoside that interferes with the ribosomal cycle by inhibiting 70S dissociation (Borovinskaya *et al.*,

2007), making this observation particularly relevant. Similarly, dimerisation factors RMF and HPF both occupy the peptidyl-transferase site (Maki *et al.*, 2000, Yoshida *et al.*, 2002, 2004) and interfere with the action of IF3, which is required for the formation of the initiation complex (Schmeing and Ramakrishnan, 2009, Yoshida *et al.*, 2009, Kato *et al.*, 2010). The same action is shared by another ribosome stabilising protein – cold shock protein Y (Agafonov *et al.*, 1999, Vila-Sanjurjo *et al.*, 2004).

Overall it appears that stability stems from the ability of the bacterium to maintain its ribosomes in the associated form. Which poses another question: why should associated ribosomes be more stable than their subunits, after all, there are several areas of exposed RNA on the surface of the 70S ribosome (Selmer *et al.*, 2006)? It is tempting to speculate that nucleolytic sites on the surface of the 70S particle would be disruptive to the cell, because it would force the cell to constantly recycle its stock of ribosomes. However, in line with the hypothesis proposed by Zundel *et al.* (2009) it is the sites at the interface of the 30S and 50S subunits that become exposed to the cytosol during dissociation that may serve as the substrate for the initial steps of rRNA degradation (see section 4.9.2 for further discussion of rRNA cleavage). In other words, ribosomal degradation is driven by their dissociation.

How does this notion correlate with what we know about the mycobacterial ribosome during stasis? Ribosomal profiling shows that 70S is the predominant form during stasis (see Figs. 4.7B, 4.8B, 4.9 and 4.12). Work on hypoxic stasis shows that there is a time dependent depletion of the ribosomes (Fig. 4.11). It appears that the depletion occurs first by the dissociation of 70S ribosomes, with a coinciding accumulation of the 50S subunit but not the 30S subunit. This process continues until no 70S ribosomes can be detected, and only a small proportion of 50S remains (Fig. 4.11). It appears that there is a bias towards the 50S subunit, and the 30S subunit is more susceptible to degradation. This course of events may reflect a more general mechanism, as the same sequence of changes has been observed during many conditions leading to

ribosomal degradation in *E. coli*, including carbon starvation (Zundel *et al.*, 2009), phosphate starvation (Davis *et al.*, 1986), heat shock (Niven, 2004) and acid stress (El-Sharoud and Niven, 2007). In all these studies 16S rRNA appeared to be less stable than 23S rRNA leading to a disparity in the level of subunits that resulted from the dissociation of 70S ribosome. Finally, 30S subunits are inherently more susceptible to heat than 50S subunits (Tolker-Nielsen and Molin, 1996).

The "50S bias" was particularly evident when analysing the composition of *Msm* ribosomes during hypoxic stasis using iTRAQ (section 4.7). There was a clear correlation between the relative increase in the levels of the 50S subunit and the time cells were in hypoxic stasis (Fig. 4.41C). This effect was particularly pronounced in the ΔdosR mutant, which was found to undergo faster ribosome destabilisation during hypoxia using ribosomal profiling (Figs. 4.9 and 4.11), rRNA profiling (Fig. 4.18) and compositional analysis (Fig. 4.41). These observations provide significant evidence in support of ribosomal association as the major mechanism of ribosomal stability in *Msm* during stasis.

During the compositional analysis there was only one large subunit protein that was significantly less abundant in static samples than during active growth – L9. Ribosomal protein L9 protrudes from the structure (Selmer *et al.*, 2006) and interacts with mRNA. It was shown to be involved in the prevention mistranslation due to mRNA slippage (Atkins and Bjork, 2009). Interestingly levels of the two ribosomally associated factors EF-Tu - needed to shuttle aminoacylated-tRNA, (Krab and Parmeggiani, 1998) and Trigger factor - chaperone for nascent proteins (Deuerling *et al.*, 1999) were also found to be lower than during active growth. The absence of L9 would lead to a severe decrease in the translational fidelity of the ribosome, while the reduction of associated EF-Tu and Trigger factor indicate reduced translational activity. It is therefore possible that associated 70S ribosomes have a decreased level of translational activity.

Overall, *Msm* does not resort to ribosomal dimerisation for stability, but rather stabilises associated 70S ribosomes. Similarly to enteric bacteria stabilised *Msm* ribosomes might not be translationally active.

4.9.1.1 Slow-growing vs fast-growing mycobacteria

Ribosomal association provides an elegant system for stabilisation. However ribosomal profiling data from slow-growing *Mbo* BCG (see Figs. 4.7D, 4.13A) do not fully conform to the hypothesis that 70S is the predominant form of ribosomes during stasis, as static cultures retain a sizeable pool of 30S and 50S subunits. The pool of dissociated subunits is smaller during stasis than during active growth (Fig. 4.7C-D), however it is difficult to assess whether or not this observation has any relevance for the stability of *Mbo* BCG ribosomes. Most of the investigations carried out in the course of this study were done in *Msm*, so the limited data regarding *Mbo* BCG do not suffice for extensive commentary. All that can be said with confidence is that like *Msm*, *Mbo* BCG ribosomes do not dimerise during stasis and that in contrast to *Msm*, no polysomes are formed in exponentially growing *Mbo* BCG.

Given the importance of ribosomal stability for long-term survival during stasis it is conceivable that slow-growing mycobacteria also possess a mechanism of stabilisation. Whether or not this mechanism is akin to that investigated in *Msm* remains to be determined and offers a clear avenue for future research.

4.9.1.2 rRNA stability in stasis

Ribosomal and rRNA stability are fundamentally linked. Indeed the degradation of ribosomes during starvation is dependent on the presence of several RNases (Kaplan and Apirion, 1975) and is believed to happen first by an endoribonuclease cutting rRNA into smaller fragments, followed by an extensive exoribonuclease digestion (Kaplan and Apirion, 1975, Deutscher, 2006, Zundel *et al.*, 2009). Most of the research done to date

has focused on the degradation of mRNA and the processing of stable RNA molecules, however little is know regarding the identity of the endoribonucleases that mediate ribosomal degradation (Deutscher, 2006, Zundel *et al.*, 2009).

Zundel *et al.* (2009) have tested the hypothesis that distinct endonucleolytic events initiate ribosomal degradation in *E. coli*. Using 23S and 16S specific northern blot probes, they were able to detect rRNA degradation fragments that retained specificity to the probes following carbon starvation. This experiment provides a rationale for the appearance of additional RNA species of distinct size observed during prolonged hypoxic stasis (Figs. 4.18 and 4.48). However it does not provide an irrefutable link between rRNA cleavage and ribosome degradation. The time-course experiment of rRNA stability during hypoxia showed that rRNA fragments are present at every time point – until the overall signal from rRNA falls bellow the level of detection. There are two possible explanations that could account for this – rRNA fragments are either stable or there is a constant turnover of ribosomes during hypoxia, and what we are detecting corresponds to a steady state level of rRNA fragments. We know from [^{3}H]-uracil incorporation studies (section 3.4.2.1) that the level of RNA synthesis is almost negligible in wild type *Msm* cultures during hypoxia, making a steady state turnover of rRNA unlikely. On the other hand fragmented 16S rRNA has been reported to assemble into 30S-like particles that can associate with 50S subunits and drive translation (Afonina *et al.*, 1991). Therefore it is possible that during hypoxia a proportion of ribosomes are subject to endonucleolytic cleavage, however this cleavage may not necessarily result in immediate ribosome degradation. Instead, this process may reflect a partitioning of the ribosomes into two populations – one, dissociated, with fragmented rRNA, less stable, but which may still provide the low translational activity required by a quiescent cell. The other, associated, with intact rRNA, stable, translationally inactive and preserved for when the cell emerges from stasis. This hypothesis is not entirely speculative – it is compatible with the rationale proposed by Maki *et al.* (2000) and El-

Sharoud (2004), and it provides a way for the cell to balance the need for ribosomal stability with the potential requirement for some level of protein synthesis during stasis.

Why then, do we not observe the fragmentation of rRNA during carbon starvation? Findings from *E. coli* clearly show that carbon starvation leads to ribosome degradation via rRNA cleavage (Zundel *et al.*, 2009, Kaplan and Apirion, 1975). However, our data show that this occurs only transiently during early (2-4 days) carbon starved stasis in *Msm* (Fig. 4.19A). This period of degradation may be necessary for physiological adaptation to carbon-limited stasis (Spector and Foster, 1993, Beste *et al.*, 2005, Berney and Cook, 2010) and once adapted the cells are able to survive in these conditions for prolonged periods of time (Smeulders *et al.*, 1999). The apparent stability of rRNA during prolonged carbon starvation is unlikely to occur due to constant *ex novo* synthesis of rRNA. Partly because the expression of rRNA is repressed during carbon starvation via a RelA – CarD mediated mechanism (Stallings *et al.*, 2009) and partly because there are no indications in our data that would suggest the presence of pre-16S and pre-23S rRNA normally observed during periods of active rRNA synthesis (Fig. 4.16). Therefore the apparent stability is most probably the result of reduced cleavage of rRNA – an effect caused either by a greater stabilisation of associated ribosomes or decreased activity of endoribonucleases. Since endoribonucleases involved in ribosomal degradation have not yet been identified it is not possible to confirm the reduced activity hypothesis. For example studies of expression levels of RNase E, which may be involved in stable RNA degradation (Deutscher, 2006), found mycobacterial RNase E to be either unaffected (Beste *et al.*, 2007), significantly down-regulated (Betts *et al.*, 2002, Berney and Cook, 2010) or significantly up-regulated during carbon starvation (Hampshire *et al.*, 2003, Archuleta *et al.*, 2005).

In summary, rRNA fragmentation plays a role in the overall stability of ribosomes. Establishing a catalogue of cellular RNases and their activity during stasis could provide further insight into the stability and catabolism of ribosomes and RNAs.

4.9.2 On the role of DosR in ribosomal stability

Loss of DosR has a destabilising effect on the ribosome and rRNA during hypoxia (Figs. 4.9 and 4.18). The question whether ribosomes are less stable because ΔdosR *Msm* fails to adapt to hypoxia, or whether loss of viability follows from a decreased stability of rRNA/ribosome, required further attention.

The stability of rRNA is closely related to viability. Davis *et al.* (1986) stipulate that ribosomal degradation during starvation is not the result of cell death, but rather its cause. They propose that excessive degradation of ribosomes leaves the cell unable to resume biosynthesis when nutrients become available again, leading to cell death. While this hypothesis is biologically valid, our findings using CCCP, rather than hypoxia, as a mediator of energy starvation, showed that loss of viability alone is sufficient to cause rRNA degradation (see Fig. 4.21). These observations indicate that rRNA stability and viability are interdependent and the loss of one leads to the loss of the other. In the case of hypoxia, viability falls simultaneously with the loss of rRNA stability, however the exact causality is not entirely clear – the outcome is most probably the result of the interplay between the two processes.

Changes in the composition of ribosomes during hypoxia provide a few important clues that point to the role of DosR in ribosomal stability. ΔdosR ribosomes contain the entire complement of integral ribosomal proteins (see section 4.7) – therefore the apparent loss of stability is unlikely to be intrinsic to the ribosomal particle. This is an important conclusion, as impaired ribosomal subunit assembly is known to lead to a decrease in the stability of the entire ribosome (Uicker *et al.*, 2007). Importantly the "50S bias" and rRNA fragmentation both occur in ΔdosR during hypoxia, just like in the wild-type strain, however they do so more rapidly and to a greater extent (Figs. 4.9, 4.11, 4.18 and 4.41). ΔdosR ribosomes during hypoxia are therefore subject to the same processes as wild type ribosomes, however they seem to be more susceptible

to these destabilising factors than their wild type counterparts. As discussed earlier, association is pivotal for the maintenance of ribosomal stability. Therefore loss of an association-promoting interaction could explain the observed loss of stability. We identified MSMEG_3935 as a possible mediator of ribosomal association – knocking out only this member of the DosR regulon led to reduced viability during prolonged hypoxia as well as an apparent decrease in rRNA stability. The impact on rRNA stability of this mutation alone did not phenocopy the loss of the regulator, showing that direct ribosomal stabilisation accounts for only a part of the stabilisation.

Overall, the function of the DosR regulon in ribosomal stability during stasis may be thought of as two-fold: it is likely to stabilise the ribosome directly via the action of MSMEG_3935 and it enables the physiological adaptations necessary for survival – therefore enhancing ribosomal stability by aiding viability.

4.9.3 MSMEG_3935 & MSMEG_1878 – keepers of the ribosome?

The best studied S30AE domain proteins – HPF and protein Y in *E. coli* and light repressed trancript A (LrtA) in the cyanobacterium *Synechococcus* PCC 7002 are inhibitors of translation (Ueta *et al.*, 2008, Agafonov *et al.*, 2001, Vila-Sanjurjo *et al.*, 2004, Tan *et al.*, 1994). Their expression and ribosomal association is induced during periods that are not conducive to bacterial growth. These conditions have so far been shown to include stress and stasis: cold shock – protein Y (Agafonov *et al.*, 2001), dark shock – LrtA (Tan *et al.*, 1994), starvation – YvyD, a *B. subtilis* S30AE protein whose expression is controlled by RelA (Drzewiecki *et al.*, 1998, Nanamiya *et al.*, 2004), stasis – HPF (Maki *et al.*, 2000) and protein Y (Maki *et al.*, 2000, Agafonov *et al.*, 2001). Interestingly their stability and ribosomal association was found to be transient and specific to the inducing conditions in all S30AE domain proteins studied thus far – the most striking example is that of LrtA (Tan *et al.* 1994). LrtA expression is induced in the dark, and leads to an accumulation of lrtA mRNA, but the transcript is rapidly degraded

when cells are exposed to light again. Its translation on the other hand, represents the majority of translational activity that occurs both in the absence of light and immediately after exposure to light (Tan *et al.*, 1994). LrtA was shown to be involved in the inhibition of translation during energy-limited conditions, but it may also act to protect the ribosome from degradation during dark stress. The fact that it is also heavily expressed immediately after light exposure suggests that it plays a role in the control of translation in the initial phases of light adaptation.

S30AE domain proteins can therefore be thought of as transient inhibitors of translation. This activity would allow the cell to control translational activity during periods that are not conducive to active growth, without having to alter the ribosomal pool at great biosynthetic and energetic cost. Moreover, their action as ribosome associating factors would also increase the stability of the ribosome by limiting the level of endonucleolytic damage to the ribosome.

The question that follows is, do MSMEG_3935 and MSMEG_1878 share this function? Their expression is induced during periods that are not conducive to growth – MSMEG_3935 and its homologue in *Mtb*, Rv0079, are induced during hypoxia (Berney and Cook, 2010, Park *et al.*, 2003). MSMEG_1878 is expressed more highly during carbon-limited conditions in *Msm* (Berney and Cook, 2010), as is its homologue in *Mtb* – Rv3241c (Betts *et al.*, 2002). We have established during this study that they do associate to the ribosome exclusively during stasis – hypoxic stasis in the case of MSMEG_3935 and both hypoxic and carbon-starved stasis in the case of MSMEG_1878. Furthermore loss of MSMEG_3935 has a negative effect on survival and rRNA stability during hypoxia. It is worthwhile noting that the detected levels of S30AE proteins do not match those of the rProteins, therefore S30AE associated ribosomes account for only a proportion of the total ribosomal population. While the direct action of either of these proteins on ribosomal activity remains to be confirmed, there is a significant body of

evidence that supports a role for S30AE domain proteins in the function and stability of the ribosome.

The domain structure of both MSMEG_1878 and MSMEG_3935 is similar to LrtA (Tan *et al.*, 1994) and has been described by Ueta *et al.* (2008) as belonging to the group of "Long HPF". It is composed of an N-terminal S30AE domain and a C-terminal region, which in the case of *Msm* proteins has no significant similarity to any protein family. The only two mycobacterial S30AE domain proteins that have a predicted homology in their C-terminal region are Mkms_1112 from *Mycobacterium sp*. KMS, a MSMEG_3935 homologue with a predicted FadR C-terminal domain (FCD) motif in the C-terminal portion of the protein (Kanehisa *et al.*, 2006); and MUL_2577 from *M. ulcerans*, a MSMEG_1878 homologue with a predicted synaptosome-associated protein 25kDA (SNAP-25) domain in the C-terminal region. Both these domains are involved in specific binding interactions – FDC binds to acyl-CoA in *E. coli* (Xu *et al.*, 2001) while SNAP-25 is a component of SNARE complexes and can be palmitoylated leading to membrane association (Risinger *et al.*, 1993). While these observations *per se* may not bear much relevance to the actual interacting partners of MSMEG_1878 and MSMEG_3935 they point to the possibility that the C-terminal domain modulates the function of "Long HPF" proteins, and may also determine the discrete localisation of ribosomes to specific cellular compartments such as the membrane.

Overall, S30AE domain proteins in *Msm* are most probably involved in ribosomal stability during stasis, in an analogous way to the activity of their homologues in other organisms. Their specific function in *Msm* is probably distinct, as MSMEG_1878, while present in hypoxia, does not completely compensate for the absence of MSMEG_3935 (see Figs. 4.47 and 4.48). For this reason we suggest to rename MSMEG_3935 as RafH Ribosome-associated factor during Hypoxia. A similar name could be used for MSMEG_1878 – RafS (Ribosome-associated factor during stasis).

The results presented in this study represent an early investigation into the function of these proteins in mycobacteria and do not irrefutably establish their role as keepers and modulators of the stationary phase ribosome. Nonetheless, we have identified very promising candidates for ribosome stabilisation factors, which may provide good targets chemotherapeutic intervention in the future.

4.9.4 The ribosome during stasis – conclusions

The findings obtained during this study can be incorporated into a model of ribosomal stability. I propose that the overall stability of mycobacterial ribosomes during stasis is governed by the ability of the cell to maintain the associated state of the 70S ribosome and not by the formation of higher order structures. Associated ribosomes most probably do not actively partake in translation, but are stored in a translationally quiescent state – this effect might be mediated by the exclusion of integral rProteins from the stabilised structure – e.g L9.

Failure to ensure complete association results in the endonucleolytic cleavage of rRNA, which will lead to the eventual degradation of the ribosome, albeit not immediately following cleavage – as seen during hypoxia. The degradation of the ribosome is unlikely to be symmetric and the degradation of 50S subunits follows that of 30S subunits. RafH and RafS may act to limit the degradation of the ribosome and potentially also control the function of ribosomes: RafH during hypoxia and RafS as a more general stasis-induced regulator. These factors aid the cell in surviving discrete periods of stasis, by stabilising at least a proportion of the ribosomal pool. The size of this pool needs to be sufficient to ensure outgrowth from stasis, otherwise the cell will not be able to cope with the internal demand for biosynthetic capability resulting in cell death.

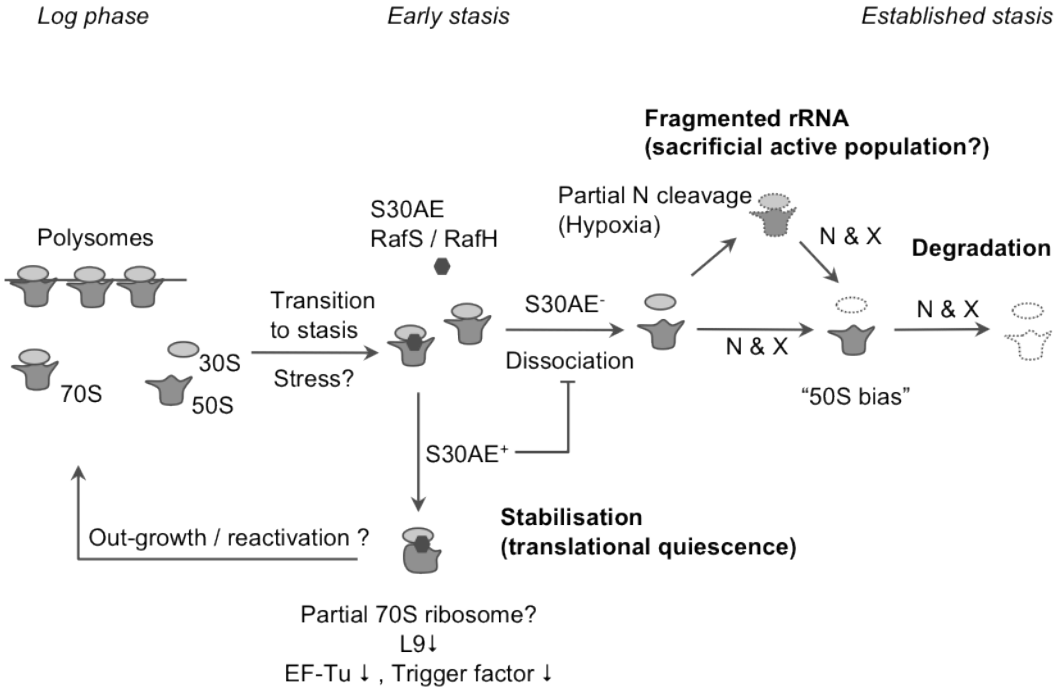


FIG. 4.49 Model of ribosomal stability during stasis. S30AE denotes RafH or RafS. N – specific endonucleases, X – specific exonucleases, L9 – Large ribosomal subunit protein L9, EF-Tu – Elongation factor EF.

5. Oxidative Stress to Nucleic Acids

5.1 Introduction and aims

ROS and RNS can lead to nucleic acid oxidation. The impact of oxidative stress to DNA has been extensively studied, as it is a source of potentially deleterious mutations (Halliwell and Gutteridge, 2007, Davis and Forse, 2009). Many recent studies have investigated oxidative damage to RNA in eukaryotic organisms, where it leads to loss of RNA stability and a reduction in the fidelity and processivity of ribosomes (see section 1.5.2). However, there are no reports in the literature regarding the levels of nucleic acid oxidation in mycobacteria, and only very few studies in other bacteria (Johnson *et al.*, 2004). Moreover there is no literature on the level of RNA oxidation *in vivo* in bacteria.

Quantifying the amount of damage caused by stress agents such as H_2O_2 would be instrumental in understanding the mechanisms by which mycobacteria cope with oxidative stress, and what repercussions such lesions may have. The aim of this chapter was to implement the analytical tools needed to assess whether and to what extent nucleic acid oxidation occurs *in vivo* in *Msm*, focusing in particular on the oxidation of RNA as a possible factor acting to destabilise mycobacterial ribosomes. Furthermore we planned to put RNA oxidation into a biological context by using transposon site hybridisation (TraSH) methodology to identify genes that are essential for the survival of *Msm* following RNA oxidation.

5.2 HPLC analysis method implementation

5.2.1 HPLC-MS method development

HPLC-MS is a well-established analytical tool for the study of oxidative damage to nucleic acids. It was successfully used to create a catalogue of nucleoside[9] modifications as well as quantifying the damage in an *in vivo* context. Extensive studies have revealed

[9] A nucleoside is composed of a nucleobase and a pentose sugar moiety.

that the hydroxylation of carbon at position 8 in the purine ring is among the most common lesions to nucleic acids due to oxidative damage, leading to the formation of 8-hydroxyguanosine – 8-OG and 8-hydroxydeoxyguanosine – 8-OdG (see Fig. 1.7, Frelon *et al.*, 2000, Cadet *et al.*, 2002, Johnson *et al.*, 2004, Hofer *et al.* 2005, Halliwell and Gutteridge, 2007). The ability to quantify these two species separately allows the simultaneous analysis of oxidative damage to DNA and RNA. This is particularly important when assessing the relative susceptibility and contribution of each type of damage to cell homeostasis.

We were able to successfully implement a method for the analysis of nucleosides. We improved on the approach reported by Hofer *et al.*, (2005) by modifying the chromatographic parameters and mass spectrometry settings. We also evaluated an alternative detection method based on electrochemistry as a possible approach to oxidative damage quantification. Electrochemical detection (ECD) measures the flow of electrons as a redox active analyte passes over the detector. The overall current is proportional to the amount of analyte present and is dependent upon the set electric potential of the electrode (see section 5.2.2)

5.2.1.1 Choice of chromatography

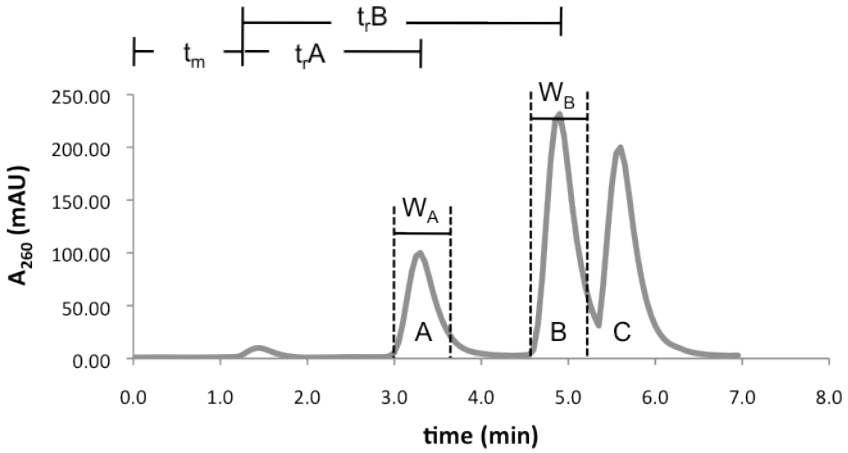
We compared the performance of three different types of column chemistry: reversed phase octadecyl (C18), phenyl and pentafluorophenyl (PFP). To assess their performance we calculated the resolution (R) of analytes as shown in Fig. 5.1 – if the numeric value of R was greater than 1.5 then the peaks were considered to be baseline resolved (see Fig. 5.1), an R value of 1.0 was considered sufficient. We tested the phenyl and C18 columns using two different buffers – an aqueous buffer containing 0.1% formic acid and 5% methanol for mass spectrometry and an aqueous buffer containing 5% methanol and 50mM sodium acetate for ECD. Two different buffers were used to accommodate for the specific requirements of the two types of detection – volatility is

essential to minimise ion suppression in mass spectrometry, while ECD requires the presence of ions to facilitate electron transfer between the analyte and the electrode. We found that phenyl columns performed better than C18 when a mass spectrometry buffer was used, allowing for a better separation of the nucleosides. In the case of the ECD buffer we found that PFP columns offered a more suitable resolution, while containing the overall run time; see Table 5.1 for a summary of R values for the nucleosides of particular interest – 8-OG, 8-OdG, guanosine (G) and 2'-deoxyguanosine (dG). Therefore I used PFP columns for ECD based analysis (see section 5.2.2).

TABLE 5.1 R values for key nucleosides using different column chemistries

Nucleoside resolution	*C18*		*Phenyl*		*PFP*
8-OG vs G	0.7[a]	7.4[b]	4.8[c]	9.6[b]	2.5[d]
8-OG vs dG	1.9[a]	3.6[b]	1.9[c]	1.1[b]	7.8[d]
8-OdG vs G	4.8[a]	13.0[b]	20.9[c]	10.8[b]	16.5[d]
8-OdG vs dG	2.9[a]	14.4[b]	21.9[c]	18.3[b]	8.0[d]

[a] buffer used: 5% Acetonitrile, 10 mM NH_4Ac
[b] buffer used: 5% methanol, 50mM NaAc (pH 5.3)
[c] buffer used: 0.1% formic acid, 5% methanol
[d] buffer used: 8% methanol, 50mM NaAc (pH 5.3)



$$R = \frac{2 \times \left(t_r B - t_r A\right)}{W_A + W_B}$$

FIG. 5.1 Definition of chromatographic resolution (R).

t_m – the time taken for the "solvent front" (injection mobile phase) to reach the detector, $t_r A$ – retention time for analyte A, W_A – peak width for analyte A.

5.2.1.2 Setting up the MRM parameters

Analogously to the study of peptides (see section 4.8.1), we chose to focus the mass spectrometric analysis on specific nucleoside species by virtue of multiple reaction monitoring (MRM). The species quantified included: Adenosine (A), 2'-dexoyadenosine (dA), G, dG, 8-OG, 8-OdG and pseudouridine (Ψ). We performed an enhanced parent ion (EPI) investigation of individual standards to determine the key parameters for MRM, including collision energy and mass transitions (see Table 2.6). Our parameters were comparable to those reported in the literature (Frelon *et al.*, 2000).

We determined the levels of the different species by first obtaining a standard curve for each analyte and then using linear regression to infer the levels of that particular analyte in each sample. We found that due to the large differences in the concentrations of the two types of nucleosides two injections were required for the analysis of each biological sample – a smaller volume injection (3 μl) to determine the level of unmodified nucleosides (A, dA, G and dG) and a larger volume injection (30 μl) to determine the levels of 8-OG and 8-OdG. In some cases the detected levels of unmodified nucleosides were outside the dynamic range of the mass spectrometer[10]. In these cases we used the absorbance at 254 nm for quantification.

[10] analyte concentration was considered to be beyond the dynamic range of the instrument when its calculated concentration no longer lay within the linear region of the standard curve.

5.2.1.3 Sample preparation evaluation

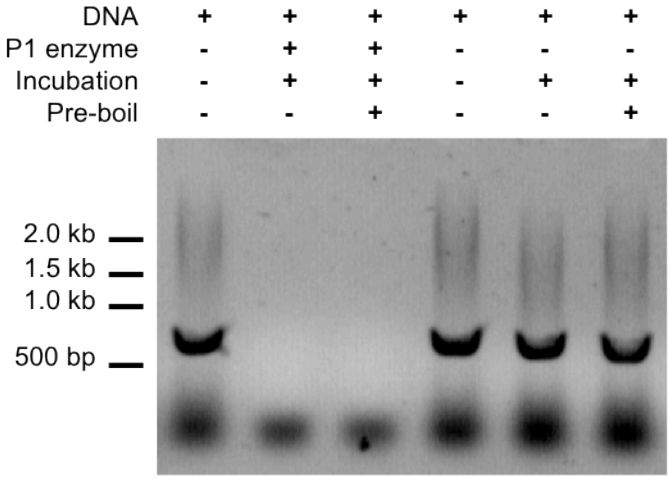


FIG. 5.2 Nuclease P1 efficiently digests DNA at 57.5˚C. Nucleic acids were extracted from a culture of wild type *Msm* (OD_{600} ~ 0.5) and incubated at 57.5˚C for 60 min in the presence or absence of P1 nuclease. The effect of boiling the nucleic acids prior to P1 digestion was tested by incubating nucleic acids at 95˚C for 5 min. The presence of intact DNA was measured by PCR using Msm_hraAFC4 and Msm_hraARC3.

Sample preparation for nucleoside analysis is based on the extraction of total nucleic acids from a cell pellet followed by an enzymatic digestion using nuclease P1 and alkaline phosphatase. Nuclease P1 digests single stranded nucleic acids to nucleotide 5'-monophosphates, while alkaline phosphatase dephosphorylates them to nucleosides. We were interested in confirming that the enzymatic step is sufficiently long to allow the complete digestion of nucleic acids. We used PCR to check for the presence of undigested DNA (see Fig. 5.2), and were unable to detect any PCR product after nucleic acids were digested for 1 h at a range of temperatures (50-57.5˚C, not all data shown). Furthermore, there was no indication of any undigested DNA fragments in P1 treated samples, which could be seen as a smear in samples that were not incubated in the presence of P1. Boiling the sample prior to digestion did not appear to affect the efficiency of digestion (see Fig. 5.2). While we did not measure the integrity of RNA following the digestion, we would expect that RNA degradation occurred to a similar if not greater extent (Sigma-Aldrich, N8630 product information sheet).

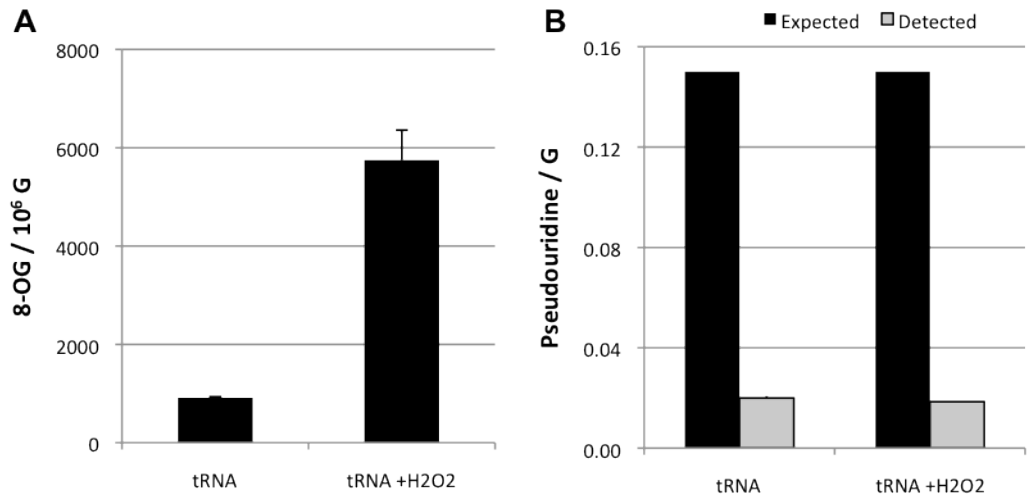


FIG. 5.3 H_2O_2 treatment causes an increase in 8-OG levels in tRNA after *in vitro* exposure. Purified tRNA was exposed to 0.1 mM H_2O_2 in the presence 1 μM Fe^{2+} and 10 μM ascorbic acid at 37˚C for 1 h. Nucleic acids were precipitated, washed, hydrolysed and analysed by HPLC-MS. Levels of 8-OG (**A**) and pseudouridine (**B**) were determined in relation to guanosine. Quantitation was performed by monitoring the following m/z transitions 245.0→125.0 for pseudouridine and 300.1→168.0 for 8-OG. Guanosine was quantified using A_{260} detected with the in-line UV spectrophotometer.

Each measurement corresponds to two independent preparations. Error bars correspond to the standard deviation (N=2).

Based on the findings presented in Fig. 5.2 we concluded that there was no need to optimise the sample preparation protocol further. We proceeded to test our method by measuring the levels of guanosine, pseudouridine and 8-OG in commercially available transfer RNA before and after exposure to H_2O_2 oxidation *in vitro* (Fig. 5.3). We were able to detect and quantify all the species of interest. H_2O_2 treatment caused a 6-fold increase in the relative amount of 8-OG, while the proportion of pseudouridine remained unchanged. The observed ratio of pseudouridine to guanosine (~0.02) was lower than expected (0.15) – we estimated that an average tRNA molecule contains 80 nucleotides, including three pseudouridines (therefore 3/(80/4) = 0.15). The reason for this discrepancy is unknown; it might be caused by an inherent bias of the extraction method, e.g. lower stability of pseudouridine compared to guanosine, or lower efficiency of the P1 nuclease to completely digest the TΨC loop. It could also be a reflection of the composition of the analysed commercial tRNAs. Nonetheless, the measured result is

consistent between samples and should therefore allow the comparative analysis we intended to carry out.

5.2.2 HPLC-ECD method development

In addition to mass spectrometry, G, dG, 8-OG and 8-OdG can be accurately detected using electrochemistry, by measuring the oxidation of these species on a glassy carbon electrode. Such analysis is more cost effective than mass spectrometry, and it has been used successfully to assay oxidative stres *in vivo* before (Hofer *et al.*, 2006).

5.2.2.1 Hydrodynamic voltammograms of nucleosides

While the exact mechanism of oxidation of these species on the electrode is not clear and is still under investigation (Goyal *et al.*, 1997, Brett *et al.*, 2000, Bolin and Cardozo-Pelaez, 2007, de-los-Santos-Alvarez *et al.*, 2007) it is well known that 8-OG and 8-OdG are readily oxidised at potentials of +400 mV[11] while G and dG are oxidised at +800mV (ESA, 2010).

By way of implementing the detection method, we set out to confirm that these values were valid for our system as well, by determining the hydrodynamic voltammograms (HDV) for G, dG, 8-OG and 8-OdG. HDV plots are obtained by measuring the oxidation/reduction of a defined amount of analyte at varying potentials (see Fig. 5.4) and are used to determine the potential at which the species of interest is oxidised/reduced.

[11] Potentials are set against a H^+/ Pt reference electrode.

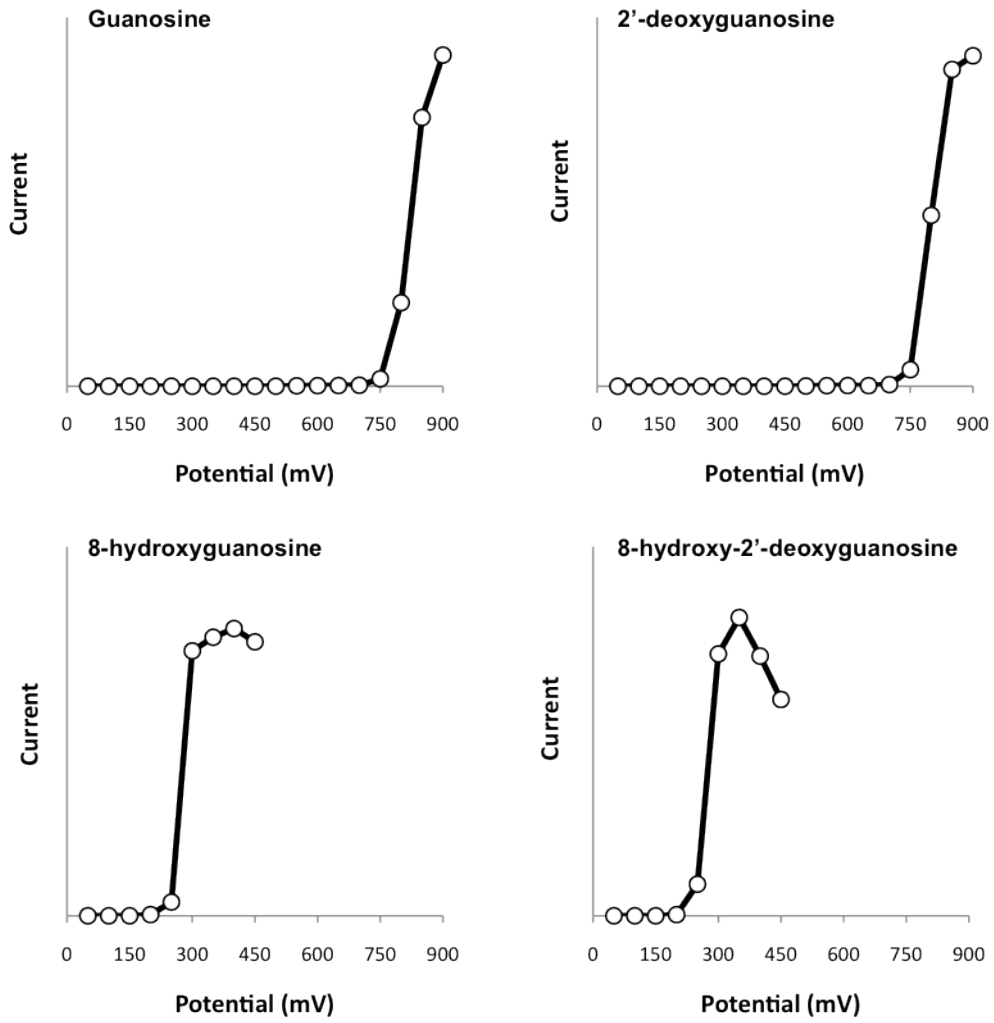


FIG. 5.4 Hydrodynamic voltammograms for guanine nucleosides and their 8-hydroxyl derivatives. Approximately 100 ng of each standard were used per injection, the oxidation was measured over a range of potentials (0 to +900 mV) by increasing the potential by 50 mV for each injection.

5.2.2.2 Sensitivity of ECD compared to mass spectrometry

A detection limit of approximately 100 fmol 8-O(d)G on column has been reported previously for HPLC-ECD systems (ESA, 2010) – a value that is comparable to that reported previously for HPLC-MS (Frelon *et al.*, 2000), therefore ECD provides a suitable alternative to mass spectrometry as a detection method for oxidative stress, both because of its selectivity and sensitivity. We were unable to achieve the same level of sensitivity as that reported by the manufacturer. The calculated limit of detection and limit of quantitation for our instrument are shown in Table 5.2.

TABLE 5.2 Detection and quantitation thresholds for 8-OG and 8-OdG using HPLC-ECD.

Nucleoside	*Limit of detection*	*Limit of quantitation*[a]
8-OG	83.5 pmol on column	229.4 pmol on column
8-OdG	56.7 pmol on column	226.8 pmol on column

[a] 3:1 signal to noise ratio

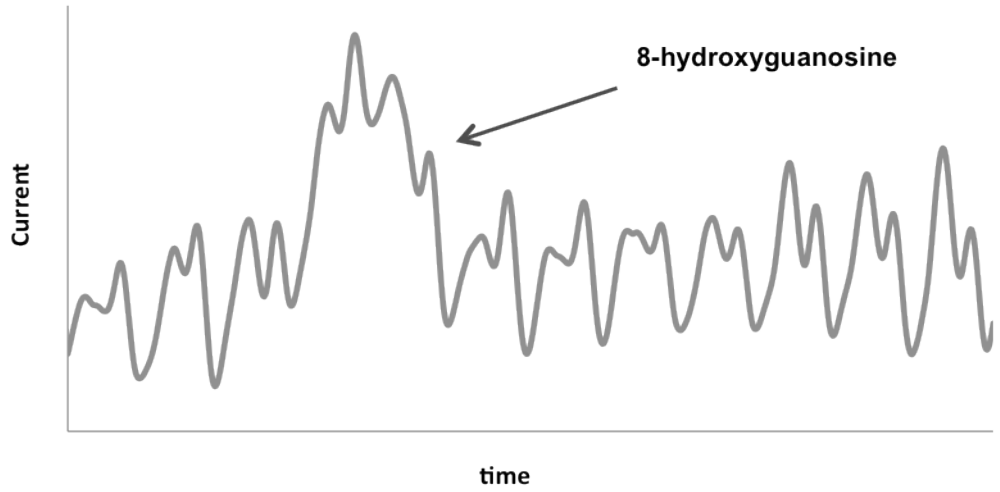


FIG. 5.5 Pump noise drastically reduces the sensitivity of our HPLC-ECD system. Approximately 100 pmol (on column) of 8-OG was loaded onto a Dionex Ultimate HPLC, with an additional mixer unit and increased dead volume to decrease pump noise. 8-OG was detected using a coulometric direct current cell set to + 400 mV on an ESA Coulochem III detector.

The calculated limit of detection for HPLC-ECD was approximately 1000-fold higher than expected. We believe that the main reason for this discrepancy lays in the high level of pump noise which affects the detector leading to a much decreased signal to noise ratio. It is clear from fig. 5.5 that small fluctuations in the pressure not only lead to baseline noise, but also affect peak shape for low abundance molecules.

Coulometric ECD electrodes are made as a porous block of glassy carbon, and are therefore very sensitive to fluctuations in system pressure. We attempted to reduce pump noise by increasing the overall volume of the system. We introduced 9 m of PEEK tubing as well as a larger mixing unit between the pump and the autosampler to dampen

the effect of the pump stroke action. We found that even fluctuations as small as ± 0.15%[12] can have a negative impact on the sensitivity of the instrument. Even though our attempt to reduce pump noise was successful, the improvement was insufficient to reach the necessary sensitivity (Fig. 5.5, Table 5.2). Attempts at measuring oxidative damage *in vivo* using HPLC-ECD did not yield data of sufficient quality to be able to make quantitative measurements (data not shown). Further steps can be taken to decrease pump noise – for example the introduction of mechanic pulse dampeners could lessen the noise further, however I was unable to pursue the optimisation of this approach and have chosen to base my analysis on HPLC-MSMS instead. Using mass spectrometry we were able to achieve limits of detection of 80 and 40 fmol for 8-OG and 8-OdG respectively, which were suitable for biological analysis.

[12] The manufacturer's tolerance for pump noise is ± 1%.

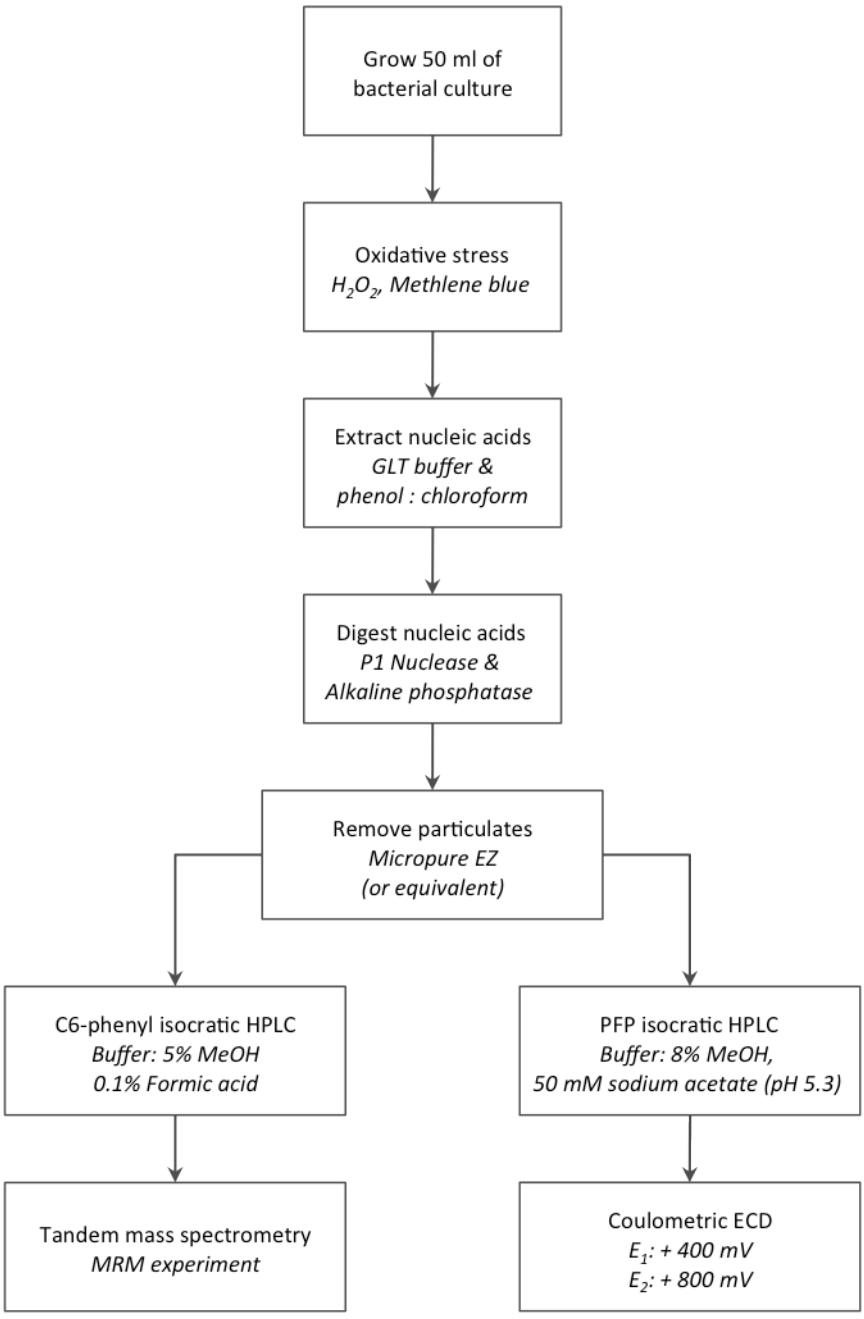


FIG. 5.6 Summary flow-chart of the nucleoside detection method.

5.3 Nucleic acid damage

5.3.1 Hydrogen peroxide oxidative damage to nucleic acids

As discussed in section 1.5.1.1, hydrogen peroxide (H_2O_2) itself is relatively inert and reacts only poorly with nucleic acids (Halliwell and Gutteridge, 2007). However, it readily decays in the presence of transition metals to give rise to highly reactive hydroxyl radicals ($OH^{\bullet}$) via the Fenton reaction (see Fig. 1.7). $OH^{\bullet}$ is believed to react with any molecule it is able to diffuse to (Halliwell and Gutteridge, 2007), therefore the damage it can cause is highly localised. *In vivo* studies in eukaryotic tissues (Hofer *et al.*, 2005, Hofer *et al.*, 2006) led to the observation that cellular RNA is more susceptible to H_2O_2 induced oxidative damage than DNA. This observation is perhaps not surprising since DNA is found in chromatin in eukaryotic cells and can therefore be considered to be physically better protected than RNA, which is more widely spread throughout the cell and therefore potentially more exposed to reacting with $OH^{\bullet}$.

We were interested in the possibility that bacterial RNA is also more susceptible to oxidative damage than DNA. If true, this observation could have important implications for the stability of mycobacterial ribosomes. We therefore started by asking a simple question – how much damage to nucleic acids occurs when mycobacterial cells are exposed to H_2O_2?

5.3.1.1 Dose dependent damage to nucleic acids

We determined earlier that 50 mM H_2O_2 is toxic to actively growing *Msm*, while 30 mM leads to a transient growth arrest (see section 3.3.1). We also found that 13 mM H_2O_2 is toxic to non-growing hypoxic cultures of *Msm* (see section 3.3.2). We used these concentrations of H_2O_2 to assess its impact on nucleic acid oxidation during active growth and hypoxic stasis.

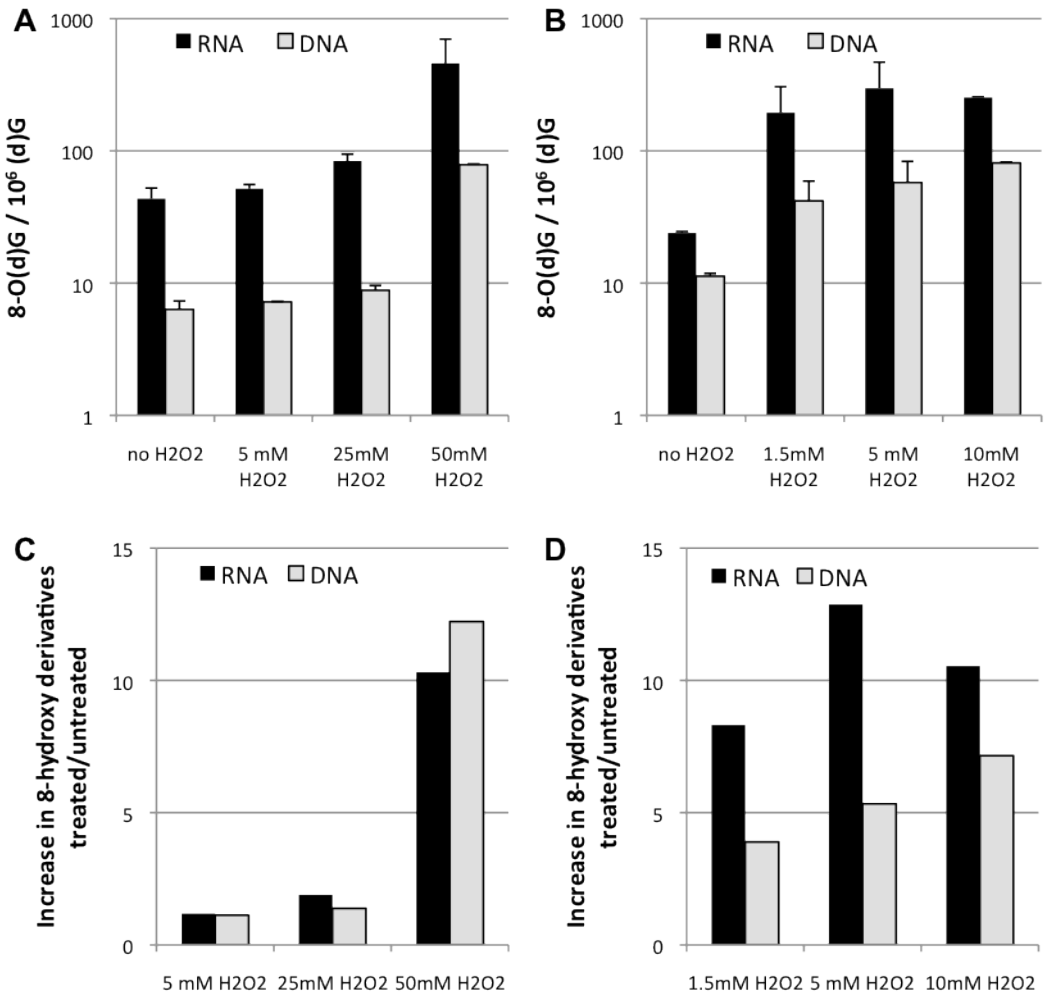


FIG. 5.7 H_2O_2 causes more detectable oxidative damage in hypoxic cultures of wild type *Msm*. H_2O_2 was added to *Msm* wild type cells grown at 37°C during normoxic active growth (**A**) or early (2 days) hypoxic stasis (**B**). Nucleic acids were extracted, hydrolysed and analysed by HPLC-MSMS. Levels of 8-OG (RNA) and 8-OdG (DNA) were determined in relation to G (RNA) or dG (DNA). Quantitation was performed by monitoring following m/z transitions 284.2→168.0 for 8-OdG and 300.1→168.0 for 8-OG. G and dG were quantified using A_{260} detected with the in-line UV spectrophotometer. The relative increase in oxidative damage compared to no treatment was calculated for cells during active growth (**C**) and hypoxic statsis (**D**).

All measurements represent three independent cultures. Error bars correspond to the standard deviation (N=3).

H_2O_2 oxidation of G/dG is more pronounced in oxygen-starved than in actively growing normoxic cultures (Fig. 5.7A-B). The correlation between the increase in oxidative lesions and H_2O_2 concentration appeared to be significantly different. Log phase cultures maintained a relatively stable overall level of 8-OG and 8-OdG when exposed to H_2O_2 concentrations of up to 25 mM. Increasing the concentration to 50 mM

resulted in a dramatic increase in the detectable levels of oxidative lesions. We measured the viability of the bacteria under these conditions and found that exposure to 25 mM H_2O_2 leads to a modest reduction in viability (approximately 15%) while 50 mM was lethal to *Msm* (data not shown). This observation suggests that there is an active mechanism of dealing with oxidative stress during exponential growth. In contrast, cells grown under hypoxic conditions show a discernible increase in the levels of both markers when exposed to as little as 1.5 mM H_2O_2. This increase is not reflected in a sharp drop of viability during the experiment – wild-type *Msm* was found to remain 70% viable when exposed to 5 mM H_2O_2 for 1 hour, this number dropped to 10% in the presence of 10 mM H_2O_2 (data not shown).

When we compared the relative increase in the level of DNA and RNA damage in response to H_2O_2 (Fig. 5.7C-D) we observed that RNA was much more susceptible to oxidation than DNA during oxygen-limiting conditions. This differential effect was much less pronounced when cells were stressed beyond what they were able to survive, suggesting that the imbalance is, at least in part, the result of an active process. The data at hand showed a significantly different level of oxidation from background only at the highest concentrations of H_2O_2. We believe that the lack of significance for lower H_2O_2 concentrations was due to our sample size. Despite this we believe that our observations are indicative of the underlying trend, and future experiments are likely to add significance to the findings. The experiment did not allow us to comment on the dynamics of oxidative damage or the role of repair in it, since it was designed to measure the effect of acute stress during a defined interval of time.

5.3.1.2 Time-course of oxidative damage

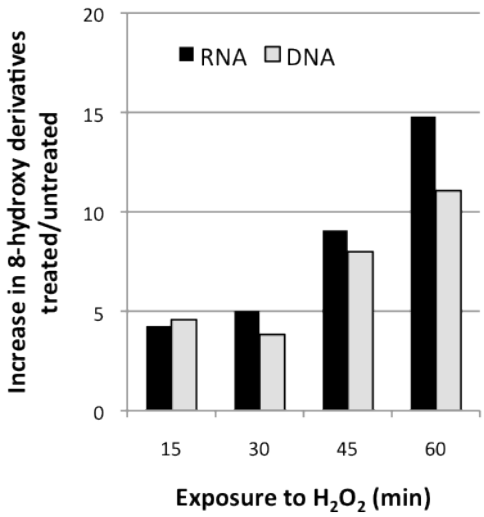


FIG. 5.8 Time-course of nucleic acid oxidation in wild type *Msm* during active growth. *Msm* wild type cells grown at 37°C and exposed to 15 mM H_2O_2 during normoxic active growth. Nucleic acids were extracted, hydrolysed and analysed by HPLC-MSMS. Levels of 8-OG (RNA) and 8-OdG (DNA) were determined in relation to G (RNA) or dG (DNA). Quantitation was performed by monitoring following m/z transitions 284.2→168.0 for 8-OdG and 300.1→168.0 for 8-OG. G and dG were quantified using A_{260} detected with the in-line UV spectrophotometer.

All measurements represent four independent cultures. Error bars correspond to the standard deviation (N=4).

We determined that the extent of oxidative damage correlates with the dose of H_2O_2. The next question we were interested in was, how does the extent of the damage correlate with the time of exposure to the insult? To address this question we exposed actively growing cells to a non-toxic concentration of H_2O_2 (15 mM) and sampled the cultures at 15-minute intervals to determine the extent of oxidative damage (see Fig. 5.8).

The number of 8-O(d)G nucleosides increased by approximately 5-fold within the first 15 minutes of exposure and remained largely unchanged for a period of 15 minutes after which it increased almost linearly for the remainder of the experiment. The R^2 value between 30 – 60 minutes of exposure was calculated to be 0.99 for both 8-OG and 8-OdG. The increases in 8-O(d)G levels were found to be significantly different (T-test, $p < 0.05$), however it is necessary to validate these data further as the number of

data points was insufficient to assume normality. The measurement at each time point is a reflection of the steady state concentration of 8-O(d)G at that point in time and is determined by the rate of repair/biosynthesis and the rate of damage. It can therefore be said that the rate of damage is similar to the rate of repair/biosynthesis for 15 min and then the rate of repair is lower than that of damage for the remainder of the experiment giving rise to the linear correlation between time and 8-O(d)G.

It is important to note that the relative increase in 8-hydroxy lesions is higher than that measured during the experiments in section 5.3.1.1. The reason for this difference may be due to a variation in cell density between the two experiments leading to a higher relative concentration of H_2O_2 per cell than in the previous experiment.

5.3.1.3 ΔdosR and oxidative damage

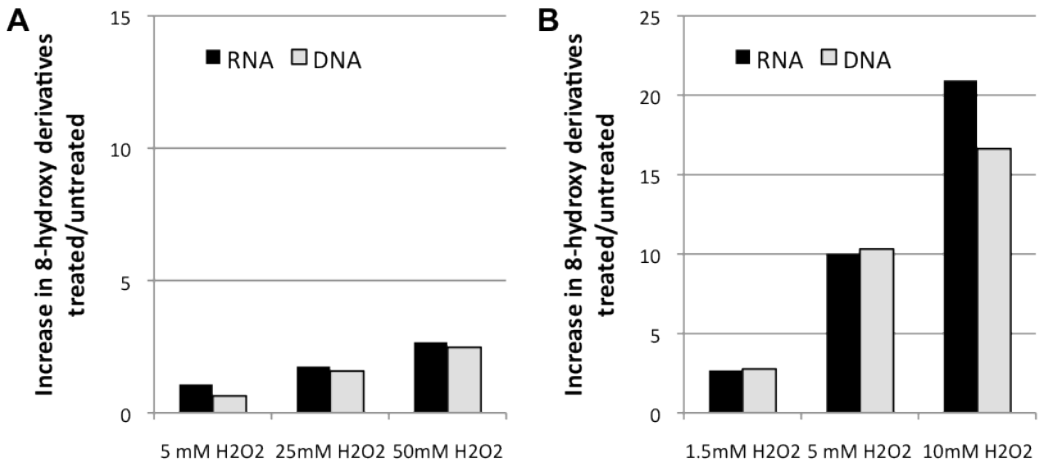


FIG. 5.9 Sub-lethal concentrations of H_2O_2 lead to a greater oxidation of cellular nucleic acids during hypoxia. The relative increase in oxidative damage compared to no treatment was calculated for *Msm* ΔdosR cells during active growth (**A**) and early (2 days) hypoxic statsis (**B**). Nucleic acids were extracted, hydrolysed and analysed by HPLC-MSMS. Levels of 8-OG (RNA) and 8-OdG (DNA) were determined in relation to G (RNA) or dG (DNA). Quantitation was performed by monitoring following m/z transitions 284.2→168.0 for 8-OdG and 300.1→168.0 for 8-OG. G and dG were quantified using A_{260} detected with the in-line UV spectrophotometer.

All measurements represent three independent cultures. Error bars correspond to the standard deviation (N=3).

We determined in section 3.3.2 that loss of DosR is unlikely to affect the ability of *Msm* to survive the exposure to H_2O_2 under hypoxic conditions. However viability is a very blunt tool to investigate shocks to a bacterial system. We therefore decided to carry out dose response experiments in ΔdosR strains of *Msm* to determine whether the degree of nucleic acid oxidation is different during hypoxia in this strain when compared to wild type.

Similarly to wild type, H_2O_2 had a higher impact on hypoxic cells, with actively growing ΔdosR *Msm* cells experiencing only a minor increase in the levels of 8-hydroxyl lesions after exposure to H_2O_2. In contrast to wild type however, the relative increase in oxidative damage of RNA and DNA occurred to a similar extent in hypoxic ΔdosR cells. However it is important to note that while the relative increase occurred to a similar extent the overall number of 8-hydroxy lesions per million (d)G was still 7-fold higher in RNA when compared to DNA. For example, after exposure of *Msm* ΔdosR to 5 mM H_2O_2 during hypoxia the number of 8-OG was 53.1 ppm (± 8.4 ppm) while the number of 8-OdG was 7.5 ppm (± 2.7 ppm).

5.3.1.4 Hydrogen peroxide – a suitable stress agent?

Using H_2O_2 we were able to show that nucleic acid oxidation occurs *in vivo* in mycobacteria. Furthermore we were able to show that like in eukaryotic cells, RNA is more susceptible to oxidative damage than DNA. The statistical significance of these observations in each experiment was limited, most probably due to the fact that the sample size was too small for each experiment. We attempted to obtain an additional measure of significance for the higher susceptibility of RNA to oxidation by carrying out a one tailed, pair-wise T-test on all our data, and we found that RNA oxidation is significantly higher than DNA oxidation following H_2O_2 stress ($p = 4.07 \times 10^{-6}$, N=49).

$OH^{\bullet}$ can react with a host of molecules leading to a wide spectrum of effects (see section 1.5.2) including lipid peroxidation, protein oxidation, protein carbonylation

(Halliwell and Gutteridge, 2007) and NAD^+/NADH imbalance (Kohanski *et al.*, 2007). Therefore using H_2O_2 to induce stress allows the investigation of the cellular response to indiscriminate oxidative stress. However, we may need to choose a different ROS donor to ask a more specific question such as what is the effect of RNA oxidation on cell physiology.

5.3.2 Methylene blue photo-oxidation

Outer shell electrons of methylene blue (MB) can be excited by visible light and can lead to the generation of singlet oxygen and superoxide (Floyd *et al.*, 2004, Floyd, 2009). It was shown that MB can induce the generation of 8-OdG and 8-OG (Czeczot *et al.*, 1991, Schneider *et al.*, 1990, Floyd, 2009) and has been used successfully to inactivate RNA viruses by virtue of photo-oxidation (Floyd *et al.*, 2004). MB photo-oxidation has bactericidal activity against several bacteria including *Pseudomonas aeruginosa* (Street *et al.*, 2009) and methicillin-resistant *Staphylococcus aureus* – MRSA (Zolfaghari *et al.*, 2009). MB photo-oxidation was also shown to lead to inhibition of ribosomal function in *E. coli* (Garvin *et al.*, 1969). Interestingly, MB is used as a redox dye to monitor the hypoxic status of static mycobacterial cultures (Wayne and Hayes, 1996). When we used it during one of our nucleoside analysis experiments we noticed an increased level of 8-OG and 8-OdG in cultures where MB was present.

Using MB to induce oxidative damage is a very attractive possibility, since we could potentially take advantage of the ability of MB to bind nucleic acids to target oxidative damage to RNA and DNA. Of course we cannot exclude the possibility that other cellular components would be damaged as well using this approach, however we feel that using MB would limit damage to other cellular components when compared to H_2O_2.

5.3.2.1 Toxicity

We wanted to establish the toxicity of MB to *Msm*. We found that in the absence of light, MB is not very toxic and cells can tolerate it at concentrations of approximately 150 μg/ml [13] (data not shown). We repeated the experiment by exposing *Msm* cultures grown in 24-well plates to red light (635 nm) and we found that MB has a significant negative effect on growth after 3h at a concentration of 1.0 μg/ml, and a significant negative effect on growth after 24h at a concentration of 0.5 μg/ml. Furthermore there is a concentration-dependent effect on viability, therefore we could control the amount of oxidative damage we induced (see Fig. 5.10).

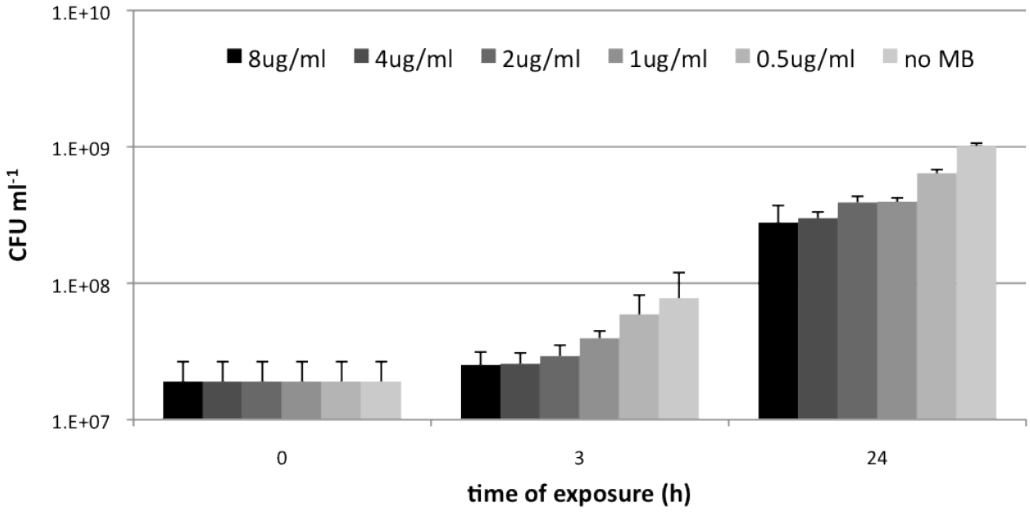


FIG. 5.10 Methylene blue photo-oxidation inhibits *Msm* wild type growth. *Msm* wild type cells were grown in 24 well plates on an orbital shaker at 37˚C. Photo-oxidation was induced by adding methylene blue and incubating the plates on a custom made LED light box (emission λ_{max} 635 nm). The viability of cells was determined by plating 10-fold serial dilutions.

All measurements represent four independent cultures. Error bars correspond to the standard deviation (N=4).

[13] Stock solution of MB is 0.5 mg/ml *w/v*.

5.3.2.2 Damage to nucleic acids

Having determined that MB photo-oxidation can inhibit mycobacterial growth, we were interested in its ability to cause oxidative damage *in vivo*. We exposed actively growing *Msm* wild type cells to MB (2 μg ml^{-1}) photo-oxidation and then determined the formation of 8-OG and 8-OdG (see Fig. 5.11).

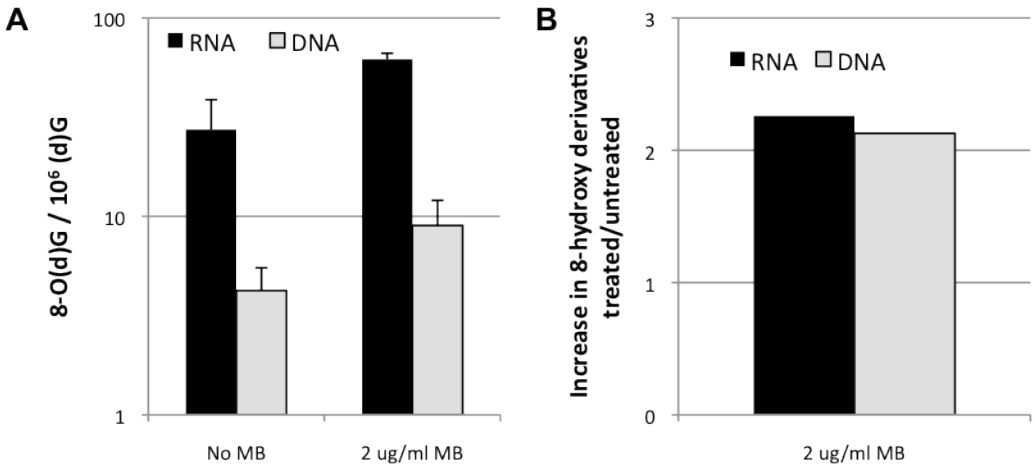


FIG. 5.11 Methylene blue photo-oxidation gives rise to 8-O(d)G in wild type *Msm in vivo*. Actively growing *Msm* wild type cells were exposed to MB (2 μg ml^{-1}) photo-oxidation at 37°C during normoxic active growth (**A**). The relative increase in oxidative damage compared to no treatment was calculated for cells during active growth (**B**) Nucleic acids were extracted, hydrolysed and analysed by HPLC-MSMS. Levels of 8-OG (RNA) and 8-OdG (DNA) were determined in relation to G (RNA) or dG (DNA). Quantitation was performed by monitoring following m/z transitions 284.2→168.0 for 8-OdG and 300.1→168.0 for 8-OG. G and dG were quantified using A_{260} detected with the in-line UV spectrophotometer.

All measurements represent three independent cultures. Error bars correspond to the standard deviation (N=3).

Analogously to challenge with H_2O_2, RNA is more susceptible to MB photo-oxidation than DNA. The increase in the level of 8-OG and 8-OdG formation we induced after exposing cells to 1 hour of photo-oxidation in the presence of 2 μg ml^{-1} of MB was significant for RNA ($p < 0.05$) but not for DNA ($p = 0.10$). The levels of damage were similar to exposing the cells to 25 mM H_2O_2 (see Figs 5.7, 5.9 and 5.11); in all cases the relative increase in 8-O(d)G was approximately 2-fold.

5.4 Exploring oxidative damage in mycobacteria using TraSH

All the results presented in section 5.3 show that nucleic acid oxidation occurs *in vivo* when cells are exposed to sources of ROS. However our observations do not inform us on the biological implications of this damage. Identifying key players in the cellular response to oxidative damage, on the other hand, could be beneficial to our understanding of the consequences of oxidation and the role that proteins involved in the amelioration of this damage would have for the survival of the cell under conditions resembling latent infection.

A global approach interrogating the essentiality of mycobacterial genes under specific conditions has been developed by Sassetti *et al.* (2001), and could be used to identify bacterial genes that are involved in dealing with oxidative damage to nucleic acids. Their transposon site hybridisation (TraSH) method requires an extensive transposon mutant library (effectively containing mutants in all non-essential genes), which is allowed to propagate in two disparate environments. The frequency of transposon insertion into each gene can be determined by isolating the total DNA after a set period of growth and analysing it by microarray, or more recently, deep sequencing. Insertions into genes that are considered to be essential for growth in a certain environment would be under-represented when compared to insertions into genes, which are not essential. Using this approach they were able to compile the first list of essential genes in *Mtb* (Sassetti *et al.*, 2001) as well as finding conditionally essential genes during infection (Sassetti and Rubin, 2003, Rengarajan *et al.*, 2005). The same approach can also be used to study specific aspects of *Mtb* infection, e.g. inhibition of phagosome acidification (Stewart *et al.*, 2005b). We decided to use this approach to find genes that are essential during oxidative stress in *Msm*.

5.4.1 Choice of mutants

As a validation step for TraSH we decided to construct knockout mutants in *Msm,* which would be more susceptible to oxidative damage than wild type. The identification of these mutants during TraSH analysis would provide a positive control that the approach was successful in identifying strains with an increased susceptibility to oxidative stress.

When choosing the appropriate mutants we assumed that the three major sources of damage in a context of infection were $OH^{\bullet}$, superoxide and peroxynitrite (Halliwell and Gutteridge, 2007). We hypothesised that proteins directly involved in the reduction/mitigation of oxidative damage would be good candidates for mutagenesis (see Fig. 5.12). There are a multitude of catalases (8), alkyl-hydroperoxidases (7) and superoxide dismutases (3) encoded in the *Msm* genome (Kanehisa *et al.*, 2006). For practical reasons we chose to knockout a subset of these genes (see Table 5.3) – KatG – MSMEG_6384, AhpC – MSMEG_4753 and two SodA homologues: MSMEG_6427 and MSMEG_6636. We also targeted two genes involved in mycothiol biosynthesis – MshA – MSMEG_0933 and Mca – MSMEG_5261 (Newton *et al.*, 2008) as well as two regulators involved the coordination of the oxidative stress response – IdeR – MSMEG_2750 (Dussurget *et al.*, 1996) and SoxR – MSMEG_5450 (Imlay, 2008). Finally we tried to knockout AlkB – MSMEG_5451, whose homologue in *E. coli* acts as an RNA alkylation repair protein (Aas *et al.*, 2001).

We reasoned that targeting several proteins at the same time would allow us to obtain at least one knock out mutant, which we could use for the validation of the TraSH experiment.

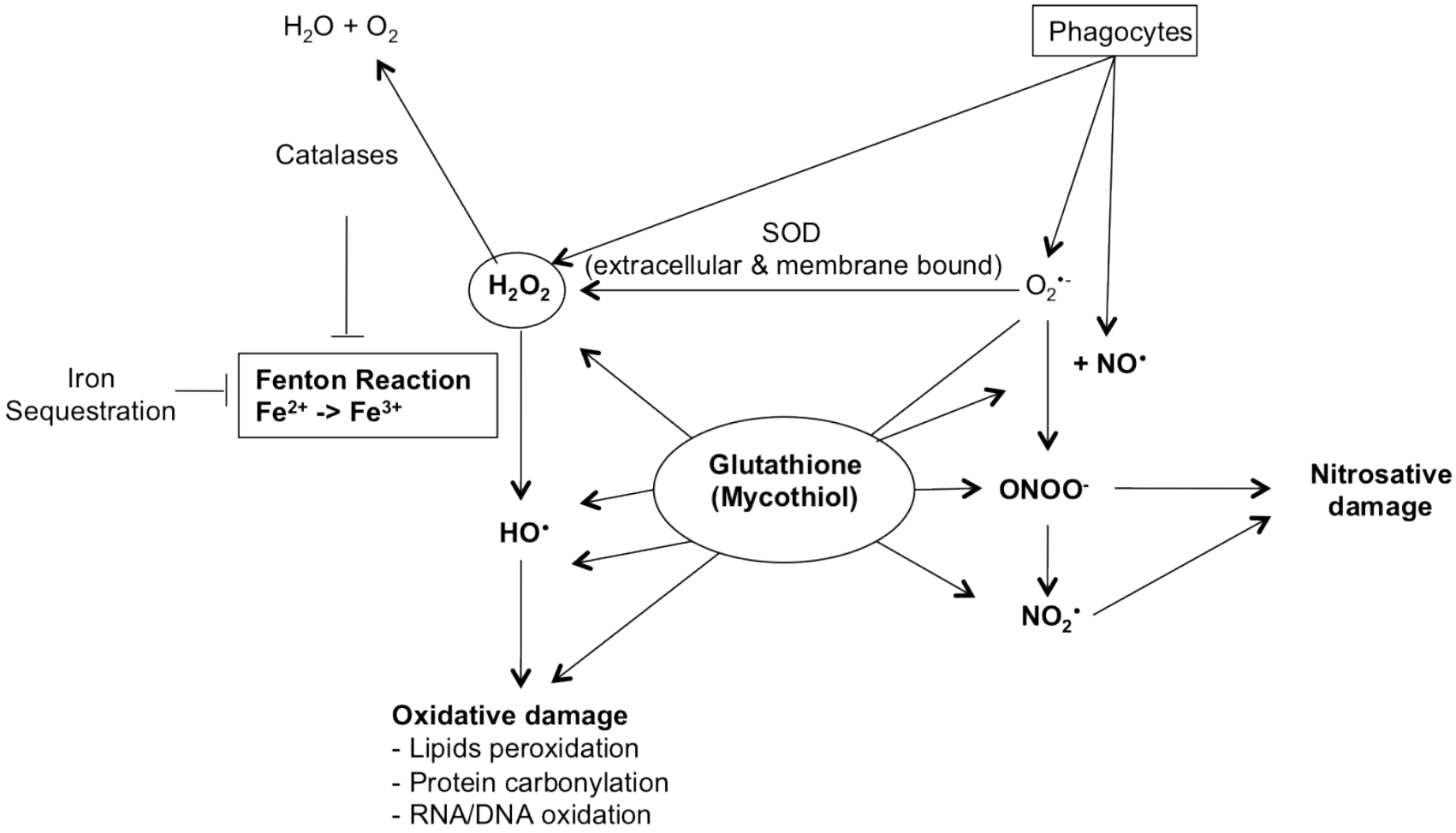


FIG. 5.12 Interplay between oxidative damage and antioxidant defences in mycobacteria during infection.

5.4.2 Mutagenesis

We used the same recombineering method (van Kessel and Hatfull, 2007) as for the knocking out of MSMEG_3935 (see section 4.8.2). In short we first created linear constructs by flanking a hygromycin cassette with approximately 500 bp up- and downstream of the gene of interest. We then electroporated the linear construct into *Msm* cells and screened for hygromycin resistance. Due to technical difficulties we were only able to obtain and confirm ΔalkB and Δmca strains. A summary of the progress for each mutant is shown in Table 5.3.

TABLE 5.3 Summary of *Msm* mutagenesis for oxidative stress TraSH.

Gene name (annotation)	*Linear construct*	*Construct insertion*[a]	*Confirmation PCR*[b]
ahpC (MSMEG_4753)	+	+	-
alkB (MSMEG_5451)	+	+	+
ideR (MSMEG_2750)	-[c]		
katG (MSMEG_6384)	-[c]		
mca (MSMEG_5261)	+	+	+
mshA (MSMEG_0933)	+	+	-
sodA I (MSMEG_6427)	-[c]		
sodA II (MSMEG_6636)	-[c]		
soxR (MSMEG_5450)	+	+	-

[a] Hygromycin resistant colonies with insert present – confirmed by PCR
[b] Insert present in the expected location as determined by PCR and restriction enzyme digestion
[c] Unsuccessful PCR for upstream or downstream fragment

Overall we were unable to obtain most of the mutants that we set out to construct. The reason in the case of *ideR*, *katG* and *sodA* lies in the technical difficulties we encountered during the generation of the mutagenic construct. We believe that re-designing the PCR primers would resolve these issues, however in light of the fact that these experiments were started at a very late stage in my PhD it was not feasible to revisit the mutagenesis and overcome the technical difficulties within the time-frame of my project.

The inability to obtain ΔsoxR, ΔmshA and ΔahpC mutants on the other hand is less obvious. The TraSH essentiality screen did not identify any of the genes we chose as essential in *Mtb* (Sassetti *et al.*, 2003). It is important to note that *Mtb* does not possess a SoxR homologue, so the inability to obtain ΔsoxR may be due to it being essential in *Msm*. However this is unlikely as SoxR was shown not to be essential in *E. coli* and *P. aeruginosa* (Palma *et al.*, 2005). Similarly MshA was shown not to be essential in *Msm* (Newton *et al.*, 2008) and AhpC was successfully mutated in *Msm* before (Dhandayuthapani *et al.*, 1996). Overall it is likely that we would be able to obtain the desired mutants if we repeated the mutagenesis. However, given the aforementioned time constraints we decided to use the two mutants we managed to create for future TraSH experiments.

5.4.3 TraSH experiment – transposon mutant library construction

The two main requirements for a successful TraSH experiment are a library containing at least 10^5 transposon insertion mutants and a robust primary selection (Murray *et al.*, 2008). As shown in Fig. 5.10 we were able to use MB photo-oxidation to induce cell death to a degree that is sufficient for TraSH analysis (Rubin, personal communication).

The construction of a transposon mutant library has been optimised for *Mtb* and *Mbo* BCG, however different researchers have had a varying degree of success in creating large enough libraries in *Msm* (Rubin, personal communication). We first made an attempt at creating an *Msm* transposon mutant library using the ϕMycoMarT7 phasmid and following the protocol described by Murry *et al.* (2008). Using this approach, optimised for *Mtb*, we obtained a library of 428 cfu ml^{-1} (±148 cfu ml^{-1}).

In an attempt to understand the reasons behind the limited library size we took a closer look at the phasmid lineage and its biology to see whether we could obtain any information that would help us to optimise the protocol for *Msm*. ϕMycoMarT7 was derived from a temperature sensitive mutant of mycobacteriophage ϕTM4 - ϕAE87

which fails to produce plaques on *Msm* at 37˚C at a multiplicity of plating of 10:1 (Ford *et al.*, 1998, Murry *et al.*, 2008). ϕTM4 appears to be a temperate phage in some mycobacterial species – it was isolated from *Mycobacterium avium* after treatment with Mitomycin C, however it does not form turbid plaques, typical of temperate phages, in *Msm* (Ford *et al.*, 1998). Therefore it is possible that ϕMycoMarT7-induced lysis of *Msm* could occur during the generation of the library, as some steps are carried out at room temperature. We therefore reasoned that performing all the steps at an elevated temperature of 42˚C, making sure that all the reagents used are also pre-heated to 42˚C would increase the efficiency of the transposon mutagenesis, while not adversely affecting *Msm* survival. When we carried out the modified experiment we obtained a marginally improved result of 977 cfu ml^{-1} (±244 cfu ml^{-1})

We envisage that a systematic approach addressing the optimal conditions for each parameter of the experiment would improve the efficiency of transposon mutagenesis. Mutagenesis could also be improved by using a different phage during the transduction – a replication deficient temperate phage in *Msm* may yield a better yield than ϕMycoMarT7. Both these approaches would require a significant amount of time, which we did not have at our disposal. We were therefore unable to optimise the mutagenesis further and consequently we were not able to carry out the planned TraSH experiment.

5.5 Discussion

5.5.1 Measuring oxidative damage in mycobacteria – what have we learned?

An important advantage of the methodology described in this chapter is the ability to measure oxidative damage to nucleic acids directly and with great sensitivity. As a result we are able to study the impact of oxidative damage to nucleic acids without having to resort to measuring such a complex and multifactorial process as cell viability. The data presented here represent an early study, as we focused mostly on the implementation of

the analytical approach at the expense of more complete biological experimentation. Nonetheless these data represent the first attempt to measure the level of RNA and DNA oxidation *in vivo* in a mycobacterial system. Importantly, we were able to obtain biologically relevant results that could form the basis for future work. Namely, we found that the relative increase in the level of oxidative damage after exposure to H_2O_2 is higher in static hypoxic cultures than in actively growing normoxic cultures. And secondly, RNA oxidation is significantly higher than DNA oxidation during exposure to oxidative stress.

In line with observations presented in Chapter 3, the susceptibility of *Msm* to oxidative stress is higher during hypoxic stasis than during normoxic growth. Why are hypoxic cells more susceptible to oxidative stress? One possibility is that hypoxic *Msm* cells have a lower level of enzymes involved in the mitigation of oxidative damage, since such enzymes would not be required in the absence of oxygen. We did not measure the activity of any of the enzymes that might limit the effect of oxidative damage, however the expression levels of *katG*, *ideR* and *ahpC* were found to be significantly higher in *Msm* growing under low oxygen conditions when compared to normoxic growth (Berney and Cooke, 2010). The relevance of this observation remains to be determined for our system, however IdeR is necessary for the limitation of iron uptake as well as the full expression of catalases, superoxide dismutases and alkyl-hydroperoxidases in *Msm* (Dussurget *et al.*, 1996). Similarly Shi *et al.* (2008) found that there is an increase in the levels of *ahpC* expression in *Mtb* during NRP-1 and a an increase in methionine sulfoxide reductase and truncated haemoglobin, both involved in ROS/RNS detoxification, during NRP-2. They also observed a minor increase in the level of *sodA* and thioredoxin during the oxygen depletion. Therefore it appears that hypoxic cells do possess antioxidant defences, whether or not the levels are comparable to actively growing cells remains to be determined.

As seen in chapter 3, [^{3}H]-uracil incorporation decreases drastically during hypoxia and levels of available energy are similarly reduced (Wayne and Hayes, 1996, Starck *et al.*, 2004, Rao *et al.*, 2008, Leistikow *et al.*, 2010). Therefore cells in hypoxia could be less capable of establishing a suitable transcriptional response to sudden oxidative damage due to a limited availability of energy. As a result hypoxic cells would be more susceptible to oxidative damage. Similarly a higher rate of RNA/DNA biosynthesis, found during active growth, would reduce the half-life of 8-hydroxy lesions, therefore limiting the impact of 8-OG and 8-OdG on the cell. However, carbon-starved stationary cells are also likely to have a limited ATP pool (Deb *et al.*, 2009, Hampshire *et al.*, 2004, Betts *et al.*, 2002), but they are not as susceptible to oxidative stress as hypoxic cultures. This observation could reflect changes in the physical properties of the cell (Smeulders *et al.*, 1999), however it might also point to the fact that low energy levels alone do not account for the susceptibility of hypoxic cells. An alternative explanation is provided by the changes in the redox state of *Msm* cultures from oxidising to reducing when cells enter hypoxia – a feature that has been exploited for the definition of NRP-1 and NRP-2 based on MB discolouration (Wayne and Hayes, 1996, Boshoff and Barry, 2005). This change is also illustrated by the susceptibility of mycobacteria to metronidazole in hypoxia both *in vitro* and *in vivo* (Wayne and Sramek, 1994, Filippini *et al.*, 2010, Via *et al.*, 2008). Under reducing conditions oxygen and consequently oxidative stress is more damaging, as demonstrated by the toxicity of oxygen to anaerobes (Halliwell and Gutteridge, 2007). One possibility is the generation of superoxide by reduced ferredoxin, if a shift towards lower potential electron carriers occurs as suggested (Berney and Cook, 2010, Boshoff and Barry, 2005).

An important consideration to make when talking about the redox state of the cell is whether we might be underestimating oxidative damage to hypoxic cultures, since chemical properties of the intracellular environment could affect the generation of 8-OG and 8-OdG. $OH^{\bullet}$ reaction with guanine can give rise to two products 8-hydroxyguanine

and 2,6-diamino-4-hydroxy-5-formamidopyrimidine – FAPyG (Halliwell and Gutteridge, 2007). The relative yield of each of these species is determined by the redox state of the reaction environment – FAPyG is favoured in reducing environments while 8-hydroxyguanine is favoured in oxidising environments (Halliwell and Gutteridge, 2007). Therefore the real extent of oxidative damage to hypoxic cultures might be even greater than shown by our data. To assess this possibility a method for measuring FAPyG by virtue of mass spectrometry would have to be implemented (Frelon *et al.*, 2000) and used for future studies of oxidative damage to nucleic acids.

Using solely the data at hand, we cannot claim that increased susceptibility to oxidative stress of hypoxic cultures is accounted for by an increased formation of 8-hydroxy lesions. The increased susceptibility is most probably caused by the interplay of several contributing factors including redox state of the cell, energy availability and antioxidant capability. The impact of oxidative stress to nucleic acids on cell viability, as well as the mechanisms by which the cell responds to it, remain to be determined. However methodology presented in this chapter, combined with genetic approaches such as TraSH, could further our understanding of how mycobacteria withstand oxidative stress in the context of infection. Studying this aspect of mycobacterial physiology could have applications that may reach as far as the clinic and the development of novel chemotherapeutic agents, since oxidative damage may play a part in the bactericidal activity of several antibiotics (Kohanski *et al.*, 2007).

5.5.2 Implications of greater susceptibility of RNA to oxidative damage

One of the key findings of this work was that the level of RNA oxidation significantly exceeds levels of DNA oxidation during exposure to H_2O_2 and MB. This fact could be indicative of a higher intrinsic susceptibility of RNA to oxidative damage. Alternatively, it could point to an active process whereby DNA lesions have a shorter half-life than their RNA counterparts. In the latter case the rate of formation of 8-OG and 8-OdG would

be comparable, but the steady state levels would differ due to an 8-OdG-specific amelioration process. 8-OdG is actively repaired in *Msm* by MutM-mediated base excision repair (Jain *et al.*, 2007), and to some extent by nucleotide excision repair (Kurthkoti *et al.*, 2008). Mutants in base excision repair enzymes as well as nucleotide excision repair enzymes were found to have higher mutation rates when exposed to H_2O_2 (Venkatesh *et al.*, 2003, Jain *et al.*, 2007, Kurthkoti *et al.*, 2008). Mutations in these strains are most likely caused by an accumulation of oxidative damage lesions, such as 8-OdG (Jain *et al.*, 2007). *Msm* strains deficient in DNA repair could be used to investigate whether the apparent higher susceptibility of RNA to oxidative damage is a result of DNA repair in *Msm*.

If differences in repair are the principal reason for the difference in susceptibility to damage, then it follows that the most probable mechanism for the remediation of oxidative damage to RNA is breakdown and *ex novo* synthesis. What does this mean for persistent mycobacteria? RNA biosynthesis is greatly reduced in hypoxic cultures (see section 3.4.2.1). In light of the limited energy availability of hypoxic cells (Wayne and Hayes, 1996, Starck *et al.*, 2004, Rao *et al.*, 2008, Leistkow *et al.*, 2010) the overall capacity for biosynthesis is probably reduced as well. Furthermore our data strongly support the possibility that RNA oxidation could occur in the *in vivo* context of hypoxic granulomas, forcing persistent cells to deal with the consequences of such damage. Despite this *Mtb* manages to survive in granulomas for several decades. This means that RNA oxidation and the associated erosion of translational fidelity (Tanaka *et al.*, 2007) and activity (Honda *et al.*, 2005) either do not have a negative impact on the survival of the cell, or the cell actively limits the damage. The information at hand is insufficient to comment on the cellular processes in place to deal with this damage. It would be tempting to speculate, however, that a selective protection of key cellular components could play a part in the process.

6. General discussion

Can RafH be a regulator of mycobacterial growth?

Habitats where bacteria exist in a permanent state of active growth are almost non-existent (Morita, 1993). Each environmental niche poses specific challenges to the organisms that inhabit it. Often, particularly in the case of many pathogens, the bacterium needs to adapt to multiple niches. In the case of *Mtb* these would include active growth in the early stages of infection, prolonged survival in the absence of oxygen and survival of the transmission to a new host. The specific physiological requirements for each are different, and mycobacteria were shown to possess the physiological plasticity that would allow them to adapt to a range of different growth rates (Berney and Cook, 2010, Beste *et al.*, 2005, Beste *et al.*, 2007, Beste *et al.*, 2009 and section 1.4). Nonetheless, a change in the environmental conditions poses a challenge to the bacterium, forcing it to trigger an adaptation mechanism. Given that adaptation is an active process that requires coordinated gene expression and protein synthesis (Ostling *et al.*, 1993, Spector and Foster, 1993), the bacterium requires sufficient time and resources to undergo the physiological transition. If this transition occurs too rapidly it is likely to result in decreased fitness of the bacterium – as exemplified by the correlation between the time spent in NRP-1 and survival in NRP-2 during the Wayne model of hypoxia (Wayne and Hayes, 1996, see 1.3.3.2).

Bacteria can extend the time of adaptation by coupling the input from related environmental stimuli in a predictive fashion. *E. coli* has evolved to survive in two drastically different environments – the mammalian intestine is defined by low oxygen levels and a temperature of approximately 37˚C, while the outside environment is characterised by higher oxygen levels and lower temperature. To increase its efficiency and chances of survival, *E. coli* co-regulates the heat shock response and aerobic respiration so that an increase in temperature results in a pre-emptive adaptation to low oxygen metabolism (Tagkopoulos *et al.*, 2008). This pre-emptive adaptation need

not be triggered. As illustrated by persisters in *E. coli* (Lewis, 2010, see 1.3.1.2) a metabolically less active fraction of a heterogeneous population of bacteria would improve the ability of the population to survive as a whole. Investigation into the mechanism of persister formation revealed that individual cells can enter this state in a stochastic manner (Balaban *et al.*, 2004), which ensures that at least a proportion of the overall population can survive an acute shock, such as antibiotic treatment.

These findings are not limited to the biology of *E. coli*; evidence from the clinic points to the existence of a heterogeneous *Mtb* population during infection ("special populations" hypothesis, Mitchison, 1979, see 1.2.3). Significantly persister-like *Mtb* can be found in the sputum of patients with active pulmonary tuberculosis (Garton *et al.*, 2008), leading to the possibility that persistent *Mtb* can also lead to infection. Whether or not persistent bacilli in sputum form the antibiotic tolerant subpopulation during infection is still not clear, but it is an interesting possibility. Moreover, *Mtb* may be capable of predictive adaptation as well. The DosR/S/T two component system responds to nitric oxide, carbon monoxide and low oxygen levels (see 1.4.2.1). The infecting mycobacterium is likely to encounter at least one of these stimuli during the initial stages of infection. If we consider that the natural state of *Mtb* appears to be latent infection, then sensing these diatomic gases offers a perfect proxy for the pre-emptive onset of the physiological changes needed to establish persistence in the hypoxic granuloma.

As outlined in sections 1.4.2.1 and 1.4.2.2 DosR plays a role in physiological adaptations of mycobacteria that would be very significant during the establishment of persistence, including energy homeostasis, nutrient storage (TAG synthase) and stress protection (HspX, USPs). The data presented here point to additional roles of the DosR regulon mediated by RafH. Our data show that RafH binding could serve as a reversible non-destructive mechanism for the global regulation of translational activity, and an important mediator of ribosomal stability. Combined, these functions could contribute

to the slow-down of metabolism needed for the establishment of persistence as well as facilitating its maintenance by stabilising the ribosome. Both functions were described previously for S30AE domain proteins such as hibernation promoting factor (HPF) and YfiA of *E. coli* and the light-repressed protein (LrtA) of *Synechococcus* PCC 7002 (see 4.9.4).

What evidence is there to support this mechanism of action for RafH? An indication for the role in slowing down metabolism comes from the inability of *Mtb* ΔdosR to efficiently reduce oxygen consumption in response to a decrease in oxygen levels during the onset of NRP-1 of the Wayne hypoxia model of persistence (Leistikow *et al.*, 2010). Further evidence for the involvement of RafH in growth regulation came from the study of genes required for growth rate adaptations in *Mbo* BCG, which identified the RafH homologue in *Mbo* BCG – Mb0082 as an essential protein for optimal growth of *Mbo* BCG in chemostats (Beste *et al.*, 2009). This result seems to be inconsistent with the hypothesis that RafH promotes a slow down in metabolism. But consider this, Mb0082 expression indicates that the DosR regulon must have been induced, suggesting that oxygen might have been somewhat limiting under the chemostat conditions used. If true, then Mb0082 could serve as a control mechanism to limit excessive growth under suboptimal conditions, which could be deleterious for the cell due to exhaustion. A similarly intriguing finding is that the W-Beijing strain of *Mtb*, which was shown to have an up-regulated DosR regulon (Reed *et al.*, 2007), does not have a growth rate defect. This result seems to be at odds with the role of RafH as a translational repressor, especially as its homologue in *Mtb* – Rv0079 is among the most induced genes of the regulon (Park *et al.*, 2003). However, a steady state increase in the level of S30AE proteins is unlikely to have the same effect on growth as a transient increase in protein levels. The rationale for this stems from the fact that an increase in the steady state concentration of ribosomes during active growth would offset the impact of a higher concentration of S30AE. For example, HPF and YfiA can both be over-

expressed in *E. coli* (Vila-Sanjurjo *et al.*, 2004, Ueta *et al.*, 2008), as there is spare capacity in the system to produce more ribosomes to counter such effects (Kurland and Mikkola, 1993, Asai *et al.*, 1999). Moreover, an induction of DosR under normoxic conditions does lead to growth retardation in *Mbo* BCG (Flores Valdez and Schoolnik, 2010) consistent with a role of RafH in translational slow-down.

It is important to note that the activity of RafH and more broadly DosR may not be unique or universal in the establishment of mycobacterial persistence. Investigations on the role of DosR in antibiotic tolerance during the Cornell model of latent tuberculosis (see 1.3.3.1) have shown that it is not essential for the re-emergence of *Mtb* infection in antibiotic treated mice (Bartek *et al.*, 2009). However the mechanism of latent infection in the Cornell model is still poorly understood, and may not reflect the adaptations required for long-term survival in the human lung. The role of RafH in the establishment of persistence has not been addressed directly by any study in the literature, however there is some evidence that it features in the growth control mechanisms of *Mtb*. A key consideration is that translational shift-down is one of the triggers for persister formation in *E. coli*, as is antibiotic treatment (Keren *et al.*, 2004, Lewis, 2010). A recent screen for multidrug tolerant mutants of *Msm* identified a number of ribosomal mutations, which led to an increased tolerance to multiple antibiotics through reduced ribosomal activity (Kaufmann *et al.*, 2010). The induction of RafH during infection would have the same effect without the need for potentially deleterious mutations of ribosomal genes. Therefore the ability to control growth by a transient slow down in metabolism could significantly aid the establishment of persistence in the context of a hypoxic granuloma.

Is ribosomal stability important for survival in mycobacterial persistence?

A reduction in the rate of translation is an early response to limiting conditions; cells that have fully adapted to a lower growth rate reduce the overall number of ribosomes

in the cell to mirror the lower requirement for biosynthesis (Beste *et al.*, 2005). The transition to a lower number of ribosomes needs to be carefully controlled – if the cell degrades too high a proportion it may not have sufficient biosynthetic capability to resume growth in more favourable conditions (Davis *et al.*, 1986). Furthermore stabilisation of excess ribosomes in an intact but inactive state is energetically more favourable than adjusting the complement of ribosomes by degradation and *ex novo* synthesis alone.

In addition to the role in growth control, S30AE domain proteins can serve as mediators of ribosomal degradation as well as stabilisation. As was discussed in section 4.9.1 ribosomal dissociation serves as an initial step in their degradation. Therefore by controlling the level of RafH and RafS the cell can exploit their association-promoting action to protect a subpopulation of ribosomes from degradation. This role is illustrated by the accelerated ribosomal degradation during early hypoxia in the ΔdosR mutant of *Msm* (see 4.3.2 and 4.7.2), which could be explained by a lack of the stabilising effect of RafH during the adaptation to hypoxia. The importance of ribosomal stabilisation during prolonged stasis is further illustrated by the decreased stability of rRNA (see 4.4.2) accompanied by a higher rate of RNA biosynthesis in ΔdosR *Msm* during hypoxic stasis (3.4.2.1). An explanation for this phenomenon can again be linked to the activity of RafH – an increased rate of ribosomal degradation forces the cell to make more rRNA than it would normally, resulting in energy depletion. Indeed, deletion of RafH alone confers a survival defect on *Msm* during prolonged hypoxic stasis (see 4.8.3). Since the phenotype of ΔrafH is less severe than that of ΔdosR, RafH alone does not account for all the functions of the DosR regulon, however it does contribute significantly towards the function of this regulon.

In addition to the intrinsic factors that affect ribosomal stability during stasis, such as RNase activity, ribosomal subunit association, energy and nutrient availability, the context of infection also poses a significant challenge to ribosomal integrity. Reactive

nitrogen and oxygen species lead to nucleic acid damage (see 1.5.1). As we were able to demonstrate for cells challenged with hydrogen peroxide, the damage is disproportionally accumulated in cellular RNA and in particular during hypoxic stasis (see 5.3.1). Both of these observations point to the ribosome as a particularly susceptible target during persistent infection. In light of the severity of the consequences of oxidative damage to RNA, which include reduced ribosomal activity and fidelity as well as reduced RNA integrity (see 1.5.2.2) it is not difficult to envisage that ribosomal stabilisation would be beneficial to the cell – particularly during prolonged periods of biosynthetic limitation.

In summary, mycobacterial persistence is not governed only by the ability of the cell to replicate, change gene expression and modify different aspects of metabolism, but it is also defined by its capacity to stabilise its complement of ribosomes. And while the work presented in this study does not irrefutably prove that RafH and RafS play a key role in this process, it undoubtedly provides ample evidence that they are prime candidates for the job, and might even provide interesting targets for the development of future therapeutics targeted specifically at non-growing mycobacteria.

7. References

Aas, P. A., M. Otterlei, P. O. Falnes, C. B. Vagbo, F. Skorpen, M. Akbari, O. Sundheim, M. Bjoras, G. Slupphaug, E. Seeberg & H. E. Krokan, (2003) Human and bacterial oxidative demethylases repair alkylation damage in both RNA and DNA. *Nature* **421**: 859-863.

Abramoff, M. D., Magelhaes, P.J., Ram, S.J., (2004) Image processing with ImageJ. *Biophotonics international* **11**: 36-42.

Adams, L. B., M. C. Dinauer, D. E. Morgenstern & J. L. Krahenbuhl, (1997) Comparison of the roles of reactive oxygen and nitrogen intermediates in the host response to *Mycobacterium tuberculosis* using transgenic mice. *Tuber Lung Dis* **78**: 237-246.

Afonina, E., N. Chichkova, S. Bogdanova & A. Bogdanov, (1991) 30S ribosomal subunits with fragmented 16S RNA: a new approach for structure and function study of ribosomes. *Biochimie* **73**: 777-787.

Agafonov, D. E., V. A. Kolb, I. V. Nazimov & A. S. Spirin, (1999) A protein residing at the subunit interface of the bacterial ribosome. *Proc Natl Acad Sci U S A* **96**: 12345-12349.

Agafonov, D. E., V. A. Kolb & A. S. Spirin, (2001) Ribosome-associated protein that inhibits translation at the aminoacyl-tRNA binding stage. *EMBO Rep* **2**: 399-402.

Al Mamun, A. A., S. Gautam & M. Z. Humayun, (2006) Hypermutagenesis in *mutA* cells is mediated by mistranslational corruption of polymerase, and is accompanied by replication fork collapse. *Molecular Microbiology* **62**: 1752-1763.

Aly, S., K. Wagner, C. Keller, S. Malm, A. Malzan, S. Brandau, F. C. Bange & S. Ehlers, (2006) Oxygen status of lung granulomas in *Mycobacterium tuberculosis*-infected mice. *J Pathol* **210**: 298-305.

Anuchin, A. M., A. L. Mulyukin, N. E. Suzina, V. I. Duda, G. I. El-Registan & A. S. Kaprelyants, (2009) Dormant forms of *Mycobacterium smegmatis* with distinct morphology. *Microbiology* **155**: 1071-1079.

Archuleta, R. J., P. Yvonne Hoppes & T. P. Primm, (2005) *Mycobacterium avium* enters a state of metabolic dormancy in response to starvation. *Tuberculosis (Edinb)* **85**: 147-158.

Asai, T., C. Condon, J. Voulgaris, D. Zaporojets, B. Shen, M. Al-Omar, C. Squires & C. L. Squires, (1999) Construction and initial characterization of *Escherichia coli* strains with few or no intact chromosomal rRNA operons. *J Bacteriol* **181**: 3803-3809.

Atkins, J. F. & G. R. Bjork, (2009) A gripping tale of ribosomal frameshifting: extragenic suppressors of frameshift mutations spotlight P-site realignment. *Microbiol Mol Biol Rev* **73**: 178-210.

Baker, R. E., W. E. Hill & C. L. Larson, (1972) Delayed Hypersensitivity Reactions Provoked by Ribosomes from Acid-Fast Bacilli I. Ribosomal Isolation, Characterization, Delayed Hypersensitivity, and Specificity. *Infect. Immun.* **6**: 258-265.

Balaban, N. Q., J. Merrin, R. Chait, L. Kowalik & S. Leibler, (2004) Bacterial persistence as a phenotypic switch. *Science* **305**: 1622-1625.

Ballesteros, M., A. Fredriksson, J. Henriksson & T. Nystrom, (2001) Bacterial senescence: protein oxidation in non-proliferating cells is dictated by the accuracy of the ribosomes. *Embo J* **20**: 5280-5289.

Barry, C. E., (2001) *Mycobacterium smegmatis*: an absurd model for tuberculosis? *Trends in Microbiology* **9**: 473-474.

Barry, C. E., 3rd, H. I. Boshoff, V. Dartois, T. Dick, S. Ehrt, J. Flynn, D. Schnappinger, R. J. Wilkinson & D. Young, (2009) The spectrum of latent tuberculosis: rethinking the biology and intervention strategies. *Nat Rev Microbiol* **7**: 845-855.

Bartek, I. L., R. Rutherford, V. Gruppo, R. A. Morton, R. P. Morris, M. R. Klein, K. C. Visconti, G. J. Ryan, G. K. Schoolnik, A. Lenaerts & M. I. Voskuil, (2009) The DosR regulon of *M. tuberculosis* and antibacterial tolerance. *Tuberculosis (Edinb)* **89**: 310-316.

Barut, M., A. Podgornik, L. Urbas, B. Gabor, P. Brne, J. Vidic, S. Plevcak & A. Strancar, (2008) Methacrylate-based short monolithic columns: enabling tools for rapid and efficient analyses of biomolecules and nanoparticles. *J Sep Science* **31**: 1867-1880.

Batni, A., N. Festjens, K. Rumbold, I. Dewerte, R. De Rycke & N. Callewaer, (2009) Construction of a *Mycobacterium bovis* BCG Transposon Insertion Library and Biochemical Charcterisation of Selected Mutants. In: Tuberculosis: Biology, Pathology and Therapy. J. L. Flynn, D. G. Russell & T. N. A. Dick (eds). Keystone, CO, USA: Keystone Symposia on Molecular and Cellular Biology, pp. 65.

Belisle, J. T. & M. G. Sonnenberg, (1998) Isolation of genomic DNA from mycobacteria. *Methods Mol Biol* **101**: 31-44.

Benčina, M., A. Podgornik & A. Štrancar, (2004) Characterization of methacrylate monoliths for purification of DNA molecules. *Journal of Separation Science* **27**: 801-810.

Berney, M. & G. M. Cook, (2010) Unique flexibility in energy metabolism allows mycobacteria to combat starvation and hypoxia. *PLoS One* **5**: e8614.

Beste, D. J., M. Espasa, B. Bonde, A. M. Kierzek, G. R. Stewart & J. McFadden, (2009) The genetic requirements for fast and slow growth in mycobacteria. *PLoS One* **4**: e5349.

Beste, D. J., E. Laing, B. Bonde, C. Avignone-Rossa, M. E. Bushell & J. J. McFadden, (2007) Transcriptomic analysis identifies growth rate modulation as a component of the adaptation of mycobacteria to survival inside the macrophage. *J Bacteriol* **189**: 3969-3976.

Beste, D. J., J. Peters, T. Hooper, C. Avignone-Rossa, M. E. Bushell & J. McFadden, (2005) Compiling a molecular inventory for *Mycobacterium bovis* BCG at two growth rates: evidence for growth rate-mediated regulation of ribosome biosynthesis and lipid metabolism. *J Bacteriol* **187**: 1677-1684.

Betts, J. C., P. T. Lukey, L. C. Robb, R. A. McAdam & K. Duncan, (2002) Evaluation of a nutrient starvation model of *Mycobacterium tuberculosis* persistence by gene and protein expression profiling. *Molecular Microbiology* **43**: 717-731.

Blanc, L. & M. Uplekar, (2003) The Present Global Burden of Tuberculosis. In: The Return of the White Plague: Global Poverty and the "New" Tuberculosis. M. Gandy & A. Zumla (eds). London: Verso, pp. 95-111.

Blokpoel, M. C., M. J. Smeulders, J. A. Hubbard, J. Keer & H. D. Williams, (2005) Global analysis of proteins synthesized by *Mycobacterium smegmatis* provides direct evidence for physiological heterogeneity in stationary-phase cultures. *J Bacteriol* **187**: 6691-6700.

Body, A. & B. H. Brownstein, (1978) Effects of detergents on ribosomal precursor subunits of *Bacillus megaterium*. *J Bacteriol* **133**: 251-255.

Boelaert, J. R., S. J. Vandecasteele, R. Appelberg & V. R. Gordeuk, (2007) The effect of the host's iron status on tuberculosis. *J Infect Dis* **195**: 1745-1753.

Bolin, C. & F. Cardozo-Pelaez, (2007) Assessing biomarkers of oxidative stress: analysis of guanosine and oxidized guanosine nucleotide triphosphates by high performance liquid chromatography with electrochemical detection. *J Chromatogr B Analyt Technol Biomed Life Sci* **856**: 121-130.

Boon, C. & T. Dick, (2002) *Mycobacterium bovis* BCG response regulator essential for hypoxic dormancy. *J Bacteriol* **184**: 6760-6767.

Boon, C., R. Li, R. Qi & T. Dick, (2001) Proteins of *Mycobacterium bovis* BCG Induced in the Wayne Dormancy Model. *J Bacteriol* **183**: 2672-2676.

Borovinskaya, M. A., R. D. Pai, W. Zhang, B. S. Schuwirth, J. M. Holton, G. Hirokawa, H. Kaji, A. Kaji & J. H. Cate, (2007) Structural basis for aminoglycoside inhibition of bacterial ribosome recycling. *Nat Struct Mol Biol* **14**: 727-732.

Boshoff, H. I. & C. E. Barry, 3rd, (2005) Tuberculosis - metabolism and respiration in the absence of growth. *Nat Rev Microbiol* **3**: 70-80.

Boshoff, H. I., M. B. Reed, C. E. Barry, 3rd & V. Mizrahi, (2003) DnaE2 polymerase contributes to in vivo survival and the emergence of drug resistance in *Mycobacterium tuberculosis*. *Cell* **113**: 183-193.

Brett, A. M. O., J. A. P. Piedade & S. H. P. Serrano, (2000) Electrochemical Oxidation of 8-Oxoguanine. *Electroanalysis* **12**: 969-973.

Brne, P., A. Podgornik, K. Bencina, B. Gabor, A. Strancar & M. Peterka, (2007) Fast and efficient separation of immunoglobulin M from immunoglobulin G using short monolithic columns. *J Chromatogr A* **1144**: 120-125.

Bustin, S. A. & T. Nolan, (2004) Pitfalls of quantitative real-time reverse-transcription polymerase chain reaction. *J Biomol Tech* **15**: 155-166.

Cadet, J., T. Douki, S. Frelon, S. Sauvaigo, J. P. Pouget & J. L. Ravanat, (2002) Assessment of oxidative base damage to isolated and cellular DNA by HPLC-MS/MS measurement. *Free Radic Biol Med* **33**: 441-449.

Carpousis, A. J., (2007) The RNA degradosome of *Escherichia coli*: an mRNA-degrading machine assembled on RNase E. *Annu Rev Microbiol* **61**: 71-87.

Castellani, R. J., A. Nunomura, R. K. Rolston, P. I. Moreira, A. Takeda, G. Perry & M. A. Smith, (2008) Sublethal RNA oxidation as a mechanism for neurodegenerative disease. *Int J Mol Sci* **9**: 789-806.

Chan, J., K. Tanaka, D. Carroll, J. Flynn & B. R. Bloom, (1995) Effects of nitric oxide synthase inhibitors on murine infection with *Mycobacterium tuberculosis*. *Infect Immun* **63**: 736-740.

Chan, K., T. Knaak, L. Satkamp, O. Humbert, S. Falkow & L. Ramakrishnan, (2002) Complex pattern of Mycobacterium marinum gene expression during long-term granulomatous infection. *Proc Natl Acad Sci U S A* **99**: 3920-3925.

Chang, Y., Q. Kong, X. Shan, G. Tian, H. Ilieva, D. W. Cleveland, J. D. Rothstein, D. R. Borchelt, P. C. Wong & C. L. Lin, (2008) Messenger RNA oxidation occurs early in disease pathogenesis and promotes motor neuron degeneration in ALS. *PLoS One* **3**: e2849.

Cirillo, S. L., S. Subbian, B. Chen, T. R. Weisbrod, W. R. Jacobs, Jr. & J. D. Cirillo, (2009) Protection of *Mycobacterium tuberculosis* from reactive oxygen species conferred by the mel2 locus impacts persistence and dissemination. *Infect Immun* **77**: 2557-2567.

Colangeli, R., A. Haq, V. L. Arcus, E. Summers, R. S. Magliozzo, A. McBride, A. K. Mitra, M. Radjainia, A. Khajo, W. R. Jacobs, Jr., P. Salgame & D. Alland, (2009) The multifunctional histone-like protein Lsr2 protects mycobacteria against reactive oxygen intermediates. *Proc Natl Acad Sci U S A* **106**: 4414-4418.

Comstock, G. W., C. Baum & D. E. Snider, Jr., (1979) Isoniazid prophylaxis among Alaskan Eskimos: a final report of the bethel isoniazid studies. *Am Rev Respir Dis* **119**: 827-830.

Converse, P. J., P. C. Karakousis, L. G. Klinkenberg, A. K. Kesavan, L. H. Ly, S. S. Allen, J. H. Grosset, S. K. Jain, G. Lamichhane, Y. C. Manabe, D. N. McMurray, E. L. Nuermberger & W. R. Bishai, (2009) Role of the dosR-dosS two-component regulatory system in *Mycobacterium tuberculosis* virulence in three animal models. *Infect Immun* **77**: 1230-1237.

Cooper, A. M., D. K. Dalton, T. A. Stewart, J. P. Griffin, D. G. Russell & I. M. Orme, (1993) Disseminated tuberculosis in interferon gamma gene-disrupted mice. *J Exp Med* **178**: 2243-2247.

Cooper, A. M., B. H. Segal, A. A. Frank, S. M. Holland & I. M. Orme, (2000) Transient loss of resistance to pulmonary tuberculosis in p47(phox$^{-/-}$) mice. *Infect Immun* **68**: 1231-1234.

Corbett, E. L., C. J. Watt, N. Walker, D. Maher, B. G. Williams, M. C. Raviglione & C. Dye, (2003) The growing burden of tuberculosis: global trends and interactions with the HIV epidemic. *Arch Intern Med* **163**: 1009-1021.

Corper, H. J. & M. L. Cohn, (1951) The viability and virulence of old cultures of tubercle bacilli; studies on 30-year-old broth cultures maintained at 37 degrees C. *Tubercle* **32**: 232-237.

Cox, R. A., (2004) Quantitative relationships for specific growth rates and macromolecular compositions of *Mycobacterium tuberculosis*, *Streptomyces coelicolor* A3(2) and *Escherichia coli* B/r: an integrative theoretical approach. *Microbiology* **150**: 1413-1426.

Cserzo, M., E. Wallin, I. Simon, G. von Heijne & A. Elofsson, (1997) Prediction of transmembrane alpha-helices in prokaryotic membrane proteins: the dense alignment surface method. *Protein Eng* **10**: 673-676.

Cunningham, A. F. & C. L. Spreadbury, (1998) Mycobacterial stationary phase induced by low oxygen tension: cell wall thickening and localization of the 16-kilodalton alpha-crystallin homolog. *J Bacteriol* **180**: 801-808.

Czeczot, H., B. Tudek, B. Lambert, J. Laval & S. Boiteux, (1991) *Escherichia coli* Fpg protein and UvrABC endonuclease repair DNA damage induced by methylene blue plus visible light in vivo and in vitro. *J. Bacteriol.* **173**: 3419-3424.

Dahl, J. L., C. N. Kraus, H. I. Boshoff, B. Doan, K. Foley, D. Avarbock, G. Kaplan, V. Mizrahi, H. Rubin & C. E. Barry, 3rd, (2003) The role of Rel^{Mtb}-mediated adaptation to stationary phase in long-term persistence of *Mycobacterium tuberculosis* in mice. *Proc Natl Acad Sci U S A* **100**: 10026-10031.

Daniel, J., C. Deb, V. S. Dubey, T. D. Sirakova, B. Abomoelak, H. R. Morbidoni & P. E. Kolattukudy, (2004) Induction of a novel class of diacylglycerol acyltransferases and triacylglycerol accumulation in *Mycobacterium tuberculosis* as it goes into a dormancy-like state in culture. *J Bacteriol* **186**: 5017-5030.

Darwin, K. H., S. Ehrt, J. C. Gutierrez-Ramos, N. Weich & C. F. Nathan, (2003) The proteasome of *Mycobacterium tuberculosis* is required for resistance to nitric oxide. *Science* **302**: 1963-1966.

Darwin, K. H. & C. F. Nathan, (2005) Role for nucleotide excision repair in virulence of Mycobacterium tuberculosis. *Infect Immun* **73**: 4581-4587.

Dasgupta, N., V. Kapur, K. K. Singh, T. K. Das, S. Sachdeva, K. Jyothisri & J. S. Tyagi, (2000) Characterization of a two-component system, devR-devS, of *Mycobacterium tuberculosis. Tuber Lung Dis* **80**: 141-159.

Davies, E. & S. Abe, (1995) Methods for isolation and analysis of polyribosomes. *Methods Cell Biol* **50**: 209-222.

Davis, B. D., S. M. Luger & P. C. Tai, (1986) Role of ribosome degradation in the death of starved *Escherichia coli* cells. *J Bacteriol* **166**: 439-445.

Davis, E. O. & L. N. Forse, (2009) DNA Repair: Key to Survival? In: Mycobacterium: Genomics and Molecular Biology. T. Parish & A. C. Brown (eds). Norfolk, UK: Caister Academic Press, pp. 79-118.

Davis, J. M., H. Clay, J. L. Lewis, N. Ghori, P. Herbomel & L. Ramakrishnan, (2002) Real-time visualization of mycobacterium-macrophage interactions leading to initiation of granuloma formation in zebrafish embryos. *Immunity* **17**: 693-702.

Davis, J. M. & L. Ramakrishnan, (2009) The role of the granuloma in expansion and dissemination of early tuberculous infection. *Cell* **136**: 37-49.

Deb, C., C. M. Lee, V. S. Dubey, J. Daniel, B. Abomoelak, T. D. Sirakova, S. Pawar, L. Rogers & P. E. Kolattukudy, (2009) A novel in vitro multiple-stress dormancy model for *Mycobacterium tuberculosis* generates a lipid-loaded, drug-tolerant, dormant pathogen. *PLoS One* **4**: e6077.

de-los-Santos-Alvarez, N., P. de-los-Santos-Alvarez, M. J. Lobo-Castanon, R. Lopez, A. J. Miranda-Ordieres & P. Tunon-Blanco, (2007) Electrochemical oxidation of guanosine and adenosine: Two convergent pathways. *Electrochemistry Communications* **9**: 1862-1866.

den Hengst, C. D. & M. J. Buttner, (2008) Redox control in actinobacteria. *Biochimica et Biophysica Acta (BBA) - General Subjects* **1780**: 1201-1216.

Desjardin, L. E., L. G. Hayes, C. D. Sohaskey, L. G. Wayne & K. D. Eisenach, (2001) Microaerophilic induction of the alpha-crystallin chaperone protein homologue (*hspX*) mRNA of *Mycobacterium tuberculosis*. *J Bacteriol* **183**: 5311-5316.

Deuerling, E., A. Schulze-Specking, T. Tomoyasu, A. Mogk & B. Bukau, (1999) Trigger factor and DnaK cooperate in folding of newly synthesized proteins. *Nature* **400**: 693-696.

Deutscher, M. P., (2006) Degradation of RNA in bacteria: comparison of mRNA and stable RNA. *Nucleic Acids Res* **34**: 659-666.

Dhandayuthapani, S., Y. Zhang, M. H. Mudd & V. Deretic, (1996) Oxidative stress response and its role in sensitivity to isoniazid in mycobacteria: characterization and inducibility of *ahpC* by peroxides in *Mycobacterium smegmatis* and lack of expression in *M. aurum* and *M. tuberculosis. J Bacteriol* **178**: 3641-3649.

Diacon, A. H., A. Pym, M. Grobusch, R. Patientia, R. Rustomjee, L. Page-Shipp, C. Pistorius, R. Krause, M. Bogoshi, G. Churchyard, A. Venter, J. Allen, J. C. Palomino, T. De Marez, R. P. van Heeswijk, N. Lounis, P. Meyvisch, J. Verbeeck, W. Parys, K. de Beule, K. Andries & D. F. Mc Neeley, (2009) The diarylquinoline TMC207 for multidrug-resistant tuberculosis. *N Engl J Med* **360**: 2397-2405.

Ding, Q., W. R. Markesbery, Q. Chen, F. Li & J. N. Keller, (2005) Ribosome dysfunction is an early event in Alzheimer's disease. *J Neurosci* **25**: 9171-9175.

Dionne, M. S., N. Ghori & D. S. Schneider, (2003) *Drosophila melanogaster* is a genetically tractable model host for *Mycobacterium marinum*. *Infect Immun* **71**: 3540-3550.

Dormandy, T., (1999) *The White Death: A History of Tuberculosis,* p. 433. The Hambledon Press, London.

Dos Vultos, T., J. Blazquez, J. Rauzier, I. Matic & B. Gicquel, (2006) Identification of Nudix hydrolase family members with an antimutator role in *Mycobacterium tuberculosis* and *Mycobacterium smegmatis*. *J Bacteriol* **188**: 3159-3161.

Downing, K. J., V. V. Mischenko, M. O. Shleeva, D. I. Young, M. Young, A. S. Kaprelyants, A. S. Apt & V. Mizrahi, (2005) Mutants of *Mycobacterium tuberculosis* lacking three of the five *rpf*-like genes are defective for growth in vivo and for resuscitation *in vitro*. *Infect Immun* **73**: 3038-3043.

Drumm, J. E., K. Mi, P. Bilder, M. Sun, J. Lim, H. Bielefeldt-Ohmann, R. Basaraba, M. So, G. Zhu, J. M. Tufariello, A. A. Izzo, I. M. Orme, S. C. Almo, T. S. Leyh & J. Chan, (2009) *Mycobacterium tuberculosis* universal stress protein Rv2623 regulates bacillary growth by ATP-Binding: requirement for establishing chronic persistent infection. *PLoS Pathog* **5**: e1000460.

Drzewiecki, K., C. Eymann, G. Mittenhuber & M. Hecker, (1998) The *yvyD* gene of *Bacillus subtilis* is under dual control of sigmaB and sigmaH. *J Bacteriol* **180**: 6674-6680.

Dukan, S., A. Farewell, M. Ballesteros, F. Taddei, M. Radman & T. Nystrom, (2000) Protein oxidation in response to increased transcriptional or translational errors. *Proc Natl Acad Sci U S A* **97**: 5746-5749.

Dussurget, O., M. Rodriguez & I. Smith, (1996) An *ideR* mutant of *Mycobacterium smegmatis* has derepressed siderophore production and an altered oxidative-stress response. *Mol Microbiol* **22**: 535-544.

Dwyer, D. J., M. A. Kohanski & J. J. Collins, (2009) Role of reactive oxygen species in antibiotic action and resistance. *Current Opinion in Microbiology* **12**: 482-489.

Dye, C. & M. Borgdorff, (2008) Global Epidemiology and Control of Tuberculosis. In: Handbook of Tuberculosis: Clinics, Diagnostics, Therapy and Epidemiology. S. Kaufman & P. van Helden (eds). Weinheim: Wiley-VCH, pp. 1-21.

El-Sharoud, W. M., (2004) Ribosome inactivation for preservation: concepts and reservations. *Sci Prog* **87**: 137-152.

El-Sharoud, W. M. & G. W. Niven, (2005) The activity of ribosome modulation factor during growth of *Escherichia coli* under acidic conditions. *Arch Microbiol* **184**: 18-24.

El-Sharoud, W. M. & G. W. Niven, (2007) The influence of ribosome modulation factor on the survival of stationary-phase *Escherichia coli* during acid stress. *Microbiology* **153**: 247-253.

ESA, (2010) Guanine Adducts. In. Chelmsford, Massachusetts: ESA Inc, pp. 3.

Fenhalls, G., L. Stevens, L. Moses, J. Bezuidenhout, J. C. Betts, P. Helden Pv, P. T. Lukey & K. Duncan, (2002) *In situ* detection of *Mycobacterium tuberculosis* transcripts in human lung granulomas reveals differential gene expression in necrotic lesions. *Infect Immun* **70**: 6330-6338.

Filippini, P., E. Iona, G. Piccaro, P. Peyron, O. Neyrolles & L. Fattorini, (2010) Activity of drug combinations against dormant *Mycobacterium tuberculosis*. *Antimicrob Agents Chemother* **54**: 2712-2715.

Finn, R. D., J. Mistry, J. Tate, P. Coggill, A. Heger, J. E. Pollington, O. L. Gavin, P. Gunasekaran, G. Ceric, K. Forslund, L. Holm, E. L. Sonnhammer, S. R. Eddy & A. Bateman, (2010) The Pfam protein families database. *Nucleic Acids Res* **38**: D211-222.

Flores Valdez, M. A. & G. K. Schoolnik, (2010) DosR-regulon genes induction in *Mycobacterium bovis* BCG under aerobic conditions. *Tuberculosis (Edinb)* **90**: 197-200.

Floyd, R. A., (2009) Serendipitous findings while researching oxygen free radicals. *Free Radic Biol Med* **46**: 1004-1013.

Floyd, R. A., J. E. Schneider, Jr. & D. P. Dittmer, (2004) Methylene blue photoinactivation of RNA viruses. *Antiviral Res* **61**: 141-151.

Flynn, J. L. & J. Chan, (2001) Tuberculosis: latency and reactivation. *Infect Immun* **69**: 4195-4201.

Flynn, J. L., J. Chan, K. J. Triebold, D. K. Dalton, T. A. Stewart & B. R. Bloom, (1993) An essential role for interferon gamma in resistance to *Mycobacterium tuberculosis* infection. *J Exp Med* **178**: 2249-2254.

Ford, M. E., C. Stenstrom, R. W. Hendrix & G. F. Hatfull, (1998) Mycobacteriophage TM4: genome structure and gene expression. *Tuber Lung Dis* **79**: 63-73.

Fox, W., G. A. Ellard & D. A. Mitchison, (1999) Studies on the treatment of tuberculosis undertaken by the British Medical Research Council tuberculosis units, 1946-1986, with relevant subsequent publications. *Int J Tuberc Lung Dis* **3**: S231-279.

Fredriksson, A., M. Ballesteros, S. Dukan & T. Nystrom, (2005) Defense against protein carbonylation by DnaK/DnaJ and proteases of the heat shock regulon. *J Bacteriol* **187**: 4207-4213.

Fredriksson, A., M. Ballesteros, S. Dukan & T. Nystrom, (2006) Induction of the heat shock regulon in response to increased mistranslation requires oxidative modification of the malformed proteins. *Molecular Microbiology* **59**: 350-359.

Fredriksson, A., M. Ballesteros, C. N. Peterson, O. Persson, T. J. Silhavy & T. Nystrom, (2007) Decline in ribosomal fidelity contributes to the accumulation and stabilization of the master stress response regulator sigmaS upon carbon starvation. *Genes Dev* **21**: 862-874.

Frelon, S., T. Douki, J. L. Ravanat, J. P. Pouget, C. Tornabene & J. Cadet, (2000) High-performance liquid chromatography--tandem mass spectrometry measurement of radiation-induced base damage to isolated and cellular DNA. *Chem Res Toxicol* **13**: 1002-1010.

Friscia, G., H. M. Vordermeier, G. Pasvol, D. P. Harris, C. Moreno & J. Ivanyi, (1995) Human T cell responses to peptide epitopes of the 16-kD antigen in tuberculosis. *Clin Exp Immunol* **102**: 53-57.

Gandy, M., (2003) Life without Germs: Contested Episodes in the History of Tuberculosis. In: The Return of the White Plague: Global Poverty and the "New" Tuberculosis. M. Gandy & A. Zumla (eds). London: Verso, pp. 15-38.

Gandy, M. & A. Zumla, (2002) The resurgence of disease: social and historical perspectives on the 'new' tuberculosis. *Soc Sci Med* **55**: 385-396; discussion 397-401.

Garbe, T. R., N. S. Hibler & V. Deretic, (1996) Response of *Mycobacterium tuberculosis* to reactive oxygen and nitrogen intermediates. *Mol Med* **2**: 134-142.

Garbe, T. R., N. S. Hibler & V. Deretic, (1999) Response to reactive nitrogen intermediates in Mycobacterium tuberculosis: induction of the 16-kilodalton alpha-crystallin homolog by exposure to nitric oxide donors. *Infect Immun* **67**: 460-465.

Garton, N. J., H. Christensen, D. E. Minnikin, R. A. Adegbola & M. R. Barer, (2002) Intracellular lipophilic inclusions of mycobacteria *in vitro* and in sputum. *Microbiology* **148**: 2951-2958.

Garton, N. J., S. J. Waddell, A. L. Sherratt, S. M. Lee, R. J. Smith, C. Senner, J. Hinds, K. Rajakumar, R. A. Adegbola, G. S. Besra, P. D. Butcher & M. R. Barer, (2008) Cytological and transcript analyses reveal fat and lazy persister-like bacilli in tuberculous sputum. *PLoS Med* **5**: e75.

Garvin, R. T., G. R. Julian & S. J. Rogers, (1969) Dye-sensitized photooxidation of the *Escherichia coli* ribosome. *Science* **164**: 583-584.

Gengenbacher, M., S. P. Rao, K. Pethe & T. Dick, (2010) Nutrient-starved, non-replicating *Mycobacterium tuberculosis* requires respiration, ATP synthase and isocitrate lyase for maintenance of ATP homeostasis and viability. *Microbiology* **156**: 81-87.

Gerdes, K., S. K. Christensen & A. Lobner-Olesen, (2005) Prokaryotic toxin-antitoxin stress response loci. *Nat Rev Microbiol* **3**: 371-382.

Ghosh, J., P. Larsson, B. Singh, B. M. Pettersson, N. M. Islam, S. N. Sarkar, S. Dasgupta & L. A. Kirsebom, (2009) Sporulation in mycobacteria. *Proc Natl Acad Sci U S A* **106**: 10781-10786.

Girardi, E., M. C. Raviglione, G. Antonucci, P. Godfrey-Faussett & G. Ippolito, (2000) Impact of the HIV epidemic on the spread of other diseases: the case of tuberculosis. *AIDS* **14 Suppl 3**: S47-56.

Glisin, V., R. Crkvenjakov & C. Byus, (1974) Ribonucleic acid isolated by cesium chloride centrifugation. *Biochemistry Easton* **13**: 2633-2637.

Gomez, J. E. & J. D. McKinney, (2004) *M. tuberculosis* persistence, latency, and drug tolerance. *Tuberculosis (Edinb)* **84**: 29-44.

Gong, X., R. Tao & Z. Li, (2006) Quantification of RNA damage by reverse transcription polymerase chain reactions. *Anal Biochem* **357**: 58-67.

Gourse, R. L., T. Gaal, M. S. Bartlett, J. A. Appleman & W. Ross, (1996) rRNA transcription and growth rate-dependent regulation of ribosome synthesis in *Escherichia coli*. *Annu Rev Microbiol* **50**: 645-677.

Goyal, R. N., N. Jain & D. K. Garg, (1997) Electrochemical and enzymic oxidation of guanosine and 8-hydroxyguanosine and the effects of oxidation products in mice. *Bioelectrochemistry and Bioenergetics* **43**: 105-114.

Gupta, A., S. Bhakta, S. Kundu, M. Gupta, B. S. Srivastava & R. Srivastava, (2009) Fast-growing, non-infectious and intracellularly surviving drug-resistant *Mycobacterium aurum*: a model for high-throughput antituberculosis drug screening. *J Antimicrob Chemother* **64**: 774-781.

Gupta, S. & D. Chatterji, (2005) Stress responses in mycobacteria. *IUBMB Life* **57**: 149-159.

Gustavsson, N., A. Diez & T. Nystrom, (2002) The universal stress protein paralogues of *Escherichia coli* are co-ordinately regulated and co-operate in the defence against DNA damage. *Molecular Microbiology* **43**: 107-117.

Gutierrez, M. C., S. Brisse, R. Brosch, M. Fabre, B. Omais, M. Marmiesse, P. Supply & V. Vincent, (2005) Ancient origin and gene mosaicism of the progenitor of *Mycobacterium tuberculosis*. *PLoS Pathog* **1**: e5.

Hager, J. W., (2004) Q TRAP(TM) mass spectrometer technology for proteomics applications. *Drug Discovery Today: TARGETS* **3**: 31-36.

Halliwell, B. & J. M. C. Gutteridge, (2007) *Free Radicals in Biology and Medicine,* p. 851. Oxford University Press, Oxford.

Hampshire, T., S. Soneji, J. Bacon, B. W. James, J. Hinds, K. Laing, R. A. Stabler, P. D. Marsh & P. D. Butcher, (2004) Stationary phase gene expression of *Mycobacterium tuberculosis* following a progressive nutrient depletion: a model for persistent organisms? *Tuberculosis (Edinb)* **84**: 228-238.

Hayakawa, H., M. Kuwano & M. Sekiguchi, (2001) Specific binding of 8-oxoguanine-containing RNA to polynucleotide phosphorylase protein. *Biochemistry* **40**: 9977-9982.

Heifets, L., J. Simon & V. Pham, (2005) Capreomycin is active against non-replicating *M. tuberculosis*. *Annals of Clinical Microbiology and Antimicrobials* **4**: 6.

Hinchey, J., S. Lee, B. Y. Jeon, R. J. Basaraba, M. M. Venkataswamy, B. Chen, J. Chan, M. Braunstein, I. M. Orme, S. C. Derrick, S. L. Morris, W. R. Jacobs, Jr. & S. A. Porcelli, (2007) Enhanced priming of adaptive immunity by a proapoptotic mutant of *Mycobacterium tuberculosis*. *J Clin Invest* **117**: 2279-2288.

Hingley-Wilson, S. M., K. E. Lougheed, K. Ferguson, S. Leiva & H. D. Williams, (2010) Individual *Mycobacterium tuberculosis* universal stress protein homologues are dispensable *in vitro*. *Tuberculosis (Edinb)*.

Hofer, T., C. Badouard, E. Bajak, J. L. Ravanat, A. Mattsson & I. A. Cotgreave, (2005) Hydrogen peroxide causes greater oxidation in cellular RNA than in DNA. *Biol Chem* **386**: 333-337.

Hofer, T., E. Marzetti, J. Xu, A. Y. Seo, S. Gulec, M. D. Knutson, C. Leeuwenburgh & E. E. Dupont-Versteegden, (2008) Increased iron content and RNA oxidative damage in skeletal muscle with aging and disuse atrophy. *Exp Gerontol* **43**: 563-570.

Hofer, T., A. Y. Seo, M. Prudencio & C. Leeuwenburgh, (2006) A method to determine RNA and DNA oxidation simultaneously by HPLC-ECD: greater RNA than DNA oxidation in rat liver after doxorubicin administration. *Biol Chem* **387**: 103-111.

Honaker, R. W., R. L. Leistikow, I. L. Bartek & M. I. Voskuil, (2009) Unique roles of DosT and DosS in DosR regulon induction and *Mycobacterium tuberculosis* dormancy. *Infect Immun* **77**: 3258-3263.

Honda, K., M. A. Smith, X. Zhu, D. Baus, W. C. Merrick, A. M. Tartakoff, T. Hattier, P. L. Harris, S. L. Siedlak, H. Fujioka, Q. Liu, P. I. Moreira, F. P. Miller, A. Nunomura, S. Shimohama & G. Perry, (2005) Ribosomal RNA in Alzheimer disease is oxidized by bound redox-active iron. *J Biol Chem* **280**: 20978-20986.

Hopewell, P., (2008) Clinical Features of Tuberculosis. In: Handbook of Tuberculosis: Clinics, Diagnostics, Therapy and Epidemiology. S. Kaufman & P. van Helden (eds). Weinheim: Wiley-VCH, pp. 89-114.

Hu, Y., J. A. Mangan, J. Dhillon, K. M. Sole, D. A. Mitchison, P. D. Butcher & A. R. Coates, (2000) Detection of mRNA transcripts and active transcription in persistent *Mycobacterium tuberculosis* induced by exposure to rifampin or pyrazinamide. *J Bacteriol* **182**: 6358-6365.

Hu, Y. M., P. D. Butcher, K. Sole, D. A. Mitchison & A. R. M. Coates, (1998) Protein synthesis is shutdown in dormant *Mycobacterium tuberculosis* and is reversed by oxygen or heat shock. *FEMS Microbiology Letters* **158**: 139-145.

Imlay, J. A., (2008) Cellular Defenses against Superoxide and Hydrogen Peroxide. *Annual Review of Biochemistry* **77**: 755-776.

Imlay, J. A. & S. Linn, (1987) Mutagenesis and stress responses induced in *Escherichia coli* by hydrogen peroxide. *J Bacteriol* **169**: 2967-2976.

Ioanoviciu, A., E. T. Yukl, P. Moenne-Loccoz & P. R. de Montellano, (2007) DevS, a heme-containing two-component oxygen sensor of *Mycobacterium tuberculosis*. *Biochemistry* **46**: 4250-4260.

Iona, E., F. Giannoni, M. Pardini, L. Brunori, G. Orefici & L. Fattorini, (2007) Metronidazole plus rifampin sterilizes long-term dormant *Mycobacterium tuberculosis*. *Antimicrob Agents Chemother* **51**: 1537-1540.

Iost, I., J. Charollais, J. Vinh & D. Pflieger, (2008) Characterization of *E. coli* ribosomal particles : combined analysis of whole proteins by mass spectrometry and of proteolytic digests by liquid chromatography-tandem mass spectrometry. *Methods Mol Biol* **432**: 321-341.

Ito, R., H. Hayakawa, M. Sekiguchi & T. Ishibashi, (2005) Multiple enzyme activities of *Escherichia coli* MutT protein for sanitization of DNA and RNA precursor pools. *Biochemistry* **44**: 6670-6674.

Jain, R., P. Kumar & U. Varshney, (2007) A distinct role of formamidopyrimidine DNA glycosylase (MutM) in down-regulation of accumulation of G, C mutations and protection against oxidative stress in mycobacteria. *DNA Repair (Amst)* **6**: 1774-1785.

Jelenc, P. C., (1980) Rapid purification of highly active ribosomes from *Escherichia coli*. *Anal Biochem* **105**: 369-374.

Jindani, A., V. R. Aber, E. A. Edwards & D. A. Mitchison, (1980) The early bactericidal activity of drugs in patients with pulmonary tuberculosis. *Am Rev Respir Dis* **121**: 939-949.

Johnson, N. A., R. McKenzie, L. McLean, L. C. Sowers & H. M. Fletcher, (2004) 8-Oxo-7,8-Dihydroguanine Is Removed by a Nucleotide Excision Repair-Like Mechanism in *Porphyromonas gingivalis* W83. *J. Bacteriol.* **186**: 7697-7703.

Kana, B. D., B. G. Gordhan, K. J. Downing, N. Sung, G. Vostroktunova, E. E. Machowski, L. Tsenova, M. Young, A. Kaprelyants, G. Kaplan & V. Mizrahi, (2008) The resuscitation-promoting factors of *Mycobacterium tuberculosis* are required for virulence and resuscitation from dormancy but are collectively dispensable for growth in vitro. *Mol Microbiol* **67**: 672-684.

Kana, B. D., E. E. Machowski, N. Schechter, J.-S. Teh, H. Rubin & V. Mizrahi, (2009) Electron Transport and Respiration in Mycobacteria. In: Mycobacterium: Genomics and Molecular Biology. T. Parish & A. C. Brown (eds). Norfolk, UK: Caister Academic Press, pp. 35-64.

Kanehisa, M., S. Goto, M. Hattori, K. F. Aoki-Kinoshita, M. Itoh, S. Kawashima, T. Katayama, M. Araki & M. Hirakawa, (2006) From genomics to chemical genomics: new developments in KEGG. *Nucleic Acids Res* **34**: D354-357.

Kaplan, R. & D. Apirion, (1975) Decay of ribosomal ribonucleic acid in *Escherichia coli* cells starved for various nutrients. *J Biol Chem* **250**: 3174-3178.

Kaplan, R. & D. Apirion, (1975) The fate of ribosomes in *Escherichia coli* cells starved for a carbon source. *J Biol Chem* **250**: 1854-1863.

Kashino, S. S., D. R. Napolitano, Z. Skobe & A. Campos-Neto, (2008) Guinea pig model of *Mycobacterium tuberculosis* latent/dormant infection. *Microbes Infect* **10**: 1469-1476.

Kato, N., K. Okabayashi & D. Mizuno, (1970) The degradation of ribosomal RNA in *E. coli* by mitomycin C and AF-5, preferential inhibitors of DNA synthesis. *J Biochem (Tokyo)* **67**: 175-184.

Kato, T., H. Yoshida, T. Miyata, Y. Maki, A. Wada & K. Namba, (2010) Structure of the 100S ribosome in the hibernation stage revealed by electron cryomicroscopy. *Structure* **18**: 719-724.

Kaufmann, B. B., J. Gomez & D. T. Hung, (2010) Assesment of Adaptive Hypermutation in Drug-Treated *Mycobacterium smegmatis* Reveals a New Mechanism for Multi-Drug Resistance. In: 16th Annual Boston Bacterial Meeting. Cambridge, MA, USA: Boston Bacterial Meeting, pp. 14.

Keane, J., S. Gershon, R. P. Wise, E. Mirabile-Levens, J. Kasznica, W. D. Schwieterman, J. N. Siegel & M. M. Braun, (2001) Tuberculosis associated with infliximab, a tumor necrosis factor alpha-neutralizing agent. *N Engl J Med* **345**: 1098-1104.

Keren, I., D. Shah, A. Spoering, N. Kaldalu & K. Lewis, (2004) Specialized persister cells and the mechanism of multidrug tolerance in *Escherichia coli*. *J Bacteriol* **186**: 8172-8180.

Kesavan, A. K., M. Brooks, J. Tufariello, J. Chan & Y. C. Manabe, (2009) Tuberculosis genes expressed during persistence and reactivation in the resistant rabbit model. *Tuberculosis (Edinb)* **89**: 17-21.

Kim, M. J., H. C. Wainwright, M. Locketz, L. G. Bekker, G. B. Walther, C. Dittrich, A. Visser, W. Wang, F. F. Hsu, U. Wiehart, L. Tsenova, G. Kaplan & D. G. Russell, (2010) Caseation of human tuberculosis granulomas correlates with elevated host lipid metabolism. *EMBO Mol Med* **2**: 258-274.

Kohanski, M. A., M. A. DePristo & J. J. Collins, (2010) Sublethal Antibiotic Treatment Leads to Multidrug Resistance via Radical-Induced Mutagenesis. *Molecular Cell* **37**: 311-320.

Kohanski, M. A., D. J. Dwyer, B. Hayete, C. A. Lawrence & J. J. Collins, (2007) A common mechanism of cellular death induced by bactericidal antibiotics. *Cell* **130**: 797-810.

Kohanski, M. A., D. J. Dwyer, J. Wierzbowski, G. Cottarel & J. J. Collins, (2008) Mistranslation of Membrane Proteins and Two-Component System Activation Trigger Antibiotic-Mediated Cell Death. *Cell* **135**: 679-690.

Kong, Q., X. Shan, Y. Chang, H. Tashiro & C. L. Lin, (2008) RNA oxidation: a contributing factor or an epiphenomenon in the process of neurodegeneration. *Free Radic Res* **42**: 773-777.

Krab, I. M. & A. Parmeggiani, (1998) EF-Tu, a GTPase odyssey. *Biochim Biophys Acta* **1443**: 1-22.

Kramberger, P., M. Peterka, J. Boben, M. Ravnikar & A. Strancar, (2007) Short monolithic columns-a breakthrough in purification and fast quantification of tomato mosaic virus. *J Chromatogr A* **1144**: 143-149.

Kumar, A., J. S. Deshane, D. K. Crossman, S. Bolisetty, B. S. Yan, I. Kramnik, A. Agarwal & A. J. Steyn, (2008) Heme oxygenase-1-derived carbon monoxide induces the *Mycobacterium tuberculosis* dormancy regulon. *J Biol Chem* **283**: 18032-18039.

Kumar, A., J. C. Toledo, R. P. Patel, J. R. Lancaster, Jr. & A. J. Steyn, (2007) *Mycobacterium tuberculosis* DosS is a redox sensor and DosT is a hypoxia sensor. *Proc Natl Acad Sci U S A* **104**: 11568-11573.

Kurland, C. G. & R. Mikkola, (1993) The Impact of Nutritional State on the Microevolution of Ribosomes. In: Starvation in Bacteria. S. Kjelleberg (ed). New York: Plenum press, pp. 225-238.

Kurthkoti, K., P. Kumar, R. Jain & U. Varshney, (2008) Important role of the nucleotide excision repair pathway in *Mycobacterium smegmatis* in conferring protection against commonly encountered DNA-damaging agents. *Microbiology* **154**: 2776-2785.

Larsen, M. H., K. Biermann, B. Chen, T. Hsu, V. K. Sambandamurthy, A. A. Lackner, P. P. Aye, P. Didier, D. Huang, L. Shao, H. Wei, N. L. Letvin, R. Frothingham, B. F. Haynes, Z. W. Chen & W. R. Jacobs, Jr., (2009) Efficacy and safety of live attenuated persistent and rapidly cleared *Mycobacterium tuberculosis* vaccine candidates in non-human primates. *Vaccine* **27**: 4709-4717.

Le Goffic, F., B. Baca & N. Moreau, (1974) A new rapid and powerful technique to obtain purified ribosomes. *FEBS Lett* **41**: 69-72.

Leistikow, R. L., R. A. Morton, I. L. Bartek, I. Frimpong, K. Wagner & M. I. Voskuil, (2010) The *Mycobacterium tuberculosis* DosR regulon assists in metabolic homeostasis and enables rapid recovery from nonrespiring dormancy. *J Bacteriol* **192**: 1662-1670.

Lewis, K., (2007) Persister cells, dormancy and infectious disease. *Nat Rev Microbiol* **5**: 48-56.

Lewis, K., (2010) Persister cells. *Annu Rev Microbiol* **64**: 357-372.

Li, Z., C. Kelley, F. Collins, D. Rouse & S. Morris, (1998) Expression of *katG* in *Mycobacterium tuberculosis* is associated with its growth and persistence in mice and guinea pigs. *J Infect Dis* **177**: 1030-1035.

Lillebaek, T., A. Dirksen, E. Vynnycky, I. Baess, V. O. Thomsen & A. B. Andersen, (2003) Stability of DNA patterns and evidence of *Mycobacterium tuberculosis* reactivation occurring decades after the initial infection. *J Infect Dis* **188**: 1032-1039.

Lin, P. L. & J. L. Flynn, (2010) Understanding Latent Tuberculosis: A Moving Target. *J Immunol* **185**: 15-22.

Lin, P. L., M. Rodgers, L. Smith, M. Bigbee, A. Myers, C. Bigbee, I. Chiosea, S. V. Capuano, C. Fuhrman, E. Klein & J. L. Flynn, (2009) Quantitative comparison of active and latent tuberculosis in the cynomolgus macaque model. *Infect Immun* **77**: 4631-4642.

Ling, J. & D. Soll, (2010) Severe oxidative stress induces protein mistranslation through impairment of an aminoacyl-tRNA synthetase editing site. *Proc Natl Acad Sci U S A* **107**: 4028-4033.

Loh, K. D., P. Gyaneshwar, E. Markenscoff Papadimitriou, R. Fong, K. S. Kim, R. Parales, Z. Zhou, W. Inwood & S. Kustu, (2006) A previously undescribed pathway for pyrimidine catabolism. *Proc Natl Acad Sci U S A* **103**: 5114-5119.

Low, K. L., P. S. Rao, G. Shui, A. K. Bendt, K. Pethe, T. Dick & M. R. Wenk, (2009) Triacylglycerol utilization is required for regrowth of in vitro hypoxic nonreplicating *Mycobacterium bovis* bacillus Calmette-Guerin. *J Bacteriol* **191**: 5037-5043.

Magnusson, L. U., A. Farewell & T. Nystrom, (2005) ppGpp: a global regulator in *Escherichia coli*. *Trends Microbiol* **13**: 236-242.

Maguire, B. A., L. M. Wondrack, L. G. Contillo & Z. Xu, (2008) A novel chromatography system to isolate active ribosomes from pathogenic bacteria. *RNA* **14**: 188-195.

Maki, Y., H. Yoshida & A. Wada, (2000) Two proteins, YfiA and YhbH, associated with resting ribosomes in stationary phase *Escherichia coli*. *Genes Cells* **5**: 965-974.

Manabe, Y. C., A. K. Kesavan, J. Lopez-Molina, C. L. Hatem, M. Brooks, R. Fujiwara, K. Hochstein, M. L. Pitt, J. Tufariello, J. Chan, D. N. McMurray, W. R. Bishai, A. M. Dannenberg, Jr. & S. Mendez, (2008) The aerosol rabbit model of TB latency, reactivation and immune reconstitution inflammatory syndrome. *Tuberculosis (Edinb)* **88**: 187-196.

Matteelli, A., A. C. Carvalho, K. E. Dooley & A. Kritski, (2010) TMC207: the first compound of a new class of potent anti-tuberculosis drugs. *Future Microbiol* **5**: 849-858.

McCune, R. M., F. M. Feldmann, H. P. Lambert & W. McDermott, (1966) Microbial persistence. I. The capacity of tubercle bacilli to survive sterilization in mouse tissues. *J Exp Med* **123**: 445-468.

McCune, R. M., F. M. Feldmann & W. McDermott, (1966) Microbial persistence. II. Characteristics of the sterile state of tubercle bacilli. *J Exp Med* **123**: 469-486.

McKinney, J. D., K. Honer zu Bentrup, E. J. Munoz-Elias, A. Miczak, B. Chen, W. T. Chan, D. Swenson, J. C. Sacchettini, W. R. Jacobs, Jr. & D. G. Russell, (2000) Persistence of *Mycobacterium tuberculosis* in macrophages and mice requires the glyoxylate shunt enzyme isocitrate lyase. *Nature* **406**: 735-738.

Miller, J. L., K. Velmurugan, M. J. Cowan & V. Briken, (2010) The type I NADH dehydrogenase of *Mycobacterium tuberculosis* counters phagosomal NOX2 activity to inhibit TNF-alpha-mediated host cell apoptosis. *PLoS Pathog* **6**: e1000864.

Mishra, S., (2009) Function prediction of Rv0079, a hypothetical *Mycobacterium tuberculosis* DosR regulon protein. *J Biomol Struct Dyn* **27**: 283-292.

Mitchison, D. A., (1965) Chemotherapy of Tuberculosis: a Bacteriologist's viewpoint. *British Medical Journal* **1**: 1331-1338.

Mitchison, D. A., (1979) Basic mechanisms of chemotherapy. *Chest* **76**: 771-781.

Mitchison, D. A., (1992) The Garrod Lecture. Understanding the chemotherapy of tuberculosis - current problems. *J Antimicrob Chemother* **29**: 477-493.

Moreira, P. I., A. Nunomura, M. Nakamura, A. Takeda, J. C. Shenk, G. Aliev, M. A. Smith & G. Perry, (2008) Nucleic acid oxidation in Alzheimer disease. *Free Radic Biol Med* **44**: 1493-1505.

Morita, R. Y., (1993) Bioavailability of Energy and the Starvation State. In: Starvation in Bacteria. S. Kjelleberg (ed). New York: Plenum press, pp. 1-24.

MRC, (1948) Streptomycin treatment of pulmonary tuberculosis. *Br Med J* **2**: 769-782.

Munoz-Elias, E. J. & J. D. McKinney, (2005) *Mycobacterium tuberculosis* isocitrate lyases 1 and 2 are jointly required for in vivo growth and virulence. *Nat Med* **11**: 638-644.

Murry, J. P., C. M. Sassetti, J. M. Lane, Z. Xie & E. J. Rubin, (2008) Transposon site hybridization in Mycobacterium tuberculosis. *Methods Mol Biol* **416**: 45-59.

Nachin, L., U. Nannmark & T. Nystrom, (2005) Differential roles of the universal stress proteins of *Escherichia coli* in oxidative stress resistance, adhesion, and motility. *J Bacteriol* **187**: 6265-6272.

Nanamiya, H., G. Akanuma, Y. Natori, R. Murayama, S. Kosono, T. Kudo, K. Kobayashi, N. Ogasawara, S. M. Park, K. Ochi & F. Kawamura, (2004) Zinc is a key factor in controlling alternation of two types of L31 protein in the *Bacillus subtilis* ribosome. *Mol Microbiol* **52**: 273-283.

Newton, G. L., N. Buchmeier & R. C. Fahey, (2008) Biosynthesis and functions of mycothiol, the unique protective thiol of Actinobacteria. *Microbiol Mol Biol Rev* **72**: 471-494.

Ng, V. H., J. S. Cox, A. O. Sousa, J. D. MacMicking & J. D. McKinney, (2004) Role of KatG catalase-peroxidase in mycobacterial pathogenesis: countering the phagocyte oxidative burst. *Mol Microbiol* **52**: 1291-1302.

Niven, G. W., (2004) Ribosome modulation factor protects *Escherichia coli* during heat stress, but this may not be dependent on ribosome dimerisation. *Arch Microbiol* **182**: 60-66.

Nomura, M., R. Gourse & G. Baughman, (1984) Regulation of the synthesis of ribosomes and ribosomal components. *Annu Rev Biochem* **53**: 75-117.

North, R. J. & Y. J. Jung, (2004) Immunity to tuberculosis. *Annu Rev Immunol* **22**: 599-623.

Nyka, W., (1971) Influence of oxidation and reduction on the acid-fastness of mycobacteria. *Infect Immun* **4**: 513-515.

Nyka, W., (1974) Studies on the effect of starvation on mycobacteria. *Infect Immun* **9**: 843-850.

Nystrom, T. & F. C. Neidhardt, (1992) Cloning, mapping and nucleotide sequencing of a gene encoding a universal stress protein in *Escherichia coli*. *Mol Microbiol* **6**: 3187-3198.

Nystrom, T. & F. C. Neidhardt, (1994) Expression and role of the universal stress protein, UspA, of *Escherichia coli* during growth arrest. *Mol Microbiol* **11**: 537-544.

O'Toole, R., M. J. Smeulders, M. C. Blokpoel, E. J. Kay, K. Lougheed & H. D. Williams, (2003) A two-component regulator of universal stress protein expression and adaptation to oxygen starvation in *Mycobacterium smegmatis*. *J Bacteriol* **185**: 1543-1554.

O'Toole, R. & H. D. Williams, (2003) Universal stress proteins and *Mycobacterium tuberculosis*. *Res Microbiol* **154**: 387-392.

Ohara, N., M. Naito, C. Miyazaki, S. Matsumoto, Y. Tabira & T. Yamada, (1997) HrpA, a new ribosome-associated protein which appears in heat-stressed *Mycobacterium bovis* bacillus Calmette-Guerin. *J Bacteriol* **179**: 6495-6498.

Oliver, J. D., (1993) Formation of Viable but Nonculturable Cells. In: Starvation in Bacteria. S. Kjelleberg (ed). New York: Plenum press, pp. 239-272.

Ostling, J., L. Holmquist, K. Flardh, B. Svenblad, A. Jouper-Jaan & S. Kjelleberg, (1993) Starvation and Recovery of Vibrio. In: Starvation in Bacteria. S. Kjelleberg (ed). New York: Plenum press, pp. 103-128.

Palma, M., J. Zurita, J. A. Ferreras, S. Worgall, D. H. Larone, L. Shi, F. Campagne & L. E. Quadri, (2005) *Pseudomonas aeruginosa* SoxR does not conform to the archetypal paradigm for SoxR-dependent regulation of the bacterial oxidative stress adaptive response. *Infect Immun* **73**: 2958-2966.

Pandey, A. K. & C. M. Sassetti, (2008) Mycobacterial persistence requires the utilization of host cholesterol. *Proc Natl Acad Sci U S A* **105**: 4376-4380.

Paramasivan, C. N., S. Sulochana, G. Kubendiran, P. Venkatesan & D. A. Mitchison, (2005) Bactericidal action of gatifloxacin, rifampin, and isoniazid on logarithmic- and stationary-phase cultures of Mycobacterium tuberculosis. *Antimicrob Agents Chemother* **49**: 627-631.

Park, H. D., K. M. Guinn, M. I. Harrell, R. Liao, M. I. Voskuil, M. Tompa, G. K. Schoolnik & D. R. Sherman, (2003) *Rv3133c/dosR* is a transcription factor that mediates the hypoxic response of *Mycobacterium tuberculosis*. *Mol Microbiol* **48**: 833-843.

Piddington, D. L., F. C. Fang, T. Laessig, A. M. Cooper, I. M. Orme & N. A. Buchmeier, (2001) Cu,Zn superoxide dismutase of *Mycobacterium tuberculosis* contributes to survival in activated macrophages that are generating an oxidative burst. *Infect Immun* **69**: 4980-4987.

Potrykus, K. & M. Cashel, (2008) (p)ppGpp: still magical? *Annu Rev Microbiol* **62**: 35-51.

Primm, T. P., S. J. Andersen, V. Mizrahi, D. Avarbock, H. Rubin & C. E. Barry, 3rd, (2000) The stringent response of *Mycobacterium tuberculosis* is required for long-term survival. *J Bacteriol* **182**: 4889-4898.

Pym, A. S., P. Domenech, N. Honore, J. Song, V. Deretic & S. T. Cole, (2001) Regulation of catalase-peroxidase (KatG) expression, isoniazid sensitivity and virulence by *furA* of *Mycobacterium tuberculosis*. *Mol Microbiol* **40**: 879-889.

Ramage, H. R., L. E. Connolly & J. S. Cox, (2009) Comprehensive functional analysis of *Mycobacterium tuberculosis* toxin-antitoxin systems: implications for pathogenesis, stress responses, and evolution. *PLoS Genet* **5**: e1000767.

Rao, S. P., S. Alonso, L. Rand, T. Dick & K. Pethe, (2008) The protonmotive force is required for maintaining ATP homeostasis and viability of hypoxic, nonreplicating *Mycobacterium tuberculosis*. *Proc Natl Acad Sci U S A* **105**: 11945-11950.

Ray, J. C., J. L. Flynn & D. E. Kirschner, (2009) Synergy between individual TNF-dependent functions determines granuloma performance for controlling *Mycobacterium tuberculosis* infection. *J Immunol* **182**: 3706-3717.

Reddy, T. B., R. Riley, F. Wymore, P. Montgomery, D. DeCaprio, R. Engels, M. Gellesch, J. Hubble, D. Jen, H. Jin, M. Koehrsen, L. Larson, M. Mao, M. Nitzberg, P. Sisk, C. Stolte, B. Weiner, J. White, Z. K. Zachariah, G. Sherlock, J. E. Galagan, C. A. Ball & G. K. Schoolnik, (2009) TB database: an integrated platform for tuberculosis research. *Nucleic Acids Res* **37**: D499-508.

Reed, M. B., S. Gagneux, K. Deriemer, P. M. Small & C. E. Barry, 3rd, (2007) The W-Beijing lineage of *Mycobacterium tuberculosis* overproduces triglycerides and has the DosR dormancy regulon constitutively up-regulated. *J Bacteriol* **189**: 2583-2589.

Rengarajan, J., B. R. Bloom & E. J. Rubin, (2005) Genome-wide requirements for *Mycobacterium tuberculosis* adaptation and survival in macrophages. *Proc Natl Acad Sci U S A* **102**: 8327-8332.

Reyrat, J. M. & D. Kahn, (2001) *Mycobacterium smegmatis*: an absurd model for tuberculosis? *Trends Microbiol* **9**: 472-474.

Rezwan, M., M. A. Laneelle, P. Sander & M. Daffe, (2007) Breaking down the wall: fractionation of mycobacteria. *J Microbiol Methods* **68**: 32-39.

Rhee, K. Y., H. Erdjument-Bromage, P. Tempst & C. F. Nathan, (2005) S-nitroso proteome of *Mycobacterium tuberculosis*: Enzymes of intermediary metabolism and antioxidant defense. *Proc Natl Acad Sci U S A* **102**: 467-472.

Rifat, D., W. R. Bishai & P. C. Karakousis, (2009) Phosphate depletion: a novel trigger for *Mycobacterium tuberculosis* persistence. *J Infect Dis* **200**: 1126-1135.

Risinger, C., A. G. Blomqvist, I. Lundell, A. Lambertsson, D. Nassel, V. A. Pieribone, L. Brodin & D. Larhammar, (1993) Evolutionary conservation of synaptosome-associated protein 25 kDa (SNAP-25) shown by Drosophila and Torpedo cDNA clones. *J Biol Chem* **268**: 24408-24414.

Roberts, D. M., R. P. Liao, G. Wisedchaisri, W. G. Hol & D. R. Sherman, (2004) Two sensor kinases contribute to the hypoxic response of *Mycobacterium tuberculosis*. *J Biol Chem* **279**: 23082-23087.

Rodriguez, G. M. & I. Smith, (2003) Mechanisms of iron regulation in mycobacteria: role in physiology and virulence. *Mol Microbiol* **47**: 1485-1494.

Russell, D. G., (2007) Who puts the tubercle in tuberculosis? *Nat Rev Microbiol* **5**: 39-47.

Russell, D. G., C. E. Barry, 3rd & J. L. Flynn, (2010) Tuberculosis: what we don't know can, and does, hurt us. *Science* **328**: 852-856.

Russell, D. G., B. C. VanderVen, S. Glennie, H. Mwandumba & R. S. Heyderman, (2009) The macrophage marches on its phagosome: dynamic assays of phagosome function. *Nat Rev Immunol* **9**: 594-600.

Russell, D. G., B. C. VanderVen, W. Lee, R. B. Abramovitch, M. J. Kim, S. Homolka, S. Niemann & K. H. Rohde, (2010) *Mycobacterium tuberculosis* wears what it eats. *Cell Host Microbe* **8**: 68-76.

Rustad, T. R., M. I. Harrell, R. Liao & D. R. Sherman, (2008) The enduring hypoxic response of *Mycobacterium tuberculosis*. *PLoS ONE* **3**: e1502.

Rustad, T. R., A. M. Sherrid, K. J. Minch & D. R. Sherman, (2009) Hypoxia: a window into *Mycobacterium tuberculosis* latency. *Cell Microbiol* **11**: 1151-1159.

Salina, E. G., Y. A. Zhogina, M. O. Shleeva, G. M. Sorokoumova, A. A. Selishcheva & A. S. Kaprelyants, (2010) Biochemical and morphological changes in dormant ("Nonculturable") *Mycobacterium smegmatis* cells. *Biochemistry (Mosc)* **75**: 72-80.

Sambrook, J. & D. Russel, (2001) *Molecular cloning - A laboratory manual*. Cold Spring Harbour Laboratory Press, Cold Spring Harbour, New York.

Sassetti, C. M., D. H. Boyd & E. J. Rubin, (2001) Comprehensive identification of conditionally essential genes in mycobacteria. *Proc Natl Acad Sci U S A* **98**: 12712-12717.

Sassetti, C. M. & E. J. Rubin, (2003) Genetic requirements for mycobacterial survival during infection. *Proc Natl Acad Sci U S A* **100**: 12989-12994.

Sassetti, M. C., H. D. Boyd & J. E. Rubin, (2003) Genes required for mycobacterial growth defined by high density mutagenesis. *Molecular Microbiology* **48**: 77-84.

Sato, A., G. Kobayashi, H. Hayashi, H. Yoshida, A. Wada, M. Maeda, S. Hiraga, K. Takeyasu & C. Wada, (2005) The GTP binding protein Obg homolog ObgE is involved in ribosome maturation. *Genes Cells* **10**: 393-408.

Scanga, C. A., V. P. Mohan, H. Joseph, K. Yu, J. Chan & J. L. Flynn, (1999) Reactivation of latent tuberculosis: variations on the Cornell murine model. *Infect Immun* **67**: 4531-4538.

Schluger, N., (2008) Chemotherapy of Tuberculosis. In: Handbook of Tuberculosis: Clinics, Diagnostics, Therapy and Epidemiology. S. Kaufman & P. van Helden (eds). Weinheim: Wiley-VCH, pp. 131-142.

Schmeing, T. M. & V. Ramakrishnan, (2009) What recent ribosome structures have revealed about the mechanism of translation. *Nature* **461**: 1234-1242.

Schnappinger, D., S. Ehrt, M. I. Voskuil, Y. Liu, J. A. Mangan, I. M. Monahan, G. Dolganov, B. Efron, P. D. Butcher, C. Nathan & G. K. Schoolnik, (2003) Transcriptional Adaptation of *Mycobacterium tuberculosis* within Macrophages: Insights into the Phagosomal Environment. *J Exp Med* **198**: 693-704.

Schneider, J. E., S. Price, L. Maidt, J. M. Gutteridge & R. A. Floyd, (1990) Methylene blue plus light mediates 8-hydroxy 2'-deoxyguanosine formation in DNA preferentially over strand breakage. *Nucleic Acids Res* **18**: 631-635.

Selmer, M., C. M. Dunham, F. V. t. Murphy, A. Weixlbaumer, S. Petry, A. C. Kelley, J. R. Weir & V. Ramakrishnan, (2006) Structure of the 70S ribosome complexed with mRNA and tRNA. *Science* **313**: 1935-1942.

Seo, A. Y., J. Xu, S. Servais, T. Hofer, E. Marzetti, S. E. Wohlgemuth, M. D. Knutson, H. Y. Chung & C. Leeuwenburgh, (2008) Mitochondrial iron accumulation with age and functional consequences. *Aging Cell* **7**: 706-716.

Shan, X., Y. Chang & C. L. Lin, (2007) Messenger RNA oxidation is an early event preceding cell death and causes reduced protein expression. *FASEB J* **21**: 2753-2764.

Shan, X., H. Tashiro & C. L. Lin, (2003) The identification and characterization of oxidized RNAs in Alzheimer's disease. *J Neurosci* **23**: 4913-4921.

Sherman, D. R., P. J. Sabo, M. J. Hickey, T. M. Arain, G. G. Mahairas, Y. Yuan, C. E. Barry, 3rd & C. K. Stover, (1995) Disparate responses to oxidative stress in saprophytic and pathogenic mycobacteria. *Proc Natl Acad Sci U S A* **92**: 6625-6629.

Sherman, D. R., M. Voskuil, D. Schnappinger, R. Liao, M. I. Harrell & G. K. Schoolnik, (2001) Regulation of the *Mycobacterium tuberculosis* hypoxic response gene encoding alpha-crystallin. *Proc Natl Acad Sci U S A* **98**: 7534-7539.

Shi, L., C. D. Sohaskey, R. J. North & M. L. Gennaro, (2008) Transcriptional characterization of the antioxidant response of *Mycobacterium tuberculosis in vivo* and during adaptation to hypoxia in vitro. *Tuberculosis* **88**: 1-6.

Shiloh, M. U. & P. A. DiGiuseppe Champion, (2010) To catch a killer. What can mycobacterial models teach us about *Mycobacterium tuberculosis* pathogenesis? *Curr Opin Microbiol* **13**: 86-92.

Shleeva, M., G. V. Mukamolova, M. Young, H. D. Williams & A. S. Kaprelyants, (2004) Formation of 'non-culturable' cells of *Mycobacterium smegmatis* in stationary phase in response to growth under suboptimal conditions and their Rpf-mediated resuscitation. *Microbiology* **150**: 1687-1697.

Shleeva, M. O., K. Bagramyan, M. V. Telkov, G. V. Mukamolova, M. Young, D. B. Kell & A. S. Kaprelyants, (2002) Formation and resuscitation of "non-culturable" cells *of Rhodococcus rhodochrous* and *Mycobacterium tuberculosis* in prolonged stationary phase. *Microbiology* **148**: 1581-1591.

Siegrist, M. S., M. Unnikrishnan, M. J. McConnell, M. Borowsky, T. Y. Cheng, N. Siddiqi, S. M. Fortune, D. B. Moody & E. J. Rubin, (2009) Mycobacterial Esx-3 is required for mycobactin-mediated iron acquisition. *Proc Natl Acad Sci U S A* **106**: 18792-18797.

Simons, S. P., T. J. McLellan, P. A. Aeed, R. P. Zaniewski, C. R. Desbonnet, L. M. Wondrack, E. S. Marr, T. A. Subashi, T. J. Dougherty, Z. Xu, I. K. Wang, P. K. LeMotte & B. A. Maguire, (2009) Purification of the large ribosomal subunit via its association with the small subunit. *Anal Biochem* **395**: 77-85.

Singh (a), B., J. Ghosh, N. M. Islam, S. Dasgupta & L. A. Kirsebom, (2010) Growth, cell division and sporulation in mycobacteria. *Antonie Van Leeuwenhoek* **98**: 165-177.

Singh, (b) R., C. E. Barry, 3rd & H. I. Boshoff, (2010) The three RelE homologs of *Mycobacterium tuberculosis* have individual, drug-specific effects on bacterial antibiotic tolerance. *J Bacteriol* **192**: 1279-1291.

Singh, R., U. Manjunatha, H. I. M. Boshoff, Y. H. Ha, P. Niyomrattanakit, R. Ledwidge, C. S. Dowd, I. Y. Lee, P. Kim, L. Zhang, S. Kang, T. H. Keller, J. Jiricek & C. E. Barry, 3rd, (2008) PA-824 Kills Nonreplicating *Mycobacterium tuberculosis* by Intracellular NO Release. *Science* **322**: 1392-1395.

Sirakova, T. D., V. S. Dubey, C. Deb, J. Daniel, T. A. Korotkova, B. Abomoelak & P. E. Kolattukudy, (2006) Identification of a diacylglycerol acyltransferase gene involved in accumulation of triacylglycerol in *Mycobacterium tuberculosis* under stress. *Microbiology* **152**: 2717-2725.

Smeulders, M. J., (1998) The Stationary Phase Survival Response of *Mycobacterium smegmatis*. In: Department of Biology. London: Imperial College London, pp. 326.

Smeulders, M. J., J. Keer, R. A. Speight & H. D. Williams, (1999) Adaptation of *Mycobacterium smegmatis* to stationary phase. *J Bacteriol* **181**: 270-283.

Smrekar, F., M. Ciringer, M. Peterka, A. Podgornik & A. Strancar, (2008) Purification and concentration of bacteriophage T4 using monolithic chromatographic supports. *J Chromatogr B Analyt Technol Biomed Life Sci* **861**: 177-180.

Solomon, J. M., G. S. Leung & R. R. Isberg, (2003) Intracellular replication of *Mycobacterium marinum* within *Dictyostelium discoideum*: efficient replication in the absence of host coronin. *Infect Immun* **71**: 3578-3586.

Sousa, E. H., J. R. Tuckerman, G. Gonzalez & M. A. Gilles-Gonzalez, (2007) DosT and DevS are oxygen-switched kinases in *Mycobacterium tuberculosis*. *Protein Sci* **16**: 1708-1719.

Spector, M. P. & J. W. Foster, (1993) Gene Expression and Survival in *S. typhymurium*. In: Starvation in Bacteria. S. Kjelleberg (ed). New York: Plenum press, pp. 201-224.

Stallings, C. L., N. C. Stephanou, L. Chu, A. Hochschild, B. E. Nickels & M. S. Glickman, (2009) CarD Is an Essential Regulator of rRNA Transcription Required for *Mycobacterium tuberculosis* Persistence. *Cell* **138**: 146-159.

Starck, J., G. Kallenius, B. I. Marklund, D. I. Andersson & T. Akerlund, (2004) Comparative proteome analysis of *Mycobacterium tuberculosis* grown under aerobic and anaerobic conditions. *Microbiology* **150**: 3821-3829.

Stewart (a), G. R., S. M. Newton, K. A. Wilkinson, I. R. Humphreys, H. N. Murphy, B. D. Robertson, R. J. Wilkinson & D. B. Young, (2005) The stress-responsive chaperone alpha-crystallin 2 is required for pathogenesis of *Mycobacterium tuberculosis*. *Mol Microbiol* **55**: 1127-1137.

Stewart (b), G. R., J. Patel, B. D. Robertson, A. Rae & D. B. Young, (2005) Mycobacterial mutants with defective control of phagosomal acidification. *PLoS Pathog* **1**: 269-278.

Story, A. & K. Citron, (2003) Private Wealth and Public Squalor: The Resurgence of Tuberculosis in London. In: The Return of the White Plague: Global Poverty and the "New" Tuberculosis. M. Gandy & A. Zumla (eds). London: Verso, pp. 95-111.

Street, C. N., A. Gibbs, L. Pedigo, D. Andersen & N. G. Loebel, (2009) In vitro photodynamic eradication of *Pseudomonas aeruginosa* in planktonic and biofilm culture. *Photochem Photobiol* **85**: 137-143.

Tabira, Y., N. Ohara, H. Kitaura, S. Matsumoto, M. Naito & T. Yamada, (1998) The 16-kDa alpha-crystallin-like protein of *Mycobacterium bovis* BCG is produced under conditions of oxygen deficiency and is associated with ribosomes. *Res Microbiol* **149**: 255-264.

Tagkopoulos, I., Y. C. Liu & S. Tavazoie, (2008) Predictive behavior within microbial genetic networks. *Science* **320**: 1313-1317.

Talaat, A. M., R. Lyons, S. T. Howard & S. A. Johnston, (2004) The temporal expression profile of *Mycobacterium tuberculosis* infection in mice. *Proc Natl Acad Sci U S A* **101**: 4602-4607.

Tan, X., M. Varughese & W. R. Widger, (1994) A light-repressed transcript found in *Synechococcus* PCC 7002 is similar to a chloroplast-specific small subunit ribosomal protein and to a transcription modulator protein associated with sigma 54. *J Biol Chem* **269**: 20905-20912.

Tanaka, M., P. B. Chock & E. R. Stadtman, (2007) Oxidized messenger RNA induces translation errors. *Proc Natl Acad Sci U S A* **104**: 66-71.

Timm, J., F. A. Post, L. G. Bekker, G. B. Walther, H. C. Wainwright, R. Manganelli, W. T. Chan, L. Tsenova, B. Gold, I. Smith, G. Kaplan & J. D. McKinney, (2003) Differential expression of iron-, carbon-, and oxygen-responsive mycobacterial genes in the lungs of chronically infected mice and tuberculosis patients. *Proc Natl Acad Sci U S A* **100**: 14321-14326.

Tolker-Nielsen, T. & S. Molin, (1996) Role of ribosome degradation in the death of heat-stressed *Salmonella typhimurium*. *FEMS Microbiol Lett* **142**: 155-160.

Traag, B. A., A. Driks, P. Stragier, W. Bitter, G. Broussard, G. Hatfull, F. Chu, K. N. Adams, L. Ramakrishnan & R. Losick, (2010) Do mycobacteria produce endospores? *Proc Natl Acad Sci U S A* **107**: 878-881.

Tsai, M. C., S. Chakravarty, G. Zhu, J. Xu, K. Tanaka, C. Koch, J. Tufariello, J. Flynn & J. Chan, (2006) Characterization of the tuberculous granuloma in murine and human lungs: cellular composition and relative tissue oxygen tension. *Cell Microbiol* **8**: 218-232.

Tsukamura, M., (1964) Effect of Rifamycin Sv on the Incorporation of ^{32}P-Phosphate, ^{35}S-Sulfate and ^{14}C-Acetate in *M. Tuberculosis*. *Jpn J Tuberc Chest Dis* **12**: 10-14.

Tyagi, J. S. & D. Sharma, (2002) *Mycobacterium smegmatis* and tuberculosis. *Trends Microbiol* **10**: 68-69.

Ueta, M., R. L. Ohniwa, H. Yoshida, Y. Maki, C. Wada & A. Wada, (2008) Role of HPF (Hibernation Promoting Factor) in Translational Activity in *Escherichia coli*. *J Biochem* **143**: 425-433.

Ueta, M., H. Yoshida, C. Wada, T. Baba, H. Mori & A. Wada, (2005) Ribosome binding proteins YhbH and YfiA have opposite functions during 100S formation in the stationary phase of Escherichia coli. *Genes Cells* **10**: 1103-1112.

Uicker, W. C., L. Schaefer, M. Koenigsknecht & R. A. Britton, (2007) The Essential GTPase YqeH Is Required for Proper Ribosome Assembly in *Bacillus subtilis*. *J. Bacteriol.* **189**: 2926-2929.

van Kessel, J. C. & G. F. Hatfull, (2007) Recombineering in *Mycobacterium tuberculosis*. *Nat Methods* **4**: 147-152.

VanderVen, B. C., R. M. Yates & D. G. Russell, (2009) Intraphagosomal measurement of the magnitude and duration of the oxidative burst. *Traffic* **10**: 372-378.

Velmurugan, K., B. Chen, J. L. Miller, S. Azogue, S. Gurses, T. Hsu, M. Glickman, W. R. Jacobs, Jr., S. A. Porcelli & V. Briken, (2007) *Mycobacterium tuberculosis nuoG* is a virulence gene that inhibits apoptosis of infected host cells. *PLoS Pathog* **3**: e110.

Venkatesh, J., P. Kumar, P. S. Krishna, R. Manjunath & U. Varshney, (2003) Importance of uracil DNA glycosylase in *Pseudomonas aeruginosa* and *Mycobacterium smegmatis*, G+C-rich bacteria, in mutation prevention, tolerance to acidified nitrite, and endurance in mouse macrophages. *J Biol Chem* **278**: 24350-24358.

Via, L. E., P. L. Lin, S. M. Ray, J. Carrillo, S. S. Allen, S. Y. Eum, K. Taylor, E. Klein, U. Manjunatha, J. Gonzales, E. G. Lee, S. K. Park, J. A. Raleigh, S. N. Cho, D. N. McMurray, J. L. Flynn & C. E. Barry, III, (2008) Tuberculous Granulomas Are Hypoxic in Guinea Pigs, Rabbits, and Nonhuman Primates. *Infect. Immun.* **76**: 2333-2340.

Vila-Sanjurjo, A., B. S. Schuwirth, C. W. Hau & J. H. Cate, (2004) Structural basis for the control of translation initiation during stress. *Nat Struct Mol Biol* **11**: 1054-1059.

Vogel, U. & K. F. Jensen, (1994) Effects of guanosine 3',5'-bisdiphosphate (ppGpp) on rate of transcription elongation in isoleucine-starved *Escherichia coli*. *J Biol Chem* **269**: 16236-16241.

Voskuil, M. I., R. W. Honaker & A. J. C. Steyn, (2009) Oxygen, Nitric Oxide and Carbon Monoxide Signalling. In: Mycobacterium: Genomics and Molecular Biology. T. Parish & A. C. Brown (eds). Norfolk, UK: Caister Academic Press, pp. 119-147.

Voskuil, M. I., D. Schnappinger, K. C. Visconti, M. I. Harrell, G. M. Dolganov, D. R. Sherman & G. K. Schoolnik, (2003) Inhibition of respiration by nitric oxide induces a *Mycobacterium tuberculosis* dormancy program. *J Exp Med* **198**: 705-713.

Voskuil, M. I., K. C. Visconti & G. K. Schoolnik, (2004) *Mycobacterium tuberculosis* gene expression during adaptation to stationary phase and low-oxygen dormancy. *Tuberculosis (Edinb)* **84**: 218-227.

Vynnycky, E. & P. E. Fine, (1997) The natural history of tuberculosis: the implications of age-dependent risks of disease and the role of reinfection. *Epidemiol Infect* **119**: 183-201.

Wada, A., K. Igarashi, S. Yoshimura, S. Aimoto & A. Ishihama, (1995) Ribosome modulation factor: stationary growth phase-specific inhibitor of ribosome functions from *Escherichia coli*. *Biochem Biophys Res Commun* **214**: 410-417.

Wada, A., R. Mikkola, C. G. Kurland & A. Ishihama, (2000) Growth phase-coupled changes of the ribosome profile in natural isolates and laboratory strains of *Escherichia coli*. *J Bacteriol* **182**: 2893-2899.

Wada, A., Y. Yamazaki, N. Fujita & A. Ishihama, (1990) Structure and probable genetic location of a "ribosome modulation factor" associated with 100S ribosomes in stationary-phase *Escherichia coli* cells. *Proc Natl Acad Sci U S A* **87**: 2657-2661.

Wallace, D. & R. Wallace, (2003) The Recent Tuberculosis Epidemic in New York City: Warning from the De-developing World. In: The Return of the White Plague: Global Poverty and the "New" Tuberculosis. M. Gandy & A. Zumla (eds). London: Verso, pp. 125-146.

Walls, T. & D. Shingadia, (2004) Global epidemiology of paediatric tuberculosis. *J Infect* **48**: 13-22.

Wang, N. & L. Li, (2008) Exploring the precursor ion exclusion feature of liquid chromatography-electrospray ionization quadrupole time-of-flight mass spectrometry for improving protein identification in shotgun proteome analysis. *Anal Chem* **80**: 4696-4710.

Warner, D. F. & V. Mizrahi, (2006) Tuberculosis chemotherapy: the influence of bacillary stress and damage response pathways on drug efficacy. *Clin Microbiol Rev* **19**: 558-570.

Wayne, L. G. & L. G. Hayes, (1996) An *in vitro* model for sequential study of shiftdown of *Mycobacterium tuberculosis* through two stages of nonreplicating persistence. *Infect Immun* **64**: 2062-2069.

Wayne, L. G. & C. D. Sohaskey, (2001) Nonreplicating persistence of *Mycobacterium tuberculosis*. *Annu Rev Microbiol* **55**: 139-163.

Wayne, L. G. & H. A. Sramek, (1979) Antigenic differences between extracts of actively replicating and synchronized resting cells of *Mycobacterium tuberculosis*. *Infect Immun* **24**: 363-370.

Wayne, L. G. & H. A. Sramek, (1994) Metronidazole is bactericidal to dormant cells of *Mycobacterium tuberculosis*. *Antimicrob Agents Chemother* **38**: 2054-2058.

Weston, S. A. & C. R. Parish, (1990) New fluorescent dyes for lymphocyte migration studies. Analysis by flow cytometry and fluorescence microscopy. *J Immunol Methods* **133**: 87-97.

WHO, (2004) The global burden of disease: 2004 update. In. Geneva: World Health Organisation, pp.

WHO, (2009) Global Tuberculosis control: A short update to the 2009 report. In. Geneva: World Health Organisation, pp.

Wilson, D. N. & K. H. Nierhaus, (2007) The weird and wonderful world of bacterial ribosome regulation. *Crit Rev Biochem Mol Biol* **42**: 187-219.

Wiuff, C., R. M. Zappala, R. R. Regoes, K. N. Garner, F. Baquero & B. R. Levin, (2005) Phenotypic tolerance: antibiotic enrichment of noninherited resistance in bacterial populations. *Antimicrob Agents Chemother* **49**: 1483-1494.

Wout, P., K. Pu, S. M. Sullivan, V. Reese, S. Zhou, B. Lin & J. R. Maddock, (2004) The *Escherichia coli* GTPase CgtAE cofractionates with the 50S ribosomal subunit and interacts with SpoT, a ppGpp synthetase/hydrolase. *J Bacteriol* **186**: 5249-5257.

Xu, J., M. D. Knutson, C. S. Carter & C. Leeuwenburgh, (2008) Iron Accumulation with Age, Oxidative Stress and Functional Decline. *PLoS ONE* **3**: e2865.

Xu, Y., R. J. Heath, Z. Li, C. O. Rock & S. W. White, (2001) The FadR-DNA complex. Transcriptional control of fatty acid metabolism in *Escherichia coli*. *J Biol Chem* **276**: 17373-17379.

Yoshida, H., Y. Maki, H. Kato, H. Fujisawa, K. Izutsu, C. Wada & A. Wada, (2002) The ribosome modulation factor (RMF) binding site on the 100S ribosome of *Escherichia coli*. *J Biochem* **132**: 983-989.

Yoshida, H., M. Ueta, Y. Maki, A. Sakai & A. Wada, (2009) Activities of *Escherichia coli* ribosomes in IF3 and RMF change to prepare 100S ribosome formation on entering the stationary growth phase. *Genes Cells* **14**: 271-280.

Yoshida, H., H. Yamamoto, T. Uchiumi & A. Wada, (2004) RMF inactivates ribosomes by covering the peptidyl transferase centre and entrance of peptide exit tunnel. *Genes Cells* **9**: 271-278.

Youmans, A. S. & G. P. Youmans, (1968) Ribonucleic acid, deoxyribonucleic acid, and protein content of cells of different ages of *Mycobacterium tuberculosis* and the ralationship to immunogenicity. *J Bacteriol* **95**: 272-279.

Young, D. B., H. P. Gideon & R. J. Wilkinson, (2009) Eliminating latent tuberculosis. *Trends Microbiol* **17**: 183-188.

Yukl, E. T., A. Ioanoviciu, P. R. de Montellano & P. Moenne-Loccoz, (2007) Interdomain interactions within the two-component heme-based sensor DevS from *Mycobacterium tuberculosis*. *Biochemistry* **46**: 9728-9736.

Zahrt, T. C. & V. Deretic, (2001) *Mycobacterium tuberculosis* signal transduction system required for persistent infections. *Proc Natl Acad Sci U S A* **98**: 12706-12711.

Zolfaghari, P. S., S. Packer, M. Singer, S. P. Nair, J. Bennett, C. Street & M. Wilson, (2009) *In vivo* killing of *Staphylococcus aureus* using a light-activated antimicrobial agent. *BMC Microbiol* **9**: 27.

Zundel, M. A., G. N. Basturea & M. P. Deutscher, (2009) Initiation of ribosome degradation during starvation in *Escherichia coli. RNA* **15**: 977-983.